Wardlaw, B.R. & Nestell, M.K., 2014. The first appearance of *Streptognathodus isolatus* in the Permian of Texas. *Permophiles 59*, 17–20.

Xia, G.Y. & Zhang, Z.C., 1985. Protozoa. In *Paleontological Atlas of North China (I) Paleozoic Volume*. Tianjin Institute of Geology and Mineral Resources, ed., Geological Publishing House, Beijing, 32–150. (in Chinese)

Xia, G.Y., Ding, Y.J., Ding, H., Zhang, W.Z., Zhang, Y., Zhao, Z. & Yang, F.Q., 1996. *On the Carboniferous–Permian Boundary Stratotype in China*. Geological Publishing House, Beijing, 200 pp. (in Chinese with English abstract)

Zhai, M.G., Guo, J.H., Li, Z., Chen, D.Z., Peng, P., Li, T.S., Hou, Q.L. & Fan, Q.C., 2007. Linking the Sulu UHP belt to the Korean Peninsula: Evidence from eclogite, Precambrian basement, and Paleozoic sedimentary basins. *Gondwana Research 12*, 388–403.

Zhang, L.X., 1960. The fusulinids in Qilian Mountains. *Geology of Qilian Mountain*, Institute of Geology and Palaeontology Chinese Academy of Science, Geological Institute of Chinese Academy of Science, eds, Science Press, Beijing, 33–53 pp. (Chinese).

Zhang, L.X., Zhou, J.P., Niu, B.X. & Wang, H., 1989. Fusulinids from Late Carboniferous Taiyuan Formation in Zibo Area, Shandong. *Acta Palaeontologica Sinica 28*(6), 803–818. (in Chinese with English summary).

Zhao, S.Y., 1982. Upper Carboniferous conodonts of the Qinshui basin, Shanxi. *Bulletin of the Tianjin Institute of Geology and Mineral Resources, Chinese Academy of Geological Sciences 4*, 97–111. (in Chinese with English abstract).

Available online at www.sciencedirect.com

ScienceDirect

Palaeoworld 26 (2017) 703–717

Palaeoworld

www.elsevier.com/locate/palwor

A new species of *Tetralophodon* from the Linxia Basin and the biostratigraphic significance of tetralophodont gomphotheres from the Upper Miocene of northern China

Shi-Qi Wang [a,b,*], Haruo Saegusa [c], Jaroon Duangkrayom [a,d], Wen He [e], Shan-Qin Chen [e]

[a] *Key Laboratory of Vertebrate Evolution and Human Origins of Chinese Academy of Sciences, Institute of Vertebrate Paleontology and Paleoanthropology, Chinese Academy of Sciences, Beijing 100044, China*

[b] *CAS Center for Excellence in Tibetan Plateau Earth Sciences, Beijing 100101, China*

[c] *Division of Earth Sciences, Institute of Nature and Environmental Sciences, University of Hyogo/Museum of Nature and Human Activities, Hyogo, Yayoigaoka 6, Sanda 669-1546, Japan*

[d] *Northeastern Research Institute of Petrified Wood and Mineral Resources, Nakhon Ratchasima Rajabhat University, Nakhon Ratchasima 30000, Thailand*

[e] *Hezheng Paleozoological Museum, Hezheng, Gansu 731200, China*

Received 1 December 2016; accepted 30 March 2017
Available online 8 April 2017

Abstract

Tetralophodont gomphotheres, i.e., *Tetralophodon*, *Paratetralophodon*, and *Anancus*, show significant morphological diversity and are of great importance for the biostratigraphy of the Upper Miocene. However, material of this group from the Upper Miocene of northern China is rare and easily to be confused with the similar taxa such as *Konobelodon* and *Stegolophodon*. The stratigraphy of this group is also unclear in China. Here we described the first mandible from northern China that can be definitely attributed to *Tetralophodon*, and erected a new species *Tetralophodon euryrostris* n. sp. Furthermore, we amended the previously reported tetralophodont gomphotheres from northern China. We attributed the type material of "*Tetralophodon exoletus*" to ?*Paratetralophodon exoletus*, the material from Lantian region ("*Tetralophodon exoletus*") to *Paratetralophodon* sp., and the material from the Qaidam Basin (*Tetralophodon* sp.) to *Tetralophodon* aff. *xiaolongtanensis*. We also discussed the stratigraphic ranges of the tetralophodont proboscideans from the Upper Miocene of China, that is, *Tetralophodon* aff. *xiaolongtanensis* from MN9, *Tetralophodon* cf. *euryrostris* from MN10, *Konobelodon robustus* from MN9–MN10, *Paratetralophodon* sp. from MN11, ?*Paratetralophodon exoletus* from MN12, and *Stegolophodon licenti* from MN13. This work is important for the study of the taxonomy and biostratigraphy of tetralophodont gomphotheres from the Upper Miocene of northern China.

Keywords: Tetralophodont gomphotheres; *Tetralophodon*; Upper Miocene; Northern China; Biostratigraphy

1. Introduction

Tetralophodont gomphotheres are an important group in the evolution of proboscideans, and proximally related to the true elephants (Tassy, 1985, 1988, 1996; Shoshani, 1996). Because tetralophodont gomphotheres are a paraphyletic group, the family hierarchy of this group is undetermined (Shoshani and Tassy, 2005) or they are attributed to the paraphyletic Gomphotheriidae (Gheerbrant and Tassy, 2009). They were dominant proboscideans in the Late Miocene of Eurasia (Göhlich, 1999). However, fossil records of tetralophodont gomphotheres from the Upper Miocene of northern China are rare, relatively to Western Europe and southern Asia, and the taxonomy of these specimens is controversial. For example, the classical taxon "*Tetralophodon exoletus* Hopwood, 1935" was erected based on the type material from the Baode region (Hopwood, 1935) (Fig. 1), and Liu et al. (1978) reported other speci-

* Corresponding author at: Key Laboratory of Vertebrate Evolution and Human Origins of Chinese Academy of Sciences, Institute of Vertebrate Paleontology and Paleoanthropology, Chinese Academy of Sciences, Beijing 100044, China. Fax: +86 10 68337001.

E-mail addresses: wangshiqi@ivpp.ac.cn (S.Q. Wang), saegusa@hitohaku.jp (H. Saegusa), jakrub2008@hotmail.com (J. Duangkrayom), hzbwg_5524668@126.com (W. He), hzbwg_chenshanqin@126.com (S.Q. Chen).

http://dx.doi.org/10.1016/j.palwor.2017.03.005
1871-174X/

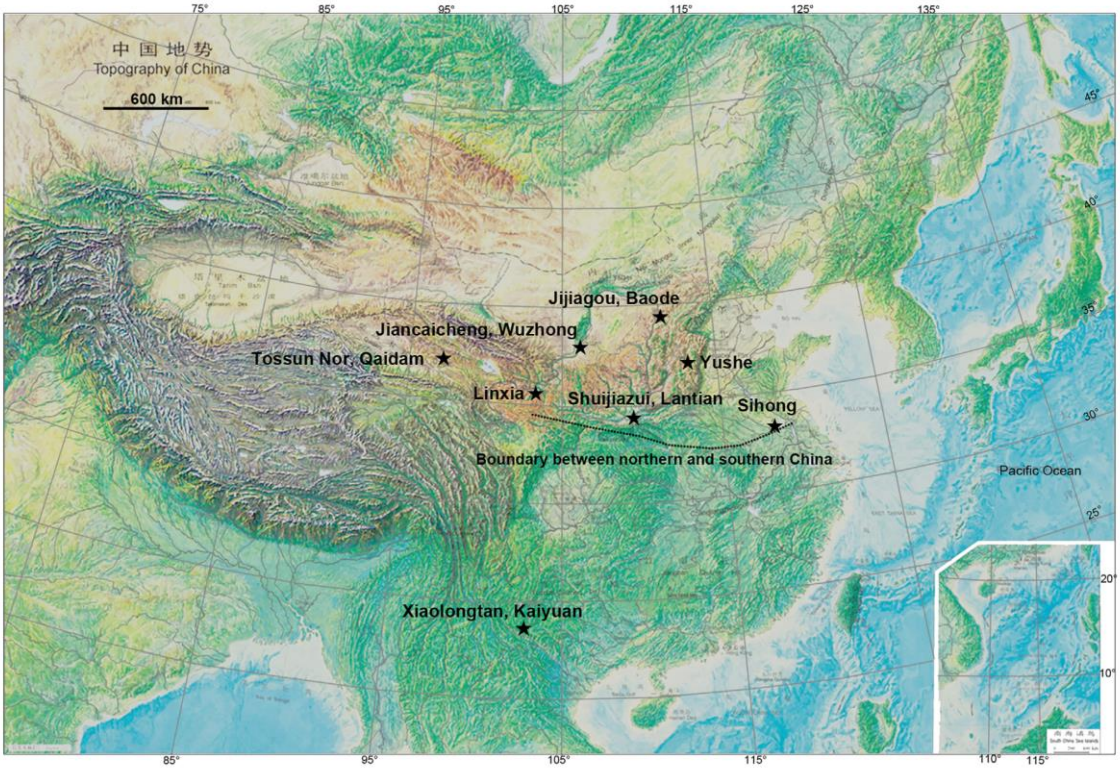

Fig. 1. Map showing the fossil localities in China bearing tetralophodont proboscideans mentioned in the present article.

mens from the Lantian region (Fig. 1). However, Tobien et al. (1988) attributed the hypodigm to "*Stegotetrabelodon exoletus*" and referred the Lantian material to "*Tetralophodon* (*Paratetralophodon*) cf. *hasnotensis*". Other researchers debated on the occurrence of *Stegotetrabelodon* in eastern Asia (Tassy, 1999; Ferreti et al., 2003). Recently recognized tetralophodont amebelodontid *Konobelodon robustus* from the Upper Miocene of the Linxia Basin (Wang et al., 2016a), which had been identified as "*Tetralophodon* sp." and "*Tetralophodon exoletus*" (Deng et al., 2004, 2013), further complicated this problem (Fig. 1). For example, can *Konobelodon* be used to name other material of *Tetralophodon* from northern China? And if so, is *Tetralophodon* really present in northern China? These questions remain to be resolved.

Besides the above material, there are other two records of tetralophodont gomphotheres from the Upper Miocene of northern China with known horizon: *Tetralophodon* sp. from the Qaidam Basin (Bohlin, 1937), *Tetralophodon* cf. *exoletus* from Wuzhong (Qiu et al., 1987) (Fig. 1). The remaining specimens of tetralophodont gomphotheres, i.e., "*Gomphotherium watzeensis*" (Hu, 1962) and "*Gomphotherium quinanensis*" (Chow and Chang, 1961) (attributed to "*Tetralophodon* (*Paratetralophodon*) cf. *hasnotensis*" and "*Stegotetrabelodon exoletus*" by Tobien et al. (1988), respectively), are represented only by molar fragments, and their precise localities and horizons are unknown.

In the Hezheng Palaeozoological Museum, there is a complete mandible of a tetralophodont gomphothere (HMV 1427). It is the first complete mandible of a tetralophodont gomphothere from China, and is clearly distinguishable from *K. robustus* from the Liushu Formation of the Linxia Basin. On the basis of the morphology of the mandible, we attributed this specimen to *Tetralophodon* and erected a new species *Tetralophodon euryrostris* n. sp. This is definitive evidence for the occurrence of the genus *Tetralophodon* in northern China. Furthermore, we amended the other material of tetralophodont gomphotheres from northern China, compared their tooth morphology with the related taxa such as *Konobelodon* and *Stegolophodon*. The stratigraphic occurrences of the tetralophodont proboscideans were also discussed based on the newly established Asian biochronological framework (Qiu et al., 2013; Wang et al., 2013). Hence this work improves the study of systematic evolution and biostratigraphy of tetralophodont gomphotheres, an important group of proboscideans, from the Upper Miocene of northern China.

2. Material and methods

2.1. Institutional abbreviations

GPAHLD: Geologisch-Paläontologische Abteilung des Hessischen Landesmuseums, Darmstadt, Germany.

HMV: Hezheng Paleozoological Museum, Hezheng, China.

IVPP: Institute of Vertebrate Paleontology and Paleoanthropology, Beijing, China.

NMHW: Naturhistorisches Museum, Vienna, Austria.

MSB: Museo del Seminario, Barcelona, Spain.

MNM: Naturhistorisches Museum, Mainz, Germany.

PMU: Palaeontological Museum, Uppsala.

UZ: Palaeontological collection in the Zoology Department, University of the Panjab, Lahore, Pakistan.

2.2. Material

The material with respect to *T. euryrostris* n. sp. is housed in HMV. It was collected by a local villager, and the precise locality cannot be traced. Judged from the sediments attached to the specimen, it was possibly excavated from the lower part of the Upper Miocene Liushu Formation of the Linxia Basin (Deng et al., 2013; Fig. 1). The material with respect to *Tetralophodon* cf. *euryrostris* and *Tetralophodon* aff. *xiaolongtanensis* is housed in IVPP. The comparative material of ?*Paratetralophodon exoletus* and *Paratetralophodon* sp. is housed in IVPP; and the other material is from previously publications (Schlesinger, 1917; Klähn, 1931; Hopwood, 1935; Osborn, 1936; Alberdi, 1971; Tobien, 1976; Sarwar, 1977; Tobien, 1978, 1980; Dong, 1987; Wang et al., 2016a).

2.3. Measurements and terminology

The terminology of the occlusal structures of bunodont molars followed Tassy (2014) (Fig. 2), and the measurements and terminology of cranium and mandible followed Tassy (2013). All measurements were taken using calipers (in mm).

3. Systematic paleontology

Order Proboscidea Illiger, 1811

Family Gomphotheriidae Hay, 1922

Genus *Tetralophodon* Falconer, 1857

Type species: *Tetralophodon longirostris* (Kaup, 1832).

Type locality and horizon: Eppelsheim of the "*Deinotherium*" sand, Germany, Vallesian (early Late Miocene) (Tassy, 1985).

Tetralophodon euryrostris n. sp.

(Figs. 3 and 4)

Etymology: *eury*-, wide; *rostris*, mouth or nose that is anteriorly protruded. The name indicates the wide mandibular symphysis and mandibular tusks relative to the other species of *Tetralophodon*.

Holotype: HMV 1427, a complete mandible, from the Late Miocene of the Linxia Basin, the precise locality is unknown.

Occurrences: ? early Late Miocene,? MN10 (reasons see below, Section 4.3), northern China.

Diagnosis: medium-sized *Tetralophodon*; mandibular symphysis and mandibular tusks relatively wide and long with a marked symphyseal groove; mandibular symphysis moderately ventrally deflected; mandibular tusks dorsally concave, oval cross-sectioned, and with a faint dorsal groove; exposed length of mandibular tusks subequal to symphyseal length; mandibular angular process blunt, slightly higher than the occlusal plane; ascending ramus perpendicular to the occlusal plane; cheek teeth showing convergent features with *Stegolophodon*, i.e., lophid straight, anterior pretrite central conules (except in the first lophids) nearly absent, posterior central conule small and low, and mesoconelets enlarged. Differing from *Tetralophodon longirostris* in wider, stronger, and more ventrally defected mandibular symphysis, and in thicker and longer mandibular tusks; differing from *Tetralophodon curvirostris* in less ventrally defected mandibular symphysis and in thicker and longer mandibular tusks; differing from *Tetralophodon gigantorostris* in shorter and thicker mandibular tusks; differing from all other species of *Tetralophodon* (the former three plus *Tetralophodon xiaolongtanensis*) and *Paratetralophodon* in the presence of convergent features of cheek teeth with *Stegolophodon*; differing from species of *Konobelodon* in shorter and suboval cross-sectioned lower tusks, in the presence of convergent features of cheek teeth with *Stegolophodon*; differing from species of *Stegolophodon* in the strong mandibular symphysis and mandibular tusks.

Description:

HMV 1427 is a complete mandible. In lateral view (Fig. 3a), the ascending ramus is low and posteriorly elongated. The coronoid process is strongly upwardly protruded and the madibular condyle is small in this view. The mandibular notch is relatively shallow. The angular process is highly positioned at the level that is slightly higher than the occlusal surface. The masseteric fossa is deep with a triangular contour. The anterior and posterior ramal borders are perpendicular to the occlusal surface. The corpus is relatively high, especially at the anterior end. The posterior mental foramen is big and oval, and is positioned at the level of the anterior end of the m2. The anterior mental foramen is small, and is anterior to the m1 alveolus. The rostrum is moderately ventrally deflected.

In dorsal view (Fig. 3b), the madibular condyle is transversely oval. The ascending ramus is thin in this view. The corpus is thick at the base part where the ascending ramus rises and tapers anteriorly. The retromolar trigon is prominent. The m1 has been shed, leaving a vacancy of the alveolus. The m2 is deeply worn of the four lophids. The right m3 has been erupted from the fourth lophid with slight wear of the first one. However, the left m3 is absent, possibly due to heteroplasia. The posterior border of the symphysis is almost in line with the anterior ends of the tooth rows. The mandibular symphysis is narrow and elongated. The interalveolar crest initials from the anterior point of the m1 alveolus, runs along the rostrum, and ends at the lateral edge of the mandibular tusk. The two interalveolar crests slightly converge in the middle part and the rostrum between the two

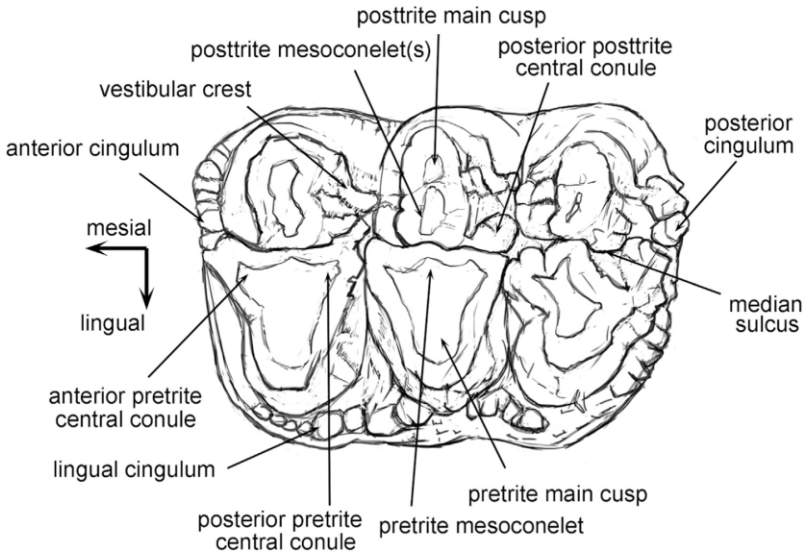

Fig. 2. Terminology used to describe a proboscidean bunodont teeth, a left moderately worn M2 of *Sinomastodon praeintemedius*.

Table 1
Mandibular measurements of *Tetralophodon euryrostris* n. sp. (HMV 1427, the holotype, in mm), after Tassy (2013).

Measurement	(mm)
Maximum length	1362
Symphyseal length	450
Alveolar distance (from the most salient point of the trigonum retromolare to the symphyseal border of the corpus)	361
Ventral length measured from the gonion (angulus mandibular) to the tip of the symphysis	999
Maximum width	402
Mandibular width measured at the root of the rami	424
Width of corpus measured at the root of the ramus	147
Width of corpus measured at the anterioralveolus (or the grinding tooth if the alveolus is entirely resorbed)	109
Posterior symphyseal width	218
Anterior symphyseal width	177
Maximum symphyseal width	186
Minimum symphyseal width	162
Maximum width of rostral trough	114
Minimum width of rostral trough	57
Internal width between anterior alveoli (or grinding teeth if the alveoli are resorbed)	78
Maximum height of corpus (measurement taken perpendicular to the ventral border of the corpus)	157
Height of corpus measured at the root of the ramus (measurement as above)	127
Rostral height measured at the symphyseal border (measurement taken perpendicular to the ventral border of the symphyseal rostrum)	122
Rostral height measured at the tip of rostrum (measurement as above)	65
Maximum mandibular height measured at the condyle perpendicular to the ventral border of the corpus	295
Maximum depth of ramus	234
Depth between gonion and coronoid processes	255
Height between gonion and condyle	182
Mid-alveolar length measured on the buccal side between the anterior alveolus (or grinding tooth if the alveolus is resorbed) and the root of the ramus	355

crests is markedly concave, forming a symphyseal groove. The anterior edge of the symphysis is anteriorly convex (Table 1).

The lower tusks (Fig. 3) are relatively robust. The lower tusks are slightly shorter than the symphyseal length. In lateral view (Fig. 3a), it is dorsally concave. In dorsal view (Fig. 3b), it is straight, showing a slightly concave dorsal surface. The anterior edge of the tusks is rounded without medial and lateral angles and the dorsal tip is polished by wear. Therefore, in apical view, the anterior end of the tusks is somewhat flattened (Fig. 3c). The cross-section of the tusks (Fig. 3d and e) is sub-oval. The medial

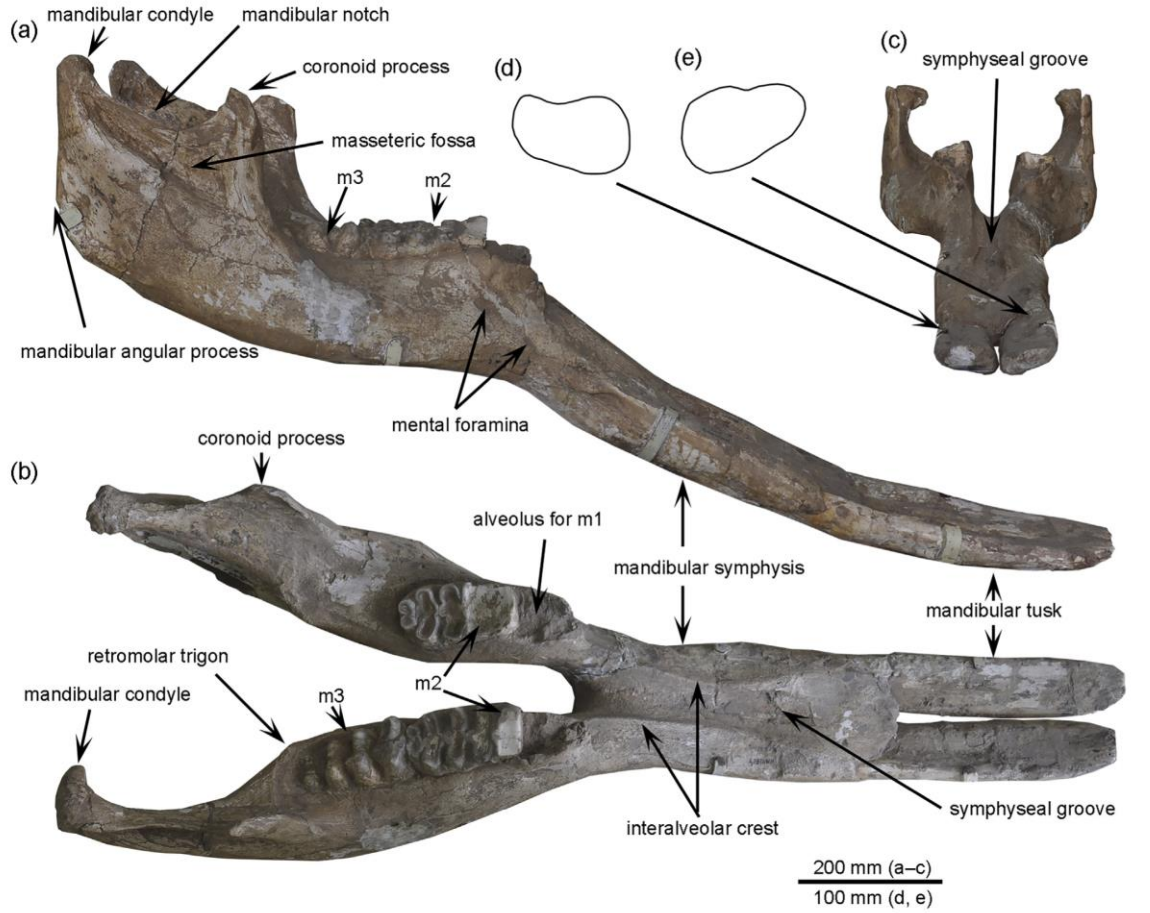

Fig. 3. Mandible with lower tusks of *Tetralophodon euryrostris* n. sp. (HMV 1427, the holotype); (a) in lateral view; (b) in dorsal view; (c) in anterior view; (d and e) cross-section of the right (d) and left (e) lower tusks at the level of the opening of the alveoli, both in anterior view.

Table 2
Measurements of mandibular tusks of *Tetralophodon euryrostris* n. sp. (HMV 1427, the holotype, in mm).

Locus	Lateral length	Medial length	Maximal diameter at the level of the alveoli	Minimal diameter at the level of the alveoli	Length of the dorsal wear facet
Left	317	300	83.27	58.19	95.28
Right	345	285	84.67	58.14	99.25

side is thick and the lateral side is thin. A shallow dorsal groove is present, but ventral groove is almost absent (Table 2).

The m2 (Fig. 4a) is a typical tetralophodont bunodont molar with a wide contour. The wear of the right one is relatively low. It is rectangular and is composed of four lophids and a strong posterior cingulid. A little cementum (or dental calculus, see Asevedo et al., 2012) seems to be deposited in the interlophids. The first lophid has been worn out, only the posterior enamel wall remaining, with a posteriorly oriented apex indicating the posterior pretrite central conule. The second lophid is deeply worn, the wear figure of the pretrite and posttrite half-lophids are interconnected with each other. This lophid is transversely straight (no anancoidy being present). Both pretrite and posttrite half-lophids are relatively antero-posteriorly compressed and the posterior pretrite central conule is pronounced. The third and fourth lophids are moderately worn. The pretrite half-lophids are antero-posteriorly compressed, showing relatively quadrate patterns, and with relatively prominent posterior pretrite central conules. The posttrite half-lophids are also antero-posteriorly compressed showing quadrate patterns, but with slightly postero-lingual orientation. Wear figures can also be observed on the posterior cingulid. It shows two compressed

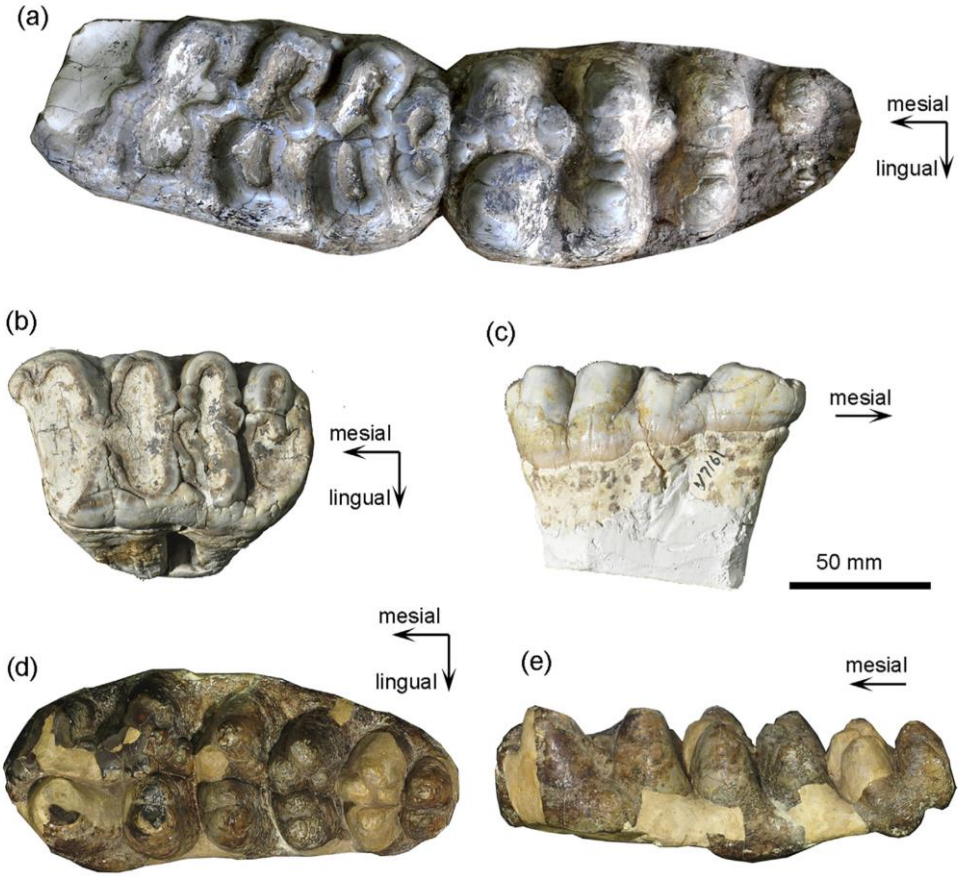

Fig. 4. Cheek teeth of *Tetralophodon* from northern China; (a) right m2 and m3 of *Tetralophodon euryrostris* n. sp., HMV 1427, the holotype, in occlusal view, from Linxia Basin; (b) left M1 of *Tetralophodon* cf. *euryrostris*, IVPP V7161, in occlusal view, from Wuzhong; (c) the same specimen as (b), in buccal view; (d) right M3 of *Tetralophodon* aff. *xiaolongtenensis*, IVPP RV37091, from Tossun Nor, Qaidam Basin, this specimen was published by Bohlin (1937, pl. 1, figs. 8, 9) as an m3 of *Tetralophodon* sp., with the original number No. 487; (e) the same specimen as (d), in lingual view.

Table 3
Measurements of cheek teeth of species of *Tetralophodon* from northern China (in mm).

Taxa	Specimen	Locus	Length	Width at the 1st loph(id)	Width at the 2nd loph(id)	Width at the 3rd loph(id)	Width at the 4th loph(id)	Width at the 5th loph(id)	Height
Tetralophodon euryrostris n. sp.	HMV 1427	left m2	147.01	68.48+	74.91	76.44	80.29		32.5+[a]
		right m2	142.37	71.05	72.35	78.85	81.12		38.26+[a]
		right m3		78.64	79.35	69.75+			58.29[b]
Tetralophodon cf. *euryrostris*	IVPP V 7161	left M1	105.86	62.59	64.62	64.61	64.07		36.96+[c]
Tetralophodon aff. *xiaolongtanensis*	IVPP RV 37091	right M3	161.48	61.8	69.79	67.78	60.20	52.06	47.99[d]

[a] Measured at the buccal side of the 4th lophid.
[b] Measured at the lingual side of the 1th lophid.
[c] Measured at the buccal side of the 4th loph.
[d] Measured at the lingual side of the 3th loph.

and contacted enamel loops. The left m2 is more deeply worn than the right one because of lacking left m3 (Table 3).

The right m3 (Fig. 4a) has four erupted lophids. Cingulids are slightly developed on the anterior and the labial margin of the first lophids and cementum not only is deposited in the intelophids but also covers the basal part of lophids. The first pretrite half-lophid is completely trifoliate. The anterior pretrite central conule is subdivided into two conules. It is anterolingually extended to link the anterior cingulid. The posterior pretrite central conule is large and isolated, linked with the main conelet by a small conule. The pretrite mesoconelet is subdivided into two conelets. The first posttrite half-lophid is composed of a main conelet and a mesoconelet. The posttrite mesoconelet is large, shows a tendency of subdivision, and is slightly anterolingually oriented. The second lophid is almost straight. Both pretrite and posttrite half-lophids are composed of a main conelet and a bisubdivided mesoconelet that is lower than the main conelet (in buccal view). The anterior pretrite central conule is almost absent, and the posterior pretrite central conule is isolated and very low (in buccal view). The third lophid is also straight. Both pretrite and posttrite half-lophids are composed of a main conelet and a relatively small mesoconelet that is lower than the main conelet. The anterior pretrite central conule is missing and the posterior one has not been erupted. Only the summits of conelets of the fourth lophid have been erupted.

Tetralophodon cf. *euryrostris*

(Fig. 4)

1987 *Tetralophodon* cf. *exoletus* Hopwood – Qiu et al., p. 48, fig. 1.

Referred material: IVPP V 7161, a deeply worn left M1, from the Jiancaicheng locality, Wuzhong, Ningxia, the early Late Miocene Ganhegou Formation (MN10) (Shen et al., 2001; Wang, W.T. et al., 2011).

Description:

This tooth is a deeply worn left M2 with a wide contour. The four lophs, except the third and fourth posttrite half-lophs, are almost completely worn. Cingula are developed on the lingual and posterior margins and surround the first posttrite half-loph. The lophs are straight and anteroposteriorly compressed, and the interlophs are anteroposteriorly narrow. Pretrite central conules appear to be relatively weak and mesoconelets are relatively strong. This tooth shows some convergent features with *Stegolophodon*, but the tooth is potentially slightly high crowned observing from the remaining last two lophs might reject its attribution to *Stegolophodon* (Fig. 4c; Table 3).

Tetralophodon aff. *xiaolongtanensis* (Chow and Chang, 1974)

(Fig. 4)

1937 *Tetralophodon* sp. – Bohlin, pl. 1, figs. 8, 9.

Referred material: IVPP RV37091, a right M3, partially broken and repaired by plaster, from Tossun Nor of the Qaidam Basin (MN9) (Wang, X.M. et al., 2011). The original number is No. 437.

Description:

The tooth is slightly worn. It is long and narrow, and is composed of five lophs. There is an unusual feature that the contour of the tooth is slightly lingually convex. Cingula are developed on the anterior and posterior ends of the tooth and no cementum is developed. The first loph is partly broken and the pretrite half-loph shows a trifoliate pattern. The second pretrite trefoil is well developed. The pretrite mesoconelet is subdivided into two strong conelets. The anterior central conule is larger than the posterior one and both of them are subdivided into two elements. The second posttrite half-loph is composed of a large main conelet and a slightly smaller mesoconelet. A very small posttrite posterior central conule is observed. The third and the fourth lophs are almost in the same pattern. The lophs are cheveroned; the pretrite mesoconelet is fused with the pretrite anterior central conule; the posterior pretrite central conule is small and subdivided; and the posttrite main conelet and mesoconelet are subequal in size and a very weak posttrite posterior central conule is likewise developed. The fifth loph is repaired by plaster. There are two large conelets developed on the posterior cingulum, as if a subdeveloped sixty loph. No tendency of anancoidy is displayed on this tooth (Table 3).

4. Comparisons and discussion

4.1. Comparison of mandibles and tusks

Mandibles of tetralophodont proboscideans (including *Konobelodon* and *Stegolophodon*) are rarely discovered from northern China. Wang et al. (2016a) reported *K. robustus* from the early Late Miocene of the Linxia Basin, which seems to be contemporary with the new material. The mandibular tusks of *K. robustus* (Fig. 5c and l) having a dorsally concave cross-section are significantly flatter and wider than those of *T. euryrostris*. The exposed length of the tusks is much longer than the symphyseal length in adults, and the two tusks are somewhat twisted and divergent. These features are clearly distinct from those in *T. euryrostris* (Fig. 5e and j). Furthermore, *T. euryrostris* seems not to be a female individual of *K. robustus*, because in the young individual of *K. robustus*, the lower tusks have been flattened and strongly divergent (generally, morphology of juveniles is closer to that of females rather than males) (Wang et al., 2016a).

Stegolophodon is an important genus in the Miocene of East and Southeast Asia. In this genus, mandibular symphysis had been significantly reduced and is acutely ventrally deflected. For example, "*Stegotetrabelodon maluvalensis*" described by Sarwar (1977) (Fig. 5m) should be attributed to *Stegolophodon*, because of the brachyodont molars, the enlargement of mesoconelets, the parallel placement of lophids, and the reduction of central conules. The symphysis of the Maluval specimen is considerably regressed with only two small sockets for mandibular tusks that should be very weak. Even in the most primitive form, such as in *Stegolophodon nasaiensis* (Tassy et al., 1992) and *Stegolophodon hueiheensis* (Chow, 1959), rostrum had been

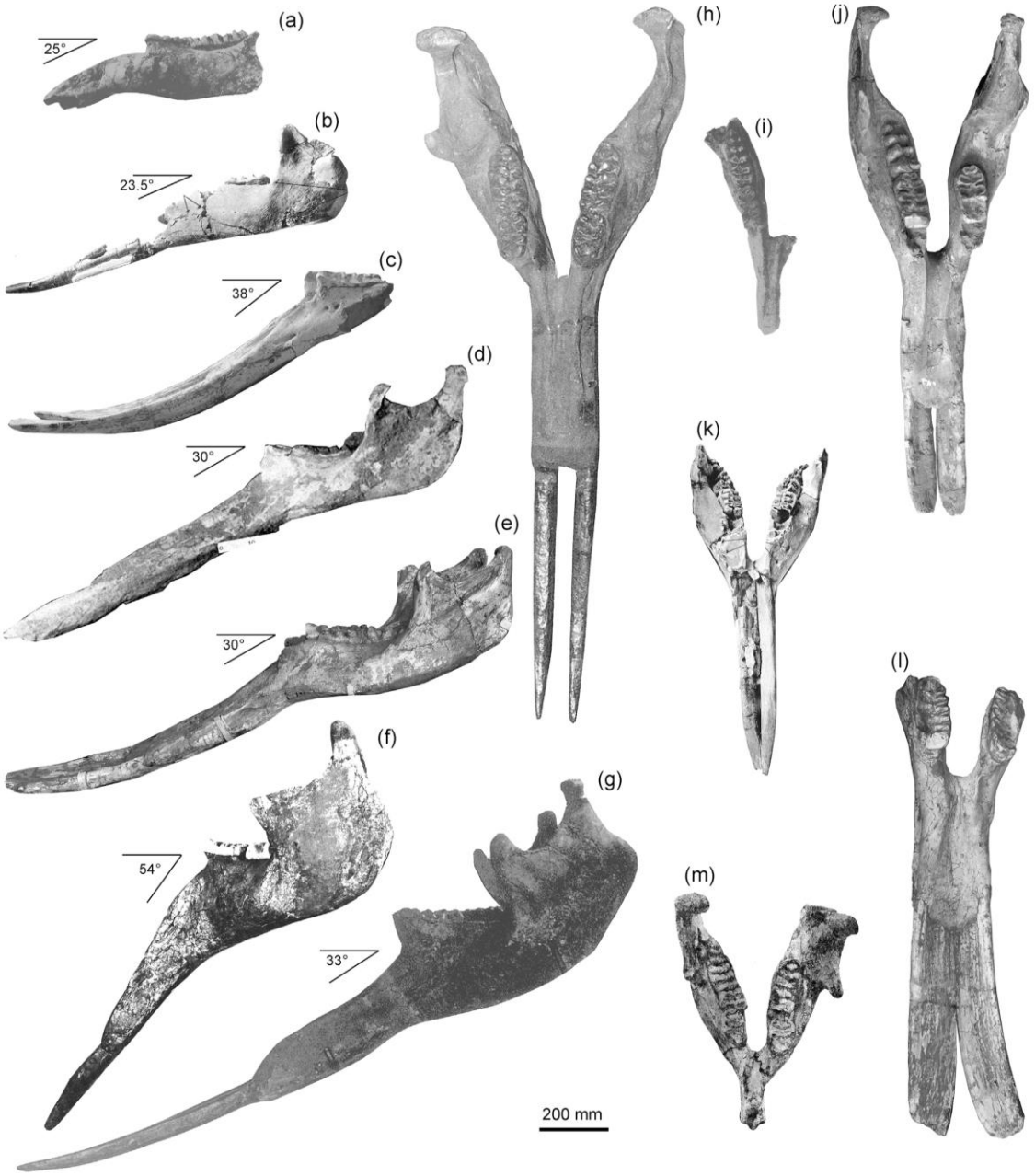

Fig. 5. Comparison of mandibles of various tetralophodont proboscideans; (a–g) in lateral view, the angle and the number near each mandible indicate the angle between the occlusal surface and the mid-symphyseal axis; (h–m) in dorsal view. (a and i) *Tetralophodon longirostris*, GPAHLD Din 111, the holotype, from Eppelsheim, Germany, reprinted from Tobien (1976, fig. 29); (b and k) *Tetralophodon longirostris*, in NMHW, from Laaerberg, Austria, reprinted from Schlesinger (1917, pl. 9, fig. 4 and pl. 10, fig. 3); (c and l) *Konobelodon robustus*, HMV 0004, the holotype, from Zhongmajia (Linxia Basin), China; (d) *Tetralophodon longirostris*, in MSB, from Polinyá, Spain, reprinted from Alberdi (1971, pl. 1, fig. 2); (e and j) *Tetralophodon euryrostris* n. sp., HMV 1427, the holotype; (f) *Tetralophodon curvirostris*, GPAHLD Din 1087, from Esselborn, Germany, reprinted from Tobien (1980, fig. 8); (g and h) *Tetralophodon gigantorostris*, MNM 1945/235, from Bermersheim, Germany, reprinted from Tobien (1980, fig. 9); (m) *Stegolophodon maluvalensis*, UZ 70/22, from Maluval (Dhok Pathan), Pakistan, reprinted from Sarwar (1977, fig. 54).

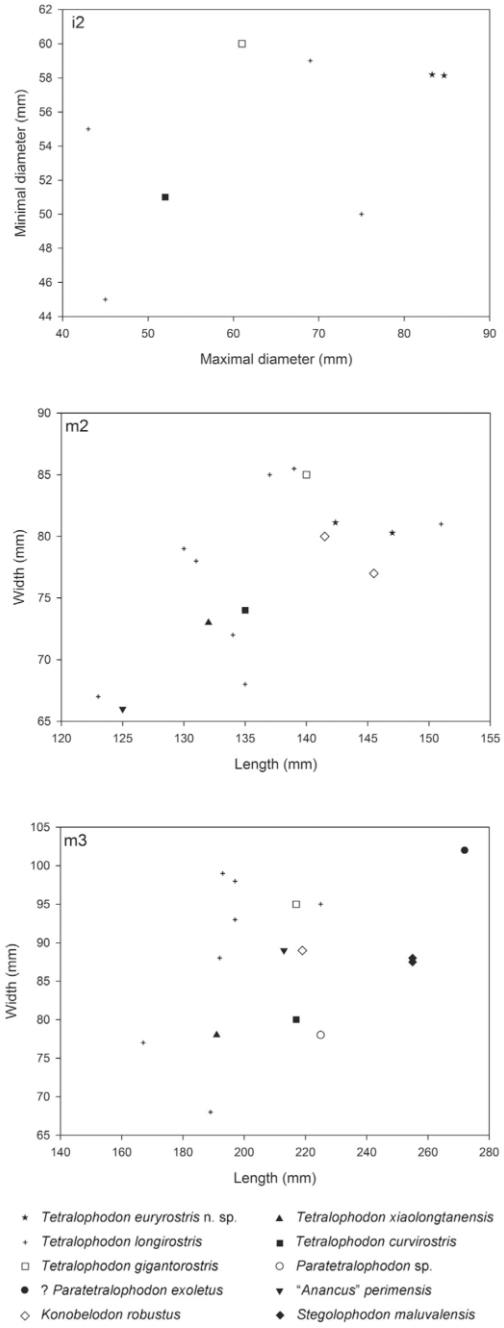

Fig. 6. Bivariate plots of tooth measurements from tetralophodont proboscideans.
Data source: *Tetralophodon xiaolongtanensis*, after Dong (1987); *Tetralophodon longirostris*, partially after Tobien (1978), the other taxa measured from the collection of NHMW; *Tetralophodon longirostris* and *Tetralophodon gigantorostris*, after Klähn (1931); ?*Paratetralophodon exoletus*, after Hopwood (1935); "*Anancus*" *perimensis*, after Osborn (1936); *Konobelodon robustus*, after Wang et al. (2016a); *Stegolophodon maluvalensis*, after Sarwar (1977); the other taxa measured by our own.

significantly reduced and is acutely ventrally deflected (the mandibular symphysis of *S. hueiheensis* is damaged, but the remaining basal part is rather small; and the mandible of *S. nasaiensis* was destroyed, but it is really rather reduced and acutely ventrally deflected). Although the morphology of the molars of the Linxia specimen is somewhat convergent with *Stegolophodon* (see below, Section 4.2.), this specimen cannot be grouped with *Stegolophodon* because of the strong mandibular symphysis and lower tusks.

Tetralophodon is the primary genus of tetralophodont gomphotheres in the Late Miocene of Eurasia (Göhlich, 1999). Firstly, "*Mastodon*" *grandincisivus* and *Tetralophodon atticus* have been synonymized by Konidaris et al. (2014) as the amebelodontid *Konobelodon atticus*. Like the Asian *K. robustus*, *K. atticus* also has flattened lower tusks, which differs from the Linxia specimen. Based on Konidaris et al. (2014), all of the tetralophodont specimens from Turolian of Eastern Europe and western Asia should be attributed to *K. atticus*. Excluding "*Mastodon*" *grandincisivus* and *T. atticus*, the remaining taxa are species of *Tetralophodon* that were widely distributed from MN8–MN11 in Europe (Göhlich, 1999). It has been noticed that *Tetralophodon* consists of polymorphic types observed in mandibles (and in teeth) (Tobien, 1976, 1978, 1980; Tassy, 1985; Ferretti et al., 2003).

The type specimen of *T. longirostris* is a right hemimandible with the m2–m3 tooth row and the symphysis, lacking lower tusks. It was discovered from Eppelsheim of the "*Deinotherium*" sand, Germany, and was first described by Kaup (1832) as "*Mastodon*" *longirostris*. The symphyseal ventral deflection is similar to that of the Linxia specimen, but the symphysis is shorter and narrower with a very deep symphyseal trough. The mandibular tusks are rather thin, with a diameter ~45 mm estimated from the alveoli (Tobien, 1978) (Fig. 6). The corpus is also lower than that of the Linxia specimen.

Schlesinger (1917) described a mandible of "*Mastodon* (*Bunolophodon*)" *longirostris* from Laaerberg, Austria (Fig. 5b and k). The mandibular symphysis is considerably destroyed. However, the right mandibular tusk is almost complete. The remaining symphysis is less downwardly deflected than that of the new specimen and the symphysis is likewise narrow. The mandibular tusk is likewise thin (with the diameters 43 × 55 mm, Fig. 6) as that of the type specimen of *T. longirostris*. These features are different from those of the Linxia specimen.

Alberdi (1971) reported a partial skeleton of *T. longirostris* from Polinyá, Spain (Fig. 5d). The symphysis shows the similar ventral deflection to that of the Linxia specimen, and the symphyseal length index (ratio of symphyseal length to total length of mandible, excluding the length of tusks) of the two specimens is very close (0.433 of the Polinyá specimen and 0.424 of the Linxia specimen). However, the symphysis of the Polinyá specimen is narrow with a V-shaped symphyseal groove (Alberdi, 1971). The tusks are relatively straight, and the exposed length is short in the Polinyá specimen, in contrast with the dorsal

curvature and the long exposed part of the tusk in the Linxia specimen.

Klähn (1931) reported "*Mastodon*" *longirostris* forma *grandis* from Esselborn of the "*Deinotherium*" sand, Germany, and this specimen has been referred to as *T. curvirostris* by Bergounioux and Crouzel (1960) and as *T. longirostris* by Tobien (1978, 1980), Tassy (1985), and Ferretti et al. (2003) (Fig. 5f). The Esselborn specimen possesses a thin and strongly deflected mandibular symphysis and thin, strongly divergent mandibular tusks (the right tusk is damaged) (Fig. 6) of which the exposed length is much shorter than the symphysis. These features are distinct from those of the Linxia specimen. Possibly, the species name "*curvirostris*" can be revived because the ventral deflection of the mandibular symphysis is marked relative to the other specimens of *T. longirostris*.

Another mandible reported by Klähn (1931), "*Mastodon*" *longirostris* forma *gigantoristris* from Bermersheim of the "*Deinotherium*" sand, Germany (Fig. 5g and h), is also an extreme case. The symphysis is moderately deflected as that of the Linxia specimen, and the symphyseal length index is 0.444, close to the Linxia specimen. However, the mandibular tusk is very thin with a diameter of 61 mm (Fig. 6), and the exposed length of the tusk is even longer than the symphyseal length. The two tusks seem to run parallel with a retentive distance (the right tusk is reconstructed). These features are distinct from the Linxia specimen. Furthermore, the symphysis of the Bermersheim specimen is somewhat narrower than that of the Linxia specimen. Tobien (1978, 1980) attributed this specimen to *Stegotetrabelodon*, a primitive elephantids. However, as Göhlich (1999) and Ferretti et al. (2003) proposed, this specimen should be referred as *Tetralophodon gigantoristris*. A similar specimen is "*Mastodon* (*Bunolophodon*)" *longirostris* from Kornberg, Austria that was described by Mottl (1969, figs. 24–26). This specimen likewise has a moderately downwardly deflected mandibular symphysis and has a symphyseal length index of 0.440. However, the mandibular tusks are broken and we do not know the exposed length of this specimen. The estimated diameter of the mandibular tusks is ~50 × 75 mm (Fig. 6). Like *T. gigantorostris* from Bermersheim, the Kornberg specimen possesses a narrower symphysis than the Linxia specimen. Considering all of the above specimens, these species of *Tetralophodon* from western and central Europe (*T. longirostris*, *T. curvirostris*, and *T. gigantorostris*) possess relatively narrower symphysis and thinner mandibular tusks, which differs from the Linxia specimen, *T. euryrostris*.

4.2. Comparison of cheek teeth

Firstly, the subject that should be compared is the only known but debated *Tetralophodon* species from northern China, "*Tetralophodon exoletus*" Hopwood, 1935. This species has been reported from three regions of the northern China, Baode, Lantian, and Linxia (Hopwood, 1935; Liu et al., 1978; Deng et al., 2004, 2013). Since *Tetralophodon exoletus* from the Linxia Basin has been identified as *K. robustus* (Wang et al., 2016a), here we will further discuss "*Tetralophodon exoletus*" only from the other two regions.

The material of "*Tetralophodon exoletus*" from two horizons of the Shuijiazui locality, Lantian region (Fig. 7) comprises "the most complete set of a tetralophodont mastodont in the Palaearctis" (Tobien et al., 1988, p. 114). Tobien et al. (1988) attributed these specimens to "*Tetralophodon* (*Paratetralophodon*) cf. *hasnotensis*" because of the ventral convexity of the upper cheek tooth rows (Fig. 7b), the relatively high crowns (Fig. 7e), the weak posttrite central conules, and the strong cementodonty, which is similar to that of *Paratetralophodon hasnotensis* from the Dhok Pathan Formation of Siwalik. It is interesting that there are two fragments of upper tusks, a right and a left one, and both possess a lateral enamel band (Fig. 7f). The enamel is very thin in cross-section view and relatively broad in lateral view. At least, enamel band is found in the tusk of *P. hasnotensis* from Dhok Pathan (Osborn, 1936, p. 364, fig. 324). We also attributed the Lantian specimens to the genus *Paratetralophodon* here. However, the Lantian specimens are distinguished from *P. hasnotensis* in lacking posterior pretrite central conule of the third loph of the intermediate cheek teeth. Therefore, the Lantian specimens might represent a separated species. The Lantian specimens also differ from the type material of "*Tetralophodon exoletus*" from Baode (Tobien et al., 1988). Here, we refer to it as *Paratetralophodon* sp. Formal naming of the Lantian specimens awaits more complete material, especially adult cranium and mandible. *T. euryrostris* differs from *Paratetralophodon* sp. in linear arrangement of conelets in lophids (no cheveron) and in the reduction of prettrite central conules. The age of the two horizons of the Shuijiazui is 8.21 and 8.07 Ma (Zhang et al., 2013), respectively, younger than the type locality of "*Tetralophodon exoletus*" (see below, Section 4.3.).

It is from Baode that yielded the type material of "*Tetralophodon exoletus*" (Hopwood, 1935) (Fig. 8). The holotype (Fig. 8a) is a right m3 with 7 lophids, and the hypodigm includes a juvenile hemimandible with p3, dp4, and m1 (Fig. 8b–d), the paratype, and some other isolated premolars and deciduous teeth. Attribution of this taxon is really a problem. On one hand, Hopwood (1935) stated that the m3 of *T. exoletus* shows similarity to "*Mastodon perimensis*" from South Asia, which was attributed to *Anancus* by Osborn (1936). However, compared with the primitive *Anancus*, *Anancus kenyensis* from Africa (Tassy, 1986; Saegusa and Hlusko, 2007), "*Tetralophodon exoletus*" has more lophids and the anancoidy of the tooth is less developed (less developed in "*Mastodon perimensis*", too). In this respect, "*Mastodon perimensis*" also differs from the African "true *Anancus*" and whether "*Mastodon perimensis*" can be really allocated to *Anancus* should be further studied. Considering the paratype, the juvenile hemimandible (Fig. 8b–d), although the symphysis is broken, there is a considerable length anterior to the tooth row. There is also an alveolar socket situated at the anterior end of the hemimandible (Fig. 8b); thus, lower tusks are present at least in this ontogenetic age. The m1 shows no tendency of anancoidy but shows a strong tendency of subdivision of conelets. Therefore, attributing this taxon to *Anancus* is difficult. On the other hand, the teeth of the paratype are similar to those of *Paratetralophodon* sp. from the Shuijiazui locality, Lantian Region (see above, the last paragraph). However, no material of mandible and lower dentition

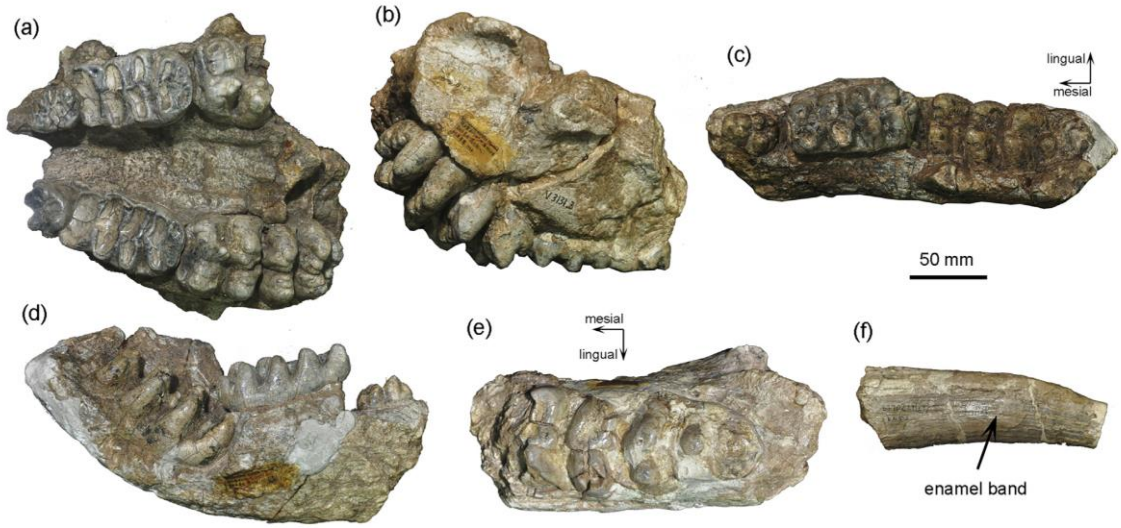

Fig. 7. Teeth and jaw fragments of *Paratetralophodon* sp., from the Shuijiazui locality, Lantian region. (a) Palate, IVPP V3131.3, in ventral view; (b) the same specimen as (a), in lateral view; (c) left hemimandible, IVPP V3130.4, in dorsal view; (d) the same specimen as (c), in medial view; (e) right m3, IVPP V3130.1, in occlusal view; (f) fragment of a right upper tusk, IVPP V3130.6, in lateral view.

of *P. hasnotensis* from Siwalik (the only known species) have been reported, and we cannot directly compare the hypodigm of "*Tetralophodon exoletus*" with *P. hasnotensis*. The age of the type locality, Sangjialianggou of Jijiagou (=Chi Chia Kou, Sang Chia Liang Kai, see Hopwood, 1935, loc. 43) is about 7.2 Ma (estimated based on Kaakinen et al., 2013, and Yue et al., 2004), which is later than *Paratetralophodon* sp. from the Shuijiazui Locality. Supposing that *Tetralophodon* might have been replaced with more derived *Paratetralophodon* in this age, here we temporarily refer to the hipodigm of "*Tetralophodon exoletus*" as ?*Paratetralophodon exoletus*, and further precise identification requires more discoveries of complete material from the type locality. Nevertheless, the attribution to *Stegotetrabelodon* by Tobien et al. (1988) is rejected here because no true-elephantid like features are displayed on the m3. *T. euryrostris* differs from ?*Paratetralophodon exoletus* in the relatively wide molar contour (Fig. 6), in the reduction of pretrite trefoils, and in the straight arrangement of conelets in lophids.

Secondly, the comparison of teeth morphology of *T. euryrostris* with *T. longirostris* and *Stegolophodon* is extremely important to this discussion. Saegusa et al. (2005) summarized morphotypes of the last two taxa and emphasized the differences between the two groups (Saegusa et al., 2005, fig. 2). Generally, the loph(id)s in *Stegolophodon* are straighter (absence of anancoidy and obliquity) than those in *T. longirostris*, especially for the lower molars; the pretrite conelets of *T. longirostris* are significantly oblique to the mid-axis. The mesoconelets of *Stegolophodon* are larger than those of *T. longirostris*, especially for the upper molars. The anterior pretrite central conules are greatly reduced as to nearly or entirely absent and the posterior pretrite central conules are also small (also see Tassy et al., 1992). From this view, *T. euryrostris* shows tooth morphology closer to *Stegolophodon* than to *T. longirostris*, especially on the slightly worn m3. Although the pretrite trefoil is well developed on the first lophid (the morphology of the first loph is conservative and often shows plesiomorphies only, see Saegusa et al. (2005)), the second and third lophids are rightly straight, and the posterior pretrite central conules of the second lophid are small and low. The mesoconelets are also relatively large, being subdivided. There are also some distinguishable features of the two. The crown height of *T. euryrostris* is larger than that of *Stegolophodon*; in *Stegolophodon*, the mesoconelet is as tall as or taller than the main conelet, whereas in *T. euryrostris*, the mesoconelet is lower than the main conelet; and rudimentary anterior pretrite central conules are present in *T. euryrostris*, but they are absent in *Stegolophodon*.

Thirdly, we will compare the new material with *T. xiaolongtanensis* from Kaiyuan, southern China, which is represented only by isolated teeth (Chow et al., 1978; Dong, 1987; Tobien et al., 1988). Relative to *T. euryrostris*, teeth of *T. xiaolongtanensis* are considerably small in size and low in crow height. The pretrite central conules are well developed, and mesoconelets are small. The loph(id)s show cheveroned structure and small conules are sparsely developed on the interloph(id)s. Cingula or cingulids are relatively marked. However, no mandibles and lower tusks are known. As Tobien et al. (1988) stated, *T. xiaolongtanensis* is possibly close to the early European *T. longirostris*, although a large geographic gap exists between Eastern Europe and southern China. It should be mentioned that Bohlin (1937) reported *Tetralophodon* sp. from Tossun Nor of the Qaidam Basin. The only complete tooth is actually an M3 rather than an m3, in contrast to Bohlin (1937), because the first and second pretrite half-lophs are slightly more mesial than the corresponding posttrite half-lophs. The crown is likewise low and the ante-

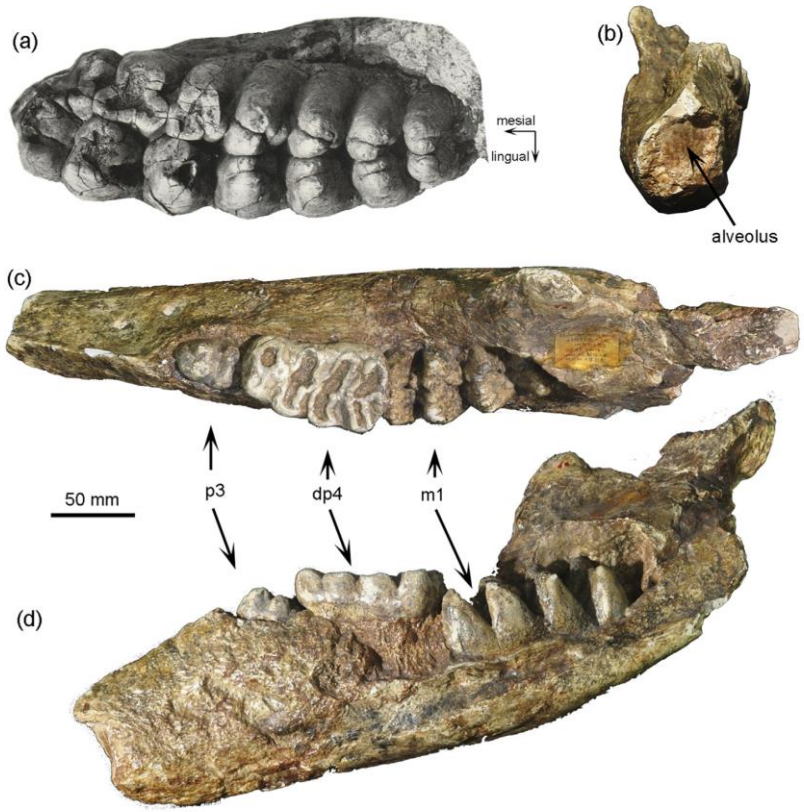

Fig. 8. Cheek teeth and jaw fragment of ?*Paratetralophodon exoletus* from Baode region. (a) Right m3, PMU M3661, the holotype, in occlusal view, from Sangjialianggou of Jijiagou (loc. 43), reprinted from Hopwood (1935, pl. 6, fig. 3); (b) right hemimandible, IVPP RV 35021, the cast of the paratype PUM M3660 of "*Tetralophodon exoletus*", in anterior view, indicating the presence of the mandibular tusks; (c) the same specimen as (b), in dorsal view; (d) the same specimen as (b), in medial view.

rior and posterior central conules are not reduced. Therefore, *Tetralophodon* sp. from the Qaidam Basin shows more similarity with *T. xiaolongtanensis* from Kaiyuan. The fossiliferous horizon of *T. xiaolongtanensis* in the Xiaolongtan Basin has been recently dated to ~12 Ma, correlated to MN8 (Li et al., 2015). The age is slightly earlier than that of the Tossun Nor of the Qaidam Basin (Wang, X.M. et al., 2011). As *T. xiaolongtanensis* is the first and the only East Asian tetralophodont gomphothere that occurred in the Middle Miocene, *Tetralophodon* sp. from the Qaidam Basin might migrate from southern China at the boundary of the Middle and Late Miocene. Here we attribute the Qaidam *Tetralophodon* as *Tetralophodon* aff. *xiaolongtanensis*. Nevertheless, *T. xiaolongtanensis* shows morphological divergence from *T. euryrostris*.

Finally, we will briefly discuss "*Tetralophodon* cf. *exoletus*" from Wuzhong (Qiu et al., 1987). It is a deeply worn M1. The lophs are straight and the crown is low. The width index is considerably wider than ?*Paratetralophodon exoletus* and *Paratetralophodon* sp. (Qiu et al., 1987). Like *T. euryrostris* from the Linxia Basin, this specimen shows a morphological convergence with *Stegolophodon*. Therefore, here we provisionally attributed this specimen to *Tetralophodon* cf. *euryrostris*. It occurs from the lower part of the Ganhegou Formation, which begins at ~10 Ma (Shen et al., 2001; Wang, W.T. et al., 2011).

4.3. Biostratigraphy of the Upper Miocene tetralophodont proboscideans in Northern China

Up to today, we recognized six species of tetralophodont proboscideans in the Upper Miocene of northern China, i.e., *K. robustus*, *Tetralophodon* aff. *xiaolongtanensis*, *T. euryrostris*, *Paratetralophodon* sp., ?*Paratetralophodon exoletus*, and *Stegolophodon licenti*. Unlike in the Middle Miocene, fossil records of proboscideans in the Upper Miocene of northern China are relatively sparse and dominated by tetralophodont rather than trilophodont proboscideans. Besides tetralophodont proboscideans, only *Predeinotherium sinese* (MN9, Linxia Basin; see Qiu et al. (2007)), *Mammut* sp. (MN11–MN12, Linxia Basin and Baode; see Hopwood (1935) and Wang et al. (2017)), and *Sinomastodon praeintermedius* (MN13, Yushe Basin; see Wang et al. (2016b)) have been discovered from the Upper Miocene of northern China. Here we will briefly summarize the occurrence

and living range of tetralophodont proboscideans in northern China and a complete biostratigraphic column of proboscideans in the Late Miocene of northern China requires more material.

In northern China, there is no remain of tetralophodont proboscideans from the strata lower than the Upper Miocene, except *S. hueiheensis* from the Lower Miocene (~MN4) of Sihong, which is just located at the boundary between northern and southern China (Fig. 1). In the Upper Miocene, the lowest tetralophodont taxon is *K. robustus* from the Linxia Basin, occurring with *Hipparion dongxiangensis*, one of the earliest hipparionine taxa in China, and ranging across MN9 and MN10 (corresponding to 11.6–8.7 Ma, see Deng et al. (2015)). It has been noticed that *K. robustus* from MN9 (Guonigou Fauna of the Linxia Basin) possesses an oval p3, and that from MN10 (Dashenggou Fauna of the Linxia Basin) possesses a sub-triangular p3. Although the difference is minor, it divides *K. robustus* into distinct morphological groups, maybe at subspecies level, which shows biostratigraphical significance (Wang et al., 2016a).

Tetralophodon aff. *xiaolongtanensis* occurs in the Tossun Nor fauna of the Qaidam Basin. This fauna has been dated to ~11–10 Ma (Wang, X.M. et al., 2011), correlated to MN9, with another one of the earliest occurrences of *Hipparion* in China. Therefore, *Tetralophodon* aff. *xiaolongtanensis* is the earliest tetralophodont gomphothere occurred in northern China.

The precise horizon of *T. euryrostris* cannot be traced. We postulated that this specimen is probably from the early Late Miocene, because the attached sediments from the specimen are kinds of fine, brownish silt stones that resemble the red *Hipparion* clay from the lower horizons of the Upper Miocene Liushu Formation in the Linxia Basin. In addition, *Tetralophodon* cf. *euryrostris* from Wuzhong occurs in the lower part of the Ganhegou Formation, which begins at ~10 Ma (Shen et al., 2001; Wang, W.T. et al., 2011), correlated to MN10. Therefore, if our taxonomical assessment is right, *T. euryrostris* from the Linxia Basin possibly has similar stratigraphyical range, that is, MN10.

Paratetralophodon sp. is from two horizons (S5 and S6) of the Shuijiazui locality, Lantian region. The two horizons have been dated to 8.21 and 8.07 Ma, respectively (Zhang et al., 2013), correlated to MN11.

The type locality of ?*Paratetralophodon exoletus* is Sangjialianggou of Jijiagou (loc. 43) of the Baode region, near the Jijiagou drainage. Based on Kaakinen et al. (2013), the fossiliferous horizon of Sangjialianggou is almost the same as Yangmugou of Jijiagou (loc. 49), which has been dated to C3Bn (Yue et al., 2004; Kaakinen et al., 2013), about 7.2 Ma, correlated to MN12.

S. licenti (the generic attribution after Saegusa et al. (2005); some researchers referred it to *Stegodon licenti*, e.g., Chen (2011)) occurs from the Hahui Formation of the Yushe Basin, which ranges from 6.5–5.9 Ma (Opdyke et al., 2013), correlated to MN13.

5. Conclusions

In this article we reported a new species of *T. euryrostris* from the Upper Miocene of the Linxia Basin. This is the only unequivocal record of *Tetralophodon* in northern China. The new species is characterized by an elongated and wide mandibular symphysis within *Tetralophodon* and by its convergence with *Stegolophodon* in tooth morphology. The age of *T. euryrostris* is postulated to be the early Late Miocene (MN10); however, the precise locality cannot be traced. Besides *T. euryrostris*, there are relatively sparse records of tetralophodont proboscideans from the Upper Miocene of the northern China, including *K. robustus* (Amebelodontidae, MN9–MN10), *Tetralophodon* aff. *xiaolongtanensis* (tetralophodont gomphothere, MN9) *Paratetralophodon* sp. (tetralophodont gomphothere, MN11), ?*Paratetralophodon exoletus* (tetralophodont gomphothere, MN12), and *S. licenti* (Stegodontidae, MN13). These taxa distinguish from each other in their mandibular and tooth morphology, and bear important biostratigraphic significance for the Upper Miocene of northern China.

Acknowledgements

We thank Tao Deng, Zhan-Xiang Qiu, Bo-Yang Sun, Su-Kuan Hou, Qin-Qin Shi, IVPP, China; U. Göhlich, Naturhistorisches Museum Wien, Austria for discussions and advice on this work. We thank Prof. Xue-Ping Ji, and an anonymous reviewer for their great suggestions in their review of this paper. This work was supported by the National Basic Research Program of China (Grant No. 2012CB821900), the Chinese Academy of Sciences (Grant No. XDB03020104), the National Natural Science Foundation of China (Grant Nos. 41372001, 41430102), and the Special Research Program of Basic Science and Technology of the Ministry of Science and Technology (Grant No. 2015FY310100-14).

References

Alberdi, M.T., 1971. Primer ejemplar complete de un *Tetralophodon longirostris* (Kaup) encontrado en España. Estudios Geológicos 27, 181–196.

Asevedo, L., Winck, G.R., Mothé, D., Avilla, L.S., 2012. Ancient diet of the Pleistocene gomphothere *Notiomastodon platensis* (Mammalia, Proboscidea, Gomphotheriidae) from lowland mid-latitudes of South America: stereomicrowear and tooth calculus analyses combined. Quaternary International 255, 42–52.

Bergounioux, F.M., Crouzel, F., 1960. *Tetralophodon curvirostris* n. sp. (Mammalia, Proboscidea) aus dem Unterpliozän (Pontien) von Esselborn (Rheinhessen). Jahresberichte und Mitteilungen Oberrheinischer Geologischer Verein 42, 109–121.

Bohlin, B., 1937. Eine tertiäre Saugetier-Fauna aus Tsaidam. Palaeontologia Sinica Series C 14, 1–111.

Chen, G.F., 2011. Remarks on the *Stegodon* Falconer, 1857 (Stegodontidae, Proboscidea) from the Late Cenozoic of China. Vertebrata PalAsiatica 49, 377–392 (in Chinese, with English summary).

Chow, M.C., 1959. New species of fossil proboscidea from South China. Acta Palaeontologica Sinica 7, 251–258 (in Chinese, with English summary).

Chow, M.C., Chang, Y.P., 1961. New mastodonts from North China. Vertebrata PalAsiatica, 245–255 (in Chinese, with English summary).

Chow, M.C., Chang, Y.P., 1974. Chinese Fossil Elephantoids. Science Press, Beijing, 74 pp. (in Chinese).

Chow, M.C., Chang, Y.P., You, Y.Z., 1978. Notes on some mastodons from Yunnan. Professional Papers of Stratigraphy and Palaeontology 7, 68–74 (in Chinese, with English summary).

Deng, T., Wang, X.M., Ni, X.J., Liu, L.P., 2004. Sequence of the Cenozoic mammalian faunas of the Linxia Basin in Gansu, China. Acta Geologica Sinica 78, 8–14.

Deng, T., Qiu, Z.X., Wang, B.Y., Wang, X.M., Hou, S.K., 2013. Late Cenozoic biostratigraphy of the Linxia Basin, northwestern China. In: Wang, X.M., Flynn, L.J., Fortelius, M. (Eds.), Fossil Mammals of Asia: Neogene Biostratigraphy and Chronology of Asia. Columbia University Press, New York, pp. 243–273.

Deng, T., Hou, S.K., Shi, Q.Q., 2015. Selection of the lower boundary stratotype of the terrestrial Upper Miocene Bahean Stage in China. Acta Geoscientica Sinica 36, 523–532 (in Chinese, with English abstract).

Dong, W., 1987. Miocene mammalian fauna of Xiaolongtan, Kaiyuan, Yunnan Province. Vertebrata PalAsiatica 25, 116–123 (in Chinese, with English summary).

Falconer, H., 1857. On the species of mastodon and elephant occurring in the fossil state in Great Britain. Part I. Mastodon. Quarterly Journal of the Geological Society of London 13, 307–360.

Ferretti, M.P., Rook, L., Torre, D., 2003. *Stegotetrabelodon* (Proboscidea, Elephantidae) from the Late Miocene of southern Italy. Journal of Vertebrate Paleontology 23, 659–666.

Gheerbrant, E., Tassy, P., 2009. L'origine et l'évolution des éléphants. Comptes Rendus Palevol 8, 281–294.

Göhlich, U.B., 1999. Order Proboscidae. In: Rössner, G.E., Heissig, K. (Eds.), The Miocene Land Mammals of Europe. Verlag Dr. Friedrich Pfeil, München, pp. 157–168.

Hay, O.P., 1922. Further observations on some extinct elephants. Proceedings of the Biological Society of Washington 35, 97–101.

Hopwood, A.T., 1935. Fossil Proboscidea from China. Palaeontologia Sinica Series C 9, 1–108.

Hu, C.K., 1962. Pliocene and Pleistocene mammalian fossils from Kansu. Vertebrata PalAsiatica 6, 88–97 (in Chinese, with English summary).

Illiger, C.D., 1811. Prodromus Systematis Mammalium et Avium Additis Terminis Zoographicis Utriusque Classis. Salfeld, Berlin, 301 pp.

Kaup, J.J., 1832. Description d'Ossements Fossiles de Mammifères Inconnus jusqu'a Présent, qui se Trouvent au Musée grand-ducal de Darmstadt. J.G. Heyer, Darmstad, 34 pp.

Kaakinen, A., Passey, B.H., Zhang, Z.Q., Liu, L.P., Pesonen, L.J., Fortelius, M., 2013. Straitigraphy and paleoecology of the classical dragon bone localities of Baode County, Shanxi Province. In: Wang, X.M., Flynn, L.J., Fortelius, M. (Eds.), Fossil Mammals of Asia: Neogene Biostratigraphy and Chronology of Asia. Columbia University Press, New York, pp. 203–217.

Klähn, H., 1931. Rheinhessisches Pliozän, besonders Unterpliozän, im Rahmen des Mitteleuropäischen Pliozäns. Geologische und Palaeontologische 18, 279–339.

Konidaris, G.E., Roussiakis, S.J., Theodorou, G.E., Koufos, G.D., 2014. The Eurasian occurrence of the shovel-tusker *Konobelodon* (Mammalia, Proboscidea) as illuminated by its presence in the late Miocene of Pikermi (Greece). Journal of Vertebrate Paleontology 34, 1437–1453.

Li, S.H., Deng, C.L., Dong, W., Sun, L., Liu, S.Z., Qin, H.F., Yin, J.Y., Ji, X.P., Zhu, R.X., 2015. Magnetostratigraphy of the Xiaolongtan Formation bearing *Lufengpithecus keiyuanensis* in Yunnan, southwestern China: constraint on the initiation time of the southern segment of the Xianshuihe–Xiaojiang fault. Tectonophysics 655, 213–226.

Liu, D.S., Li, C.K., Zhai, R.J., 1978. Pliocene vertebrate of Lantian, Shensi: Tertiary mammalian fauna of the Lantian District, Shensi. Professional Papers of Stratigraphy and Palaeontology 7, 149–200 (in Chinese, with English summary).

Mottl, M., 1969. Bedeutende Proboscidier-Neufunde aus dem Altpliozän (Pannonien) Südost-Österreichs. Österreichische Akademie der Wissenschaften, Mathemeatisch-naturwissenschaffliche Klasse, Denschriften 115, 1–50.

Opdyke, N.D., Huang, K., Tedford, R.H., 2013. The paleomagnetism and magnetic stratigraphy of the Late Cenozoic sediments of the Yushe Basin, Shanxi Province, China. In: Tedford, R.H., Qiu, Z.X., Flynn, L.J. (Eds.), Late Cenozoic Yushe Basin, Shanxi Province, China: Geology and Fossil Mammals, Volume I: History, Geology, and Magnetostratigraphy. Springer Dorsrecht Heidelberg, New York, pp. 69–78.

Osborn, H.F., 1936. Proboscidea: A Monograph of the Discovery, Evolution, Migration and Extinction of the Mastodonts and Elephants of the World. Volume I. The American Museum Press, New York, 802 pp.

Qiu, Z.X., Ye, J., Jiang, Y.J., 1987. Some mammalian fossils of Bahe Stage from Wuzhong, Ningxia. Vertebrata PalAsiatica 25, 46–56 (in Chinese, with English summary).

Qiu, Z.X., Wang, B.Y., Deng, T., Li, H., Sun, Y., 2007. First discovery of deinothere in China. Vertebrata PalAsiatica 45, 261–277 (in Chinese, with English summary).

Qiu, Z.X., Qiu, Z.D., Deng, T., Li, C.K., Zhang, Z.Q., Wang, B.Y., Wang, X.M., 2013. Neogene land mammal stages/ages of China: toward the goal to establish an Asian Land Mammal Stage/Age Scheme. In: Wang, X.M., Flynn, L.J., Fortelius, M. (Eds.), Fossil Mammals of Asia: Neogene Biostratigraphy and Chronology of Asia. Columbia University Press, New York, pp. 29–90.

Sarwar, M., 1977. Taxonomy and Distribution of the Siwalik Proboscidea. Bulletin of the Department of Zoology University of the Punjab (New Series), Article 10, 1–172.

Saegusa, H., Hlusko, L.J., 2007. New Late Miocene elephantoid (Mammalia: Proboscidea) fossils from Lemudong'O, Kenya. Kirtlandia 56, 1–8.

Saegusa, H., Thasod, Y., Ratanasthien, B., 2005. Notes on Asian stegodontids. Quaternary International 126–128, 31–48.

Schlesinger, G., 1917. Die Mastodonten des K. K. Naturhistorischen Hofmuseums Denkschriften des K. K. Naturhistorischen Hofmuseums 1, Geologisch-paläontologische Reihe 1, 1–231.

Shen, X.H., Tian, Q.J., Ding, G.Y., Wei, K.B., Chen, Z.W., Zhai, Z.Z., 2001. The late Cenozoic stratigraphic sequence and its implication to tectonic evolution, Hejiakouzi area, Ningxia Hui Autonomous Region. Earthquake Research in China 17, 156–166 (in Chinese, with English abstract).

Shoshani, J., 1996. Para- or monophyly of the gomphotheres and their position within Proboscidea. In: Shoshani, J., Tassy, P. (Eds.), The Proboscidea: Evolution and Palaeoecology of Elephants and Their Relatives. Oxford University Press, Oxford, pp. 149–177.

Shoshani, J., Tassy, P., 2005. Advances in proboscidean taxonomy & classification, anatomy & physiology, and ecology & behavior. Quaternary International 126–128, 5–20.

Tassy, P., 1985. La Place des Mastodontes Miocènes de l'Ancien Monde dans la Phylogénie des Proboscidea (Mammalia): Hypothèses et Conjectures. Dissertation for Doctoral Degree, Doctorat ès Sciences, Université Pierre et Marie Curie, Paris, 861 pp.

Tassy, P., 1986. Nouveaux Elephantoidea (Proboscidea, Mammalia) dans le Miocène du Kenya: essai de réévaluation systématique. Cahiers de Paléontologie, E'ditions du Centre National de la Recherche Scientifique, Paris, 135 pp.

Tassy, P., 1988. The classification of Proboscidea: how many cladistic classifications? Cladistics 4, 43–57.

Tassy, P., 1996. Who is who among the Proboscidea. In: Shoshani, J., Tassy, P. (Eds.), The Proboscidea: Evolution and Palaeoecology of Elephants and Their Relatives. Oxford University Press, Oxford, pp. 39–48.

Tassy, P., 1999. Miocene elephantids (Mammalia) from the Emirate of Abu Dhabi, United Arab Emirates: palaeobiogeographic implications. In: Whybrow, P.J., Hill, A. (Eds.), Fossil Vertebrates of Arabia. Yale University Press, New Haven, pp. 209–233.

Tassy, P., 2013. L'anatomie cranio-mandibulaire de *Gomphotherium angustidens* (Cuvier, 1817) (Proboscidea, Mammalia): données issues du gisement d'En Péjouan (Miocène moyen du Gers, France). Geodiversitas 35, 377–445.

Tassy, P., 2014. L'odontologie de *Gomphotherium angustidens* (Cuvier, 1817) (Proboscidea, Mammalia): données issues du gisement d'En Péjouan (Miocène moyen du Gers, France). Geodiversitas 36, 35–115.

Tassy, P., Anupandhanant, P., Ginsburg, L., Mein, P., Ratanasthien, B., Sutteethorn, V., 1992. A new *Stegolophodon* (Proboscidea, Mammalia) from the Early Miocene of northern Thailand. Géobios 25, 511–523.

Tobien, H., 1976. Zur Paläontologischen Geschichte der Mastodonten (Proboscidea, Mammalia). Mainzer Geowissenschaftliche Mitteilungen 5, 143–225.

Tobien, H., 1978. On the evolution of mastodonts (Proboscidea, Mammalia). Part 2: the bunodont tetralophodont groups. Geologisches Jahrbuch Hessen 106, 159–208.

Tobien, H., 1980. A note on the mastodont taxa (Proboscidea, mammalia) of the "Dinotheriensande" (Upper Miocene, Rheinhessen, Federal Republic of Germany). Mainzer Geowissenschaftliche Mitteilungen 9, 187–201.

Tobien, H., Chen, G.F., Li, Y.Q., 1988. Mastodonts (Proboscidea, Mammalia) from the Late Neogene and Early Pleistocene of the People's Republic of China. Part II: historical account: the genera *Tetralophodon*, *Anancus*, *Stegotetrabelodon*, *Zygolophodon*, *Mammut*, *Stegolophodon*. Mainzer Geowissenschaftliche Mitteilungen 17, 95–220.

Wang, S.Q., Shi, Q.Q., He, W., Chen, S.Q., 2016a. A new species of the tetralophodont amebelodontine *Konobelodon* Lambert, 1990 (Proboscidea, Mammalia) from the Late Miocene of China. Geodiversitas 38, 65–97.

Wang, S.Q., Ji, X.P., Jablonski, N.G., Su, D.F., Ge, J.Y., Ding, C.F., Yu, T.S., Li, W.Q., Duangkrayom, J., 2016b. The oldest cranium of *Sinomastodon* (Proboscidea, Gomphotheriidae), discovered in the uppermost Miocene of southwestern China: implications for the origin and migration of this taxon. Journal of Mammalian Evolution 23, 155–173.

Wang, S.Q., Li, Y., Duangkrayom, J., He, W., Chen, S.Q., 2017. The early Mammut from the Upper Miocene of northern China, and its implications for the evolution and differentiation of Mammutidae. Vertebrata PalAsiatica 55 (in press) http://www.ivpp.cas.cn/cbw/gjzdwxb/pressonline/201704/t20170410_4772851.html.

Wang, W.T., Zhang, P.Z., Kirby, E., Wang, L.H., Zhang, G.L., Zheng, D.W., Chai, C.Z., 2011. A revised chronology for Tertiary sedimentation in the Sikouzi Basin: implications for the tectonic evolution of the northeastern corner of the Tibetan Plateau. Tectonophysics 505, 100–114.

Wang, X.M., Xie, G.P., Li, Q., Qiu, Z.D., Tseng, Z.J., Takeuchi, G.T., Wang, B.Y., Fortelius, M., Rosenström-Fortelius, A., Wahlquist, H., Downs, W.R., Zhang, C.F., Wang, Y., 2011. Early explorations of Qaidam Basin (Tibetan Plateau) by Birger Bohlin — reconciling classic vertebrate fossil localities with modern biostratigraphy. Vertebrata PalAsiatica 49, 285–310.

Wang, X.M., Flynn, L.J., Fortelius, M., 2013. Toward a continental Asian biostratigraphic and geochronologic framework. In: Wang, X.M., Flynn, L.J., Fortelius, M. (Eds.), Fossil Mammals of Asia: Neogene Biostratigraphy and Chronology of Asia. Columbia University Press, New York, pp. 1–25.

Yue, L.P., Deng, T., Zhang, Y.X., Wang, J.Q., Zhang, R., Yang, L.R., Heller, F., 2004. Magnetostratigraphy of stratotype section of the Baode stage. Journal of Stratigraphy 28, 48–63 (in Chinese, with English abstract).

Zhang, Z.Q., Kaakinen, A., Liu, L.P., Lunkka, J.P., Sen, S., Gose, W.A., Qiu, Z.D., Zheng, S.H., Fortelius, M., 2013. Mammalian biochronology of the Late Miocene Bahe Formation. In: Wang, X.M., Flynn, L.J., Fortelius, M. (Eds.), Fossil Mammals of Asia: Neogene Biostratigraphy and Chronology of Asia. Columbia University Press, New York, pp. 187–202.

Journal of Systematic Palaeontology, 2017
Vol. 15, No. 8, 601–615, http://dx.doi.org/10.1080/14772019.2016.1208687

Taylor & Francis
Taylor & Francis Group

Morphological and ecological diversity of Amebelodontidae (Proboscidea, Mammalia) revealed by a Miocene fossil accumulation of an upper-tuskless proboscidean

Shi-Qi Wang[a,b]*, Tao Deng[a,b], Jie Ye[a], Wen He[c] and Shan-Qin Chen[c]

[a]*Key Laboratory of Vertebrate Evolution and Human Origins of the Chinese Academy of Sciences, Institute of Vertebrate Paleontology and Paleoanthropology, Chinese Academy of Sciences, Beijing 100044, China;* [b]*CAS Center for Excellence in Tibetan Plateau Earth Sciences, Beijing 100101, China;* [c]*Hezheng Paleozoological Museum, Hezheng 731200, China*

(Received 5 January 2016; accepted 22 June 2016; published online 10 August 2016)

Amebelodontidae is the most taxonomically and morphologically diverse group of proboscideans. However, relative to the morphological variation of the mandible and mandibular tusks, ecological and phylogenetic differentiations within Amebelodontidae have been largely debated. Here we evaluate a middle Miocene fossil accumulation of a new amebelodontid, *Aphanobelodon zhaoi* gen. et sp. nov. This species lacks upper tusks, which is unique in elephantiforms. The mandible and mandibular tusk morphologies of *A. zhaoi* are similar to those of the genus *Platybelodon*, which is the typical representative of one of the two main amebelodontid branches (the other branch is represented by *Amebelodon*). We suggest that *Amebelodon* potentially used its mandible and mandibular tusks to dig for food in relatively hard substrates; whereas *Platybelodon* is more specialized and possibly used its mandibular tusks for cutting soft vegetation. *Aphanobelodon zhaoi* morphology indicates that it is an offshoot of the platybelodont clade within Amebelodontidae, because it has primitive undifferentiated states of the mandible and mandibular tusks. Cladistic analysis indicates that *Aphanobelodon*, *Platybelodon* and *Torynobelodon* comprise a monophyletic group within Amebelodontidae. This study enhances our knowledge regarding proboscidean evolutionary history in terms of morphology, taxonomy and biology.

http://zoobank.org/urn:lsid:zoobank.org:pub:8F30BAC7-4245-4952-BFCF-884E3DB839F6

Keywords: Amebelodontidae; functional morphology; evolution; proboscidean

Introduction

The family Amebelodontidae is a group of peculiar proboscideans that possess an extremely elongated mandibular symphysis and flattened mandibular tusks (Barbour 1927; Borissiak 1929; Osborn 1936). It is also the most diverse proboscidean family, and nine genera have been established (Gheerbrant & Tassy 2009; Sanders *et al*. 2010). Amebelodontids vary in mandibular symphysis and mandibular tusk morphology, and also in the inner structure of the mandibular tusks (i.e. dentinal tubulars in *Platybelodon* and *Torynobelodon*, compared with concentric laminations in other genera) (S.-Q. Wang *et al.* 2015). It has been debated why amebelodontids developed various types of mandibular symphysis and mandibular tusks, how these extinct proboscideans used their shovel-like mandible and tusks, and whether they show distinct ecological positions (Barbour 1927; Borissiak 1929; Osborn 1936; Lambert 1992; Semprebon *et al.* 2011; S.-Q. Wang *et al.* 2015). Furthermore, amebelodontid phylogeny has also debated, because strong parallel evolution appears to be present (Shoshani 1996; Prado & Alberdi 2008; S.-Q. Wang *et al.* 2015).

Here, we report on a fossil accumulation of a new proboscidean taxon. This accumulation (Fig. 1, Supplemental Fig. S1), containing a single species, includes an adult male, two adult females, four subadults and three juveniles (Supplemental Table S1). Most of the individuals are completely preserved and all of the bones are articulated (Fig. 1, Supplemental Fig. S2). Thus, this material provides complete osteological and anatomical information for the new taxon, and also provides insights into various aspects of biology, such as sexual dimorphism, ontogeny and dietary preference. Although most of these skeletons have not been prepared except for a female skull (HMV1880), this material provides sufficient information for anatomical and taxonomic evaluation of the taxon. Here, our description and discussion are mainly based on the one prepared skull. Analysis of the entire skeleton will be performed in the future.

*Corresponding author. Email: wangshiqi@ivpp.ac.cn

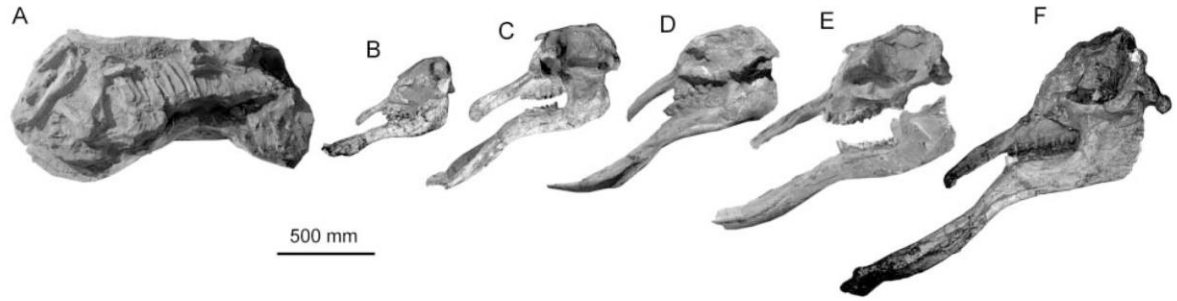

Figure 1. Selected individuals from the fossil accumulation of *Aphanobelodon zhaoi* gen. et sp. nov. showing the age-sex structure and burial state, all in lateral view. **A,** skeleton of HMV1916, baby; **B,** skull of HMV1912, juvenile; **C,** skull of HMV1918, subadult ?male; **D,** skull of HMV1920, subadult ?female; **E,** cranium and mandible of HMV1880, adult female, the holotype (horizontally reversed); **F,** skull of HMV1919, adult male.

Abbreviations

Institutional abbreviation: **HMV**, Hezheng Paleozoological Museum, Hezheng, China. Other abbreviations: **CI**, consistency index; **MN**, European Mammal Neogene-Zone; **MPT**, most parsimonious tree; **RI**, retention index.

Geological setting

The material of the new taxon was discovered in the Zhangenbao Formation exposed in Maerzuizigou quarry, northern China (Fig. 2A). Sediments of the Zhangenbao Formation are dominated by sandstones and siltstones

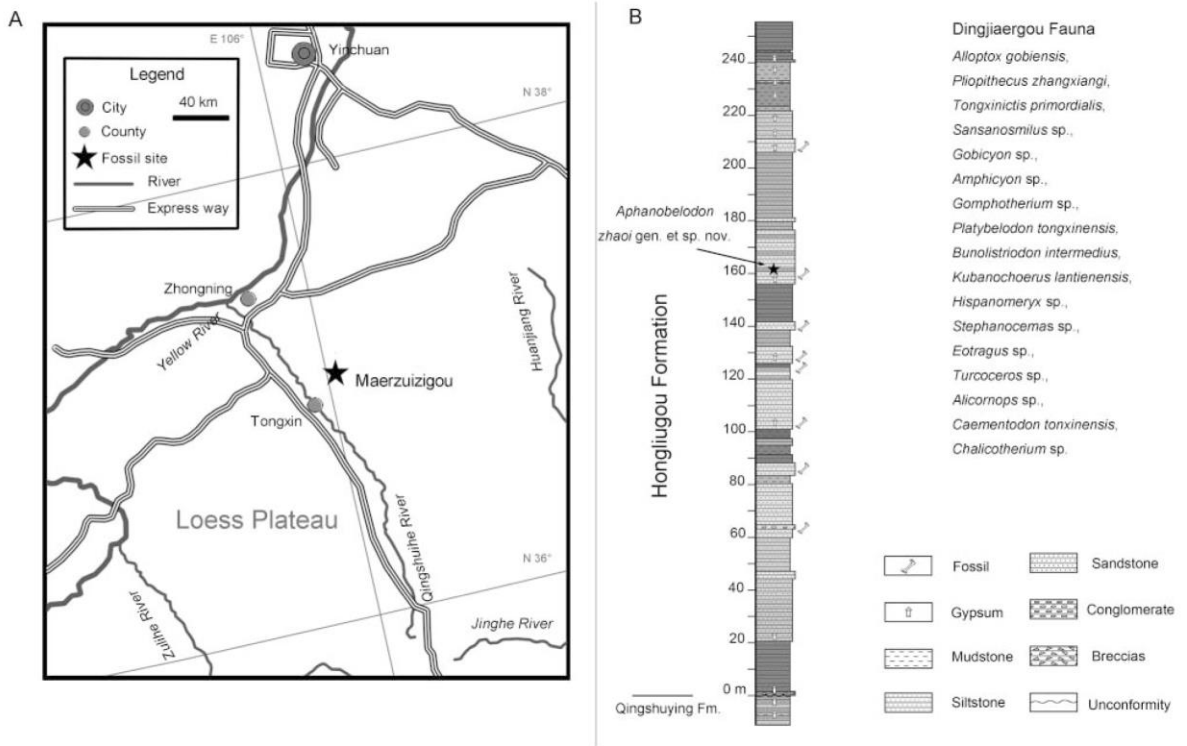

Figure 2. Geographical and geological information on the study material. **A,** location of the Maerzuizigou quarry **B,** the Jinggou section of the Miocene Zhangenbao Formation (for a detailed description, see Supplemental data). The star in panel **B** indicates the horizon (No. 19) of the Maerzuizigou quarry that yielded *Aphanobelodon zhaoi* gen. et sp. nov. The faunal list is revised from Guan (1988) and Qiu *et al.* (1999).

Figure 3. Habitat reconstruction of *Aphanobelodon zhaoi* gen. et sp. nov. of the Dingjiaergou Fauna during the early middle Miocene, by Yu Chen (the artist has granted permission to use the illustration).

punctuated by mudstones (Fig. 2B). The fossil accumulation was discovered in horizon 19 of the Zhangenbao Formation. Detailed description of the sedimentology is given in the Supplemental data (after S.-Q. Wang *et al.* 2016b). The lithofacies of the Zhangenbao Formation comprise blocky or tabular organic-rich sandstones and siltstones, which potentially indicates marshy floodplain or lake-margin wetland deposits (Allen & Collinson 1986). Only one species, *Aphanobelodon zhaoi* gen. et sp. nov., has been identified from this fossil accumulation. In the adjacent area (Tongxin), more than 10 quarries yielding 27 mammalian taxa have been reported (Guan 1988; Qiu *et al.* 1999; S.-Q. Wang & Ye 2015; S.-Q. Wang *et al.* 2015) (Fig. 3). These taxa constitute the Dingjiaergou fauna that is correlated with MN6 (Qiu *et al.* 1999). Three proboscidean taxa have been discovered previously in this fauna: *Platybelodon tongxinensis*, *Protanancus tobieni* and *Gomphotherium* sp. (Ye & Jia 1986; Guan 1988; S.-Q. Wang *et al.* 2015).

Material and methods

Material

All of the material of *Aphanobelodon zhaoi* gen. et sp. nov. is housed in the HMV (Supplemental Table S1). The comparative taxa included *Phiomia serridens*, *Serbelodon barbourensis*, *Archaeobelodon filholi*, *Protanancus tobieni*, *Pr. chinjiensis*, *Amebelodon fricki*, *Platybelodon danovi*, *Pl. tongxinensis*, *Pl. grangeri*, *Torynobelodon dangheensis* and *Torynobelodon barnumbrowni*; these species cover all shovel-tusker morphotypes (Matsumoto 1922, 1924; Barbour 1927, 1932; Borissiak 1929; Osborn & Granger 1932; Frick 1933; Osborn 1936; Tobien 1973; Tassy 1983, 1984; Ye & Jia 1986; Guan 1988, 1991, 1996; Ye *et al.* 1989; S.-Q. Wang *et al.* 2013, 2015; S.-Q. Wang & Ye 2015). It should be noted that '*Pl. grangeri'* from the Moergen Fauna of Tunggur, China, shows a higher evolutionary grade than the *Pl. grangeri* type specimen from the Tairum Nor Fauna (S.-Q. Wang *et al.* 2013). The '*Pl. grangeri'* from the Moergen fauna possesses a complete fourth lophid in m2 and displays a stronger (and relatively shorter) mandibular symphysis; therefore, in the present paper, we refer to it as tetralophodont *Platybelodon* (a new species). Moreover, *Pl. tongxinensis* from the Tongxin area, China, has often been assigned as *Pl. danovi* in recent publications (Ye & Jia 1986; Guan 1988, 1991, 1996; Qiu *et al.* 1999; S.-Q. Wang *et al.* 2013), and *Torynobelodon dangheensis* was considered a *Platybelodon* species by B.-Y. Wang & Qiu (2002).

Measurements and terminology

Cranial and mandibular measurements follow Tassy (2013). All measurements were taken using calipers. The terminology of occlusal structures of gomphotheriid cheek teeth follows Tassy (2014), and the terminology of the cranium and mandible follows Tassy (2013) and Ferretti (2010). Rock colour description follows the Munsell colour chart (Landa & Fairchild 2005), and the grain size subdivision is based on the Wentworth grain size chart (Krumbein & Aberdeen 1937).

Microwear study

The feeding preference of the new taxon was determined by microwear analyses, with the main procedures based on those described in Calandra *et al.* (2010). Shearing facet casts of the second loph of the M3 in HMV1919, HMV1880 and HMV1921 were made, and digital microphotographs were taken. In each 0.4 mm × 0.4 mm digital microphotograph, the scratches and pits were quantified, and results were compared to extant proboscidean and ungulate microwear databases to determine the dietary categories of browser versus grazer (Solounias & Semprebon 2002). The cast-making protocol was based on that of Solounias & Moelleken (1992). The microwear data of *Platybelodon grangeri* and extant elephants is from Semprebon *et al.* (2016, fig. 3B).

Cladistic analysis

A cladistic analysis was performed to investigate the possible phylogenetic interrelationships of our new taxon and shovel-tusked elephantiforms. The data matrix contains 38 unordered characters and 18 taxa, in which *Deinotherium* was the outgroup (see Supplemental appendices S1 and S2). In particular, characters 0, 6−11, 14, 23, 29, 30, 31, 32, 35 and 37 were included, because they represent known morphological variations among gomphothere taxa. The remaining characters were chosen based on their previously suggested importance in gomphotheriid and elephantid phylogenetics (Shoshani 1996; Tassy 1996; Prado & Alberdi 2008). Cladograms were obtained from a parsimony analysis carried out using the TNT 1.1 program (Goloboff *et al.* 2003). The reported results were based on MPTs and a strict consensus rule tree. Node support was calculated by a bootstrap analysis (1000 replicates). Data for the examined taxa were obtained from previous publications (Andrews 1906; Matsumoto 1924; Barbour 1927, 1929; Borissiak 1929; Osborn & Granger 1932; Frick 1933; Mottl 1969; Tobien 1973; Tassy 1983, 1986; Lambert 1990; Guan 1991; B.-Y. Wang & Qiu 2002; S.-Q. Wang *et al.* 2013, 2015; Konidaris *et al.* 2014).

Body mass estimation

We estimated the body masses of individuals of *Aphanobelodon zhaoi* based on their humerus lengths (when the humeral length of the individual could be measured). The equation is a linear regression function with the formula $\log_{10}(\text{mass in kg}) = -4.145 + 2.635\ (\log_{10}X)$, where X (in mm) is the length of the humerus (Christiansen 2004). The body mass data of extant elephants were taken from Nowak (1999), and other estimates of body masses of fossil elephantiforms were from Christiansen (2004) using the same method.

Systematic palaeontology

Order **Proboscidea** Illiger, 1811
Family **Amebelodontidae** Barbour, 1927
Genus ***Aphanobelodon*** gen. nov.

Type species. *Aphanobelodon zhaoi* sp. nov.

Etymology. *Aphano-*, invisible, indicating lack of upper tusks; *belodon*, front tooth, a masculine root typical of longirostrine elephantiforms.

Diagnosis. Upper permanent tusks always absent in every ontogenetic age and both sexes. Rostrum slender, elongated. Mandible extremely elongated and expanded in the distal part; lower tusks flattened as in *Platybelodon*, however with internal concentric lamination; Dp4, M1, and M2 bunodont and trilophodont; molars with incipient secondary trefoils, incipient pseudo-anancoidy, strong choerodonty and heavy cementodonty.

Aphanobelodon zhaoi sp. nov.
(Figs 4, 5)

Etymology. Dedicated to Mr Rong Zhao who discovered and excavated the material.

Diagnosis. As for the genus.

Type locality and horizon. Maerzuizigou quarry (37°05′21.8″N′, 106°00′58.4″E, Fig. 2A), horizon 19 of the Zhangenbao Formation (previously named the Hongliugou Formation, but renamed because of synonymy) (Fig. 2B), middle Miocene, MN6 (Qiu *et al.* 1999; S.-Q. Wang & Ye 2015; S.-Q. Wang *et al.* 2015, 2016b).

Occurrence. Early middle Miocene, MN6, East Asia.

Holotype. HMV1880: a complete cranium with associated mandible and partial skeleton, adult female, dental age XX (Tassy 2013).

Paratypes. See Supplemental Table S1; all of the material is from the same locality and horizon as the holotype.

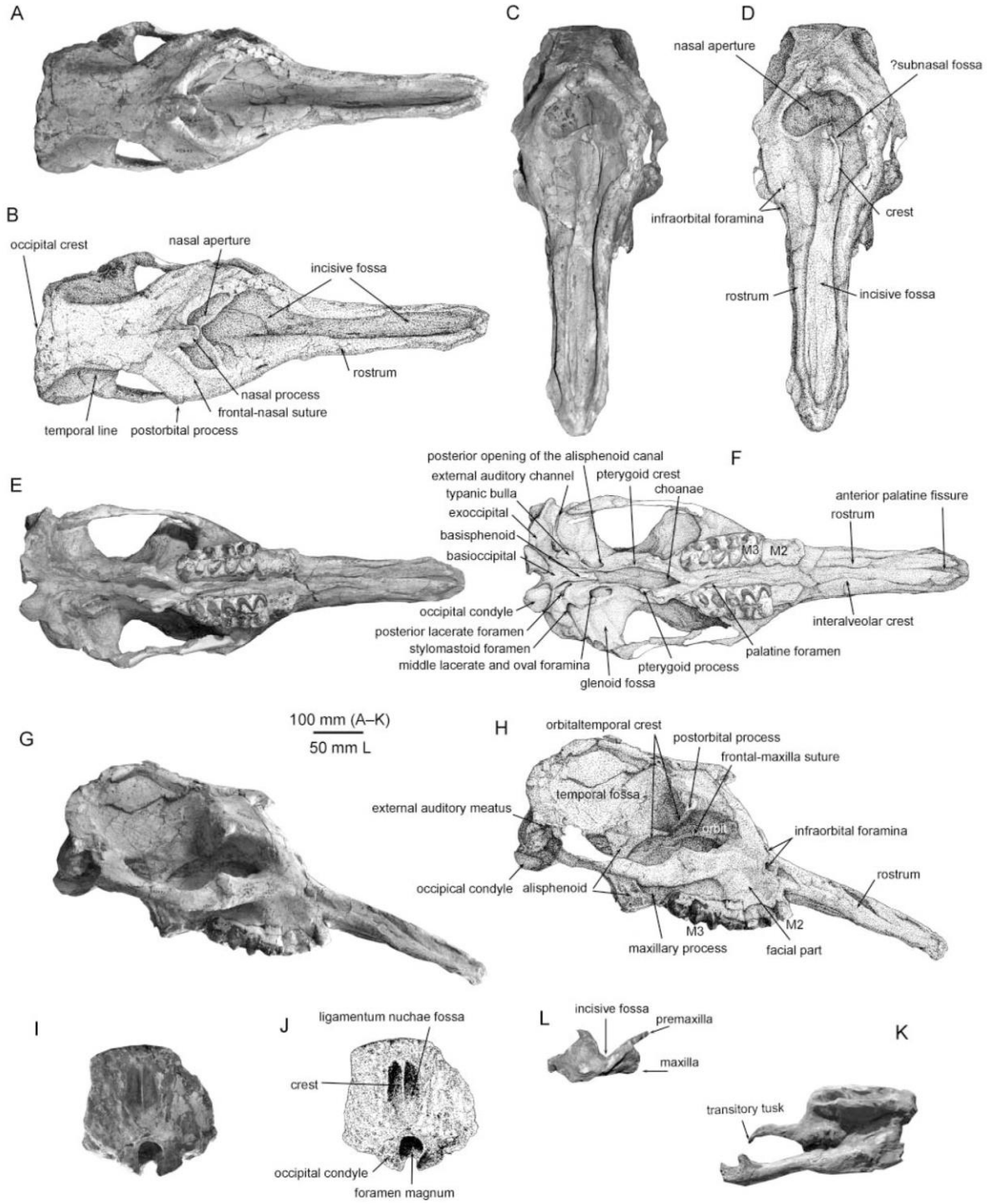

Figure 4. Crania of *Aphanobelodon zhaoi* gen. et sp. nov. (all parts show HMV1880, the type specimen, except K, which shows HMV1916, a juvenile). **A,** dorsal view; **B,** sketch and annotations of A; **C,** anterodorsal view; **D,** sketch and annotations of C; **E,** ventral view; **F,** sketch and annotations of E; **G,** lateral view; **H,** sketch and annotations of G; **I,** posterior view; **J,** sketch and annotations of I; **K,** skull of HMV1916, showing the small transitory upper tusk; **L,** apical view of the tip of the premaxillae showing the closed incisive alveolar sockets.

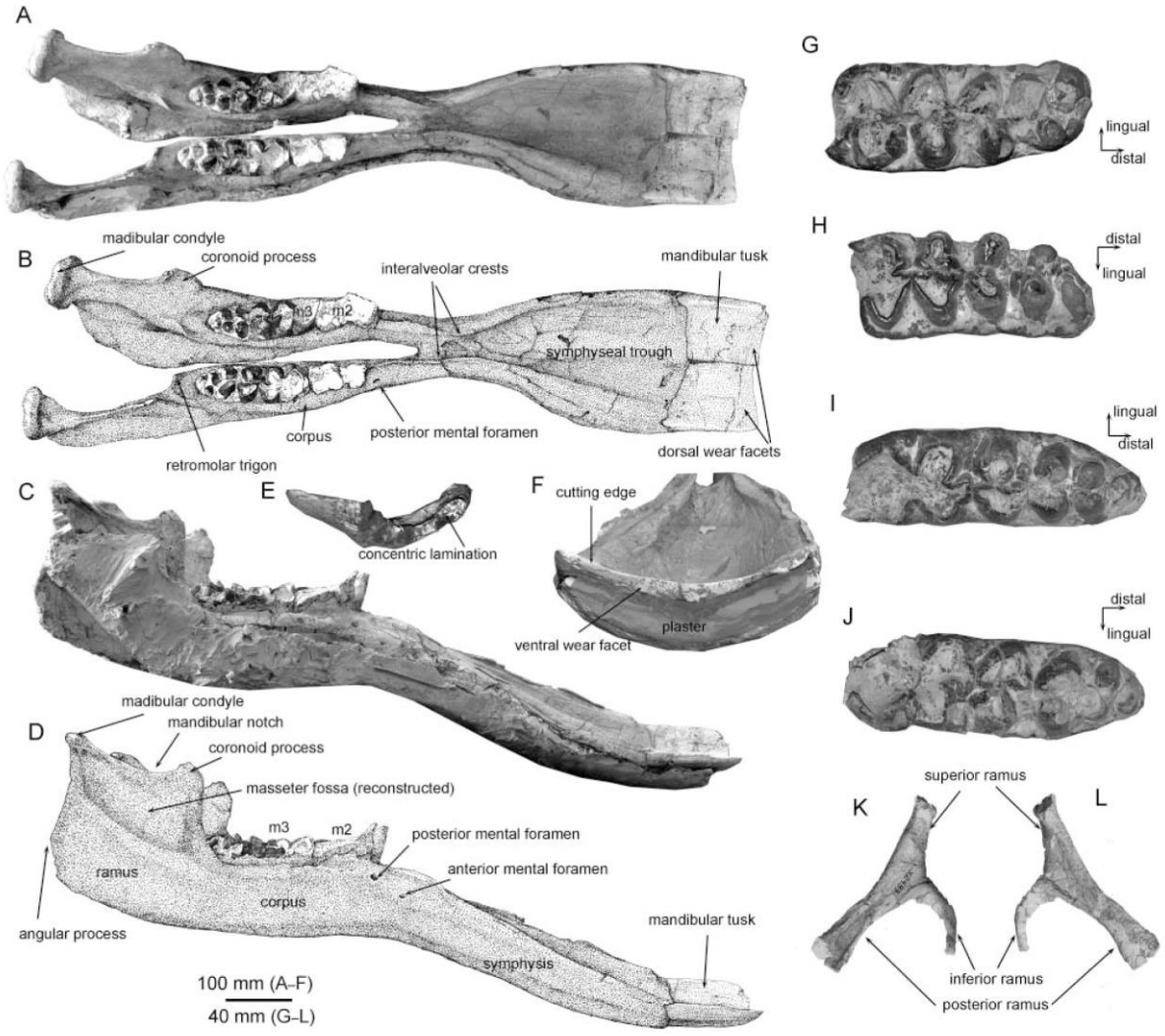

Figure 5. Mandibles, cheek teeth and stylohyoid of *Aphanobelodon zhaoi* gen. et sp. nov. (all parts show HMV1880, the type specimen, except E, which shows HMV1918, a subadult). **A,** mandible, in dorsal view; **B,** sketch and annotations of A; **C,** mandible, in lateral view (lateral side is covered by plaster); **D,** sketch and annotations of C (the masseter fossa is reconstructed); **E,** HMV1918, apical view of the lower tusks, showing the concentric lamination in the cross section of the left lower tusk; **F,** apical view of the lower tusks, showing the sharp cutting edge of the lower tusks; **G,** right M3, in occlusal view; **H,** left M3, in occlusal view; **I,** left m3, in occlusal view; **J,** right m3, in occlusal view; **K,** left stylohyoid, in lateral view; **L,** left stylohyoid, in medial view.

Description

Cranium. See Figure 4, Supplemental Table S2. In dorsal view (Fig. 4A, B), the cranium is anteroposteriorly elongated and laterally compressed with little lateral expansion of zygomatic arches. The occipital crest is almost straight, not anteriorly concave. The two temporal lines converge from the posterolateral flanges of the two temporal fossae, run parallel along the lateral edges of the nearly rectangular braincase, and diverge before they reach the postorbital processes. The sutures of the anterior edge of the frontal bones are visible, and the frontal is in contact with the nasal, premaxillary and maxilla bones from medial to lateral. The nasal bone extends laterally along the superior rim of the nasal aperture, and possesses a strongly protruded nasal process. The contour of the nasal aperture forms two anterolaterally expanded lateral wings, and the superior rim of the nasal aperture reaches the level of the two postorbital processes. The two premaxillae anterior to the nasal aperture are very broad at first, enclosing a large incisive fossa. Then, the two premaxillae steeply taper and prominently protrude, forming

a slender rostrum. The incisive fossa also tapers and runs through the entire length of the rostrum.

In anterodorsal view (Fig. 4C, D), the nasal aperture is fabaceous. Although the opening is broad, no clear step-like perinasal fossae (Tassy 1994, 2014) are visible. In the type specimen, although deformed by vertical pressure, there is a crest in the middle line of the base part of the incisive fossa (Ferretti 2010). This crest may be bifurcated at the ventral border of the nasal aperture, enclosing a small subnasal fossa. To our knowledge, this crest is not observed in other elephantiforms. The infraorbital foramina are duplicated – there is a large, subcircular ventral opening and a small, slit-like dorsal one. In the long and narrow rostrum, the distal part of the incisive fossa is relatively wide, and is bordered by two crest-like bony walls. These two walls are homologous to the incisive sockets of the other elephantiforms. From the apical view of the rostrum (Fig. 4L), the incisive fossa is deep and V-shaped, and the bones (premaxillae at dorsal part and maxillae at ventral part) are very thin. No openings for tusks are developed.

In ventral view (Fig. 4E, F), the occipital condyle is sub-triangular. The two condyles are divergent, forming a sharp intercondyloid notch. The basioccipital tapers anteriorly and is fused with the basisphenoid by a tough basal tuberosity. The tympanic bulla is not laterally expanded; is irregular shaped with a prominent anteromedial angle; and is surrounded by foramina: a posterior, triangular posterior lacerate foramen (*foramen metoticum*), and a lateral, large and rounded stylomastoid foramen. The middle lacerate foramen and oval foramen (*foramen ovale*) are confluent and located beneath the anterior margin of the bulla. A rounded posterior opening of the alisphenoid canal is anterior to the anterior edge of the bulla and links the confluent opening of the middle lacerate and oval foramina by a shallow groove. The glenoid fossa is large, with an anterior slop that is inclined dorsally. The exoccipital is strong, anterolaterally elongated. Between the glenoid fossa and the exoccipital, there is a broad and shallow groove for the external auditory channel. The choanae are narrow with a sharp apex on the anterior rim. Lateral to the choanae, a strong pterygoid process is laterally hooked, and the pterygoid crest extends posteriorly to the tympanic bulla. The palate is deformed by transverse pressure. The palatine foramen is slit-like. The zygomatic process of the maxilla is not strong. Two interalveolar crests extend anteriorly along the narrow rostrum, and slightly converge in the middle. The anterior palatine fissure is weak.

In lateral view (Fig. 4G, H), the braincase is low. However, in the presumed male specimen HMV1919, the braincase is relatively raised (Fig. 1F). The temporal fossa is anteroposteriorly expanded. The basicranium is almost not erected, the occipital condyle does not posteroventrally protrude, and a notch for the external auditory meatus is posterior to the zygomatic arch. The orbitotemporal crest extends posteroventrally to reach the anterior edge of the alisphenoid. A large fissure is located beneath the anterior margin of the alisphenoid, in which the optic foramen, the anterior lacerate foramen (*foramen orbitale*) and the round foramen (*foramen rotundum*) are present. The anterior edge of the alisphenoid turns anteroinferiorly to the pterygoid process and wraps up the posterior end of the maxillary process. The orbit is relatively small and the anterior rim is located at the level of the anterior part of the M3, and the postorbital process is just at the level of the posterior end of the tooth row. In the orbit, the transverse suture between the frontal and the maxilla clearly runs from the anterior rim to the anterior margin of the orbitotemporal crest. The facial part of the maxilla is anteriorly elongated, and that ventral to the zygomatic process is low. The infraorbital foramina are just anterior to the zygomatic process of the maxilla, and they are relatively distant from the anterior rim of the orbit. The rostrum is slim and slightly downwardly inclined.

In posterior view (Fig. 4I, J), the occipital surface is subcircular. The foramen magnum is also subcircular and surrounded by two fabaceous occipital condyles. The ligamentum nuchae fossa is dorsoventrally oval and divided into two parts by a thin crest in the middle.

Mandible. See Figure 5A–D, Supplemental Table S3. In dorsal view (Fig. 5A, B), the left hemimandible is slightly deformed by the transverse pressure, and the right one is not deformed. The madibular condyle forms a transversely cylindrical bar. The corpus is narrow and tapers anteriorly. The retromolar trigone is prominent. The posterior border of the symphysis is distant from the anterior end of the tooth row. The symphysis is elongated and trough-shaped. The basal part of the symphysis is narrow and steeply widens distally. No transverse ledge is present at the narrowest part of the symphysis. The two interalveolar crests run along the lateral margins of the deep symphyseal trough. The anterior edge of the symphysis is only slightly anteriorly convex. This is intermediate between *Platybelodon*, in which this edge is almost straight, and *Amebelodon*, in which this edge forms an anteriorly oriented apex.

In lateral view (Fig. 5C, D), in order to protect the specimen, plaster has not been removed; therefore, the masseter fossa in Figure 5D is reconstructed. The ramus of the mandible is long and low. The coronoid process is blunt, and the mandibular condyle is small. The mandibular notch is shallow. The angular process is slightly protruded, and is at the level of the occlusal surface. The anterior and posterior ramal borders are perpendicular to the occlusal surface and less posteriorly inclined. The corpus is relatively high. The posterior mental foramen is relatively big, and is positioned at the level of the anterior

end of the tooth row. The anterior mental foramen is small. The symphysis is moderately ventrally deflected.

Teeth. See Figures 1, 4 and 5. The upper tusks are absent in all specimens except the newborn HMV1917, in which the left tusk is tiny, ventrally bent and covered by enamel (Fig. 4K). It is identified as a transitory upper tusk. All the rostria of all crania are slender with a relatively wide incisive fossa that cannot support tusks (Figs 1, 3). The sockets for upper tusks are closed (Fig. 4L). Thus, upper tusks were evidently not developed in this taxon, rather than shed or not exposed to the alveoli. This feature is unique not only in Amebelodontidae but also in Elephantiformes (tuskless males have also been reported in some populations of *Elephas maximus*, but it is not a stable character in *Elephas maximus*; see Kurt *et al.* 1995).

The lower tusk (Fig. 5A−F) is broad and flattened, as in *Platybelodon*. No tubular structures but concentric lamination is present on the cross section, as observed from the anterior breakage of the lower tusk in HMV1918 (Fig. 5E). The exposed length is much smaller than the length of the symphysis. The lower tusk is slightly dorsally curved in lateral view. In basal view, the left tusk is slightly left-handedly twisted, and mirrors the right one. In dorsal view, the two tusks are slightly convergent with both nearly orthogonal anteromedial and anterolateral angles. The anterior edge of the tusk is slightly concave. In apical view, the tusk is very thin, forming a sharp cutting edge (Fig. 5F). The wear facet is present on both dorsal and ventral sides of the tusk. The dorsal facet is long, and the ventral one short (both in the distal-apical direction) (Fig. 5A−D, F). Measurements of HMV1880 (left/right, in mm): lateral exposed length, 146/150; medial exposed length, 111/100; maximal width (at alveolus), 114/111; height, 24/25; length of the wear facet on the dorsal surface, 65.5/64.5.

Both M2 and m2 are worn to the roots without any remains of enamel. Both are rectangular and presumably have three loph(id)s.

The M3 (Fig. 5G, H) is anteroposteriorly rectangular and composed of five lophs. Chevroning and pseudoanancoidy are present on the second to fourth lophs, and the last loph is much incipient. Pretrite trefoils are present on the first two lophs with symmetrical anterior and posterior central conules. The third and fouth pretrite half-lophs only have a mesoconelet and an anterior central conule. Posttrite half-lophs are relatively simple. The first three posttrite half-lophs have incipient posterior posttrite central conules, and the second loph also has a small anterior posttrite central conule. The third posttrite half-loph is subdivided into three main cusps. Cementum is very heavy, and small conules are developed in the interlophs, thus showing strong cementodonty and choerodonty. Cingula are present on the anterior, lingual and posterior margins of the tooth. Measurements (left/right, in mm): length, 155/163; width at loph 1, 67/71.5; loph 2, 65.5/66; loph 3, 61.5/63.5; loph 4, 59/57; height at the posttrite side of loph 3, 48/51.5.

The m3 (Fig. 5I, J) is anteroposteriorly oval and composed of five lophids plus a strong posterior cingulid. The first two lophids are deeply worn. The third pretrite half-lophid is trifoliate, and the posterior central conule is also present on the third posttrite half lophid. The fourth and fifth pretrite and posttrite half-lophids are rather simple, and only have a main cuspid with somewhat subdivision on its summit. Cementum is very heavy (cementodonty), and small conules are developed in the interlophids (choerodonty), similar to those in the M3. Cingulid is prominent on the posterior end, which is composed of a strong cuspid, and absent on the other margins of the tooth. Measurements (left/right, in mm): length, 185/184; width at lophid 1, 59/59; lophid 2, 61.5/58.5; lophid 3, 60/58.5; lophid 4, 57/58.5; height at the posttrite side of lophid 4, 47/50.

Stylohyoid. The left stylohyoid (Fig. 5K, L), the only remainder of the hyoid apparatus, looks like a bifurcated antler. The superior and the posterior rami are nearly arranged in line with one another. Both rami are strong and rod-like. The proximal end of the superior ramus is oval, and is connected to the tympanohyal cartilage. The posterior ramus is longer than the superior one, and has a groove on its lateral side. The distal end of the posterior ramus is flat, where the *m. digastricus posterior* is attached. The inferior ramus is hook-like with a tapering and slightly medially oblique tip. It is slender relative to the other two rami. The morphology of the stylohyoid is typical of gomphotheres (Shoshani & Tassy 2005).

Comparisons and discussion

Comparison of cranium

The cranium of *Aphanobelodon zhaoi* displays some plesiomorphies. The braincase is relatively low; the basicranium is not or only slightly erect. These features are common in trilophodont amebelodontids and trilophodont gomphotheres. In *Serbelodon barbourensis*, the basicranium is somewhat more erect, which is a slightly derived feature (Frick 1933). We do not know this feature in *Amebelodon*, in which a cranium has not been explicitly assigned. However, in *Konobelodon* from China (S.-Q. Wang *et al.* 2016a), the braincase is clearly moderately domed and the basicranium is clearly moderately erected. Therefore, these common elephantiform traits were also present in the lineage of Amebelodontidae (considered a monophyletic group).

The facial part of *Aphanobelodon zhaoi* is very developed, showing an anteriorly elongated face and a basally expanded incisive fossa. These features are also observed

in *Platybelodon grangeri* (S.-Q. Wang *et al.* 2013). In *Archaeobelodon* aff. *filholi*, the facial part is also anteriorly elongated, but the incisive fossa is not basally expanded. Sanders *et al.* (2010) considered an anteriorly elongated facial part to be a diagnostic character of Amebelodontidae. Based on this feature, they put *Progomphotherium* into Amebelodontidae. However, a relatively anteriorly elongated facial part is also observed in *Gomphotherium annectens*, a primitive species in Gomphotheriidae (Tassy 1994). In *Konobelodon* from China (S.-Q. Wang *et al.* 2016a), the facial part is substantially shortened, similar to that of *Tetralophodon longirostris*. Therefore, we consider the shortening of the facial part to be a common elephantiform trend that also occurred in Amebelodontidae.

A step-like perinasal fossa is described in *Gomphotherium angustidens* (Tassy 1994, 2013) and considered an important nasal modification in elephantiforms. This feature appears also to be present in some amebelodontids such as *Archaeobelodon* aff. *filholi* (Tassy 1986) and in *Konobelodon* from China (S.-Q. Wang *et al.* 2016a). In *Aphanobelodon zhaoi*, the nasal aperture is laterally enlarged, but no clear step-like perinasal fossa can be observed. A similar morphology is also seen in *Platybelodon grangeri* (S.-Q. Wang *et al.* 2013). The perinasal fossa may be secondarily lost with the development of the enlarged basal part of the incisive fossa.

The tympanic bulla of *Aphanobelodon zhaoi* is not laterally expanded, similar to that of *Phiomia* (Andrews 1906). This feature is also observed in *Platybelodon grangeri* (S.-Q. Wang *et al.* 2013). Except for the absence of upper tusks and the slenderness of the rostrum, the cranium of *Aphanobelodon zhaoi* resembles *Platybelodon* in all aspects.

Comparison of mandible

As a typical amebelodontid, the mandible of *Aphanobelodon zhaoi* resembles that of *Platybelodon* more than any other. In dorsal view, the mandibular symphysis of *Aphanobelodon zhaoi* strongly expands laterally in the distal part, which is similar to that of *Platybelodon* (Osborn & Granger 1932; S.-Q. Wang *et al.* 2013), in contrast to the not or slightly laterally expanded mandibular symphysis in *Archaeobelodon*, *Serbelodon*, *Protanancus*, *Amebelodon* and *Konobelodon* (Barbour 1927; Frick 1933; Tobien 1973; Tassy 1986; S.-Q. Wang *et al.* 2015, 2016a). Furthermore, in *Aphanobelodon zhaoi*, the anterior edge of the mandibular symphysis is slightly anteriorly convex. This feature is more similar to the straight anterior end of the mandibular symphysis in *Platybelodon* and *Torynobelodon* (Barbour 1932; Osborn & Granger 1932; S.-Q. Wang *et al.* 2013) than to that of the other amebelodontids displaying an anterior apex (Barbour 1927). In lateral view, the mandibular symphysis of *Aphanobelodon zhaoi* is deflected moderately downward, like that in *Platybelodon*; this shows a contrast to the strongly downward-deflected mandibular symphysis in *Amebelodon* and *Konobelodon* (Barbour 1927; Lambert 1990; S.-Q. Wang *et al.* 2016a). The mandibular resemblance between *Aphanobelodon* and *Platybelodon* reflects the close phylogenetic relationship of the two genera and will be further discussed below.

In *Aphanobelodon zhaoi*, there are also some mandibular features that are distinct from those of *Platybelodon*. For example, the ascending ramus of *Aphanobelodon zhaoi* is vertical to the occlusal plan, and this feature is shared widely among other amebelodontids. However, in *Platybelodon* (except *Platybelodon danovi* from the Caucasus), the ramus is strongly posteriorly inclined (Borrissiak 1929; S.-Q. Wang *et al.* 2013). Furthermore, in *Platybelodon grangeri* and the tetralophodont *Platybelodon*, there is a strong transverse ledge at the base of the mandibular symphysis (S.-Q. Wang *et al.* 2013). However, this ledge is likewise missing in *Aphanobelodon zhaoi* and the other amebelodontids.

Comparison of lower tusks

In *Aphanobelodon zhaoi*, the lower tusks are extremely wide and thin. Wear facets are distributed on both dorsal and ventral sides of the tusks. The dorsal facet is long, and the ventral one short. The anterior edge of the lower tusks is sharp, forming a cutting edge, and the anteromedial and anterolateral angles are sharp, forming two nearly right angles (Fig. 5A−F). These morphologies are similar to those of *Platybeldon* and *Torynobelodon barnumbrowni*. The dimensions of the lower tusk of *Ap. zhaoi* are smaller than those of *Platybelodon tongxinensis* and *Pl. grangeri*, and similar to those of *Pl. danovi* (Fig. 6A). However, the internal structure of *Aphanobelodon zhaoi* displays concentric lamination, which is also observed in *Archaeobelodon*, *Serbelodon*, *Protanancus* and *Amebelodon*, and distinct from the tubular structure in *Platybeldon* and *Torynobelodon* (Osborn & Granger 1932; Tassy 1986; Ye & Jia 1986; Lambert 1990; S.-Q. Wang *et al.* 2013, 2015; Konidaris *et al.* 2014).

Comparison of cheek teeth

The cheek tooth morphology of *Aphanobelodon zhaoi* is typical amebelodontid. The contours of M3 and m3 are narrow and long. Posttrite central conules and pseudoanancoidy are developed. The cheek teeth of *Ap. zhaoi* resemble those of *Platybeldon* more than those of the other amebelodontids, because of the strong cementodonty and choerodonty. The dimensions of M3 and m3 are also in the ranges of *Pl. tongxinensis* and *Pl. grangeri* (Fig. 6B, C). In the teeth sample of *Platybeldon* we obtained, the anterior posttrite central conule is always

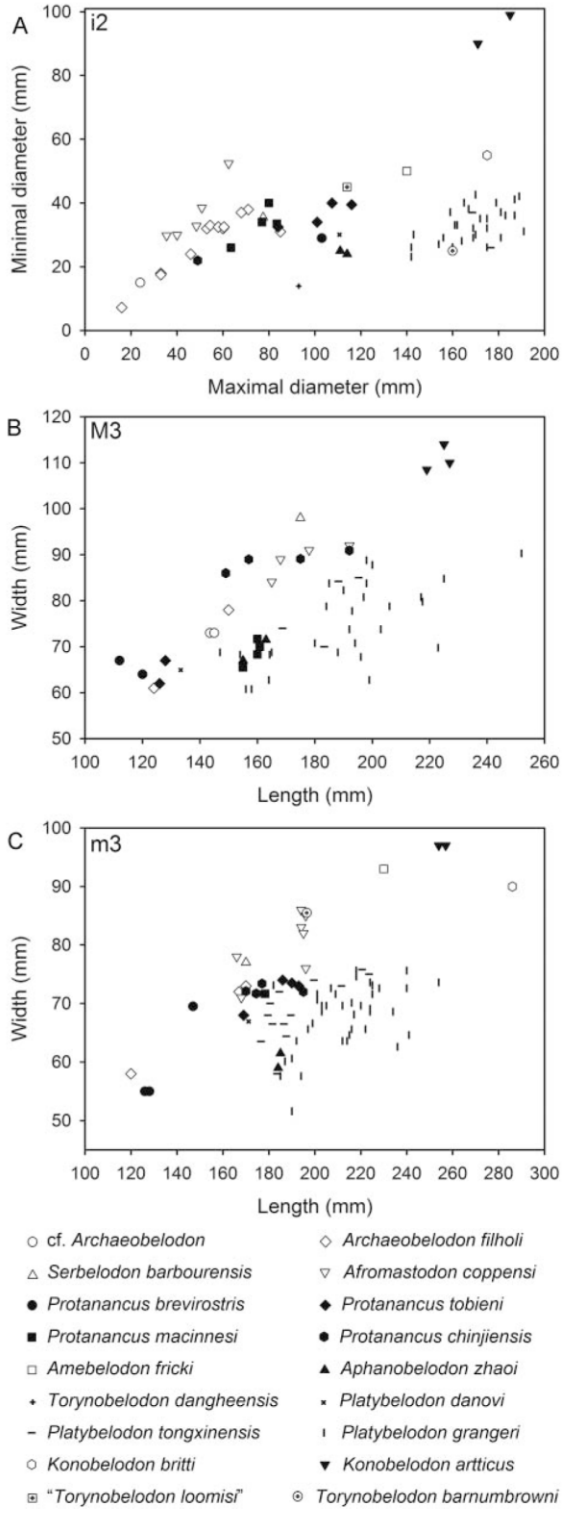

Figure 6. Bivariate plots for various amebelodontid teeth measurements. **A,** cross-section measurements of lower tusks; **B,** occlusal measurements of M3; **C,** occlusal measurements of m3.

absent in the second loph of upper molars (S.-Q. Wang *et al.* 2013). However, it is present in M3 of *Ap. zhaoi*. This element is also often present in *Protanancus* and *Amebelodon* (Barbour 1927; Lambert 1990; S.-Q. Wang *et al.* 2015). This was the only difference that we could find between the cheek teeth of *Platybeldon* and *Ap. zhaoi*; however, this difference seems not to be an important feature.

Feeding behaviour and ecological differentiation of Amebelodontidae

Research using various approaches has been carried out to infer the feeding behaviour of shovel-tuskers. Barbour (1927), Borissiak (1929) and Osborn (1936) hypothesized that shovel-tuskers (i.e. *Amebelodon*, *Platybelodon* and *Torynobelodon*) were marsh dwellers that scooped up aquatic plants using their shovel-like tusks. Lambert (1992) opposed this hypothesis based on morphology and microwear studies of upper and lower tusks of shovel-tuskers; he considered that *Amebelodon* used its upper and lower tusks in various ways, whereas *Platybelodon* and *Torynobelodon barnumbrowni* had lower tusks that were specialized for cutting vegetation. Semprebon *et al.* (2016) reconstructed the dietary habit of *Pl. grangeri* from the Linxia Basin, China based on microwear analysis and confirmed that *Platybelodon* was generally a browser. S.-Q. Wang *et al.* (2015) discussed the competition and replacement between *Protanancus* and *Platybelodon* in East Asia, from which evidence was partly based on microwear study.

Although the sample size is limited (most specimens are not prepared), we studied the microwear of shearing surfaces of the M3 of the three adult *Aphanobelodon zhaoi*. The result showed that the diet of *Ap. zhaoi* is in the range of browsers and close to mix-feeders. However, *Platybelodon grangeri* appears to be slightly more specialized as a browser than *Ap. zhaoi* (Fig. 7).

This result can be further confirmed from the analyses of morphology of lower tusks and mandible. In *Aphanobelodon zhaoi*, the lower tusks are extremely wide and thin. The anterior edge of the lower tusks is sharp, forming

Data sources: *Aphanobelodon zhaoi* gen. et sp. nov., present paper; cf. *Archaeobelodon*, from Tassy (1986); *Ar. filholi*, from Tobien (1973); *Serbelodon barbourensis*, from Frick (1933); *Afromastodon coppensi*, from Pickford (2003); *Protanancus brevirostris* and *Pr. tobieni*, from S.-Q. Wang *et al.* (2015); *Pr. macinnesi*, from Tassy (1986); *Pr. chinjiensis*, from Tassy (1983); *Amebelodon fricki*, from Barbour (1927); *Torynobelodon dangheensis*, from B.-Y. Wang & Qiu (2002); *Pl. danovi*, from Borissiak 1929; *Pl. tonxingensis* and *Pl. grangeri* (including the tetralophodon *Platybelodon*) from S.-Q. Wang *et al.* (2013); *Konobelodon britti*, from Lambert (1990); *K. atticus*, from Schlesinger (1917, 1922) and Konidaris *et al.* (2014); *Torynobelodon barnumbrowni*, from Barbour (1932); '*T. loomisi*', from Barbour (1929).

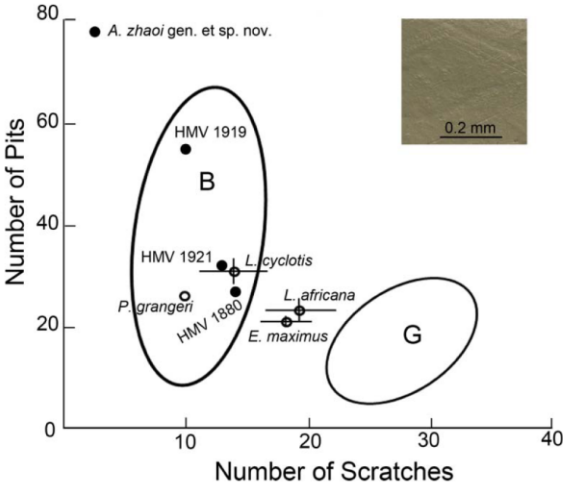

Figure 7. Bivariate plot of the average scratch versus average pit results of extant elephants, *Platybelodon grangeri* and *Aphanobelodon zhaoi* gen. et sp. nov., redrawn after Semprebon *et al.* (2016, fig. 3B). Oval outlines = Gaussian confidence ellipses (p = 0.95) on the centroid of the comparative extant grazer (G) and browser (B) samples adjusted by sample size. The insert is a photomicrograph of an enamel surface in HMV1921.

a cutting edge, and the anteromedial and anterolateral angles are sharp, forming two nearly right angles (Fig. 5A, B, F). This morphology is similar to those of *Platybeldon* and *Torynobelodon barnumbrowni*, which indicates vegetation-cutting behaviour, as Lambert (1992) stated. However, in *Amebelodon*, *Serbelodon* and *Protanancus*, the lower tusks are not as wide and thin as those in *Ap. zhaoi*. The anterior edge is blunt without sharp anteromedial and anterolateral angles. This morphology indicates that the tusks are attrited on hard substrate, possibly for digging.

Phylogenetic position of *Aphanobelodon zhaoi* in Amebelodontidae

It is easy to attribute *Aphanobelodon zhaoi* to Amebelodontidae based on its flattened lower tusks. Thus far, nine genera have been attributed to the family, including seven shovel-tuskers, *Archaeobelodon*, *Serbelodon*, *Protanancus*, *Amebelodon*, *Platybelodon*, *Torynobelodon* and *Konobelodon* (Shoshani 1996; Tassy 1996; Prado & Alberdi 2008; Konidaris *et al.* 2014; S.-Q. Wang *et al.* 2015), and, controversially, two non-shovel-tuskers, *Progomphotherium* and *Afromastodon* (Sanders *et al.* 2010). Here we confine our discussion to the shovel-tuskers. Among these taxa, *Platybelodon*, *Torynobelodon* and *Konobelodon* have tubular structure in their low tusks (Osborn & Granger 1932; Ye & Jia 1986; Tassy 1986; Lambert 1990; Konidaris *et al.* 2014; S.-Q. Wang *et al.* 2015), and the others have concentric lamination. *Aphanobelodon zhaoi* has concentric lamination in its lower tusks. However, its lower tusk is more flattened than that of any members of *Archaeobelodon*, *Serbelodon*, *Protanancus* and *Amebelodon*. The width-height ratio of its lower tusk falls into the variation range of *Platybelodon* (Fig. 6A), and the mandibular shape is more similar to that of *Platybelodon* than any other genus. This makes it difficult to determine the phylogenetic relationship within Amebelodontidae.

A cladistic analysis was carried out to determine the phylogenetic position of *Aphanobelodon zhaoi* within Amebelodontidae. Two MPTs were obtained (Fig. 8A, B). The topologies of the two MPTs yielded different positions of *Protanancus chinjiensis* (as the sister group of *Amebelodon* or *Amebelodon* + *Konobelodon*). In both MPTs, the position of *Aphanobelodon zhaoi* was stable; however, it was nested into species of *Platybelodon*. '*Platybelodon' dangheensis*, an isolated species in the early Miocene, MN3 (B.-Y. Wang & Qiu 2002), was stably clustered with the American late Miocene *Torynobelodon barnumbrowni*, sharing two synapomorphies – the incipient posttrite trefoils and the very short and broad symphysis. Therefore, we suggest that the genus name *Torynobelodon* is valid, and only includes two species, *T. barnumbrowni* and *T. dangheensis*.

Excluding *Torynobelodon*, *Aphanobelodon zhaoi* constitutes the sister group of *Platybelodon*. Guan (1991) considered *Pl. tongxinensis* from the Dingjiaergou fauna (Ye & Jia 1986; Ye *et al.* 1989, 1990; Guan 1988) as a junior synonym of *Pl. danovi*, and this view was accepted by subsequent researchers (Qiu *et al.* 1999; S.-Q. Wang *et al.* 2013). However, based on our comparison, there are two important differences between the type mandible of *Pl. danovi* and *Pl. tongxinensis*. First, the cross section of type material is relatively narrow in *Pl. danovi* (Fig. 6A); second, the mandibular ramus of *Pl. danovi* is not posteriorly inclined (Borissiak 1929, pl. 4, fig. 3). Furthermore, the presence of tubular structure in the type specimen of *Pl. danovi* is questionable (Tobien 1973, p. 252). Therefore, it is better to revive *Pl. tongxinensis* as a valid species.

S.-Q. Wang *et al.* (2013) demonstrated the morphological differences between *Platybelodon grangeri* from the Tairum Nor Fauna (from lower horizons in the Tunggur Formation) and the Moergen Fauna (from upper horizons in the Tunggur Formation). *Platybelodon* from the Moergen Fauna differs from other species of *Platybelodon* because it possesses complete tetralophont M2 and m2. It is also distinct from other species of *Platybelodon* because it possesses a wider symphysis that is closer to the tooth rows (Osborn & Granger 1932, fig. 5). Therefore, we suggest establishing a new species for *Platybelodon* from the Moergen Fauna of Tunggur, and here we have temporarily referred to it as tetralophodont *Platybelodon*.

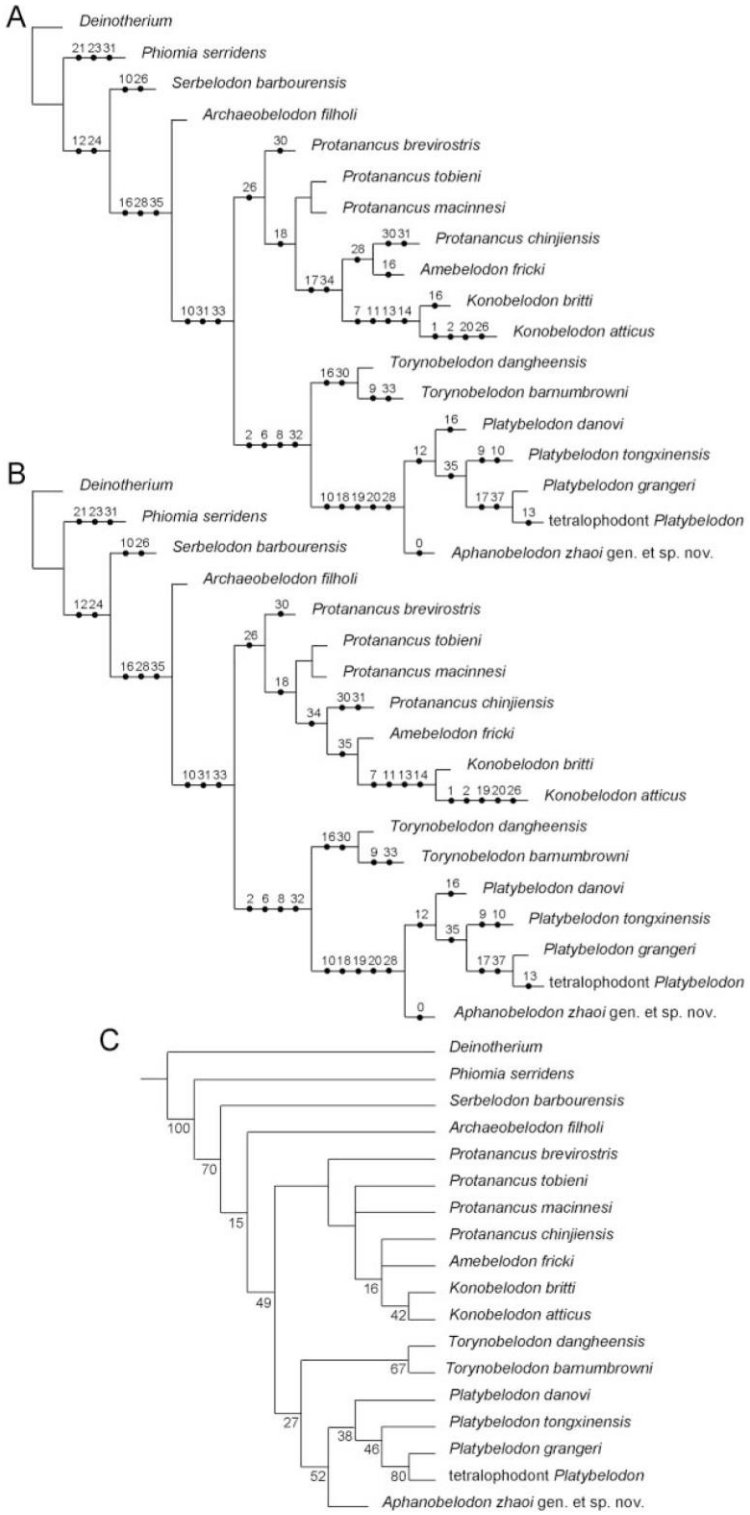

Figure 8. Phylogenetic reconstruction of shovel-tusked elephantiforms. **A, B,** MPTs from cladistic analysis of the proboscideans, based on the characters provided in Supplemental Appendix S1 and the data matrix in Supplemental Appendix S2. Tree length = 91, CI = 0.637; RI = 0.720; the numbers above each circle represent the supporting characters; **C,** the strict consensus tree from the two MPTs; the number at each node represents the bootstrap support value.

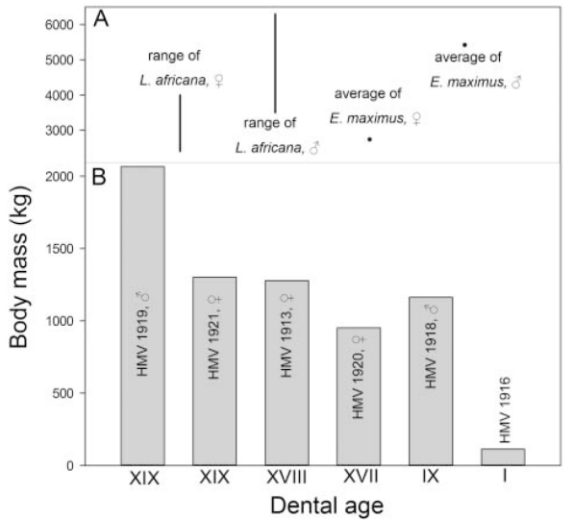

Figure 9. Body mass estimation of *Aphanobelodon zhaoi* gen. et sp. nov. and comparison with extant elephants. **A,** body mass data of extant elephants from Norwak (1999); **B,** body mass estimation of *Aphanobelodon zhaoi* gen. et sp. nov., based on Christiansen (2004).

Konobelodon was first established as a subgenus of *Amebelodon* that contained shovel-tuskers with tetralophodont intermediate cheek teeth and tubular structures in the mandibular tusks (Lambert 1990), but recently was upgraded to genus level, with the taxon enlarged to include the Eurasian '*Mastodon' grandincisivus* (Konidaris *et al.* 2014; S.-Q. Wang *et al.* 2016a). *Konobelodon* was thought to be derived from *Platybelodon* by some researchers (Konidaris *et al.* 2014) because of the presence of tubular structures in the mandibular tusks. However, the mandibular morphology does not support a close relationship between *Konobelodon* and *Platybelodon*. In *Konobelodon*, the ramus is not posteriorly inclined and the symphysis is strongly downwardly deflected. These features are similar to those of *Amebelodon*, and our phylogenetic reconstruction also supports the close relationship of the two genera. However, it should be noted that in our phylogeny, the presence of tubular structures in the mandibular tusks is no longer regarded as a synapomorphy. S.-Q. Wang *et al.* (2015) demonstrated biomechanical advantages of the tubular structures in *Platybeldon*. Therefore, the occurrence of the tubular structure is potentially due to parallel evolution (having evolved three times, in *Torynobelodon*, *Platybelodon* and *Konobelodon*, in our phylogenetic reconstruction) induced by competition and selection pressure.

To summarize, based on our phylogenetic reconstruction, we recognized two monophyletic groups in Amebelodontidae (Fig. 8C): one includes *Protanancus*, *Amebelodon* and *Konobelodon*; and the other includes *Torynobelodon*, *Aphanobelodon* and *Platybelodon*. The former can be referred to as Amebelodontinae and the latter as Platybelodontinae; *Archaeobelodon* and *Serbelodon* are plesions.

Sexual dimorphism and body mass estimation

The size distribution of the three adult individuals of *Aphanobelodon zhaoi* is notably bimodal. The length of the cranium of HMV1919 is 1016 mm and those of HMV1880 and HMV1921 are 895 mm and 808 mm, respectively. The mandible length of HMV1919 is 1550 mm and those of HMV1880 and HMV1921 are 1127 mm and 1201mm, respectively. This is easily interpreted as sexual dimorphism. The braincase of HMV1880 (and of HMV1921) is low, and the superior rim of the nasal aperture is at the level of the two postorbital processes (Fig. 1E). However, in HMV1919, the braincase is relatively domed and the superior rim of the nasal aperture is clearly posterior to the postorbital process (Fig. 1F). Similar sexual dimorphism was also observed in *Platybelodon grangeri* (S.-Q. Wang *et al.* 2013, fig. 3; S.-Q. Wang & Deng 2016), and possibly also *Gomphotherium angustidens* (Tassy 2013, fig. 15A, D; S.-Q. Wang & Deng 2016).

The body mass of the adult male (HMV1919) was estimated to be 2066.76 kg and that of the adult female (HMV1921) to be 1302.33 kg, only 63% that of the adult male, which indicates strong sexual dimorphism (Supplemental Table S1; Fig. 9). Two subadults very close to the adult dental age are estimated to be 950.98 kg and 1278.34 kg, respectively, and were identified as two females (Supplemental Table S1; Fig. 9). However, a subadult with younger dental age was estimated at 1162.53 kg, which is close to the adult female, and thus was identified as a young male (Supplemental Table S1; Fig. 9). The baby is only estimated to be 112.98 kg (Supplemental Table S1; Fig. 9). The estimated body masses of *Aphanobelodon zhaoi* are much smaller than the lower limit of extant elephants (Fig. 9). Furthermore, they are also smaller than estimated body masses of the fossil elephantiform taxa (i.e. *Mammuthus primigenius* 3179.50−9837.41 kg, *Elephas antiquus* 5762.53−12266.55 kg, *Mammut americanum* 4004.44−5390.60 kg and *Serbelodon barbourensis* 3211.10 kg); and are similar to those of *Archaeobelodon filholi* 2029.45 kg, *Gomphotherium angustidens* 2069.42 kg and *G. productum* 1309.98−1874.35 kg (Christiansen 2004).

Conclusions

In the present study, we report an interesting proboscidean taxon, *Aphanobelodon zhaoi*, that possessed a shovel-

tusked mandible and lacked permanent upper tusks. This is a unique feature combination – like a combination of *Deinotherium* and *Platybelodon*. Based on our cladistic analysis, *Aphanobelodon zhaoi* is the sister group of *Platybelodon* and, along with *Torynobelodon*, constitutes a monophyletic group in Amebelodontidae. The mandible of *Aphanobelodon* is not as specialized as that of *Platybelodon*, which is more suitable for cutting vegetation. This study enhances our knowledge regarding the evolutionary diversification of proboscideans in terms of morphology, taxonomy and biology.

Acknowledgements

We are grateful to Z.-X. Qiu, P. Tassy, U. Göhlich and M. Pickford for useful discussions. We thank Y. Chen and S. Wang for the reconstruction work. We thank two reviewers for their important advice to improve this manuscript. This work was supported by the National Basic Research Program of China (Grant Number 2012CB821900), the Chinese Academy of Sciences (Grant Number XDB03020104), the National Natural Science Foundation of China (Grant Numbers 41372001, 41430102) and the Special Research Program of Basic Science and Technology of the Ministry of Science and Technology (Grant No. 2015FY310100-14).

Supplemental data

Supplemental material for this article can be accessed online at: http://dx.doi.org/10.1080/14772019.2016.1208687.

References

Allen, P. & **Collinson, J.** 1986. Lakes. Pp. 63–94 in H. Reading (ed.) *Sedimentary environments and facies*. Blackwell Scientific Publications, Oxford.

Andrews, C. W. 1906. *A descriptive catalogue of the Tertiary vertebrata of the Fayûm, Egypt*. British Museum (Natural History), London, 324 pp.

Barbour, E. H. 1927. Preliminary notice of a new proboscidean *Amebelodon fricki*, gen. et sp. nov. *Bulletin of the Nebraska State Museum*, **1**, 131–134.

Barbour, E. H. 1929. *Torynobelodon loomisi*, gen. et sp. nov. *Bulletin of the Nebraska State Museum*, **1**, 147–153.

Barbour, E. H. 1932. The mandible of *Platybelodon barnumbrowni*. *Bulletin of the Nebraska State Museum*, **1**, 251–258.

Borissiak, A. A. 1929. On a new direction in the adaptive radiation of mastodonts. *Palaeobiologica*, **2**, 19–33.

Calandra, I., **Göhlich, U. B.** & **Merceron, G.** 2010. Feeding preferences of *Gomphotherium subtapiroideum* (Proboscidea, Mammalia) from the Miocene of Sandelzhausen (Northern Alpine Foreland Basin, southern Germany) through life and geological time: evidence from dental microwear analysis. *Paläontologische Zeitschrift*, **84**, 205–215.

Christiansen, P. 2004. Body size in proboscideans, with notes on elephant metabolism. *Zoological Journal of the Linnean Society*, **140**, 523–549.

Ferretti, M. P. 2010. Anatomy of *Haplomastodon chimborazi* (Mammalia, Proboscidea) from the late Pleistocene of Ecuador and its bearing on the phylogeny and systematics of South American gomphotheres. *Geodiversitas*, **32**, 663–721.

Frick, C. 1933. New remains of trilophodont-tetrabelodont mastodons. *Bulletin of the American Museum of Natural History*, **56**, 505–652.

Gheerbrant, E. & **Tassy, P.** 2009. L'origine et l'évolution des éléphants. *Comptes Rendus Palevol*, **8**, 281–294.

Goloboff, P. A., **Farris, J. S.** & **Nixon, K. C.** 2003. *TNT: tree analysis using new technology*. Program and documentation, available from the authors [updated at www.zmuc.dk/public/phylogeny, accessed 17 May 2013].

Guan, J. 1988. The Miocene strata and mammals from Tongxin, Ningxia and Guanghe, Gansu. *Memoirs of Beijing Natural History Museum*, **42**, 1–21.

Guan, J. 1991. The character analysis and phylogeny discussion on the shovel tusk mastodonts. *Memoirs of Beijing Natural History Museum*, **50**, 1–21.

Guan, J. 1996. On the shovel-tusked elephantoids from China. Pp. 124–135 in J. Shoshani & P. Tassy (eds) *The Proboscidea: evolution and palaeoecology of elephants and their relatives*. Oxford University Press, Oxford.

Illiger, C. D. 1811. *Prodromus systematis mammalium et avium additis terminis zoographicis uttriusque classis*. Salfeld, Berlin, 301 pp.

Konidaris, G. E., **Roussiakis, S. J.**, **Theodorou, G. E.** & **Koufos, G. D.** 2014. The Eurasian occurrence of the shoveltusker *Konobelodon* (Mammalia, Proboscidea) as illuminated by its presence in the Late Miocene of Pikermi (Greece). *Journal of Vertebrate Paleontology*, **34**, 1437–1453.

Krumbein, W. C. & **Aberdeen, E.** 1937. The sediments of Barataria Bay. *Journal of Sedimentary Research*, **7**, 3–17.

Kurt, F., **Hartl, G. B.** & **Tiedemann, R.** 1995. Tuskless bulls in Asian elephant *Elephas maximus*. History and population genetics of a man-made phenomenon. *Acta Theriologica*, Suppl. **3**, 125–143.

Lambert, W. D. 1990. Rediagnosis of the genus *Amebelodon* (Mammalia, Proboscidea, Gomphotheriidae), with a new subgenus and species, *Amebelodon* (*Konobelodon*) *britti*. *Journal of Paleontology*, **64**, 1032–1040.

Lambert, W. D. 1992. The feeding habits of the shovel-tusked gomphotheres: evidence from tusk wear patterns. *Paleobiology*, **18**, 132–147.

Landa, E. R. & **Fairchild, M. D.** 2005. Charting color from the eye of the beholder. *American Scientist*, **93**, 436–443.

Matsumoto, H. 1922. Revision of *Palaeomastodon* and *Moeritherium*. *Palaeomastodon intermedius*, and *Phiomia osborni*, new species. *American Museum Novitates*, **51**, 1–6.

Matsumoto, H. 1924. A revision of *Palaeomastodon* dividing it into two genera, and with descriptions of two new species. *Bulletin of the American Museum of Natural History*, **50**, 1–58.

Mottl, M. 1969. Bedeutende Proboscidier-Neufunde aus dem Altpliozän (Pannonien) Südost-Österreichs. *Österreichische Akademie der Wissenschaften, Mathemeatisch-naturwissenschaffliche Klasse, Denschriften*, **115**, 1–50.

Nowak, R. M. 1999. *Walker's mammals of the World*. 6th edition. Johns Hopkins University Press, Baltimore, 1936 pp.

Osborn, H. F. 1936. *Proboscidea: a monograph of the discovery, evolution, migration and extinction of the mastodonts*

and elephants of the World, Volume 1. American Museum Press, New York, 802 pp.

Osborn, H. F. & **Granger, W.** 1932. *Platybelodon grangeri*, three growth stages, and a new serridentine from Mongolia. *American Museum Novitates*, **537**, 1–13.

Pickford, M. 2003. New Proboscidea from the Miocene strata in the lower Orange River Valley, Namibia. *Memoir Geological Survey Namibia*, **19**, 207–256.

Prado, J. L. & **Alberdi, M. T.** 2008. A cladistic analysis among trilophodont gomphotheres (Mammalia, Proboscidea) with special attention to the south American genera. *Palaeontology*, **51**, 903–915.

Qiu, Z.-X., **Wu, W.-Y.** & **Qiu, Z.-D.** 1999. Miocene mammal faunal sequence of China: palaeozoogeography and Eurasian relationships. Pp. 443–455 in G. E. Rössner & K. Heissig (eds) *The Miocene land mammals of Europe*. Verlag Dr. Friedrich Pfeil, Munich.

Sanders, W. J., **Gheerbrant, E.**, **Harris, J. M.**, **Saegusa, H.** & **Delmer C.** 2010. Proboscidea. Pp. 161–251 in L. Werdelin & W. J. Sanders (eds) *Cenozoic mammals of Africa*. University of California Press, Berkeley.

Schlesinger, G. 1917. Die Mastodonten des K. K. naturhistorischen Hofmuseums. *Denkschriften des K. K. Naturhistorischen Hofmuseums, Geologisch-paläontologische Reihe*, **1**, 1–231.

Schlesinger, G. 1922. Die Mastodonten der Budapester Sammlungen. *Geologica Hungarica, Editio Separata*, **2**, 1–284.

Semprebon, G. M., **Deng, T.**, **Hasjanova, J.** & **Solounias, N.** 2016. An examination of the dietary habits of *Platybelodon grangeri* from the Linxia Basin of China: Evidence from dental microwear of molar teeth and tusks. *Palaeogeography, Palaeoclimatology, Palaeoecology,* **457**, 109–116.

Shoshani, J. 1996. Para- or monophyly of the gomphotheres and their position within Proboscidea. Pp. 149–177 in J. Shoshani & P. Tassy (eds) *The proboscidea: evolution and palaeoecology of elephants and their relatives*. Oxford University Press, Oxford.

Shoshani, J. & **Tassy, P.** 2005. Advances in proboscidean taxonomy & classification, anatomy & physiology, and ecology & behavior. *Quaternary International*, **126–128**, 5–20.

Solounias, N. & **Moelleken, S. M. C.** 1992. Tooth microwear analysis of *Eotragus sansaniensis* (Mammalia: Ruminantia), one of the oldest known bovids. *Journal of Vertebrate Paleontology*, **12**, 113–121.

Solounias, N. & **Semprebon, G.** 2002. Advances in the reconstruction of ungulate ecomorphology with application to early fossil equids. *American Museum Novitates*, **3366**, 1–49.

Tassy, P. 1983. Les Elephantoidea Miocènes du Plateau du Potwar, Groups de Siwalik, Pakistan. Ire Partie: Cadre chronologique et géographique, Mammutidés, Amébélodontidés. *Annales de Paléontologie*, **69**, 99–136.

Tassy, P. 1984. Le mastodonte à dents étroites, le grade trilophodonte et la radiation initiale des Amebelodontidae. Pp. 459–473 in E. Buffetaut, J. M. Mazin & E. Salmon (eds) *Actes du symposium paléontologique Georges Cuvier*. Impressions le Serpentaire, Montbéliard.

Tassy P. 1986. *Nouveaux Elephantoidea (Proboscidea, Mammalia) dans le Miocène du Kenya: essai de réévaluation systématique*. Cahiers de Paléontologie, E'ditions du Centre National de la Recherche Scientifique, Paris, 135 pp.

Tassy, P. 1994. Gaps, parsimony, and early Miocene elephantoids (Mammalia), with a re-evaluation of *Gomphotherium annectens* (Matsumoto, 1925). *Zoological Journal of the Linnean Society*, **112**, 101–117.

Tassy, P. 1996. Who is who among the Proboscidea? Pp. 39–48 in J. Shoshani & P. Tassy (eds) *The Proboscidea: evolution and palaeoecology of elephants and their relatives*. Oxford University Press, Oxford.

Tassy, P. 2013. L'anatomie cranio-mandibulaire de *Gomphotherium angustidens* (Cuvier, 1817) (Proboscidea, Mammalia): données issues du gisement d'En Péjouan (Miocène moyen du Gers, France). *Geodiversitas*, **35**, 377–445.

Tassy, P. 2014. L'odontologie de *Gomphotherium angustidens* (Cuvier, 1817) (Proboscidea, Mammalia): données issues du gisement d'En Péjouan (Miocène moyen du Gers, France). *Geodiversitas*, **36**, 35–115.

Tobien, H. 1973. On the evolution of mastodonts (Proboscidea, Mammalia), Part 1: the bunodont trilophodont groups. *Notizblatt des Hessischen Landesamtes für Bodenforschung zu Wiesbaden*, **101**, 202–276.

Wang, B.-Y. & **Qiu, Z.-X.** 2002. A new species of *Platybelodon* (Gomphotheriidae, Proboscidea, Mammalia) from early Miocene of the Danghe area, Gansu, China. *Vertebrata PalAsiatica*, **40**, 291–299.

Wang, S.-Q. & **Ye, J.** 2015. Paleobiological implications of new material of *Platybelodon danovi* from the Dingjiaergou Fauna, western China. *Historical Biology*, **27**, 987–997.

Wang, S.-Q. & **Deng, T.** 2016. Female preference promotes asynchronous sex evolution in Elephantiformes. *Vertebrata PalAsiatica*, **54**, 51–66.

Wang, S.-Q., **He, W.** & **Chen, S.-Q.** 2013. Gomphotheriid mammal *Platybelodon* from the Middle Miocene of Linxia Basin, Gansu, China. *Acta Palaeontologica Polonica*, **58**, 221–240.

Wang, S.-Q., **Shi, Q.-Q.**, **He, W.**, **Chen, S.-Q.** & **Yang, X.-W.** 2016a. A new species of the tetralophodont amebelodontine *Konobelodon* (Proboscidea, Mammalia) from the Late Miocene of China. *Geodiversitas*, **38**, 65–97.

Wang, S.-Q., **Deng, T.**, **Tang, T.**, **Xie, G.-P.**, **Zhang, Y.-G.** & **Wang, D.-Q.** 2015. Evolution of *Protanancus* (Proboscidea, Mammalia) in East Asia. *Journal of Vertebrate Paleontology*, **35**, e881830, doi: 10.1080/02724634.2014.881830.

Wang, S.-Q., **Zong, L.-Y.**, **Yang, Q.**, **Sun, B.-Y.**, **Li, Y.**, **Shi, Q.-Q.**, **Yang, X.-W.**, **Ye, J.** & **Wu, W.-Y.** 2016b. Biostratigraphic subdividing of the Neogene Dingjiaergou mammalian fauna, Tongxin County, Ningxia Province, and its background for the uplift of the Tibetan Plateau. *Quaternary Sciences*, **36**, 789–809.

Ye, J. & **Jia, H.** 1986. *Platybelodon* (Proboscidea, Mammalia) from the Middle Miocene of Tongxin, Ningxia. *Vertebrata PalAsiatica*, **24**, 139–151.

Ye, J., **Qiu, Z.-X.** & **Chen, J.-Z.** 1989. Comparative study of a juvenile skull of *Platybelodon tongxinensis*. *Vertebrata PalAsiatica*, **27**, 284–300.

Ye, J., **Wu, W.-Y.** & **Jia, H.** 1990. Reconstruction of the jaw-closing muscles of *Platybelodon tongxinensis* (Amebelodontidae, Proboscidea) and discussion of cranial evolution from long-jawed mastodont to short-jawed elephantid. *Vertebrata PalAsiatica*, **28**, 284–295.

Journal of Paleontology, 93(2), 2019, p. 385–397

0022-3360/19/1937-2337
doi: 10.1017/jpa.2018.65

JOURNAL OF PALEONTOLOGY
A PUBLICATION OF THE Paleontological SOCIETY

New *Olonbulukia* material and its related assemblage reveal an early radiation of stem Caprini along the north of the Tibetan Plateau

Shi-Qi Wang,[1,2] Qing Yang,[3] Ya Zhao,[3] Chun-Xiao Li,[1,4] Qin-Qin Shi,[1] Li-Yi Zong,[3] and Jie Ye[1]

[1]Key Laboratory of Vertebrate Evolution and Human Origins of the Chinese Academy of Sciences, Institute of Vertebrate Paleontology and Paleoanthropology, Chinese Academy of Sciences, Beijing, China <wangshiqi@ivpp.ac.cn>, <lichunxiao@ivpp.ac.cn>, <shiqinqin@ivpp.ac.cn>, <jieye@hotmail.com>
[2]Chinese Academy of Sciences Centers for Excellence in Life and Paleoenvironment, and in Tibetan Plateau Earth Sciences, Beijing, China
[3]Ningxia Geological Museum, Yinchuan 750000, China <1048852529@qq.com>, <376542383@qq.com>, <455011213@qq.com>
[4]University of Chinese Academy of Sciences, Beijing 100049, China

Abstract.—Living Caprini are dominant bovids in the pan-Tibetan area that are strongly adapted to dry steppe and high-mountain meadow habitats. Some taxa with Holarctic distributions, e.g., *Ovis* Linnaeus, 1758, were thought to originate on the Tibetan Plateau and subsequently dispersed elsewhere, which was depicted as an 'out of Tibet' story. However, except for some information on a stem caprine assemblage from the Qaidam Basin, the early evolution of Caprini around the Tibetan Plateau is poorly known. Here, we report new material of *Olonbulukia tsaidamensis* Bohlin, 1937, which was a member of this stem caprine assemblage, from the Wuzhong region, northern China, confirming the similarity of the Wuzhong Fauna and 'Qaidam Fauna.' Based on a biometric study of horncores from the 'Qaidam' and Wuzhong faunas, we recognize six taxa from this stem caprine assemblage: *O. tsaidamensis*, *O.* sp., *Qurliqnoria cheni* Bohlin, 1937, *Tossunnoria pseudibex* Bohlin, 1937, ?*Protoryx* cf. *P. enanus* Köhler, 1987, and cf. *Pachytragus* sp. Among these taxa, *Q. cheni* and *T. pseudibex* are probably related to some extant Tibetan endemic species, e.g., the Tibetan antelope, *Pantholops hodgsonii* (Abel, 1826), and the Himalayan tahr, *Hemitragus jemlahicus* (Smith, 1826). Others might be ancestral to the Turolian caprine assemblages and even possibly gave rise to the extant Caprina. This work reveals an early radiation of stem caprines along the northern side of the rising Tibetan Plateau and indicates a mixed pattern of pan-Tibetan stem caprine evolution prior to their dispersal out of the Tibetan Plateau.

Introduction

Bohlin (1937) reported the 'Qaidam (= Tsaidam) Fauna' from the Qaidam Basin (Fig. 1) in the northern part of the Tibetan Plateau. Among the fossil assemblages in the early paleontological history of China, this fauna is distinctive in the occurrence of various specialized bovids that are seldom recovered elsewhere (i.e., *Olonbulukia* Bohlin, 1937, *Qurliqnoria* Bohlin, 1937, *Tossunnoria* Bohlin, 1937, and *Tsaidamotherium* Bohlin, 1935a). The most specialized bovid, *Tsaidamotherium*, which has a very odd horncores (Bohlin, 1935a; Shi, 2014), was attributed to Ovibovinae or Urmiatheriinae, and its phylogenetic position has been substantially debated (Köhler, 1987; Gentry, 1992; Bibi et al., 2009; Chen and Zhang, 2009). Other taxa were grouped as presumed with Caprinae (Gentry, 2000), and were recently changed to Caprini based on both morphological and molecular evidence (Bibi et al., 2009; Hassanin et al., 2012). *Qurliqnoria* is hypothesized to be the ancestor of the extant Tibetan antelope or chiru, *Pantholops hodgsonii* (Abel, 1826) (Gentry, 1968, 2000; Deng et al., 2011). *Tossunnoria pseudibex* Bohlin, 1937 seems to be related to the extant Himalayan tahr, *Hemitragus jemlahicus* (Smith, 1826), or goats (*Capra* spp.) (Bohlin, 1937; Gentry, 1971, 2000). Therefore, 'Qaidam Fauna' bovids could represent an early radiation of endemic stem Caprini on the Tibetan Plateau. Except for the above-named taxa, there are still several types of horncores with relatively unspecialized morphology, which Bohlin (1937) referred to as 'Antilope gen. et sp. indet.' I–IV. However, these unnamed taxa have been inadequately noticed by subsequent researchers (but see Bibi and Güleç, 2008).

The 'Qaidam Fauna' was considered the earliest *Hipparion* fauna in northern China, because of the occurrence of early hipparions, early tetralophodont gomphotheres, an early *Acerorhinus*, and some primitive cervids (i.e., *Lagomeryx* Roger, 1904 and *Dicrocerus* Lartet, 1837) that were thought to be middle Miocene relicts (Qiu et al., 1987). Recently, Wang et al. (2011) studied Bohlin's field records and investigated the stratigraphy of the fossiliferous region; consequently, they recognized two fossil assemblages in the 'Qaidam Fauna,' the late middle Miocene Olongbuluk Fauna (ca. 15–12.5 Myr) and early late Miocene Tuosu Fauna (ca. 12–10.5 Myr). Therefore, the 'Qaidam Fauna' was a fossil assemblage complex, and we refer to the 'Qaidam Fauna' using quotation marks.

Recently, we discovered a horncore of *Olonbulukia tsaidamensis* Bohlin, 1937 and possibly stem Caprini dental material from the Wuzhong Building Material Plant (Jiancaichang locality, Wuzhong), Ningxia Province, China (Fig. 1) from the early late Miocene Ganhegou Formation. This is

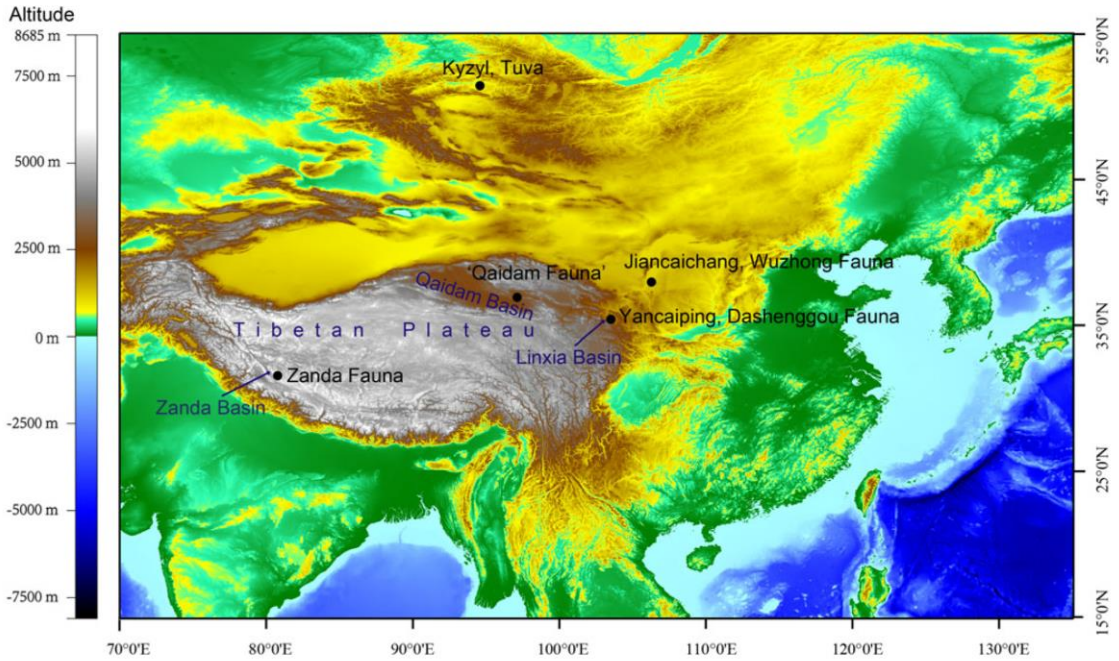

Figure 1. Topology of eastern Asia with related fossil localities in the present article, emphasizing the Tibetan Plateau. The map was downloaded from the public source, General Bathynetric Chart of the Oceans (https://www.gebco.net/).

the first report of *Olonbulukia* outside of the Qaidam Basin. This locality was previously reported by Qiu et al. (1987), with the discovery of *Qurliqnoria cheni* Bohlin, 1937. The occurrence of *O. tsaidamensis* and *Q. cheni*, with recent palaeomagnetic data of the Ganhegou Formation (ca. 10 Ma, see Shen et al., 2001), proves that the fossil assemblage from the Jiancaichang locality (denoted herein as the Wuzhong Fauna) is comparable to the classic Tuosu Fauna. In the same period, fossils were rarely discovered from northern China. Therefore, an in-depth study of the bovid assemblages of these two faunas is helpful in understanding the radiation of caprines, which are very important members of today's dry and cold Holarctic habitats (Geist, 1987).

Materials and methods

Horncore biometric study and 3D models.—We used three biometric parameters to characterize horncore morphology. (1) Mediolateral compression was inferred by basal anteroposterior diameter (DAP)/transverse diameter (DT); data were measured using calipers. (2) Curvature (unit / mm) was represented by the mean curvature of horncore anterior and posterior edges; to obtain these data, we took photographs of the direct lateral view of the horncore (Fig. 2.1) and extracted the outlines of the anterior and posterior edges (Fig. 2.2); then, we used the least-squares method to fit a circle by the sample points of the outlines, and calculated the curvature of the regressed circle (Fig. 2.3, 2.4). Calculation was performed using a set of self-programmed MATLAB (MathWorks, Inc.; ver. R2016a) codes. (3) Oblique angle was represented by the angle between the medial sagittal plane and the vertical plane that passes through the long axis of the pedicle; to obtain these data, we acquired the 3D surface digital models of the horncores using an Artec 3D Spider scanner and measured the angle on the 3D models using the Materialise 3-matic program (ver. 9.0) (Fig. 2.5, 2.6). All of the 3D models (see Supplemental data SI 1–17) are available in the public online repository Dryad. Other biometric data were measured using calipers.

One-way ANOVA.—Student's t-tests were performed to test the statistical significance of differences in horncore curvature and oblique angle between *Olonbulukia* and *Qurliqnoria*, and mediolateral compression between *O. tsaidamensis* and *Olonbulukia* sp. Equal variance was hypothesized, and differences were considered significant if the double-tailed test was < 0.05.

Repositories and institutional abbreviations.—IVPP = Institute of Vertebrate Paleontology and Paleoanthropology, Chinese Academy of Sciences, Beijing (IVPP RV is the prefix for the specimens that were previously published under informal numbering systems); NGM = Ningxia Geological Museum, Yinchuan, Ningxia, China. All of the specimens examined here are housed in IVPP, except one from NGM. Comparative materials were from previous publications. Ruminant tooth terminology follows that used by Bärmann and Rössner (2011).

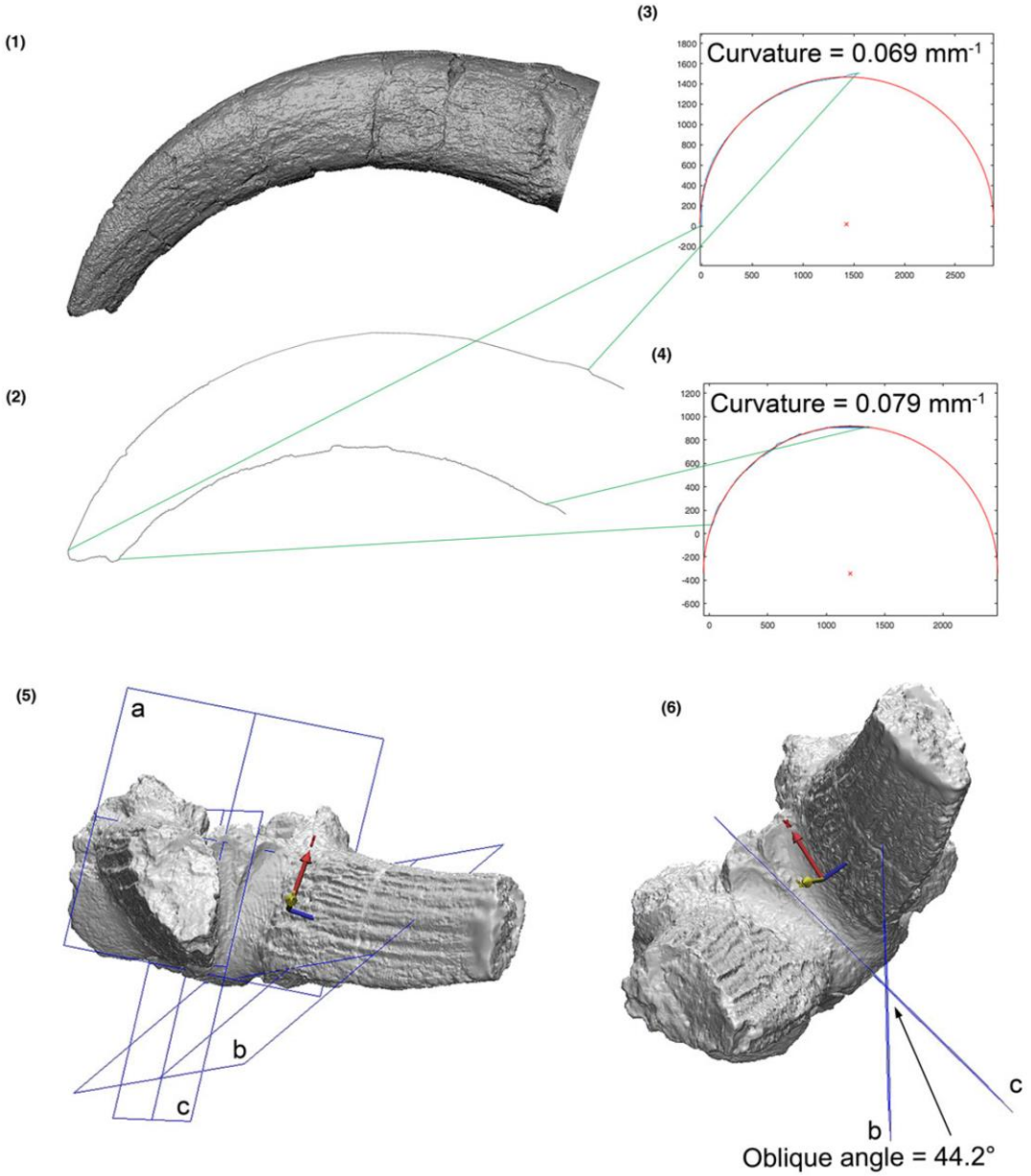

Figure 2. Horncore biometric data acquisition: (**1**) photo of a horncore (*Olonbulukia tsaidamensis*, IVPP RV37008, taken from 3D digital model) in lateral view; (**2**) outlines of the horncore in Figure 2.1; the green lines denote the sections of anterior and posterior edges; (3, 4) circle fitting of the anterior (**3**) and posterior (**4**) edges of the horncore; the blue lines denote the horncore ontlines and the red lines denote the fitted circles; (**5**) sectioning plane on the 3D digital horncore model (*Qurliqnoria cheni*, IVPP RV37100); a = horizon plane, b = vertical plane through the pedicle long axis, c = medial sagittal plane; (**6**) oblique angle measurement, or the angle between the b and c planes. The red, blue, and yellow arrows represent the X, Y, and Z coordinates that were arbitrarily generated by the 3-matic program; the arrowhead of the blue arrow is hidden by the 3D model of the horncore body.

Systematic paleontology

Order Artiodactyla Owen, 1848
Family Bovidae Gray, 1821
Subfamily Antilopinae Gray, 1821 (sensu Kingdon, 1982)
Genus *Olonbulukia* Bohlin, 1937

Type species.—*Olonbulukia tsaidamensis* Bohlin, 1937.

Diagnosis.—Medium-sized bovid with mediolaterally compressed horncore that possesses an anterior keel. The horncore has a weak spiral structure with strong posterior bending (curvature 0.04–0.10/mm). The oblique angle of the pedicle is small (15–30°). The top of the cranium is vaulted, and the profile of the dorsal cranium is curved dorsally instead of straight, resembling that of *Protoryx* Major, 1891. (Revised from Bohlin, 1937.)

Occurrence.—Qaidam Basin and Wuzhong regions, China; middle Miocene and early late Miocene (late Tunggurian and early Bahean, Chinese Land Mammal Age), which were correlated to MN 6–9.

Olonbulukia tsaidamensis Bohlin, 1937
Figure 3.1–3.3; Table 1

Holotype.—IVPP RV37008 [Bohlin's (1937) field no. 356], a brain case with both horncores; the ventral surface is deeply weathered.

Diagnosis.—The horncore is strongly compressed with DAP/DT 1.6–1.9 (at the horncore base). Otherwise as for the genus.

Occurrence.—Bohlin Camp (BB, 165), Qaidam Basin, basal red beds (Olongbuluk Fauna), middle Miocene, ca. 15 Ma (Wang et al., 2011).

Description.—The right horncore (Fig. 3.1–3.3) is strongly lateromedially compressed. The horncore cross section at the base is a compressed oval. This shape is retained throughout the preserved length, and only becomes slightly smaller distally (Fig. 3.1.1–3.1.3). The long axis of the cross section at the right horncore base is slightly oblique to the midsuture of the frontal bone by an angle of 19.7°, suggesting that the two long axes of horncore cross sections posteriorly diverge by ~40°. No less than 1/3 of the distal part of the horncore is broken. In lateral and medial views, the preserved horncore portion shows a posterior curvature. In anterior and posterior views, the horncore is slightly laterally oblique. The horncore is slightly homonymous. Strong furrows are present along the entire length of the horncore. An anterior keel is present, but is not as sharp as that of the type specimen. The pedicle is moderately long, with the anterior edge longer than the posterior edge. The anterior opening of the supraorbital channel is small and located at the proximal base slightly lateral to the anterior edge of the pedicle, which is relatively close to the midsuture of the frontal bone. No groove surrounds the supraorbital foramen. The postcornual fossa is weak and close to the horncore base.

The remaining frontal bone can be subdivided into three surfaces. (1) The cerebral surface is anterodorsally bordered by the midsuture of the frontal bone and posterodorsally bordered by the frontal-parietal suture; it is triangular and deeply concave with many digital impressions. The midsuture of the frontal bone is half-crescent-shaped. The anterior part is strongly thickened, extends posterodorsally, and thins. The frontal-parietal suture forms a right angle. (2) The orbital surface is located laterally. However, the thin orbital rim was broken. This surface is smoothly concave. The posterior opening of the supraorbital channel is located at the deepest point of the orbital surface and is almost at the same level as the anterior opening. (3) The frontal sinus surface is small; it is located at the anteroventral part of the bone. The frontal sinus is irregular and shallow on the surface. However, we do not know whether the excavation of the frontal sinus in the horncore is present.

Materials.—IVPP V23373, a right horncore with partial frontal bone; the distal part of the horncore is broken.

Locality and age of the new material.—The Wuzhong Building Material Plant (Jiancaichang locality), Northeast Quarry (IVPP no. NXWZ201502), 37°49'50.46"N, 106°07'12.08"E, 1169.0H (Fig. 1), early late Miocene Ganhegou Formation, Bahean, correlated to ~MN 9.

Remarks.—*Olonbulukia tsaidamensis* is a stem caprine species with relatively specialized horncores for its age. The horncore is remarkably laterally compressed with strong posterior curvature. The holotype is from the Bohlin Camp (BB, 165) of the Olongbuluk Fauna, Qaidam Basin, ca. 15 Ma of the middle Miocene (Wang et al., 2011). This age is very early, even for stem caprines. *Olonbulukia tsaidamensis* also occurred in the early late Miocene Tuosu Fauna but was never found outside of the Qaidam Basin prior to this study. The newly discovered horncore from the Wuzhong Fauna displays almost identical morphology with the holotype, except for smaller dimensions, possibly due to a younger ontogenetic stage. The Jancaicheng site of the Wuzhong Fauna is ca. 10 Ma, very close to and probably slightly later than the Tuosu Fauna of the Qaidam Basin. The new horncore is the first report of *O. tsaidamensis* outside of the Qaidam Basin.

Antilopinae gen. indet. sp. indet.
Figure 3.4–3.9; Table 2

Description.—The P3 and P4 (Fig. 3.4–3.6) are moderately worn. In occlusal view (Fig. 3.4), the P3 is semicircular with a straight labial wall and a rounded lingual wall. The labial cone is relatively anteriorly positioned. The anterior style is also strong, labially protruded. The posterior style is relatively blunt. The fossa is strongly anteriorly positioned. It is fabaceous with a small central fold on the posterolingual crista. The dentinal area of posterolabial and posterolingual cristae is very large, and a shallow posterior fossa is developed on the posterolingual crista. This fossa is narrow and cuts through the posterior wall of the tooth enamel at the lingual side of the posterior style. In buccal view (Fig. 3.5), the labial cone is high and sharp. The ribs of the labial cone

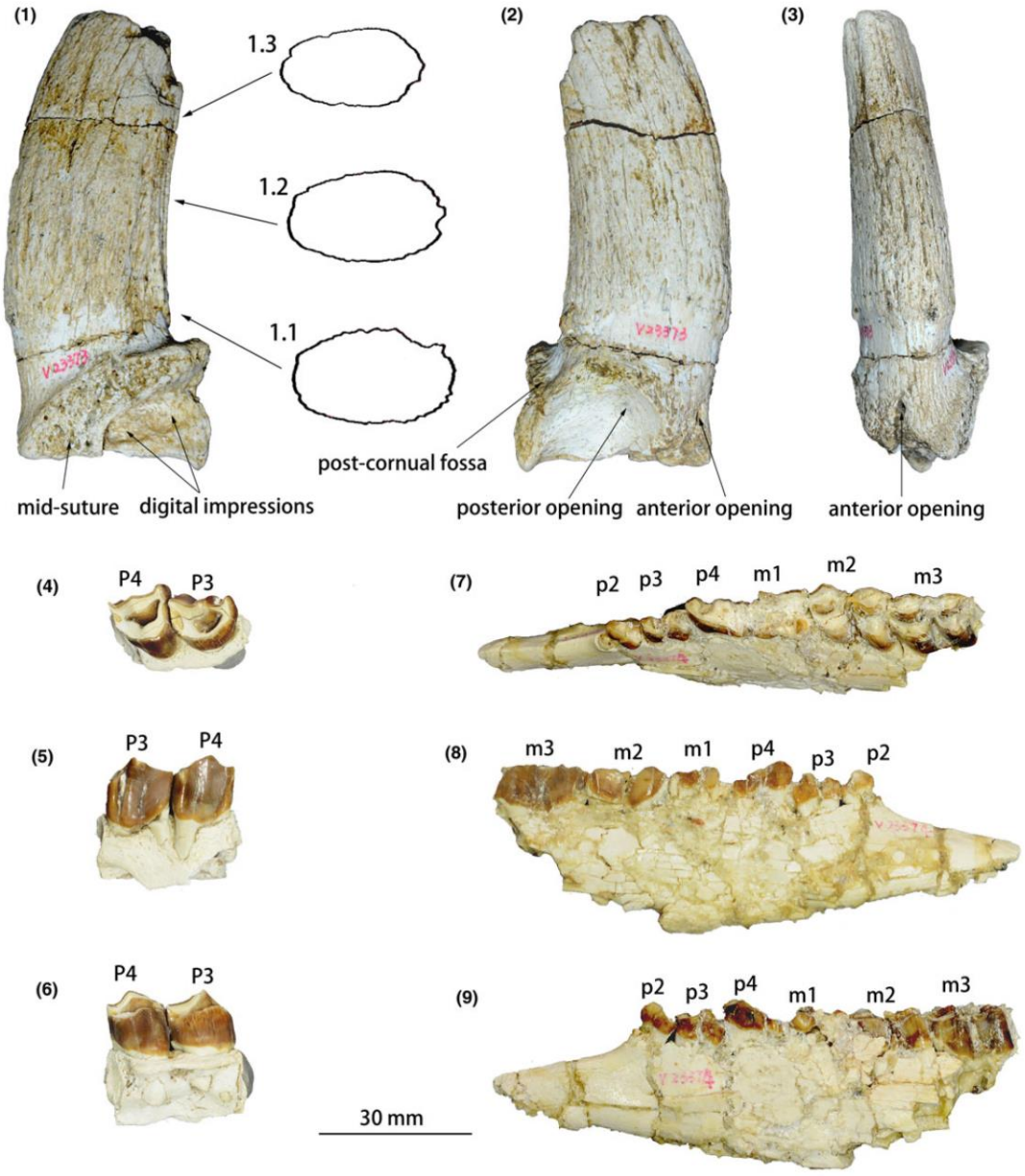

Figure 3. Stem caprines from the Jiancaichang locality, Wuzhong (Wuzhong Buliding Material Plant), China, Bahean age (ca. 10 Ma), late Miocene: (**1–3**) *Olonbulukia tsaidamensis*, IVPP V23373, right horncore with fragmentary frontal bone remains, in medial (**1**), lateral (**2**), and anterior (**3**) views (anterior at left and lateral at top), with cross sections at 0 (**1.1**), 37.8 (**1.2**), and 59.1 (**1.3**) mm distal to the pedicle; (**4–6**) Antilopinae gen. indet. sp. indet., NGM WJCCD-10-N-006, right P3 and P4, in occlusal (**4**), buccal (**5**), and lingual (**6**) views; (**7–9**) Antilopinae gen. indet. sp. indet., IVPP V23374, right hemimandible with p2–m3 tooth row, in occlusal (**7**), lingual (**8**), and buccal (**9**) views. Notes: M/m = upper/lower molar; P/p = upper/lower premolar.

Table 1. Information and biometric data of the horncores discussed in this study. * = type specimen; ** = both horncores preserved.

Taxon	Number	Bohlin taxonomy	Bolin field no.	Age (Miocene)	Locus	Anterior curvity (mm^{-1})	Posterior curvity (mm-1)	Long axis (mm)	Short axis (mm)	Oblique angle (°)
Olonbulukia tsaidamensis	V23373 (SI 1)	(Wuzhong specimen)	–	late	right	0.0693	0.0543	45.3	26.5	19.7
	RV37008* (SI 4)	*O. tsaidamensis*	356	middle	right**	0.0691	0.794	55.4	32.3	16.0
	RV37093 (SI 5)	*O. tsaidamensis*	429	late	left	0.0918	0.0705	48.6	27.1	22.6
	RV37094 (SI 6)	Antilope gen. et sp. indet. III	514	late	left	0.0665	0.0476	46.4	27.7	25.3
Olonbulukia sp.	RV37095 (SI 7)	?*Olonbulukia* sp.	423	late	right	0.0795	0.0699	54.1	36.8	26.6
	RV37096 (SI 8)	Antilope gen. et sp. indet. II	479	late	left	0.0658	0.0840	38.1	25.7	–
	RV37097 (SI 9)	Antilope gen. et sp. indet. II	486	late	right	0.0751	0.0598	40.2	28.9	27.8
	RV37098 (SI 10)	Antilope gen. et sp. indet. II	499	late	left	0.0424	0.0623	38.1	25.9	27.7
Qurlignoria cheni	RV37100* (SI 11)	*Qurlignoria cheni*	441	late	right**	0.0336	0.0208	48.4	30.0	44.2
	RV37101 (SI 12)	*Qurlignoria cheni*	491	late	right	0.0469	0.0217	43.0	31.5	53.8
	RV37102 (SI 13)	*Qurlignoria* sp.	508	late	left**	0.0362	0.0245	39.1	27.5	56.4
	RV37103	*Qurlignoria* sp.	531	late	left	0.0227	0.0164	42.0	27.1	–
Tussunnoria pseudibex	RV37086* (SI 14)	*Tussunnoria pseudibex*	481	late	right	0.1022	0.0643	75.4	43.3	32.0
	RV37087 (SI 15)	*Tussunnoria pseudibex*	449	late	right	0.0543	0.0602	69.0	36.7	33.8
cf. *Pachytragus* sp.	RV37104 (SI 16)	Antilope gen. et sp. indet. I	492	late	left**	0.0667	0.0752	37.4	29.0	45.2
?*Protoryx* cf. *P. enanus*	RV37099 (SI 17)	Antilope gen. et sp. indet. IV	451	middle	right	0.0987	0.0881	40.9	30.7	19.4

and anterior style are strong and columnar-like, and are close to each other. The rib of the posterior style is weak.

In occlusal view (Fig. 3.4), the P4 is shorter and wider than the P3, and its width is greater than the length. The labial cone is medially positioned. The anterior and posterior styles are equally developed, and both labially protrude. The fossa is also anteriorly positioned like that of P3, and the shape of the fossa is inverted trapezoid. The lingual cone is relatively anteriorly positioned and displays a strong posterolingual crista. A small, shallow posterior fossa that cuts through the posterior enamel wall is also present, but this fossa is much smaller than that of the P3. In buccal view (Fig. 3.5), the buccal cone is also high and sharp, as is the posterior style (the top of the anterior style is broken). The ribs of the anterior and posterior styles are strong and columnar-like. The rib of the labial cone is also columnar-like, but it is relatively weak.

The left hemimandible is deeply weathered (Fig. 3.7–3.9). The tooth row is almost complete except regarding the third lobe of the m3. However, the tooth row is deeply worn. The premolar row is moderately long relative to the molar row (Table 2). The p2 is small. The anterolabial cristid is hook-like and extends from the mesolabial conid. The mesolingual conid is juxtaposed with the mesolabial conid, and a thin posterolingual cristid extends from the mesolingual conid. The posterolabial and posterolingual conids are interconnected.

The p3 is longer than the p2. The anterior conid and anterior stylid are fork-like, and link to the mesolabial conid by the anterolabial cristid. The transverse cristid is posteriorly oblique and connected to a slightly inflated mesolingual conid. A thin posterolingual cristid is also present. There is a groove between the mesolabial and posterolabial conids. The posterolabial and posterolingual conids are deeply worn and interconnected.

The p4 is much larger than the p3. However, morphology of the two teeth is very similar, except for the stronger mesolingual and posterolingual conids of the p4.

The m1 is so deeply worn that nearly all of the enamel is worn down. The shape is relatively quadrate, which is the only character that can be observed.

The two m2 lobes are of equal dimensions. The metaconid is more lingually prominent than the entoconid. The mesostylid and metastylid are weak, but this feature might be due to the deep wear. The entoconid protrudes posteriorly. The protoconid and hypoconid show rounded labial walls. A small ectostylid is present. The anterior cingulid (goat fold) is absent. No ribs can be seen on the lingual wall.

The third m3 lobe is broken. The anterior two lobes are narrower than the two lobes of the m2. Both metaconid and entoconid are slightly inflated. The mesostylid and metastylid are slightly protruded. The protoconid and hypoconid also have rounded labial walls, and a very small ectostylid occurs between

Table 2. Tooth measurements of Antilopinae gen. indet. sp. indet. from the Jiangcaichang locality. Measured at: * = lingual cone; ** = mesolabial cone; *** = mesolingual cone; **** = anterior cone; ***** = metaconid cone.

Number	Locus	Length (mm)	Width (mm)	Height (mm)
NGM WJCCD-10-N-006 (SI 1)	P3	12.72	11.33	13.50*
	P4	11.58	13.75	13.13*
IVPP V23373 (SI 3)	p2	7.7	4.55	5.33+**
	p3	9.95	10.64	6.34+***
	p4	12.33	6.62	5.90+****
	m1	11.99	9.24	4.43+*****
	m2	16.13	10.54	7.33+*****
	m3	~20	10.03	9.37+*****
	Premolar length (mm)	27.56	–	–
	Molar length (mm)	~45	–	–
	Tooth row length (mm)	~74.5	–	–
	Premolar/molar length ratio	0.612	–	–

the two conids. The anterior cingulid cannot be observed. As in the m2, no lingual ribs can be observed.

Materials.—IVPP V23374, a left cheek tooth row (p2–m3) with broken hemimandible, from the Jiancaichang locality, Northeast Quarry (IVPP no. NXWZ201502, coordinates as above); NGM WJCCD-10-N-006, right P3 and P4 with partial bone of the upper jaw, also from the Jiancaichang locality, coordinates not recorded.

Remarks.—The teeth remains from the Jancaicheng site, Wuzhong Fauna, coincide in morphology with Miocene stem caprines (Bohlin, 1935b). At this site, two stem caprines have been reported, *Olonbulukia tsaidamensis* and *Qurliqnoria cheni* (Qiu et al., 1987). However, teeth of these two species are yet unknown to us. The new material might belong to either of the two species, or another uncovered one. Here we refer these teeth to Antilopinae gen. indet. sp. indet.

Results

Comparisons.—The newly discovered horncore from the Jiancaichang locality (Wuzhong Fauna) shows great similarity to that of the type specimen of *Olonbulukia tsaidamensis* from the Qaidam Basin (Bohlin, 1937). Previous studies showed that horncore growth generates at the tip (Dove, 1935; Janis and Scott, 1987). It seems that a constant development velocity is retained and maintains a constant horncore curvature. The horncore body is vertically erect, and the vertical plane that passes through the long axis of the pedicle is close to the medial sagittal plane with an angle between the two planes (oblique angle of the pedicle) of 19.7° (16.0° in the type specimen) (Fig. 4.2). The pedicle is moderately long, and the supraorbital foramen is close to the elongation line of the anterior edge of the horncore body. These features are distinct from those of other stem caprine genera. For example, in *Qurliqnoria*, the DAP/DT ranges 1.364–1.616, curvature ranges 0.020–0.034/mm, and the oblique angle of the pedicle ranges 44.2–56.4° (Table 1). These biometrics are greatly distinct from *Olonbulukia*. Furthermore, in *Qurliqnoria*, the pedicle is relatively low, and the supraorbital foramen is more laterally remote to the horncore elongation line. In *Tossunnoria*, the horncore is very short and thick, and the two horncores greatly diverge, which substantially differs from that of *Olonbulukia*.

One difference between the Wuzhong specimen and the type specimen is that the Wuzhong specimen is smaller. All of the biometric differences are proportional, which is easily interpreted as a result of ontogeny. The Wuzhong specimen is comparable in size to some referred specimens from the 'Qaidam Fauna,' as described below. Furthermore, the postcornual fossa in the Wuzhong specimen is smaller and less clear than that of the Qaidam specimens. As a result, we are confident that the Wuzhong specimen belongs to *Olonbulukia tsaidamensis*.

Biometric study of horncores from the 'Qaidam Fauna'.—Stem caprine remains from the 'Qaidam Fauna' reported by Bohlin (1937) (Fig. 5) represent the most abundant material from this group during the middle and early late Miocene of northern China. Bohlin (1937) reported a total of nine taxa based on the horncores. Except for the named *Olonbulukia tsaidamensis* (Fig. 5.1, 5.2, 5.13), ?*Olonbulukia* sp. (Fig. 5.14), *Qurliqnoria cheni* (Fig. 5.3, 5.4, 5.18), *Qurliqnoria* sp. (Fig. 5.5, 5.6), and *Tossunnoria pseudibex* (Fig. 5.19–5.22) with relatively specialized horncore morphology, other unnamed taxa (i.e., "Antilope gen. et sp. indet." I [Fig. 5.9–5.11], II [Fig. 5.15–5.17], III [Fig. 5.12], and IV [Fig. 5.7, 5.8]) have relatively unspecialized horncores. This rigorous classification seems to inadequately account for individual variation, especially for elucidating ontogeny. Qiu et al. (1987) considered *Qurliqnoria cheni*, and *Qurliqnoria* sp. to be the same species.

We further studied the taxonomy of all groups in this fauna based on biometric analyses. In curvature vs. mediolateral compression plane (Fig. 4.1), the sample points are distributed in three regions. *Qurliqnoria* samples cluster at the left half of the plane, which indicates straighter horncores in *Qurliqnoria* than in other taxa. In the upper right part of the plane are the *Olonbulukia tsaidamensis* samples, which include the Wuzhong specimen and Antilope gen. et sp. indet. III., and the *Tossunnoria pseudibex* samples, indicating that these taxa have curved and strongly compressed horncores. In the lower right part of the plane are samples of the other taxa. It is noticeable that Antilope gen. et sp. indet. I and IV are located at the lowest right part of the plane, which indicates relatively rounded horncores with strong curvatures.

In oblique angle vs. mediolateral compression plane (Fig. 4.2), the *Qurliqnoria* samples cluster in the right half with Antilope gen. et sp. indet. I, which indicates strongly oblique horncores. *Tossunnoria pseudibex* samples are located at the middle-upper part of the plane, indicating that the horncore oblique angle of *Tossunnoria* is intermediate between those of *Qurliqnoria* and *Olonbulukia*. Other samples are in the right part of the plane and are separated into the upper *O. tsaidamensis* and Antilope gen. et sp. indet. III, and lower *O.* sp. and Antilope gen. et sp. indet. II, which is like curvature vs. mediolateral compression plane. Also as in curvature vs. mediolateral compression plane, Antilope gen. et sp. indet. IV is in the lower left corner of the plane and is relatively distant from the *Olonbulukia* sp. and Antilope gen. et sp. indet. II samples.

Based on the biometric analysis and morphological comparison of stem caprine horncores from the 'Qaidam' and Wuzhong faunas, we recognize the following groups:

(1) *Tossunnoria pseudibex* (Fig. 5.19–5.23; SI 14, 15) shows the most specialized horncore morphology. The horncore is very short and thick (this feature is not reflected in our biometric analysis) with strong mediolateral compression.
(2) All *Qurliqnoria* specimens (Fig. 5.3–5.6, 5.18; SI 11–13) had straight horncores that are very oblique to the middle sagittal plane, which differs substantially from the other groups. We agree with the assertion of Qiu et al. (1987) that Bohlin's *Q. cheni* and *Q.* sp. represent ontogenetic or individual variation and belong to one species.
(3) Bohlin's Antilope gen. et sp. indet. III, a complete left horncore (Fig. 5.12; SI 6), can be grouped with *Olonbulukia tsaidamensis* (Fig. 5.1, 5.2, 5.13; SI 4, 5). Bohlin (1937) also stated that this horncore is very similar to that of *Olonbulukia*, and might be a young individual. This horncore

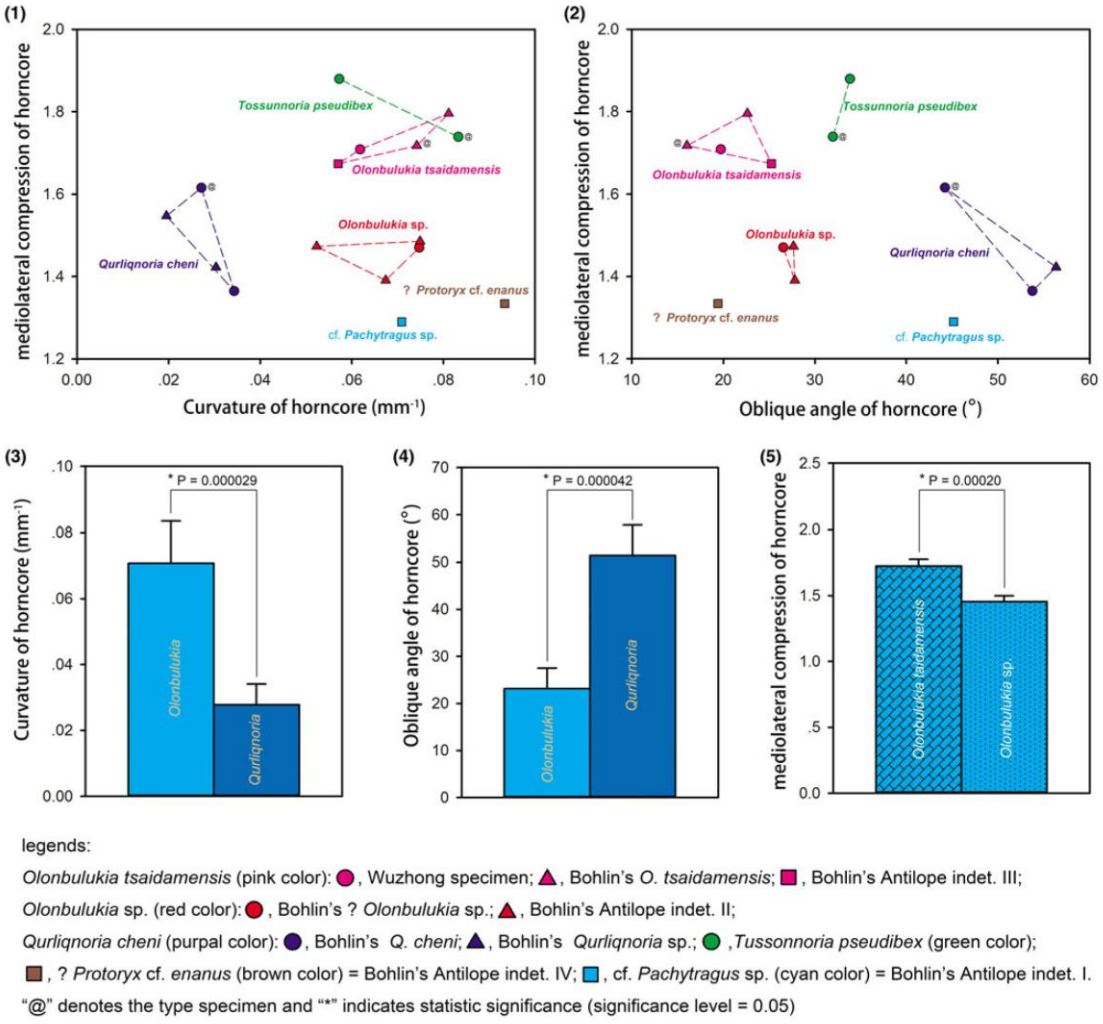

Figure 4. Biometric data and statistics of stem caprine horncores from Wuzhong and Qaidam Basin: (**1**) bivariate plot of curvature (average curvature of the anterior and posterior edges of horncore) vs. mediolateral compression (DAP/DT); (**2**) bivariate plot of oblique angle (angle between the medial sagittal plane and the vertical plane passing through the long axis of the pedicle) vs. mediolateral compression; (**3–5**) arithmetic mean (bars) and standard deviation (errors) of curvature (**3**), oblique angle (**4**), and mediolateral compression (**5**) between two groups; in addition, student's t-tests were performed on each pair.

differs from the type specimen based on the more rapid tapering and shorter pedicle. As we discussed above, the horncore elongates from the bone tissue at the tip. In this process, curvature is maintained. The shorter pedicle can also be interpreted as a younger ontogenetic stage.

(4) Bohlin's ?*Olonbulukia* sp. (Fig. 5.14; SI 7) and Antilope gen. et sp. indet. II (Fig. 5.15–5.17; SI 8–10) are similar based on biometric analysis. This group has similarly curved but less laterally compressed horncores than *Olonbulukia tsaidamensis*. The anterior keel of these horncores is relatively blunt relative to *O. tsaidamensis*. Bohlin's ? *Olonbulukia* sp. is larger than Antilope gen. et sp. indet. II. However, this difference can be interpreted as a result of ontogeny. In the present paper, we refer to this group as *Olonbulukia* sp.

(5) Bohlin's Antilope gen. et sp. indet. I (Fig. 5.9–5.11; SI 16) shows clearly distinct morphology from *Olonbulukia* and *Qurliqnoria*. The horncore oblique angle is large, close to that of *Q. cheni*, and the horncore curvature is strong and like that of *Olonbulukia.* The cross section displays an approximate round-cornered triangle (Fig. 5.11.1). A deep groove runs longitudinally along the posterior surface of the horncore. The morphology seems consistent with the diagnosis of *Pachytragus* Schlosser, 1904 from Samos, Greece (Schlosser, 1904) and is very similar to that of *P. crassicornis* Schlosser, 1904 (Schlosser,

Figure 5. Stem caprines published by Bohlin (1937), from the Qaidam Basin (photos taken on 3D digital models): (**1, 2**) *Olonbulukia tsaidamensis*, IVPP RV37008 (type specimen), brain case with both horncores, Bohlin's field no. 356 (also below), middle Miocene Olongbuluk Fauna (MMOF), in anterior (**1**) and lateral views (**2**); (**3, 4**) *Qurliqnoria cheni*, IVPP RV37100 (type specimen), both horncores with frontal remains, no. 441, late Miocene Tuosu Fauna (LMTF), in anterior (**3**) and lateral views (**4**) (the distal part of both horncores has been lost, but were figured by Bohlin, 1937, pl. 3, figs. 6, 7); (**5, 6**) *Q. cheni*, IVPP RV37102, both horncores with frontal remains, no. 508, LMTF, in anterior (**5**) and lateral (**6**) views; (**7, 8**) ?*Protoryx* cf. *P. enanus*, IVPP RV37099, right horncore with frontal remains, no. 451, MMOF, in lateral (**7**) and anterior (**8**) views, with cross section at the base (**8.1**) (anterior at top, lateral at right); (**9–11**) cf. *Pachytragus* sp., IVPP RV37104, both horncores with frontal remains, no. 492, LMTF, in anterior (**9**), lateral (**10**), and dorsal (**11**) views, with cross section at the base (**11.1**) (anterior at top, lateral at left); (**12**) *O. tsaidamensis*, IVPP RV37094, left horncore with frontal remains, no. 514, in lateral view, LMTF; (**13**) *O. tsaidamensis*, IVPP RV37093, left horncore with frontal remains, no. 429, in lateral view, LMTF; (**14**) *O.* sp., IVPP RV37095, right horncore with frontal remains, no. 423, in lateral view, LMTF; (**15**) *O.* sp., IVPP RV37096, right horncore, no. 479, in lateral view, LMTF; (**16**) *O.* sp., IVPP RV37097, right horncore with frontal remains, no. 486, in lateral view, LMTF; (**17**) *O.* sp., IVPP RV37098, left horncore with frontal remains, no. 499, in lateral view, LMTF; (**18**) *Q. cheni*, IVPP RV37101, right horncore with frontal remains, no. 491, in lateral view, LMTF; (**19–22**) *Tossunnoria pseudibex*, IVPP RV37086 (type specimen), brain case with both horncores, no. 481, in dorsal (**19**), lateroventral (**20**), ventral (**21**), and anterior (**22**) views, LMTF; (**23**) *T. pseudibex*, IVPP RV37087, fragmentary brain case with both horncores, no. 449, in anterior view, LMTF.

1904; Kostopoulos, 2005), but the specimen is smaller. Bibi and Güleç (2008) suggested that this specimen might belong to *Caprotragoides* Thenius, 1979 or *Tethytragus* Azanza and Morales, 1994. In our opinion, although the dimensions of the cross section fall into the range of the *Caprotragoides-Tethytragus-Gentrytragus* group (Bibi and Güleç, 2008, fig. 8), the subtriangular shape of the cross section and strong obliquity of horn pedicle differ from those in *Caprotragoides* and its affinities with an oval cross section and less obliquity (Köhler, 1987; Azanza and Morales, 1994; Bibi and Güleç, 2008). Because of the incompleteness of the specimen, we prefer to assign this specimen to cf. *Pachytragus* sp. rather than to *Caprotragoides* or *Tethytragus*.

(6) Bohlin's Antilope gen. et sp. indet. IV (Fig. 5.7, 5.8; SI 17), an incomplete right horncore, also displays morphology distinct from *Olonbulukia* and *Qurliqnoria*. The horncore cross section is oval (Fig. 5.8.1) and more rounded than any *Olonbulukia* and *Qurliqnoria* specimen and have more backward bending. It is also anteriorly positioned relative to the orbit. This specimen occurred in the middle Miocene Olongbuluk Fauna, which is geologically older than most of the other *Olonbulukia* samples, except for the type specimen (Fig. 6). The horncore morphology is like that of the middle Miocene *Protoryx enanus* Köhler, 1987 from western Turk (Köhler, 1987), although the generic attribution of the *P. enanus* sample has been questioned (Gentry, 2000). The cross-sectional dimensions of Bohlin's Antilope gen. et sp. indet. IV also fall into the ranges for *P. enanus* (see Köhler, 1987). Alternatively, this specimen is also like *Caprotragoides* and *Tethytragus*, but is larger. Nevertheless, Köhler (1987) considered that *T. langai* Azanza and Morales, 1994 = *C. potwaricus* (Köhler, 1987), *P. enanus*, and *P. solignaci* (Robinson, 1972) belong to the same lineage. Here, we refer this specimen to ?*P.* cf. *P. enanus* because of the sample limitations.

We performed one-way ANOVAs to test if there are statistically significant differences in the biometric data between *Olonbulukia* and *Qurliqnoria*, and species within *Olonbulukia*. The results showed that the horncore curvature and the pedicle oblique angle differed strongly and significantly between the two genera ($p < 0.05$ for both traits; Fig. 4.3, 4.4). Therefore, these two characters efficiently discriminate these two genera. Horncore mediolateral compression also strongly significantly differed between *O. tsaidamensis* and *O.* sp. ($p < 0.05$; Fig. 4.5).

Discussion

The Wuzhong specimen is the only *Olonbulukia* record aside from specimens from the type locality, the Qaidam Basin (Fig. 1). In the Qaidam Basin, the type specimen is from the middle Miocene Olongbuluk Fauna (ca. 15–12.5 Myr, see Wang et al., 2011; Fig. 6); whereas most of the other specimens are from the early late Miocene Tuosu Fauna (ca. 11–10 Myr, see Wang et al., 2011). The age of the Wuzhong Fauna is ca. 10 Ma, which corresponds to the beginning of the Ganhegou Formation (Shen et al., 2001; S.Q. Wang et al., 2016) (Fig. 6). Therefore, *O. tsaidamensis* is probably one of the earliest stem caprines (if both the attribution and dating are correct) and crossed the middle/late Miocene boundary. Another stem caprine, *Qurliqnoria cheni*, was also reported in the Wuzhong Fauna (Qiu et al., 1987). However, we did not see this specimen. The sympatry of *Olonbulukia tsaidamensis* and *Qurliqnoria cheni* indicates a close relationship of the Tuosu and Wuzhong faunas, and the age of the two faunas should be very similar. Nevertheless, mammalian fauna from ca. 10 Ma is rare in northern China (Qiu et al., 1987). Another very specialized genus from the Tuosu Fauna, *Tsaidamotherium*, was also reported from the Yangcaiping locality, Linxia Basin (Shi, 2014) (Fig. 1). This locality was attributed to the Dashenggou Fauna. Therefore, further studies should be carried out to examine whether *Olonbulukia* and/or other stem caprine genera also existed in the Wuzhong and Dashenggou faunas.

The stem caprine assemblage from the 'Qaidam' and Wuzhong faunas displays a mixed appearance. Although *Olonbulukia* seems to have no modern descendants, Gentry (2000) proposed that *Olonbulukia* could be related to *Protoryx carolinae* Major, 1891 from the Pikemi fauna (Turolian) of Greece. *Protoryx* is an unspecialized Turolian caprine that is widely distributed across eastern Europe, northern Africa, western and central Asia, and even China (Bohlin, 1935b; Gentry, 1971, 2000; Köhler, 1987; Dmitrieva and Serdyuk, 2011). Two other taxa—cf. *Pachytragus* sp. and ?*Protoryx* cf. *P. enanus*—display strong morphological similarity to the western analogues *Pachytragus crassicornis* and *Protoryx enanus* from the late and middle Miocene of the Mediterranean region (Schlosser, 1904; Köhler, 1987), which also indicates an exchange of caprine related groups between the Mediterranean and eastern Asian regions during this period. ?*Protoryx* cf. *P. enanus* might be very closely related to the ancestor of the Caprini-Hippotragini-Alcelaphini clade, because it is very similar to *Tetrytragus* and *Caprotragoides*, as discussed by Gentry (2000) and Bibi et al. (2009).

Alternatively, *Qurliqnoria* survived longer, as was reported from Kyzyl, Tuva (MN 11, 12; Dmitrieva and Serdyuk, 2011) and the Zanda Basin (MN 13–15; Deng et al., 2011; Wang et al., 2013) (Fig. 1). This genus was considered the ancestor of the extant Tibetan antelope (*Pantholops hodgsonii*) (Gentry, 1968, 2000; Deng et al., 2011). *Tossunnoria pseudibex* was also thought to be related to the extant Himalayan tahr (*Hemitragus jemlahicus*) or goats (*Capra* spp.) (Bohlin, 1937; Gentry, 2000). *Qurliqnoria* and *Tossunnoria* records are restricted to eastern Asia and the Tibetan Plateau. Therefore, the presence of *Qurliqnoria* and *Tossunnoria* from the Tuosu Fauna might indicate an early endemic radiation of stem caprines that eventually adapted the cold and dry habitats induced by the rising Tibetan Plateau.

Deng et al. (2011) demonstrated a scenario in which the Pliocene Zanda fauna on the Tibetan Plateau (Zanda Basin, Figs. 1, 6) had pre-emptively adapted to cold weather, and then expanded to the northern tundra during the Pleistocene Ice Ages. In this fauna, one taxon—*Protovis himalayensis* Wang, Xie, and Takeuchi, 2016 (5.24–3.10 Myr)—was shown to be a direct ancestor of worldwide species of *Ovis* Linnaeus, 1758 (X.M. Wang et al., 2016) (Fig. 6). Based on a calibrated molecular phylogeny, *Ovis* is the most basal taxon in the clade Caprina, which consists of at least *Ovis*, *Ammotragus* Blyth, 1840, *Pseudois* Hodgson, 1846, *Hemitragus* Hodgson, 1841, and *Capra* Linnaeus, 1758. The occurrence age of Caprina is

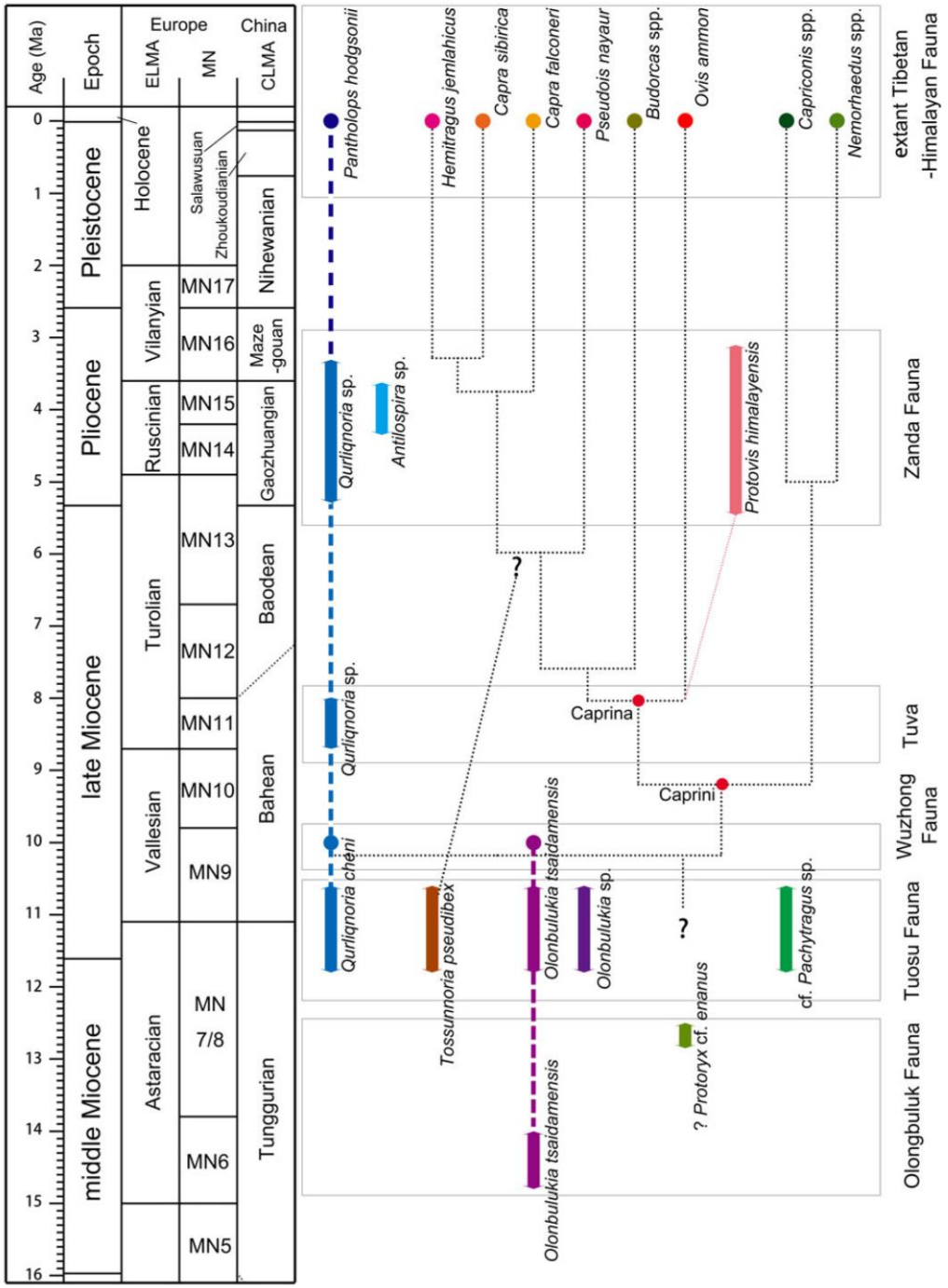

Figure 6. Stem and crown Caprini succession in the pan-Tibetan region and their possible phylogenetic relationship. Extant Tibetan-Himalayan caprines after Castelló (2016). Phylogeny and differential ages after Bibi (2013) and X.M. Wang et al. (2016). CLMA = Chinese Land Mammal Age; ELMA = European Land Mammal Age; MN = European Mammal Neogene System.

ca. 8 Ma (Bibi, 2013). Ropiquet and Hassanin (2004) demonstrated that caprines might have originated in the isolated mountains of the Mediterranean mega-archipelago; however, this is somewhat debatable. In our opinion, the Tibetan Plateau, with the formation of isolated mountainous terrains, is a more likely area for caprine origin than the Mediterranean mega-archipelago. Based on the occurrence of *Protovis* Wang, Xie, and Takeuchi, 2016 on the Tibetan Plateau, the common ancestor of Caprina could have evolved ca. 8 Ma on and/or around the rising Tibetan Plateau (except for the Indian subcontinent). The stem caprines in the Tuosu and Wuzhong faunas ca. 10 Ma provide ideal precursors of Caprina, because there are both small temporal and spatial gaps (Fig. 6). *Olonbulukia tsaidamensis* seems a bit too specialized to be the ancestor of Caprina because of the substantially compressed horncore. Although *Tossunnoria* was thought to be related to *Hemitragus* and/or *Capra*, it also displayed a specialized horncore, which weakened its potential as an ancestor of Caprina. Alternatively, nonspecialized horncores (e.g., ?*Protoryx* cf. *P. enanus*, cf. *Pachytragus* sp., and *Olonbulukia* sp. in the present study) are ideal candidates for elucidating the origin of Caprina.

According to Deng and Ding (2015), the Tibetan Plateau reached a relatively high elevation during the middle Miocene, which hindered megamammalian faunal exchange between southern and northern sides along the Tibetan Plateau. Simultaneously, a stem caprine assemblage (as we see in the 'Qaidam' and Wuzhong faunas) was shaped along the northern Tibetan Plateau and lasted until at least the early late Miocene. This stem caprine assemblage shows a composite appearance of two groups. One relatively specialized group includes at least *Qurliqnoria cheni* and *Tossunnoria pseudibex*, which are related to some endemic Tibetan taxa; the other even group perhaps includes ?*Protoryx* cf. *P. enanus* and cf. *Pachytragus* sp., possibly with *Olonbulukia* sp., pertaining to the common caprines that spread across Eurasia and Mediterranean regions in the Turolian. In particular, certain members might have given rise to the extant Caprina, which is an interesting issue and should be studied further.

Conclusions

(1) The new horncore from Jiancaichang locality, Wuzhong, northern China is similar to *Olonbulukia tsaidamensis* that also occurred in the 'Qaidam Fauna.' With the occurrence of *Qurliqnoria cheni*, the Wuzhong Fauna shows high similarity to the Tuosu Fauna and is similar in age.

(2) The stem caprine horncores from the 'Qaidam Fauna' can be divided into the following groups based on biometric analyses. *Tossunnoria pseudibex* is the same as Bohlin's definition; *Qurliqnoria cheni* includes Bohlin's *Q. cheni* and *Q.* sp.; *Olonbulukia tsaidamensis* consists of Bohlin's *O. tsaidamensis* and Antilope gen. et sp. indet. III; *Olonbulukia* sp. includes Bohlin's ?*O.* sp. and Antilope gen. et sp. indet. II; Bohlin's Antilope gen. et sp. indet. IV can be attributed to ?*Protoryx* cf. *P. enanus*; and Bohlin's Antilope gen. et sp. indet. I can be attributed to cf. *Pachytragus* sp.

(3) The stem caprine assemblages from the 'Qaidam Fauna' show a combined appearance. *Qurliqnoria* and *Tossunnoria* are probably related to some extant Tibetan endemic caprine species. Other taxa belong to other Turolian caprine species and might have given rise to the extant Caprina. These results indicate a pan-Tibetan origin of Caprina and indicate a pan-Tibetan evolutionary pattern of some megafaunas prior to dispersal from Tibet.

Acknowledgments

We thank Z. Qiu and T. Deng for useful discussion of the study. We thank M. Eckstut, from Liwen Bianji, Edanz Editing China (www.liwenbianji.cn/ac), for editing the English text of a draft of this manuscript. This work was supported by the Chinese Academy of Sciences (grant nos. XDB26000000, XDA20070203, QYZDY-SSW-DQC022), the National Natural Science Foundation of China (grant nos. 41430102, 41372001), the Natural Science Foundation of Ningxia (grant no. NZ17227), the Special Research Program of Basic Science and Technology of the Ministry of Science and Technology (grant no. 2015FY310100-14), and All China Commission of Stratigraphy Project (grant no. DD20160120-04).

Accessibility of supplemental data

Data available from the Dryad Digital Repository: http://doi.org/10.5061/dryad.736cj0j.

SI 1. *Olonbulukia tsaidamensis*, IVPP V23373, right horncore with fragmentary frontal bone remains.

SI 2. Antilopinae gen. indet. sp. indet., NGM WJCCD-10-N-006, right P3 and P4.

SI 3. Antilopinae gen. indet. sp. indet., IVPP V23374, right hemimandible with p2–m3 tooth row.

SI 4. *Olonbulukia tsaidamensis*, IVPP RV37008 (type specimen, Bolin's field number [same below], no. 356), brain case with both horncores.

SI 5. *Olonbulukia tsaidamensis*, IVPP RV37093 (no. 429), left horncore with frontal remains.

SI 6. *Olonbulukia tsaidamensis*, IVPP RV37094 (no. 514), left horncore.

SI 7. *Olonbulukia* sp., IVPP RV37095 (no. 423), right horncore with frontal remains.

SI 8. *Olonbulukia* sp., IVPP RV37096 (no. 479), right horncore.

SI 9. *Olonbulukia* sp., IVPP RV37097 (no. 486), right horncore with frontal remains.

SI 10. *Olonbulukia* sp., IVPP RV37098 (no. 499), left horncore with frontal remains.

SI 11. *Qurliqnoria cheni*, IVPP RV37100 (type specimen, no. 441), both horncores with frontal remains.

SI 12. *Qurliqnoria cheni*, IVPP RV37101 (no. 491), right horncore with frontal remains.

SI 13. *Qurliqnoria cheni*, IVPP RV37102 (no. 508), both horncores with frontal remains.

SI 14. *Tossunnoria pseudibex*, IVPP RV37086 (type specimen, no. 481), brain case with both horncores.

SI 15. *Tossunnoria pseudibex*, IVPP RV37087 (no. 449), fragmentary brain case with both horncores.

SI 16. cf. *Pachytragus* sp, IVPP RV37099 (no. 492), right horncore with frontal remains.

SI 17. ?*Protoryx* cf. *P. enanus*, IVPP RV37104 (no. 451), both horncores with frontal remains.

References

Abel, C., 1826, On the supposed unicorn of the Himalayas: Philosophical Magazine and Journal, v. 68, p. 232–234.

Azanza, B., and Morales, J., 1994, *Tethytragus* nov. gen. et *Gentrytragus* nov. gen.: deux nouveaux bovidés (Artiodactyla, Mammalia) du Miocène moyen, relations phylogénétiques des bovidés anté-vallésiens: Proceedings of the Koninklijke Akademie van Wetenschappen, v. 97, p. 249–282.

Bärmann, E.V., and Rössner, G.E., 2011, Dental nomenclature in Ruminantia: towards a standard terminological framework: Mammalian Biology, v. 76, p. 762–768, doi:10.1016/j.mambio.2011.07.002.

Bibi, F., 2013, A multi-calibrated mitochondrial phylogeny of extant Bovidae (Artiodactyla, Ruminantia) and the importance of the fossil record to systematics: BMC Evolutionary Biology, v. 13, p. 166, doi:10.1186/1471-2148-13-166.

Bibi, F., and Güleç, E.S., 2008, Bovidae (Mammalia: Artiodactyla) from the late Miocene of Sivas, Turkey: Journal of Vertebrate Paleontology, v. 28, p. 501–519, doi:10.1671/0272-4634(2008)28[501:BMAFTL]2.0.CO;2.

Bibi, F., Bukhsianidze, M., Gentry, A.W., Geraads, D., Kostopoulos, D., and Vrba, E.S., 2009, The fossil record and evolution of Bovidae: state of the field: Palaeontologia Electronica, v. 12, p. 1–10.

Blyth, E., 1840, Letter February 11: 1840 Proceedings of the Zoological Society of London, v. 1, p. 11–19.

Bohlin, B., 1935a, *Tsaidamotherium hedini*, n. g., n. sp.: Geografiska Annaler, v. 71, p. 66–74.

Bohlin, B., 1935b, Cavicorner der Hipparion-Fauna Nord-Chinas: Palaeontologia Sinica, ser. C, v. 9, p. 1–166.

Bohlin, B., 1937, Eine tertiäre Saugetier-Fauna aus Tsaidam: Palaeontologia Sinica, ser. C, v. 14, p. 1–111.

Castelló, R.J., 2016, Bovids of the World: Antelopes, Gazelles, Cattle, Goats, Sheep, and Relatives: Princeton, New Jersey, Princeton University Press, 664 p.

Chen, G.F., and Zhang, Z.Q., 2009, Taxonomy and evolutionary process of Neogene Bovidae from China: Vertebrata PalAsiatica, v. 47, p. 265–281.

Deng, T., and Ding, L., 2015, Paleo-altimetry reconstructions of the Tibetan Plateau: progress and contradictions: National Science Review, v. 93, p. 92–95, doi:10.1093/nsr/nwv062.

Deng, T., Wang, X.M., Fortelius, M., Li, Q., Wang, Y., Tseng, Z.J., Takeuchi, G.T., Saylor, J.E., Säilä, L.K., and Xie, G.P., 2011, Out of Tibet: Pliocene wooly rhino suggests high-plateau origin of ice age megaherbivores: Science, v. 333, p. 1285–1288, doi:10.1126/science.1206594.

Dmitrieva, E.L., and Serdyuk, N.V., 2011, Hippotraginae (Bovidae, Artiodactyla, Mammalia) from the late Miocene of Tuva: Paleontological Journal, v. 45, p. 665–673, doi:10.1134/S0031030111060050.

Dove, W.F., 1935, The physiology of horn growth: a study of the morphogenesis, interaction of tissues, and the evolutionary processes of a Mendelian recessive character by means of transplantation of tissues: The Journal of Experimental Zoology, v. 69, p. 347–405.

Geist, V., 1987, On the evolution of the Caprinae, *in* Lovari, S., ed., The Biology and Management of Mountain Ungulates: London, Croom Helm, p. 3–40.

Gentry, A.W., 1968, The extinct bovid genus *Qurliqnoria* Bohlin: Journal of Mammalogy, v. 49, p. 769.

Gentry, A.W., 1971, The earliest goats and other antelopes from Samos *Hipparion* Fauna: Bulletin of the British Museum (Natural History), Geology, v. 20, p. 229–296.

Gentry, A.W., 1992, The subfamilies and tribes of the family Bovidae: Mammal Review, v. 22, p. 1–32.

Gentry, A.W., 2000, Caprinae and Hippotragini (Bovidae, Mammalia) in the upper Miocene, *in* Vbra, E.S., and Schaller, G.B., eds., Antelopes, Deer and Relatives: Fossil Record, Behavioral Ecology, Systematics and Conservation: New Haven, Connecticut, Yale University Press, p. 65–83.

Gray, J.E., 1821, On the natural arrangement of vertebrose animals: London Medical Repository, v. 15, p. 296–310.

Hassanin, A., Delsuc, F., Ropiquet, A., Hammer, C., Jansen van Vuuren, B., Matthee, C., Ruiz-Garcia, M., Catzeflis, F., Areskoug, V., Nguyen, T.T., and Couloux, A, 2012, Pattern and timing of diversification of Cetartiodactyla (Mammalia, Laurasiatheria), as revealed by a comprehensive analysis of mitochondrial genomes: Comptes Rendus Biologies, v. 335, p. 32–50, doi:10.1016/j.crvi.2011.11.002.

Hodgson, B.H., 1841, Classified catalogue of mammals of Nepal, corrected to end of 1840, first printed in 1832: Calcutta Journal of Natural History, v. 2, p. 212–221.

Hodgson, B.H., 1846, Description of a new species of Tibetan antelope: Journal of the Asiatic Society of Bengal, v. 15, p. 334–343.

Janis, C.M., and Scott, K.M., 1987, The interrelationships of higher ruminant families with special emphasis on the members of the Cervoidea: Amercan Museum Novitates, v. 2893, p. 1–85.

Kingdon, J., 1982, East African Mammals: An Atlas of Evolution in Africa, IIIC: London, Academic Press, 404 p.

Köhler, M., 1987, Boviden des türkischen Miozäns (Känozoikum und Braunkohlen der Türkei) : Paleontologia i Evolució, v. 21, p. 133–246.

Kostopoulos, D.S., 2005, The Bovidae (Mammalia, Artiodactyla) from the late Miocene of Akkaşdağı, Turkey: Geodiversitas, v. 27, p. 747–791.

Lartet, É., 1837, Notice sur les ossements fossiles des terrains tertiaires de Simorre, de Sansan, etc., et sur la découverte récente d'un emâchoire de singe fossile: Comptes Rendus Hebdomaires l'Academie de Sciences, v. 4, p. 1–583.

Linnaeus, C., 1758, Systema Naturae per Regna Tria Naturae (tenth edition), Volume 1, Regnum Animale: Stockholm, Laurentii Salvii, 824 p

Major, C.I.F., 1891, Considérations nouvelles sur la faune des vertébrés du Miocène supérieur dans l'Île de Samos: Comptes Rendus Hebdomadaires des Séances de l'Académie des Sciences, Paris, v. 113, p. 608–610.

Owen, R., 1848, The Archetype and Homologies of the Vertebrate Skeleton: London, J. van Voorst, 203 p.

Qiu, Z.X., Ye, J., and Jiang, Y.J., 1987, Some mammalian fossils of Bahe Stage from Wuzhong, Ningxia: Vertebrata PalAsiatica, v. 25, p. 46–56.

Robinson, P., 1972, *Pachytragus solignaci*, a new species of caprine bovid from the late Miocene Beglia Formation of Tunisia: Notes du Service Géologique de Tunisie, v. 37, p. 73–94.

Roger, O., 1904, Wirbeltierreste aus dem Obermiozän der bayrisch-schwäbischen Hochebene, V: Bericht des Naturwissenschaftlichen Vereins für Schwaben und Neuburg, Augsburg, v. 36, p. 1–19.

Ropiquet, A., and Hassanin, A., 2004, Molecular phylogeny of caprines (Bovidae, Antilopinae): the question of their origin and diversification during the Miocene: Journal of Zoological Systematics and Evolutionary Research, v. 43, p. 49–60, doi:10.1111/j.1439-0469.2004.00290.x.

Schlosser, M., 1904, Die fossiles Cavicornis von Samos: Beiträge zur Paläontologie und Geologie Österreich-Ungarn, v. 17, p. 21–118.

Shen, X.H., Tian, Q.J., Ding, G.Y., Wei, K.B., Chen, Z.W., and Chai, C.Z., 2001, The late Cenozoic stratigraphic sequence and its implication to tectonic evolution, Hejiakouzi Area, Ningxia Hui Autonomous Region: Earthquake Research in China, v. 17, p. 156–166.

Shi, Q.Q., 2014, New species of *Tsaidamotherium* (Bovidae, Artiodactyla) from China sheds new light on the skull morphology and systematics of the genus: Science China: Earth Science, v. 57, p. 258–266, doi:10.1007/s11430-013-4722-2.

Smith, C.H., 1826–1827, The seventh order of the Mammalia: The Ruminantia, *in* Griffith, E., Smith, C.H., and Pidgeon, E., eds., The Animal Kingdom, the Class Mammalia, Arranged by the Baron Cuvier, with Specific Discriptions: London, Willian Clowes, Charing Cross, v. 4, p. 1–498.

Thenius, E., 1979, Zur systematischen Stellung und verbreitung von *Gazella stehlini* aus dem Miozän Europas: Anzeiger der Österreichische Akademie der Wissenschaften Mathematisch-Naturwissenschaftliche Klasse, v. 116, p. 9–13.

Wang, S.Q., Zong, L.Y., Yang, Q., Sun, B.Y., Li, Y., Shi, Q.Q., Yang, X.W., Ye, J., and Wu, W.Y., 2016, Biostratigraphic subdividing of the Neogene Dingjia'ergou mammalian fauna, Tongxin County, Ningxia Province, and its background for the uplift of the Tibetan Plateau: Quaternary Sciences, v. 36, p. 789–809, doi:10.11928/j.issn.1001-7410.2016.0402.

Wang, X.M., Xie, G.P., Li, Q., Qiu, Z.D., Tseng, Z.J., Takeuchi, G.T., Wang, B.Y., Fortelius, M., Rosenström, F.A., Wahlquist, H., Downs, W.R., Zhang, C.F., and Wang, Y., 2011, Early explorations of Qaidam Basin (Tibetan Plateau) by Birger Bohlin—reconciling classic vertebrate fossil localities with modern biostratigraphy: Vertebrata PalAsiatica, v. 49, p. 285–310.

Wang, X.M., Li, Q., Xie, G.P., Saylor, J.E., Tseng, Z.J., Takeuchi, G.T., Deng, T., Wang, Y., Hou, S.K., Liu, J., Zhang, C.F., Wang, N., and Wu, F.X., 2013, Mio-Pleistocene Zanda Basin biostratigraphy and geochronology, pre-Ice Age fauna, and mammalian evolution in western Himalaya: Palaeogeography, Palaeoclimatology, Palaeoecology, v. 374, p. 81–95, doi:10.1016/j.palaeo.2013.01.007.

Wang, X.M., Xie, G.P., and Takeuchi, G., 2016, Out of Tibet: an early sheep from the Pliocene of Tibet, *Protovis himalayensis*, gen. et sp. nov. (Bovidae, Caprini), and origin of Ice Age mountain sheep: Journal of Vertebrate Paleontology, v. 5, p. 1–12, doi:10.1018/02724634.2016.1169190.

Accepted: 28 June 2018

Palaeogeography, Palaeoclimatology, Palaeoecology 515 (2019) 162–171

Contents lists available at ScienceDirect

Palaeogeography, Palaeoclimatology, Palaeoecology

journal homepage: www.elsevier.com/locate/palaeo

Yunnan, a refuge for trilophodont proboscideans during the late Miocene aridification of East Asia

Shi-Qi Wang [a,b,*], Xue-Ping Ji [c], Tao Deng [a,b], Li-Ya Fu [d], Jia-Hua Zhang [d], Chun-Xiao Li [a,e], Zi-Ling He [f]

[a] Key Laboratory of Vertebrate Evolution and Human Origins of Chinese Academy of Sciences, Institute of Vertebrate Paleontology and Paleoanthropology, Chinese Academy of Sciences, Beijing 100044, China
[b] CAS Center for Excellence in Tibetan Plateau Earth Sciences, Beijing 100101, China
[c] Department of Paleoanthropology, Yunnan Institute of Cultural Relics and Archaeology, Kunming 650118, China
[d] Museum of Chuxiong Yi Nationality Autonomous Prefecture, Chuxiong 675000, China
[e] University of Chinese Academy of Sciences, Beijing 100049, China
[f] Yuanmou Man Meuseum, Yuanmou 651399, China

ARTICLE INFO

Article history:
Received 29 March 2017
Received in revised form 18 June 2017
Accepted 29 July 2017
Available online 3 August 2017

Keywords:
Biogeography
Tibetan Plateau
Paratethys Sea
Dynamics of genera
Biostratigraphy

ABSTRACT

Fossil elephantimorph proboscideans are very common in Miocene faunas of East Asia. However, their evolution and migration associated with ecological pressure have been studied little, especially in China. In the present article, analyses of the dynamics of the elephantimorph genera of northern and southern China were performed. The results indicate considerable depression of elephantimorph proboscidean diversity in northern China and continuous success of this group in the Yunnan region (southern China) during the late Miocene. Notably, all trilophodont elephantimorph proboscideans were extinct by the end of the middle Miocene in northern China and did not recover until the latest Miocene. However, trilophodont and tetralophodont elephantimorph proboscideans coexisted throughout the late Miocene in the Yunnan region. Therefore, we interpret the Yunnan region as a late Miocene refuge for proboscideans, especially trilophodonts, from severe aridity in northern China caused by uplift of the Tibetan Plateau and retreat of the Paratethys Sea. Further analysis of the dynamics of coexisting genera indicates that the components of elephantimorph proboscidean assemblages in northern China display patterns distinct from those of Yunnan/Southeast Asia and Siwalik. Therefore, ecological barriers between northern China and Siwalik and between northern China and Yunnan/Southeast Asia are hypothesized to have existed by as early as the middle Miocene. The latter barrier occasionally opened, e.g. at the boundary between the middle and late Miocene, and thus provided a pathway for the survival of trilophodont proboscideans escaping from ecological pressures in northern China.

1. Introduction

The rapid elevation of the Tibetan Plateau and the retreat of the Paratethys Sea caused by the convergence of the Indian and Eurasia plates in the Cenozoic greatly affected the climate of the Central and East Asia during the late Miocene and Pliocene, with inland desertification and establishment of the monsoon-dominated climate system (Fig. 1A) (Harrison et al., 1992; Ramstein et al., 1997; An et al., 2001; Guo et al., 2001, 2002, 2008; Zheng et al., 2004; Molnar, 2005; Zhang et al., 2007; Ge et al., 2012; Liu and Dong, 2013). As a result, continuous cooling and aridification occurred in northern China (An et al., 2001; Guo et al., 2001, 2004, 2008; Liu and Dong, 2013; Zhang et al., 2013). Deposition of loess–paleosol successions as early as ~22 Ma represents the initial stages of this change (Guo et al., 2001, 2008); while the appearance of the "*Hipparion* red clay" aged ~11 Ma (Xu et al., 2009; Deng et al., 2015a) and the prevalence of such strata from ~8 Ma (Guo et al., 2001, 2004; Zheng et al., 2004; Yue et al., 2004; Molnar, 2005) suggest the amplification of aridity in northern China. Correspondingly, biogeographic differentiation between northern and southern China began in the early Miocene, and by the late Miocene, a distinct biogeographic contrast between northern and southern China (Fig. 1A) had been established (Qiu and Li, 2005; Deng et al., 2015b). However, detailed studies of the biogeographic evolution of individual taxa, especially proboscideans, have not previously been reported.

In the late Miocene of northern China, mammalian faunas underwent dramatic turnovers. The most important faunal turnover occurred at ~11 Ma, the beginning of the late Miocene (Qiu and Qiu, 1995; Z.-X. Qiu et al., 1999, 2013; Deng, 2006; Wang et al., 2011; Deng et al., 2013). Low-crowned and short-legged middle Miocene herbivores, presumed to have lived in dense forest, were largely replaced with high-

* Corresponding author at: Institute of Vertebrate Paleontology and Paleoanthropology, Chinese Academy of Sciences, Beijing 100044, China.
E-mail address: wangshiqi@ivpp.ac.cn (S.-Q. Wang).

http://dx.doi.org/10.1016/j.palaeo.2017.07.034
0031-0182/

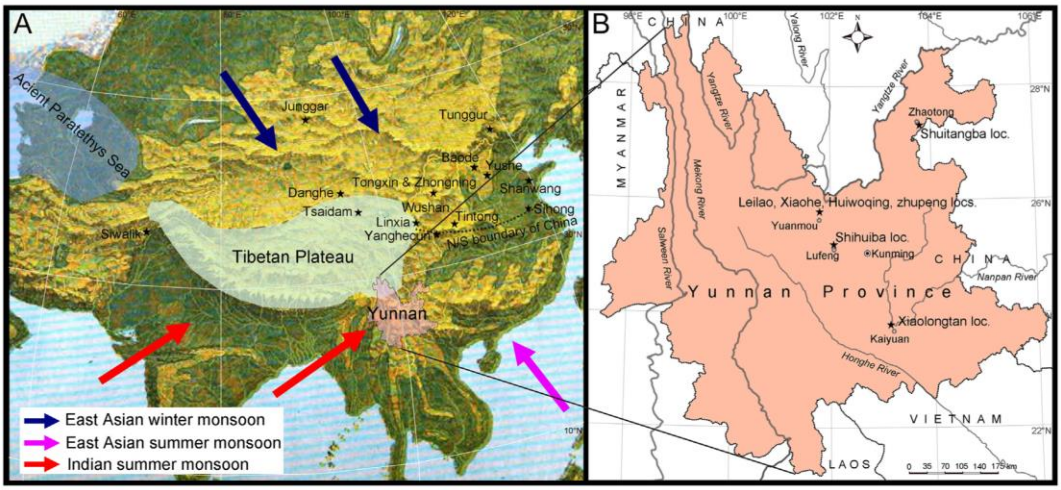

Fig. 1. Maps showing fossil localities and geographic and geoclimatic factors relevant to the present study. A, topological map of East Asia with the locations of the Tibetan Plateau and the Paratethys Sea, the relevant fossil localities (except those in Yunnan), and the major orientations of monsoons; B, map of Yunnan Province with Miocene elephantimorph fossil localities.

crowned and long-legged late Miocene members of the "*Hipparion* fauna", which indicate a savannah woodland environment, similar to that of current East Africa. For proboscideans, in this faunal turnover, tetralophodonts replaced trilophodonts in northern China (Liu et al., 1978; Deng et al., 2013; Wang et al., 2016b). As far as we know, all trilophodont taxa, including mammutids (*Zygolophodon*), gomphotheres (*Gomphotherium*), amebelodontids (*Platybelodon*), and choerolophodontids (*Choerolophodon*), were entirely extinct by the end of the middle Miocene, and two tetralophodont taxa, *Tetralophodon* aff. *xiaolongtanensis* (tetralophodont gomphotheres) from the Tsaidam Basin (Bohlin, 1937; Wang et al., 2011) and *Konobelodon robustus* (tetralophodont amebelodontids) from the Linxia Basin (Wang et al., 2016b), occurred at the beginning of the late Miocene. Trilophodont proboscideans did not recover in northern China until ~7 Ma, when *Mammut* cf. *obliquelophus* occurred at ~7 Ma (Baode and Linxia basins) (Hopwood, 1935) and *Sinomastodon praeintermedius* at ~6 Ma (Yushe Basin) (Hopwood, 1935; Flynn et al., 1991; Tedford et al., 1991; Opdyke et al., 2013; Wang et al., 2016a).

The terrestrial mammalian faunal turnover at ~11 Ma was not restricted to northern China but was a global event (Janis, 1982; MacFadden, 1992). This event seems to have been caused by a combination of both intrinsic evolutionary factors and global environmental change. For proboscideans, the replacement of trilophodonts with tetralophodonts (in gomphotheres and amebelodontids) occurred in western, central and eastern Europe, western Asia (Tassy, 1990; Göhlich, 1999), and in the Indian subcontinent (Tassy, 1983). However, only in northern China did no trilophodonts persist across the boundary between the middle and late Miocene.

For this study, we analyzed and compared the dynamics of the elephantimorph genera of northern China with those of Yunnan and the adjacent areas during the Miocene. The results indicate considerable depression of elephantimorph proboscidean diversity in northern China and continuous success of this group in the Yunnan region (Fig. 1B) during the late Miocene. Therefore, Yunnan and Southeast Asia (e.g. Thailand and Myanmar) were found to have been a refuge for proboscideans from northern China during the late Miocene aridification. Further studies should expand this analysis to other groups of mammals. However, from this study, we can infer that Yunnan and Southeast Asia played an important role as a refuge maintaining mammal diversity with continuous cooling and aridification in northern China during the late Miocene, and this strongly affected the faunal assemblage of the Pliocene.

2. Material and methods

2.1. Abbreviations

AMNH, American Museum of Natural History, New York, USA; CX, Museum of Chuxiong Yi Nationality Autonomous Prefecture, Chuxiong, China; IVPP, Institute of Vertebrate Paleontology and Paleoanthropology, Beijing, China; MN, the European Mammal Neogene-Zone; NHMW, Naturhistorisches Museum Wien, Vienna, Austria; YV, Yunnan Institute of Cultural Relics and Archaeology, Kunming, China.

2.2. Terminology and classification

The terminology of the occlusal elements of gomphotheriid cheek teeth follows Tassy (1996). The classification of elephantimorph proboscideans (Fig. 2) is mainly after Gheerbrant and Tassy (2009). Trilophodonts and tetralophodonts represent evolutionary grades, but are not formal taxonomic categories in phylogenetic meaning.

2.3. Biochronology and dynamics of genera

The biochronology of proboscideans from northern China and Yunnan were studied based on both previous data (Hopwood, 1935; Bohlin, 1937; Teilhard and Trassaert, 1937; Chow, 1959; Liu et al., 1978; Yan et al., 1983; Tobien et al., 1988; Deng et al., 2003; Wang et al., 2003, 2011) and our own researches (Wang and Deng, 2011; Wang, 2014; Wang et al., 2013, 2015a, b, c, 2016a, b, c, 2017a, b, c, d). However, several results have not yet been published. Previously published data were used for the corresponding biochronology of Southeast Asia (von Koenigswald, 1959; Chow and Zhai, 1962; Tobien, 1975; Dong, 1987; Tassy et al., 1992; Saegusa et al., 2005; Ji and Zhang, 2006; Chavasseau et al., 2009; Chavasseau et al., 2013; Ji et al., 2013; Li et al., 2015; Duangkrayom et al., 2017), and the biochronology of Siwalik is after Tassy (1983). To establish a common temporal scale with relatively high resolution, the European Mammal Neogene (MN) system was used. The starting point ages and the durations of MN intervals are after Steininger (1999). However, one change should be noted here: we subdivided the MN7/8 age into an early period and a later period, denoted "MN7" and "MN8" respectively. The approximate boundary between these intervals is at ~12.5 Ma. No mammalian fossil records from earlier than ~12.5 Ma are known from the middle Miocene of southern China (Li et al., 2015). *Tetralophodon xiaolongtanensis*, the

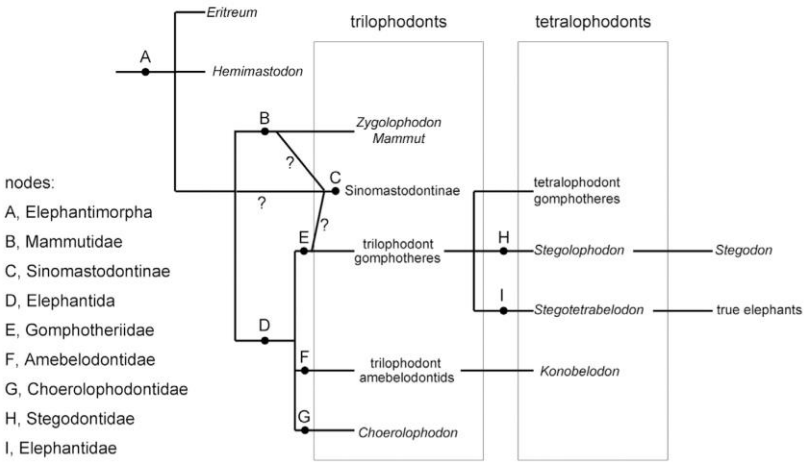

Fig. 2. Abbreviated classification of elephantimorphs, mainly after (Gheerbrant and Tassy, 2009), slightly revised.

earliest tetralophodont gomphotheres from East and Southeast Asia, occurred after ~12.5 Ma (Chavasseau et al., 2009; Li et al., 2015). Therefore, separation of MN7 and MN8 is meaningful. Results are shown in Table 1, in which the detailed explanations for each taxon in each MN are provided in on-line Supplementary material 1.

Based on the information in Table 1, we calculated the numbers of genera of elephantimorphs present in each MN unit in three areas: northern China, Yunnan/Southeast Asia, and Siwalik. The dynamics of the genera present in each area from MN4 to MN13 were then plotted. In particular, we calculated the numbers of trilophodonts and the ratios of trilophodonts to total elephantimorphs for each MN unit in each area. Furthermore, we determined which genera were common to any two areas, calculated the rates of common genera to total genera of elephantimorphs (coexistence rate) between any two areas, and plotted coexistence rate curves (to indicate the dynamics of the common genera) from MN6 to MN13.

3. Results

The elephantimorph genera in each MN unit from MN4 to MN13 were determined (Table 1) in northern China, Yunnan and Southeast Asia, and Siwalik. The Arabian–African continent was the evolutionary and spreading center of proboscideans (Kappelman et al., 2003; Sanders et al., 2004). Because of the relative proximity of Siwalik to Arabia, this area was populated by proboscideans earlier and more easily than were other areas of Eurasia. Therefore, the elephantimorphs of Siwalik were introduced as a control. However, it should be noted that the taxa listed in Table 1 do not necessarily constitute a complete list; these results are strongly affected by the precision of taxonomic identification and stratigraphic correlation, as well as by the incidence of findings. However, with the error balanced statistically, these results provide an overall view of the faunal turnover of elephantimorph proboscideans in these regions.

Table 1
Elephantimorph genera of each MN unit in northern China, Yunnan/Southeast Asia, and Siwalik. The detailed explanations for each taxon in each MN are provided in on-line Supplementary material 1.

	MN4	MN5	MN6	MN7	MN8	MN9	MN10	MN11	MN12	MN13
Northern China	**C**	**C**	**C**	**C**	**C**					
	Pr	**Pr**	**Ap**	**To?**		K	K	K		
		Pl	**Pl**	**Pl**	**Pl**					
	G	**G**	**G**	**G**	**G**	Te	Te	Pa	?Pa	An
	Sl									St
			Si	**Si**	**Si**					**Si**
			Z	**Z**	**Z**				**M**	**M**
Yunnan and Southeast Asia			**Pr?**	**Pr?**						
			G	**G**	Te	Te	?Te	Te	Te	
	Sl	Sl	Sl	Sl	Sl	Sl	?Sl	Sl	Sl	St
						?Si	**?Si**	**Si**	**Si**	**Si**
					Z	**Z**	**?Z**	**?M?**	**?M**	**?M**
								Sm?	**Sm?**	
Siwalik	**C**	**C**	**C**	**C**	**C**	**C**	**C**	**C**	**C**	**C?**
			Pr	**Pr**	**Pr**	K?	K?	K		
	G	**G**	**G**	**G**	**G**	?Te	?Te	Pa	Pa	Pa?
								An	An	An?
			Sl	Sl	Sl	?Sl	?Sl	Sl	Sl	St
			Si	**Si**	**Si**					
			Z	**Z**	**Z**	**Z**	**?Z**	**M?**	**M?**	**?M?**
										E

Abbreviations: An, *Anancus*; Ap, *Aphanobelodon*; C, *Choerolopodon*; E, Elephantidae, indet.; G, *Gomphotherium*; K, *Konobelodon*; M, *Mammut*; Pa, *Paratetralophodon*; Pl, *Platybelodon*; Pr, *Protanancus*; Si, *Sinomastodon* or sinomastodontines; Sl, *Stegolophodon*; Sm, *Sinomammut*; St, *Stegodon*; Te, *Tetralophodon*; To, *Torynobelodon*. Bold fonts represent trilophodont taxa. The front "?" indicates that the presence of this taxon is postulated (i.e. the same taxon or a director ancestor/descendant is present in both the preceding and subsequent ages), or indicates that this taxon is undetermined. The hind "?" indicates that the age of this taxon is postulated.

Based on the information in Table 1, we plotted the numbers of genera present from MN4 to MN13 in these three areas (Fig. 3A). The diversity (in terms of the number of genera) dramatically increased between MN5 and MN6 in all three areas (Fig. 3A). In this period, all of these proboscideans except for *Stegolophodon* were trilophodont elephantimorphs. Across the boundary between the middle and late Miocene, the diversity (number of genera) in Siwalik, used as a control, was almost invariable (although genus compositions changed dramatically). The diversity of elephantimorphs in northern China declined dramatically, however. It is notable that elephantimorph diversity increased in Southeast Asia; this phenomenon indicates a continuously warm and humid environment and also suggests inflow of elephantimorphs into this area, as discussed below.

The fate of trilophodont elephantimorphs was also evaluated (Fig. 3C–E). Prior to MN9, trilophodont elephantimorphs comprised almost 100% of elephantimorphs in northern China, except for the occasional occurrence of *Stegolophodon* in MN4 in Sihong (migrated from southern China). However, after MN9, the percentage of trilophodont elephantimorphs dropped to zero. As mentioned above, the trilophodont/tetralophodont replacement event occurred at the boundary of the middle and late Miocene. Only after MN12 did the trilophodont component of the elephantimorph assemblage partially recover (Fig. 3C). In Siwalik, the percentage of trilophodont elephantimorphs declined continuously. Replacement of trilophodonts with tetralophodonts also occurred in this region between MN8 and MN9 but not as suddenly as in northern China (Fig. 3E). However, in Yunnan/Southeast Asia, the ratio of trilophodont elephantimorphs did not decline greatly at this boundary and increased slightly during the late Miocene until it reached the same level as that of the middle Miocene (Fig. 3D).

To further investigate the migration of elephantimorphs between northern China and Southeast Asia, we enumerated the genera from MN6 to MN13 that coexisted in any two of the three areas. The results are provided in Table 2. Based on these results, we calculated the coexistence rate of elephantimorph genera between regions (Fig. 3B). Interestingly, the resemblance of elephantimorph assemblages between Siwalik and Yunnan (Southeast Asia) indicated by the coexistence rate curve maintains a high level throughout the entire Miocene, which indicates intensive faunal exchange between these two regions. The resemblance of these faunal components between Siwalik and northern China is high in the middle Miocene but drops dramatically after MN9 and does not recover until the latest Miocene (MN13). However, the resemblance between elephantimorph genera of northern China and Yunnan remains very low, except in the latest Miocene.

4. Discussion

4.1. Trilophodonts and tetralophodonts, evolutionary grades and their ecological adaptations

In the present paper, we use the terms trilophodonts (= trilophodont elephantimorphs) and tetralophodonts (=tetralophodont elephantimorphs) (Fig. 2). These terms only indicate the evolutionary grades, rather than natural groups. In Eurasia, most of the early elephantimorphs are trilophodonts, including Mammutidae, Choerlophodontidae, Gomphotheriidae, and Amebelodontidae. These trilophodonts were presumably forests dwellers and feed as browsers or, at most, mixed feeders (Fox and Fisher, 2004; Calandra et al., 2010; Semprebon et al., 2016). Tetralophodonts evolved within Amebelodontidae, Gomphotheriidae, and Stegodontidae. In the former two groups, tetralphodonts largerly or totally replaced trilophodonts mainly by the end of middle Miocene in Eurasia, although the earliest tetralophodont gomphothere might appear as early as in MN6 (Tassy, 1985). Here we denote tri−/tetralophodont (in amebelodontids and gomphotheres) replacement event. This replacement event may be urged by the ecological pressure induced by the global climate change as continuous colding and drying beginning at the late middle Miocene (~14 Ma) (Zachos et al., 2001). Tetralophodonts seems to possess better

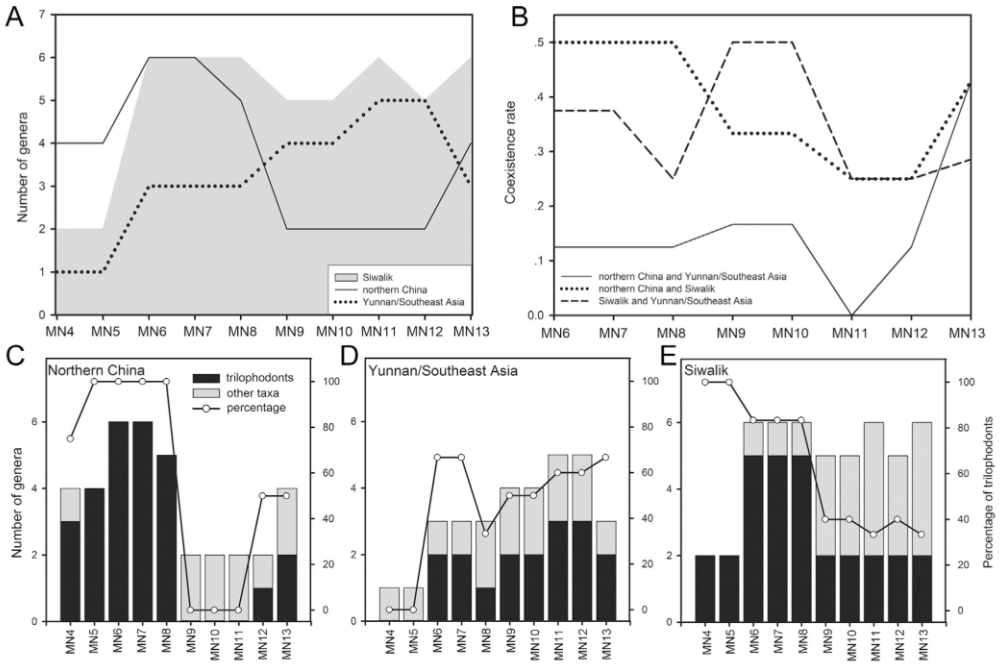

Fig. 3. Histograms for comparisons of elephantimorph turnover throughout the Miocene in northern China, Yunnan/Southeast Asia, and Siwalik. A, numbers of elephantimorphs genera present from MN4 to MN13; B, coexistence rates between regions from MN6 to MN13; C–E, dynamics of trilophodont genera present compared with total genera and percentage of trilophodonts from MN4 to MN13.

Table 2
Coexisting genera of elephantimorphs from MN6 to MN13 between northern China, Yunnan/Southeast Asia, and Siwalik.

	MN6	MN7	MN8	MN9	MN10	MN11	MN12	MN13
Northern China and Yunnan (Southeast Asia)	**G**	**G**	**Z**	Te	?Te		**?M**	**?M**
								Si
								St
Yunnan (Southeast Asia) and Siwalik	**G**	**G**		?Te	?Te			
	Pr?	**Pr?**	**Z**	**Z**	**?Z**	**M?**	**M?**	**M?**
	Sl	Sl	Sl	?Sl	?Sl	Sl	Sl	St
Northern China and Siwalik	**C**	**C**	**C**	K?	K?	K		
	G	**G**	**G**	?Te	?Te	Pa	?Pa	?An
	Si	**Si**	**Si**					St
	Z	**Z**	**Z**				**M?**	**M?**

Abbreviations: see Table 1.

adaptability for more hash and more abrasive foods than trilophodonts. Logically, one more loph(id) in each cheech teeth withstands more weathering of the teeth. Furthermore, the true elephantids, which shows great adaptability for cold and dry environments in the Ice Age, were derived from tetralophodont gomphotheres (Maglio, 1973). The opposite case is *Stegolophodon*, the tetralophodont stegodonts, which occurred earlier (early Miocene in Southeast Asia) than the other tetralophodonts (Saegusa, 1996). However, it might only live in warm and humid environments, as the tooth crowns are pronounced brachyodont (Tassy et al., 1992). Finally, mammutids and choerolophodontids never evolved to the tetralophodont grade. They were never very aboundant in species and population, and may live in forests or even have semi-aquatic habits (Saunders, 1996; Pickford, 2005).

4.2. Role of *Serridentinus gobiensis* Osborn and Granger, 1932 and its relatives

Serridentinus gobiensis was first described by Osborn and Granger (1932) based on a right dentary with complete symphysis and mandibular tusks (Fig. 4A, B, E, S1A, B, E). The type locality is the middle Miocene Tunggur Formation of Zhuwuguer, Tunggur, northern China, which has been dated at ~12.4–11.6 Ma (Wang et al., 2003). Tobien (1972) attributed this specimen to the genus *Zygolophodon*. In the type specimen of "*Serridentinus gobiensis*", the straight ventral border and ventrally bulging mandibular angle (Fig. 4A) look more like those of a mammutid (Tobien, 1972). However, the anterior and posterior pretrite central conules of the molars (Fig. 4E) are not thin-crest-like, as is typical of *Zygolophodon turicensis*, and the posttrite half-lophids are not greatly anteroposteriorly compressed to show a cutting edge. Therefore, attribution of "*Serridentinus gobiensis*" to *Zygolophodon* is in doubt. For similar reasons, attribution of "*Serridentinus metachinjiensis* Osborn, 1929" from Siwalik to *Zygolophodon* (Tassy, 1983), and more broadly, "the robust type of *Zygolophodon turicensis*", is likewise in doubt. Detail comparison of "the robust type of *Zygolophodon turicensis*" and the "true *Zygolophodon*" are provided in on-line Supplementary material 2.

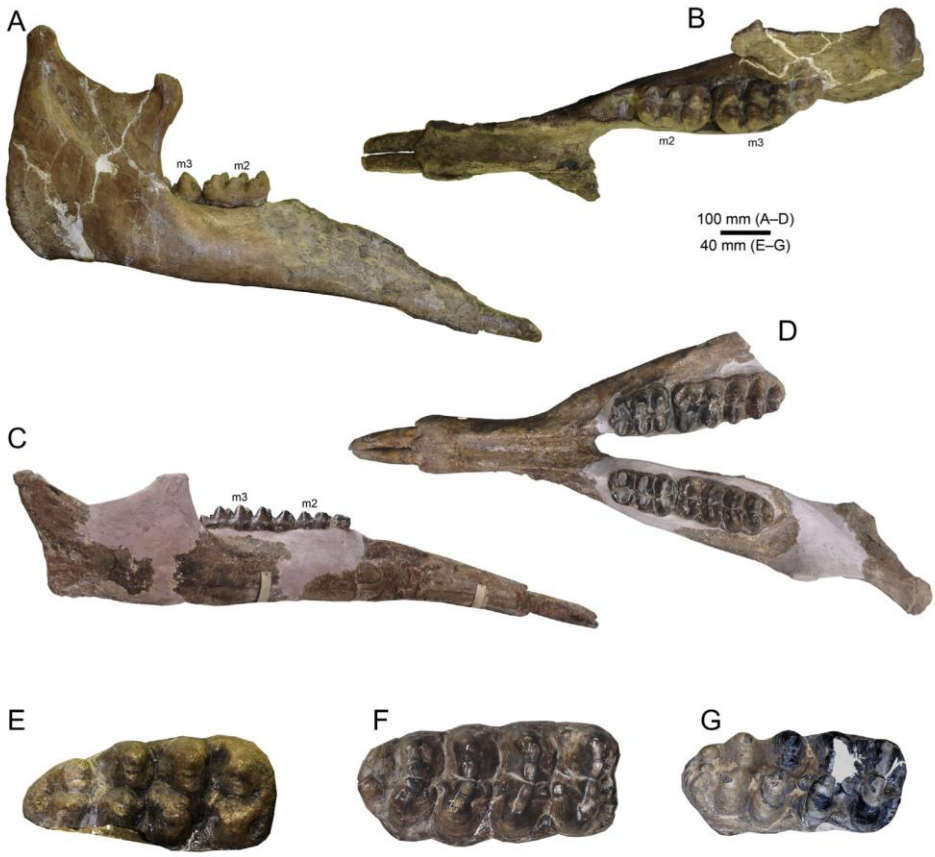

Fig. 4. Mandibles and teeth of sinomastodontines. A, B, and E, AMNH 26461, the type specimen of "*Seridentinus gobiensis*", from the Zhunwuguer locality, Tunggur region, the mandible in lateral (A) and dorsal (B) views, and the right m3 in occlusal view (E); C, D, and F, CX C1134ZA94, mandible of "*Zygolophodon gobiensis*" from the Huiwoqing locality, Yuanmou Basin, in lateral (C) and dorsal (D) views, and the left m3 (horizontally reversed) in occlusal view (F); G, YV ZY-00025, *Sinomastodon praeintermedius*, right m3 in occlusal view, from the Shuitangba locality, Zhaotong Basin.

Zong (1997) described "*Zygolophodon gobiensis*" from the Huiwoqing locality (possibly correlated to ~MN11) (Fig. 4C, D, F) of the late Miocene Yuanmou Basin, Yunnan (southern China), based on a nearly complete mandible. This mandible is very similar to the type mandible of "*Serridentinus gobiensis*", especially its moderately elongated symphysis and the closely apposed pair of mandibular tusks with a subcircular cross-section (Fig. 4B, D). The tooth morphology of the Huiwoqing specimen is very similar to the type specimen of "*Serridentinus gobiensis*", except the tendency of increasing lophid number in m3. We suggest that the Huiwoqing specimen can be attributed to the same genus as the type mandible of "*Serridentinus gobiensis*" (and "*Serridentinus metachinjiensis*") but not necessarily to the same species.

Wang et al. (2016a) described the cranium of *Sinomastodon praeintermedius* from the Shuitangba locality of the late Miocene Zhaotong Basin, Yunnan, with an age ~ 6.5–6.0 Ma. In comparing the morphology of the lower cheek teeth, we observe strong similarity between the Huiwoqing "*Zygolophodon gobiensis*" and *Sinomastodon praeintermedius* (Fig. 4F, G). The teeth of both specimens show intermediate morphology between zygodonty and bunodonty. The anterior and posterior pretrite central conules are thick-crest-like, and the posttrite half-lophids are moderately subdivided. Only is the crown hight of the latter slightly higher. Therefore, *Sinomastodon praeintermedius* may have evolved directly from the form of "*Zygolophodon gobiensis*" from the Huiwoqing locality. All of these taxa should be ascribed to Sinomastodontinae Wang et al., 2012, but further study of this problem exceeds the scope of this article. Nevertheless, we identified a unique pattern of migration and evolution for this elephantimorph proboscidean group, from the middle Miocene "*Serridentinus gobiensis*" of northern China to the late Miocene "*Zygolophodon gobiensis*" of southern China, and finally to the latest Miocene *Sinomastodon praeintermedius* and early Pliocene *Sinomastodon intermedius* of northern and southern China. In this article, we simply use the term sinomastodontines to denote "*Serridentinus gobiensis*", "*Serridentinus metachinjiensis*", and "*Zygolophodon gobiensis*" from the Huiwoqing locality.

4.3. Turnover of elephantimorphs in the Miocene of northern China

Both the rapid elevation of the Tibetan Plateau and the retreat of the Paratethys Sea contributed to aridification and the establishment of the monsoon-dominated climate system in East Asia during the Miocene–Pliocene (Harrison et al., 1992; Ramstein et al., 1997; An et al., 2001; Molnar, 2005; Zhang et al., 2007; Guo et al., 2008; Sun et al., 2010; Liu and Dong, 2013). Three temporal points in the Miocene are notable: ~22 Ma, ~11 Ma, and ~8 Ma. The date ~22 Ma represents the emergence of the East Asian monsoon and the beginning of aridification, as revealed by the loess–paleosol succession of the Qinan section (Guo et al., 2002, 2008). The date ~11 Ma, which approximately corresponds to the boundary between the middle and late Miocene, represents the enhancement of the aridification and monsoon system, as reflected by the occurrence of the aeolian records of the *Hipparion* red clay in several localities of northern China (Xu et al., 2009), and by records from the North Pacific (Rea et al., 1998). The date ~8 Ma represents the intensity of the monsoon system, which corresponds to extensive occurrences of the *Hipparion* red clay in northern China (Guo et al., 2001, 2004; Zheng et al., 2004; Yue et al., 2004; Molnar, 2005).

Determining the extent to which climate evolution affects faunal turnover is an interesting problem. During the Miocene in northern China, these two elements did not fully match. Based on precisely dated events, the proboscideans reached northern China around 21 Ma, as represented by cf. *Gomphotherium* from the Nanyu section, Wushan region (unpublished data), which is located very close to the Qinan section. This invasion event was followed by occurrences of *Choerolophodon* and *Protanancus* (Wang and Deng, 2011; Wang et al., 2015a) recorded from ~MN4 in the Dalonggou section. *Zygolophodon* and sinomastodontines of the same age may occur in northern China, but proboscidean records from the early Miocene are rare in any region. All of these taxa are trilophodonts. However, one tetralophodont taxon, *Stegolophodon hueiheensis*, occurred in MN4 in Sihong (Chow, 1959). This taxon may have migrated from southern China, because records of *Stegolophodon* are abundant in Southeast Asia throughout MN3 to MN13 of the Miocene (von Koenigswald, 1959; Tobien, 1975; Tassy et al., 1992; Chavasseau et al., 2009; Chavasseau et al., 2013; Wang et al., 2015c). This occurrence also represents the first exchange of elephantimorphs between northern and southern China. During the middle Miocene, the diversity of elephantimorphs increased dramatically, especially for amebelodontids, with the occurrences of *Platybelodon*, *Aphanobelodon*, and *Torynobelodon* (Wang et al., 2013, 2017a). This radiation was not confined to elephantimorph proboscideans; it also occurred among other large mammalian groups. Evidence of this event can be observed in outcrops of many regions of northern China, e.g. in the Junggar, Tunggur, Tongxin, Linxia, and Tintong areas (Qiu and Qiu, 1995; Qiu et al., 1999; Ye et al., 2012; Deng et al., 2013; Deng, 2016; Wang et al., 2016c). This event clearly corresponded to the Mid-Miocene Optimum (Zachos et al., 2001; Deng, 2016). The warm and humid environment of this interval promoted the rapid radiation of proboscideans. In this period, trilophodont elephantimorphs were dominant, and no tetralophodont taxa of this age have been reported from northern China.

A dramatic faunal change occurred at the boundary between the middle and late Miocene (Qiu and Qiu, 1995; Z.-X. Qiu et al. 1999, 2013; Deng, 2006; Wang et al., 2011; Deng et al., 2013). This change is herein denoted the tri−/tetralophodont replacement event. Three trilophodont taxa, *Choerolophodon*, *Zygolophodon*, and sinomastodontines, became extinct, and two trilophodont genera, *Platybelodon* and *Gomphotherium*, were replaced with corresponding tetralophodont taxa, *Konobelodon* and *Tetralophodon*, respectively. The latter is represented by *T.* aff. *xiaolongtanensis* from the Tsaidam Basin (Bohlin, 1937; Wang et al., 2011). This species is probably migrated from Yunnan, as *T. xiaolongtanensis* occurred at the latest middle Miocene in Yunnan (Dong, 1987; Li et al., 2015). The tri−/tetralophodonts replacement event also occurred in other areas of Eurasia (Tassy, 1983, 1990; Göhlich, 1999), therefore, this event may have been driven by intrinsic evolutionary causes. However, the amplification of aridification at ~11.6 Ma in northern China (Rea et al., 1998) may have severely affected the local elephantimorphs and enhanced the effect of the tri−/tetralophodonts replacement event. None of the trilophodont genera persisted across the middle/late Miocene boundary, as far as we know.

The aeolian *Hipparion* red clay was widespread in northern China by ~8 Ma, which has led to the conclusion that the aridification of northern China strengthened dramatically at this time (Guo et al., 2001, 2004; Zheng et al., 2004; Yue et al., 2004; Molnar, 2005). However, the evidence of faunal turnover in northern China does not seem to support this conclusion. Abundant murids from Lingtai, as well as deer and moschids from Baode, Yushe, and Huade indicate a relatively humid environment (Qiu, 1979; Flynn et al., 1991; Tedford et al., 1991; Zheng and Zhang, 2000; Yue et al., 2004). For elephantimorphs, a pronounced event is the recovery of trilophodonts: the occurrence of *Mammut* and *Sinomostodon*. Recent studies indicate that the East Asian summer monsoon strengthened at ~8–7 Ma in northern China, which resulted in a relatively humid steppe–forest environment (Li et al., 2008). The strengthening of the Indian summer monsoon may also have contributed to this climatic change (Zheng et al., 2004). Wang et al. (2016a) demonstrated the northward migration of *Sinomostodon* and stegodontids from Yunnan to northern China in the latest Miocene. *Mammut* may have migrated into northern China (Hopwood, 1935; Tobien et al., 1988) via paths along the northern side of the Tibetan Plateau, along with *Paratetralophodon* and *Anancus*, as indicated by the occurrence of *M. obliquelophus* at several ~MN11–MN12 localities in Eurasia (Markov, 2008). However, the possibility that *Mammut* migrated from Yunnan/Southeast Asia cannot be excluded.

4.4. Turnover of elephantimorphs in the Miocene of Yunnan/Southeast Asia

In southern China, the climate remained warm and humid throughout the entire Miocene because of the dominant summer monsoon produced by the elevation of the Tibetan Plateau (Zheng et al., 2004). However, Tertiary deposits are rare in southern China, except in Yunnan Province. Even in Yunnan, fossil records of the early and middle Miocene are absent, except for the Xiaolongtan Formation, of which the deposition began in the latest middle Miocene (Li et al., 2015). In the adjacent areas of Southeast Asia, e.g. Thailand and Myanmar, fossil records from the early and middle Miocene are also sparse (Chavasseau et al., 2009; Chavasseau et al., 2013). Therefore, we know little about early and middle Miocene elephantimorphs in this region. Nevertheless, *Stegolophodon nasaiensis*, the most primitive *Stegolophodon*, has been reported from the early Miocene of Thailand (Tassy et al., 1992). *Stegolophodon* is the earliest known tetralophodont and is believed to have originated from this area and spread to other regions (Saegusa, 1996; Wang et al., 2015c). Records from the middle Miocene of Thailand indicate the existence of *Protanancus*, which may have migrated directly from Siwalik (Saegusa et al., 2005). *Gomphotherium* cf. *browni* has also been recorded from strata that may have been deposited at the same time (Chavasseau et al., 2009). In MN8 of the latest middle Miocene, a true tetralophodont, *Tetralophodon xiaolongtanensis*, occurred in Xiaolongtan (Dong, 1987; Tobien et al., 1988; Li et al., 2015), and *T.* cf. *xiaolongtanensis* also occurred in Thailand (Chavasseau et al., 2009). The presence of *Zygolophodon* in Xiaolongtan (Chow et al., 1978) is the earliest record of a mammutid in this region. *Zygolophodon* of Xiaolongtan may have migrated from northern China, because both the Xiaolongtan specimens and the northern Chinese *Zygolophodon* have relatively small pretrite mesoconelets, which may represent inherent morphological similarity (Tobien et al., 1988). Duangkrayom et al. (2017) reported *Zygolophodon* from Thailand, which may represent the southernmost distribution of *Zygolophodon* in Eurasia. The morphology of *Zygolophodon* from Thailand is very similar to that of *Zygolophodon* from Xiaolongtan.

Sinomastodontines may also occur in this region by the end of middle Miocene, although explicit fossil records of this arrival have not been discovered. There are several hypotheses on the occurrence of sinomastodontines in Yunnan region. One is that they immigrated from northern China, as descendants of "*Serridentinus gobiensis*". Alternatively, sinomastodontines immigrated from Siwalik, derived from "*Serridentinus metachinjiensis*". Or more extendedly, sinomastodontines may has a pan-Asian distribution during MN6–MN8 and persisted in Yunnan area during the Late Miocene. However, "*Serridentinus metachinjiensis*" shows less similarity to "*Serridentinus gobiensis*" and the Huiwoqing specimen than that between the latter two, because the distal ends of the posterior pretrite central conules are more inflated, and the posttrite half lophids are more subdivided in both "*Serridentinus gobiensis*" and the Huiwoqing specimen than those in the Siwalik "*Serridentinus metachinjiensis*". Furthermore, sinomastodontines have also not been discovered from the middle Miocene of Yunnan and Southeast Asia. For these two reasons, we preferred the assumption that sinomastodontines in the late Miocene of Yunnan were migrated from northern China. If this hypothesis is true, the southward migrations of *Zygolophodon* and sinomastodontines may have been affected by the ecological pressure of aridification in northern China.

In the late Miocene of Yunnan, although fossil records remain incomplete (with MN10 missing and MN11 rare), elephantimorphs were very abundant. In the Xiaohe Formation of the Yuanmou Basin (~MN12), *Tetralophodon xiaolongtanensis* was replaced with *T. xiaoheensis*, a more derived taxon (Ji and Zhang, 2006). A highly derived *Stegolophodon*, *S. stegodontoides*, has also been reported (Wang et al., 2015c). These two taxa may also occur in the slightly higher Shihuiba Formation of the Lufeng region. Another taxon of interest from the Xiaohe Formation is "*Zygolophodon gobiensis*", which has been ascribed to Sinomastodontinae in the present article. Compared with the contemporary *Mammut obliquelophus* from the north, "*Zygolophodon gobiensis*" is characterized by rather bunodont cheek teeth and longer mandibular symphysis. Meanwhile, *Sinomammut*, a very rare and peculiar mammutids (Mothé et al., 2016) discovered from the boundary of northern and southern China (Yanghecun locality), may exist in Bahean age of MN11 or MN12 (Wang et al., 2014). Furthermore, in the Zhaotong Formation (MN13), "*Zygolophodon gobiensis*" was replaced with the presumed brevirostine *Sinomastodon praeintermedius*, and *Stegolophodon stegodontoides* with the true stegodont *Stegodon zhaotongensis* (Saegusa, 1996; Saegusa et al., 2005; Ji et al., 2013; Jablonski et al., 2014; Wang et al., 2016a). These two groups also invaded northern China in this interval and continued to flourish in the Pliocene of Yunnan. *Mammut* was also present in the Shihuiba Formation to the Zhaotong Formation (Wang et al., 2016a), but these fossils are very rare. Records of *Mammut* from the Pliocene have not yet been discovered.

4.5. Migration of elephantimorphs between northern China, Yunnan/Southeast Asia, and other regions

A rather isolated pattern of elephantimorph components in northern China compared with the two adjacent areas is indicated by the coexistence curves (Fig. 3B). Here, we hypothesize the existence of barriers between northern China and Southeast Asia, and between northern China and Siwalik, which obstructed proboscidean migration (Fig. 5).

Two types of barriers, geographical and environmental barriers, contributed to faunal isolation (MacFadden, 1992). Both types were absent between Siwalik and Southeast Asia, where elephantimorph resemblance persisted continuously between the two areas (Fig. 5). The exchange of elephantimorph proboscideans between Siwalik and northern China is unclear because relevant fossil records are sparse (Fig. 5A). However, the elevation of the Tibetan Plateau between these two areas strongly affected faunal exchange. Evidence has been reported that at least in the middle Miocene, the Tibetan Plateau had reached a relatively high level, which prevented faunal exchange between these two regions (Deng et al., 2015b; Deng and Ding, 2015). *Choerolophodon*, *Gomphotherium*, *Zygolophodon*, and sinomastodontines may have arrived in these two regions in the early Miocene, and then evolved independently (Fig. 5A). It is notable that *Platybelodon*, which flourished in the middle Miocene of northern China and fully replaced the native *Protanancus* (Wang et al., 2015a), never reached Siwalik (Deng and Ding, 2015) (Fig. 5B). Therefore the barrier between northern China and Siwalik was established by the middle Miocene (Fig. 5B). In the late Miocene, because the Tibetan Plateau had reached a high latitude, the exchange of elephantimorph proboscideans was entirely blocked, and the occurrences of *Paratetralophodon*, *Anancus* and *Mammut* in northern China may have migrated via paths along the northern Tibetan Plateau (Fig. 5C).

Although no geographic blockage existed between northern and southern China, the resemblance of elephantimorph genera between these two areas remained low (Fig. 3B). An environmental barrier seems to have persisted throughout most of the Miocene but opened occasionally. It is unknown if this barrier was already established in the early Miocene. However, *Stegolophodon*, at least, is known to have entered northern China (Fig. 5A) and reached Japan (Saegusa, 1996; Saegusa et al., 2005). *Stegolophodon* was soon extinct in northern China as the barrier became established during the middle Miocene. The first opening of this barrier may have occurred in MN8–MN9; sinomastodontines and *Zygolophodon* may have migrated from northern China (Fig. 5B), as discussed above. It should be noted that *Tetralophodon* aff. *xiaolongtanensis* occurred in the Tsaidam Basin of northern China and may have migrated directly from Yunnan (Fig. 5B). The unexpected occurrence of the only deinothere from the earliest late Miocene of the Linxia Basin of northern China (Qiu et al., 2007),

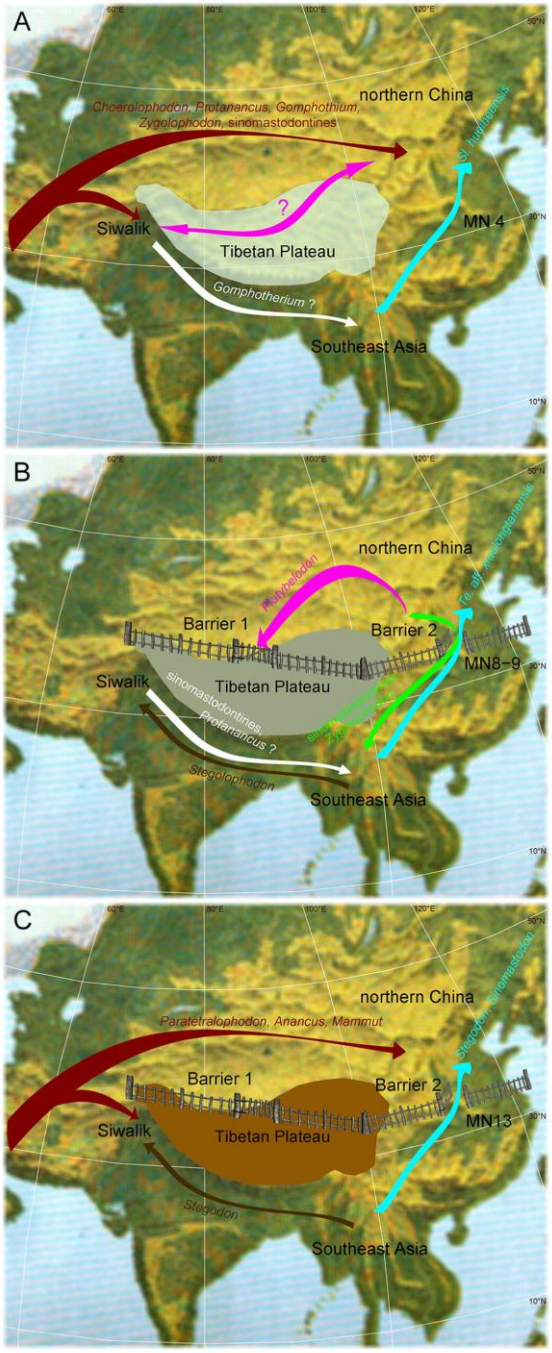

Fig. 5. Schematic maps showing the migrations of elephantimorphs between northern China, Southeast Asia, and other regions in the early (A), middle (B), and late (C) Miocene. Hypothetical barriers between northern China and Southeast Asia (barrier 1) and between northern China and Siwalik (barrier 2) are marked on panels B and C. Note the discontinuous opening of barrier 2.

Prodeinotherium sinense, may also have migrated this way, but this hypothesis should be investigated further. The second opening of this barrier may have occurred in MN13 of the latest Miocene, as discussed by Wang et al. (2016a). As the summer monsoon strengthened, northern China became more humid than it was throughout most of the late Miocene (Li et al., 2008), and *Stegodon* and *Sinomastodon* invaded northern China during this time (Fig. 5C). However there seems to have been no southward migration of elephantimorphs, because *Anancus* has not yet been discovered in the latest Miocene or early Pliocene of Yunnan. Overall, Yunnan (and Southeast Asia) functioned as a refuge for elephantimorphs from northern China. It accommodated relict trilophodont elephantimorphs, i.e. *Zygolophodon* and sinomastodontines, during the severe aridification that occurred in the late Miocene in northern China, and from there, *Stegodon* and *Sinomastodon* migrated to northern China. In the early Pleistocene, with the onset of glaciation, this refuge again enabled the survival of *Stegodon* and *Sinomastodon* (Wang et al., 2016a).

5. Conclusions

In this study, we interpreted that Yunnan and Southeast Asia played a role as a refuge for elephantimorphs from northern China during aridification in the late Miocene. Because of the severe aridification of northern China that began in the late Miocene, all trilophodont proboscideans were extinct in this region by the end of the late Miocene, and tetralophodont proboscideans dominated for most of the late Miocene. However, trilophodont proboscideans coexisted with tetralophodonts throughout the late Miocene in southern China, where the environment remained warm and humid. Therefore, we proposed that an environmental barrier was present between northern and southern China and resulted in low resemblance of genus compositions between the two regions during the entire Miocene. This barrier opened at least twice in the Miocene, which enabled exchange of taxa between northern China and Yunnan, such as the migration of *Zygolophodon* and sinomastodontines to the south and of *Tetralophodon* to the north at the boundary between the middle and late Miocene, and of *Stegodon* and *Sinomastodon* to the north in the latest Miocene.

Acknowledgments

We thank J. Meng, AMNH, USA for preparation of the comparative material. We thank Cheng-Long Deng, Yi-Kun Li, Xiu-Xi Wang, China, for discussions of the chronostratigraphy. We thank Jie Ye, Su-Kuan Hou, Qin-Qin Shi, Bo-Yang Sun, Yu Li, Xiang-Wen Yang, IVPP, China, for attending the field works. We thank Edanz Editing China for the improvement of English. This work was supported by the Chinese Academy of Sciences (Grant No. XDPB05), the National Natural Science Foundation of China (Grant Nos. 41372001, 41430102), the Key Research Program of Frontier Sciences, CAS (no grant number), the Special Research Program of Basic Science and Technology of the Ministry of Science and Technology (Grant No. 2015FY310100-14), the Yunnan Natural Science Foundation (2010CC010), and the Program of Reset of the Human Origin in Chuxiong Yi Nationality Autonomous Prefecture (no grant number).

Conflict of interest

The authors declare that they have no conflict interests.

Author contributions

S.-Q.W. and T.D. designed the study; C.-X.L. conducted the analysis; S.-Q.W., X.-P.J., and T.D. studied the biostratigraphy; all authors except T.D. and C.-X.L. studied the specimens; S.-Q.W. wrote the paper.

Appendix A. Supplementary data

Supplementary data to this article can be found online at http://dx.doi.org/10.1016/j.palaeo.2017.07.034.

References

An, Z.-S., Kutzbach, J.E., Prell, W.L., Porter, S.C., 2001. Evolution of Asian monsoons and phased uplift of the Himalaya-Tibetan plateau since Late Miocene times. Nature 411, 62–66.

Bohlin, B., 1937. Eine tertiäre Saugetier-Fauna aus Tsaidam. Palaeontol. Sin. Ser. C 14, 1–111.

Calandra, I., Göhlich, U.B., Merceron, G., 2010. Feeding preferences of *Gomphotherium subtapiroideum* (Proboscidea, Mammalia) from the Miocene of Sandelzhausen (Northern Alpine Foreland Basin, southern Germany) through life and geological time: evidence from dental microwear analysis. Paläontol. Z. 84, 205–215.

Chavasseau, O., Chaimanee, Y., Yamee, C., Tian, P., Rugbumrung, M., Marandat, B., Jaeger, J.-J., 2009. New Proboscideans (Mammalia) from the middle Miocene of Thailand. Zool. J. Linnean Soc. 155, 703–721.

Chavasseau, O., Khyaw, A.A., Chaimanee, Y., Coster, P., Emonet, E.-G., Soe, A.N., Rugbumrung, M., Tun, S.T., Jaeger, J.-J., 2013. Advances in the biochronology and biostratigraphy of the continental Neogene of Myanmar. In: Wang, X.-M., Flynn, L.J., Fortelius, M. (Eds.), Fossil Mammals of Asia: Neogene Terrestrial Mammalian Biostratigraphy and Chronology of Asia. Columbia University Press, New York, pp. 461–474.

Chow, M.-C., 1959. New species of fossil Proboscidea from South China. Acta Palaeontol. Sin. 7, 251–258.

Chow, M.-C., Zhai, R.-J., 1962. Description of a new species of *Stegodon* from Chaotung, Yunnan. Vert. PalAsiat. 6, 138–147.

Chow, M.-C., Chang, Y.-P., You, Y.-Z., 1978. Notes on some mastodonts from Yunnan. Prof. Papers Stratigr. Palaeontol. 7, 68–74.

Teilhar de Chardin, P., Trassaert, M., 1937. The proboscidians of south-eastern Shansi. Palaeontol. Sin. Ser. C 13, 1–58.

Deng, T., 2006. Chinese Neogene mammal biochronology. Vert. PalAsiat. 44, 143–163.

Deng, T., 2016. Records and characteristics of the mammalian faunas of northern China in the Middle Miocene Climatic Optimum. Quat. Sci. 36, 810–819.

Deng, T., Ding, L., 2015. Paleo-altimetry reconstructions of the Tibetan Plateau: progress and contradictions. Nat. Sci. Rev. 93, 92–95.

Deng, T., Wang, W.-M., Yue, L.-P., 2003. Recent advances of the establishment of the Shanwang Stage in the Chinese Neogene. Vert. PalAsiat. 41, 314–323.

Deng, T., Qiu, Z.-Y., Wang, B.-Y., Wang, X.-M., Hou, S.-K., 2013. Late Cenozoic biostratigraphy of the Linxia Basin, northwestern China. In: Wang, X.-M., Flynn, L.J., Fortelius, M. (Eds.), Fossil Mammals of Asia: Neogene Terrestrial Mammalian Biostratigraphy and Chronology of Asia. Columbia University Press, New York, pp. 243–273.

Deng, T., Hou, S.-K., Shi, Q.-Q., 2015a. Selection of the lower boundary stratotype of the terrestrial Upper Miocene Bahean Stage in China. Acta Geosci. Sin. 36, 523–532.

Deng, T., Wang, X.-M., Wang, S.-Q., Li, Q., Hou, S.-K., 2015b. Evolution of the Chinese Neogene mammalian faunas and its relationship to uplift of the Tibetan Plateau. Adv. Earth Science 30, 407–415.

Dong, W., 1987. Miocene mammalian fauna of Xiaolongtan, Kaiyuan, Yunnan Province. Vert. PalAsiat. 25, 116–123.

Duangkrayom, J., Wang, S.-Q., Deng, T., Jintasakul, P., 2017. The first Neogene record of *Zygolophodon* (Mammalia, Proboscidea) in Thailand: implications for the mammutid evolution and dispersal in Southeast Asia. J. Paleontol. 91:179–193. http://dx.doi.org/10.1017/jpa.2016.143.

Flynn, L.J., Tedford, R.H., Qiu, Z.-X., 1991. Enrichment and stability in the Pliocene mammalian fauna of North China. Paleobiology 17, 246–265.

Fox, D.L., Fisher, D.C., 2004. Dietary reconstruction of Miocene *Gomphotherium* (Mammalia, Proboscidea) from the Great Plains region, USA, based on the carbon isotope composition of tusk and molar enamel. Palaeogeogr. Palaeoclimatol. Palaeoecol. 206, 311–335.

Ge, J.-Y., Guo, Z.-T., Zhan, T., Yao, Z.-Q., Deng, C.-L., Oldfield, F., 2012. Magnetostratigraphy of the Xihe loess-soil sequence and implication for late Neogene deformation of the West Qinling Mountains. Geophys. J. Int. 189, 1399–1408.

Gheerbrant, E., Tassy, P., 2009. L'origine et l'évolution des éléphants. Comptes Rendus Palevol 8, 281–294.

Göhlich, U.B., 1999. Order Proboscidea. In: Rössner, G.E., Heissig, K. (Eds.), The Miocene Land Mammals of Europe. Verlag Dr. Friedrich Pfeil, München, pp. 157–168.

Guo, Z.-T., Peng, S.-Z., Hao, Q.-Z., Biscaye, P.E., Liu, T.-S., 2001. Origin of the Miocene-Pliocene red-earth formation at Xifeng in Northern China and implications for paleoenvironments. Palaeogeogr. Palaeoclimatol. Palaeoecol. 170, 11–26.

Guo, Z.-T., Ruddiman, W.F., Hao, Q.-Z., Wu, H.-B., Qiao, Y.-S., Zhu, R.-X., Peng, S.-Z., Wei, J.-J., Yuan, B.-Y., Liu, T.-S., 2002. Onset of Asian desertification by 22 Myr ago inferred from loess deposits in China. Nature 416, 159–163.

Guo, Z.-T., Peng, S.-Z., Hao, Q.-Z., Biscaye, P.E., An, Z.-S., Liu, T.-S., 2004. Late Miocene-Pliocene development of Asian aridification as recorded in the red-earth formation in northern China. Glob. Planet. Chang. 41, 135–145.

Guo, Z.-T., Sun, B., Zhang, Z.-S., Peng, S.-Z., Xiao, G.-Q., Ge, J.-Y., Hao, Q.-Z., Qiao, Y.-S., Liang, M.-Y., Liu, J.-F., Yin, Q.-Z., Wei, J.-J., 2008. A major reorganization of Asian climate by the early Miocene. Clim. Past 4, 153–174.

Harrison, T.M., Copeland, P., Kidd, W.S.F., Yin, A., 1992. Raising Tibet. Science 255, 1663–1670.

Hopwood, A.T., 1935. Fossil Proboscidea from China. Palaeontol. Sin. Ser. C 9, 1–108.

Jablonski, N.G., Su, D.F., Flynn, L.J., Ji, X.-P., Deng, C.-L., Kelley, J., Zhang, Y.-G., Yin, J.-Y., You, Y.-S., Yang, X., 2014. The site of Shuitangba (Yunnan, China) preserves a unique, terminal Miocene fauna. J. Vertebr. Paleontol. 34, 1251–1257.

Janis, C., 1982. Evolution of horns in ungulates: ecology and paleoecology. Biol. Rev. 57, 261–318.

Ji, X.-P., Zhang, J.-H., 2006. Proboscidea Illiger, 1811. In: Qi, G.-Q., Dong, W. (Eds.), *Lufengpithecus hudienensis* Site. Science Press, Beijing, pp. 177–188.

Ji, X.-P., Jablonski, N.G., Su, D.F., Deng, C.-L., You, Y.-S., Kelley, J., 2013. Juvenile hominoid cranium from the terminal Miocene of Yunnan, China. Chin. Sci. Bull. 58, 3771–3779.

Kappelman, J., Rasmussen, D.T., Sanders, W.J., Feseha, M., Bown, T., Copeland, P., Crabaugh, J., Fleagle, J., Glantz, M., Gordon, A., Jacobs, B., Maga, M., Muldoon, K., Pan, A., Pyne, L., Richmond, B., Ryan, T., Seiffert, E.R., Sen, S., Todd, L., Wiemann, M.C., Winkler, A., 2003. Oligocene mammals from Ethiopia and faunal exchange between Afro-Arabia and Eurasia. Nature 426, 549–552.

Li, F.-J., Rousseau, D.-D., Wu, N.-Q., Hao, Q.-Z., Pei, Y.-P., 2008. Late Neogene evolution of the East Asian monsoon revealed by terrestrial mollusk record in Western Chinese Loess Plateau: from winter to summer dominated sub-regime. Earth Planet. Sci. Lett. 274, 439–447.

Li, S.-H., Deng, C.-L., Dong, W., Sun, L., Liu, S.-Z., Qin, H.-F., Yin, J.-Y., Ji, X.-P., Zhu, R.-X., 2015. Magnetostratigraphy of the Xiaolongtan formation bearing *Lufengpithecus keiyuanensis* in Yunnan, southwestern China: constraint on the initiation time of the southern segment of the Xianshuihe–Xiaojiang fault. Tectonophysics 655, 213–226.

Liu, X.-D., Dong, B.-W., 2013. Influence of the Tibetan plateau uplift on the Asian monsoon-arid environment evolution. Chin. Sci. Bull. 58, 4277–4291.

Liu, D.-S., Li, C.-K., Zhai, R.-J., 1978. Pliocene vertebrates from Lantian. Shensi. Prof. Papers Stratigr. Palaeontol. 7, 149–200.

MacFadden, B.J., 1992. Fossil Horses: Systematics, Paleobiology, and Evolution of the Family Equidae. Cambridge Universit Press, Cambridge.

Maglio, V.J., 1973. Origin and evolution of the Elephantidae. Trans. Amer. Philos. Soc. (N. Ser.) 63, 1–149.

Markov, G.N., 2008. The Turolian proboscideans (Mammalia) of Europe: preliminary observations. Hist. Natural. Bulg. 19, 153–178.

Molnar, P., 2005. Mio-Pliocene growth of the Tibetan Plateau and evolution of Asian climate. Palaeontol. Electron. 8, 1–23.

Mothé, D., Avilla, L.S., Zhao, D.-S., Xie, G.-P., Sun, B.-Y., 2016. A new Mammutidae (Proboscidea, Mammalia) from the late Miocene of Gansu Province, China. Anais Acad. Brasil. Ciênc. 88, 65–74.

Opdyke, N.D., Huang, K., Tedford, R.H., 2013. The paleomagnetism and magnetic stratigraphy of the Late Cenozoic sediments of the Yushe Basin, Shanxi Province, China. In: Tedford, R.H., Qiu, Z.-X., Flynn, L.J. (Eds.), Late Centozoic Yushe Basin, Shanxi Province, China: Geology and Fossil Mammals. Volume I: History, Geology, and Magnetostratigraphy. Springer, Dordrecht, pp. 69–78.

Osborn, H.F., 1929. New Eurasiatic and American proboscideans. Am. Mus. Novit. 393, 1–28.

Osborn, H.F., Granger, W., 1932. *Platybelodon grangeri*, three growth stages, and a new serridentine from Mongolia. Am. Mus. Novit. 537, 1–13.

Pickford, M., 2005. *Choerolophodon pygmaeus* (Proboscidea Mammalia) from the Middle Miocene of southern Africa. S. Afr. J. Sci. 101, 175–177.

Qiu, Z.-D., 1979. Some mammalian fossils from the Pliocene of inner Mongolia and Gansu (Kansu). Vert. PalAsiat. 17, 222–235.

Qiu, Z.-D., Li, C.-K., 2005. Evolution of Chinese mammalian faunal regions and elevation of the Qinghai-Xizang (Tibet) Plateau. Sci. China Earth Sci. 48, 1246–1258.

Qiu, Z.-X., Qiu, Z.-D., 1995. Chronological sequence and subdivision of Chinese Neogene mammalian faunas. Palaeogeogr. Palaeoclimatol. Palaeoecol. 116, 41–70.

Qiu, Z.-X., Wu, W.-Y., Qiu, Z.-D., 1999. Miocene mammal faunal sequence of China: palaeozoogeography and Eurasian relationships. In: Rössner, G.E., Heissig, K. (Eds.), The Miocene Land Mammals of Europe. Verlag Dr. Friedrich Pfeil, München, pp. 443–455.

Qiu, Z.-X., Wang, B.-Y., Deng, T., Li, H., Sun, Y., 2007. First discovery of deinothere in China. Vert. PalAsiat. 45, 261–277.

Qiu, Z.-X., Qiu, Z.-D., Deng, T., Li, C.-K., Zhang, Z.-Q., Wang, B.-Y., Wang, X.-M., 2013. Neogene land mammal stages/ages of China: toward the goal to establish an Asian land mammal stage/age scheme. In: Wang, X.-M., Flynn, L.J., Fortelius, M. (Eds.), Fossil Mammals of Asia: Neogene Terrestrial Mammalian Biostratigraphy and Chronology of Asia. Columbia University Press, New York, pp. 29–90.

Ramstein, G., Fluteau, F., Besse, J., Joussaume, S., 1997. Effect of orogeny, plate motion and land-sea distribution on Eurasian climate change over the past 30 million years. Nature 386, 788–795.

Rea, D.K., Snoeckx, H., Joseph, L.H., 1998. Late Cenozoic eolian deposition in the North Pacific: Asian drying, Tibetan uplift, and cooling of the northern hemisphere. Paleoceanography 13, 215–224.

Saegusa, H., 1996. Stegodontidae: evolutionary relationships. In: Shoshani, J., Tassy, P. (Eds.), The Proboscidea: Evolution and Palaeoecology of Elephants and Their Relatives. Oxford University Press, Oxford, pp. 178–190.

Saegusa, H., Thasod, Y., Ratanasthien, B., 2005. Notes on Asian stegodontids. Quat. Int. 126–128, 31–48.

Sanders, W.J., Kappelman, J., Rasmussen, D.T., 2004. New large–bodied mammals from the late Oligocene site of Chilga, Ethiopia. Acta Palaeontol. Pol. 49, 365–392.

Saunders, J.J., 1996. North American Mammutidae. In: Shoshani, J., Tassy, P. (Eds.), The Proboscidea: Evolution and Palaeoecology of Elephants and Their Relatives. Oxford University Press, Oxford, pp. 271–279.

Semprebon, G.M., Deng, T., Hasjanova, J., Solounias, N., 2016. An examination of the dietary habits of *Platybelodon grangeri* from the Linxia Basin of China: evidence from dental microwear of molar teeth and tusks. Palaeogeogr. Palaeoclimatol. Palaeoecol. 457, 109–116.

Steininger, F.F., 1999. Chronostratigraphy, geochronology and biochronology of the Miocene "European land mammal megazones" (ELMMZ) and the Miocene "mammal-zones (MNZones)". In: Rössner, G.E., Heissig, K. (Eds.), The Miocene Land Mammals of Europe. Verlag Dr. Friedrich Pfeil, München, pp. 9–24.
Sun, J.-M., Ye, J., Wu, W.-Y., Ni, X.-J., Bi, S.-D., Zhang, Z.-Q., Liu, W.-M., Meng, J., 2010. Late Oligocene–Miocene mid-latitude aridification and wind patterns in the Asian interior. Geology 38, 515–518.
Tassy, P., 1983. Les Elephantoidea Miocènes du Plateau du Potwar, Groups de Siwalik, Pakistan. Ann. Paleontol. 69 (99–136, 235–297, 317–354).
Tassy, P., 1985. La place des mastodontes Miocènes de l'ancien monde dans la phylogénie des Proboscidea (Mammalia): hypothèses et conjectures. Unpublished Thèse Doctorat ès Sciences. Université Pierre et Marie CURIE, Paris.
Tassy, P., 1990. The "proboscidean datum event:" how many proboscideans and how many events? In: Lindsay, E.H., Fahlbusch, V., Mein, P. (Eds.), European Neogene Mammal Chronology. Plenum Press, New York, pp. 237–252
Tassy, P., 1996. Dental homologies and nomenclature in the Proboscidea. In: Shoshani, J., Tassy, P. (Eds.), The Proboscidea: Evolution and Palaeoecology of Elephants and Their Relatives. Oxford University Press, Oxford, pp. 21–25.
Tassy, P., Anupandhanant, P., Ginsburg, L., Mein, P., Ratanasthien, P., Sutteethorn, V., 1992. A new *Stegolophodon* (Proboscidea, Mammalia) from the early Miocene of northern Thailand. Géobios 25, 511–523.
Tedford, R.H., Flynn, L.J., Qiu, Z.-X., Opdyke, N.D., Downs, W.R., 1991. Yushe Basin, China: paleomagnetically calibrated mammalian biostratigraphic standard for the Late Neogene of Eastern Asia. J. Vertebr. Paleontol. 11, 519–526.
Tobien, H., 1972. Status of the genus *Serridentinus* Osborn 1923 (Proboscidea, Mammalia) and related forms. Mainz. Geowiss. Mitt. 1, 143–191.
Tobien, H., 1975. The structure of the mastodont molar (Proboscidea, Mammalia). Part 2: the zygodont and the zygobunodont patterns. Mainz. Geowiss. Mitt. 4, 195–233.
Tobien, H., Chen, G.-F., Li, Y.-Q., 1988. Mastodonts (Proboscidea, Mammalia) from the Late Neogene and Early Pleistocene of the People's Republic of China. Part II: the genera *Tetralophodon*, *Anancus*, *Stegotetrabelodon*, *Zygolophodon*, *Mammut*, *Stegolophodon*. Mainz. Geowiss. Mitt. 17, 95–220.
von Koenigswald, G.H.R., 1959. A mastodon and other fossil mammals from Thailand. Rep. Investig. Royal Departm. Mines 2, 25–28.
Wang, S.-Q., 2014. *Gomphotherium inopinatum*, a basal *Gomphotherium* species from the Linxia Basin, China, and other Chinese members of the genus. Vert. PalAsiat. 52, 183–200.
Wang, S.-Q., Deng, T., 2011. The first *Choerolophodon* (Proboscidea, Gomphotheriidae) skull from China. Sci. China Earth Sci. 54, 1326–1337.
Wang, X.-M., Qiu, Z.-D., Opdyke, N.D., 2003. Litho-, bio-, and magnetostratigraphy and paleoenvironment of Tunggur Formation (Middle Miocene) in central Inner Mongolia, China. Am. Mus. Novit. 3411, 1–31.
Wang, X.-M., Xie, G.-P., Li, Q., Qiu, Z.-D., Tseng, Z.J., Takeuchi, G.T., Wang, B.-Y., Fortelius, M., Rosenström-Fortelius, A., Wahlquist, H., Downs, W.R., Zhang, C.-F., Wang, Y., 2011. Early explorations of Qaidam Basin (Tibetan Plateau) by Birger Bohlin—reconciling classic vertebrate fossil localities with modern biostratigraphy. Vert. PalAsiat. 49, 285–310.
Wang, Y., Jin, C.-Z., Deng, C.-L., Wei, G.-B., Yan, Y.-L., 2012. The first *Sinomastodon* (Gomphotheriidae, Proboscidea) skull from the Quaternary in China. Chin. Sci. Bull. 57, 4726–4734.
Wang, S.-Q., He, W., Chen, S.-Q., 2013. Gomphotheriid mammal *Platybelodon* from the Middle Miocene of Linxia Basin, Gansu, China. Acta Palaeontol. Pol. 58, 221–240.
Wang, S.-Q., Zhao, D.-S., Xie, G.-P., Sun, B.-Y., 2014. An Asian origin for *Sinomastodon* (Proboscidea, Gomphotheriidae) inferred from a new Upper Miocene specimen from Gansu of China. Sci. China Earth Sci. 57, 2522–2531.
Wang, S.-Q., Deng, T., Tang, T., Xie, G.-P., Zhang, Y.-G., Wang, D.-Q., 2015a. Evolution of *Protanancus* (Proboscidea, Mammalia) in East Asia. J. Vertebr. Paleontol. 35 (e881830), 1–13.
Wang, S.-Q., Duangkrayom, J., Yang, X.-W., 2015b. Occurrence of the *Gomphotherium angustidens* group in China, based on a revision of *Gomphotherium connexum* (Hopwood, 1935) and *Gomphotherium shensiensis* Chang and Zhai, 1978: continental correlation of *Gomphotherium* species across the Palearctic. Paläontol. Z. 89, 1073–1086.
Wang, S.-Q., Fu, L.-Y., Zhang, J.-H., Li, T.-G., Ji, X.-P., Duangkrayom, J., Han, R.-T., 2015c. New material of *Stegolophodon* from the Upper Miocene Xiaohe Formation, Yuanmou Basin, Yunnan Province. Quat. Sci. 35, 573–583.
Wang, S.-Q., Ji, X.-P., Jablonski, N.G., Su, D.F., Ge, J.-Y., Ding, C.-F., Yu, T.-S., Li, W.-Q., Duangkrayom, J., 2016a. The oldest cranium of *Sinomastodon* (Proboscidea, Gomphotheriidae), discovered in the uppermost Miocene of southwestern China: implications for the origin and migration of this taxon. J. Mamm. Evol. 23, 155–173.
Wang, S.-Q., Shi, Q.-Q., He, W., Chen, S.-Q., Yang, X.-W., 2016b. A new species of the tetralophodont amebelodontine *Konobelodon* Lambert, 1990 (Proboscidea, Mammalia) from the Late Miocene of China. Geodiversitas 38, 65–97.
Wang, S.-Q., Zong, L.-Y., Yang, Q., Sun, B.-Y., Li, Y., Shi, Q.-Q., Yang, X.-W., Ye, J., Wu, W.-Y., 2016c. Biostratigraphic subdividing of the Neogene Dingjiaergou mammalian fauna, Tongxin County, Ningxia province, and its background for the uplift of the Tibetan Plateau. Quat. Sci. 36, 789–809.
Wang, S.-Q., Deng, T., Ye, J., He, W., Chen, S.-Q., 2017a. Morphological and ecological diversity of Amebelodontidae (Proboscidea, Mammalia) revealed by a Miocene fossil accumulation of an upper-tuskless proboscidean. J. Syst. Palaeontol. 15:601–615. http://dx.doi.org/10.1080/14772019.2016.1208687.
Wang, S.-Q., Saegusa, H., Duangkrayom, J., He, W., Chen, S.-Q., 2017b. A new species of *Tetralophodon* from the Linxia Basin and the biostratigraphic significance of tetralophodont gomphotheres from the Upper Miocene of northern China. Palaeoworld http://dx.doi.org/10.1016/j.palwor.2017.03.005.
Wang, S.-Q., Yu, L., Duangkrayom, J., Yang, X.-W., He, W., Chen, S.-Q., 2017c. A new species of *Gomphotherium* (Proboscidea, Mammalia) from China and the evolution of *Gomphotherium* in Eurasia. J. Vertebr. Paleontol.:1–15 e1318284. http://dx.doi.org/10.1080/02724634.2017.131828.
Wang, S.-Q., Yu, L., Duangkrayom, J., He, J., W., Chen, S.-Q., 2017d. The early *Mammut* from the Upper Miocene of northern China, and its implications for the evolution and differentiation of Mammutidae. Vert. PalAsiat. 55, 233–256.
Xu, Y., Yue, L.-P., Li, J.-X., Sun, L., Sun, B., Zhang, J.-Y., Ma, J., Wang, J.-Q., 2009. An 11-Ma-old red clay sequence on the Eastern Chinese Loess Plateau. Palaeogeogr. Palaeoclimatol. Palaeoecol. 284, 383–391.
Yan, D.-F., Qiu, Z.-D., Meng, Z.-Y., 1983. Miocene stratigraphy and mammals of Shanwang, Shandong. Vert. PalAsiat. 21, 210–222.
Ye, J., Wu, W.-Y., Ni, X.-J., Bi, S.-D., Sun, J.-M., Meng, J., 2012. The Duolebulejin Section of northern Junggar Basin and its stratigraphic and environmental implication. Sci. China Earth Sci. 42, 1523–1532.
Yue, L.-P., Deng, T., Zhang, Y.-X., Wang, J.-Q., Zhang, R., Yang, L.-R., Heller, F., 2004. Magnetostratigraphy of stratotype section of the Baode stage. J. Stratigr. 28, 48–63.
Zachos, J.C., Pagani, M., Sloan, L., Thomas, E., Billups, K., 2001. Trends, rhythms, and aberrations in global climate 65 Ma to present. Science 292, 686–693.
Zhang, Z.-S., Wang, H.-J., Guo, Z.-T., Jiang, D.-B., 2007. What triggers the transition of palaeoenvironmental patterns in China, the Tibetan Plateau uplift or the Paratethys Sea retreat? Palaeogeogr. Palaeoclimatol. Palaeoecol. 245, 317–331.
Zhang, Z.-G., Han, W.-X., Fang, X.-M., Song, C.-H., Li, X.-Y., 2013. Late Miocene–Pleistocene aridification of Asian inland revealed by geochemical records of lacustrine-fan delta sediments from the western Tarim Basin, NW China. Palaeogeogr. Palaeoclimatol. Palaeoecol. 377, 52–61.
Zheng, S.-H., Zhang, Z.-Q., 2000. Late Miocene-early pleistocene micromammals from Wenwanggou of Liangtai, Gansu, China. Vert. PalAsiat. 38, 58–71.
Zheng, H.-B., Powell, C.A., Rea, D.K., Wang, J.-L., Wang, P.-X., 2004. Late Miocene and mid-Pliocene enhancement of the East Asian monsoon as viewed from the land and sea. Glob. Planet. Chang. 41, 147–155.
Zong, G.-F., 1997. A new evidence of dividing in the Neogene Stratigraphy of Yuanmou Basin. Mem. Beijing Nat. Hist. Mus. 56, 159–173.

Journal of Vertebrate Paleontology

ISSN: 0272-4634 (Print) 1937-2809 (Online) Journal homepage: http://www.tandfonline.com/loi/ujvp20

A new species of Gomphotherium (Proboscidea, Mammalia) from China and the evolution of Gomphotherium in Eurasia

Shi-Qi Wang, Yu Li, Jaroon Duangkrayom, Xiang-Wen Yang, Wen He & Shan-Qin Chen

To cite this article: Shi-Qi Wang, Yu Li, Jaroon Duangkrayom, Xiang-Wen Yang, Wen He & Shan-Qin Chen (2017) A new species of Gomphotherium (Proboscidea, Mammalia) from China and the evolution of Gomphotherium in Eurasia, Journal of Vertebrate Paleontology, 37:3, e1318284, DOI: 10.1080/02724634.2017.1318284

To link to this article: http://dx.doi.org/10.1080/02724634.2017.1318284

Journal of Vertebrate Paleontology e1318284 (15 pages)

DOI: 10.1080/02724634.2017.1318284

ARTICLE

A NEW SPECIES OF *GOMPHOTHERIUM* (PROBOSCIDEA, MAMMALIA) FROM CHINA AND THE EVOLUTION OF *GOMPHOTHERIUM* IN EURASIA

SHI-QI WANG,*[1,2] YU LI,[1,3] JAROON DUANGKRAYOM,[1,4] XIANG-WEN YANG,[1,3] WEN HE,[5] and SHAN-QIN CHEN[5]
[1]Key Laboratory of Vertebrate Evolution and Human Origins of Chinese Academy of Sciences, Institute of Vertebrate Paleontology and Paleoanthropology, Chinese Academy of Sciences, Beijing 100044, China, wangshiqi@ivpp.ac.cn;
[2]Chinese Academy of Sciences Center for Excellence in Tibetan Plateau Earth Sciences, Beijing 100101, China;
[3]University of Chinese Academy of Sciences, Beijing 100049, China;
[4]Northeastern Research Institute of Petrified Wood and Mineral Resources, Nakhon Ratchasima Rajabhat University, Nakhon Ratchasima 30000, Thailand;
[5]Hezheng Paleozoological Museum, Hezheng, Gansu Province 731200, China

ABSTRACT—*Gomphotherium* is a stem taxon of Elephantida that was widespread in Africa, Eurasia, and North America during the Miocene. However, the evolution of this genus is greatly debated because of morphological variation among the species of *Gomphotherium*. In the present work, we describe a cranium and accompanying material of *Gomphotherium* from the late middle Miocene Hujialiang Formation of Linxia Basin, China. The new material shows dental similarities to *G. subtapiroideum* from the middle Miocene of Europe; however, it displays some cranial, mandibular, and dental feature combinations that are distinct from the known species of *Gomphotherium*. Therefore, a new species, *G. tassyi*, is established. We further study the phylogeny of *Gomphotherium* by cladistic analysis and recognize four groups. The most basal '*G. annectens* group' is a paraphyletic group that includes *G. annectens, G. cooperi, G. sylvaticum*, and *G. hannibali*. The African taxa, *G. libycum* and *G. pygmaeus*, constitute a monophyletic group that has not been named. The '*G. angustidens* group' is a monophyletic group that includes *G. inopinatum, G. mongoliense, G. connexum*, and *G. angustidens*. In addition, the 'derived *Gomphotherium* group,' which includes *G. subtapiroideum, G. tassyi, G. wimani, G. browni, G. productum*, and *G. steinheimense*, was widely distributed in Eurasia and North America during the middle and late Miocene.

http://zoobank.org/urn:lsid:zoobank.org:act:28B89A74-7FF6-41DB-BA3C-C4CDD200A30F

SUPPLEMENTAL DATA—Supplemental materials are available for this article for free at www.tandfonline.com/UJVP

Citation for this article: Wang, S.-Q., Y. Li, J. Duangkrayom, X.-W. Yang, W. He, and S.-Q. Chen. 2017. A new species of *Gomphotherium* (Proboscidea, Mammalia) from China and the evolution of *Gomphotherium* in Eurasia. Journal of Vertebrate Paleontology. DOI: 10.1080/02724634.2017.1318284.

INTRODUCTION

Gomphotherium is a long-lived and widely distributed proboscidean genus. It existed for at least 15.0 Ma, from the early Miocene (ca. 19.5 Ma) of Africa (Sanders et al., 2010) to the end of the Hemphillian (ca. 4.5 Ma) of North America (Fisher, 1996). *Gomphotherium* is also a morphologically diverse genus. More than a dozen species are considered valid, and more than 30 junior synonyms of those species have been proposed (Shoshani and Tassy, 1996). However, Shoshani (1996) and Tassy (1996a) indicated that *Gomphotherium* is a paraphyletic group; thus, from a phylogenetic perspective, '*Gomphotherium*' appears to be an artificial taxon.

Many previous studies, mainly based on evolutionary grade but also on cladistics, have provided a framework for designating subgroups of *Gomphotherium* (Osborn, 1936; Tobien, 1973; Tassy, 1985; Shoshani and Tassy, 1996; Sanders et al., 2010). According to Tassy (1985), the '*G. annectens* group' (i.e., *G. annectens, G. cooperi, G. sylvaticum*, and *G. hannibali*) includes the stem taxa of this genus. The '*G. angustidens* group' (i.e., *G. inopinatum, G. angustidens, G. connexum*, and *G. subtapiroideum*) is an important group of Eurasian *Gomphotherium*; however, whether *G. subtapiroideum* can be placed in this group is questionable based on newly discovered material (Göhlich, 2010; Wang et al., 2015). Sanders et al. (2010) proposed the 'pygmy *Gomphotherium* group' as a grade (not a clade) including *G. pygmaeus* and some other small specimens that occurred in Afro-Arabia. However, the validity of *G. pygmaeus* was questioned by Tassy et al. (2013). Wang (2014) proposed that the '*G. productum* group' contained *G. productum, G. steinheimense*, and *G. wimani*, but whether it is a natural group should be tested.

At Hezheng Paleozoological Museum, there is an almost complete cranium with associated remains that can be attributed to *Gomphotherium*. These specimens were discovered from the late middle Miocene Hujialiang Formation (MN7/8) of Linxia Basin, China (Fig. 1). The cranium shows some derived features within *Gomphotherium*. The new material contributes to elucidating the evolution and phylogeny of *Gomphotherium*, especially for the Old World species.

Institutional Abbreviations—**AMNH**, American Museum of Natural History, New York, U.S.A.; **HMV**, Hezheng Paleozoological Museum, Hezheng, China; **IVPP**, Institute of

*Corresponding author.
Color versions of one or more of the figures in the article can be found online at www.tandfonline.com/ujvp

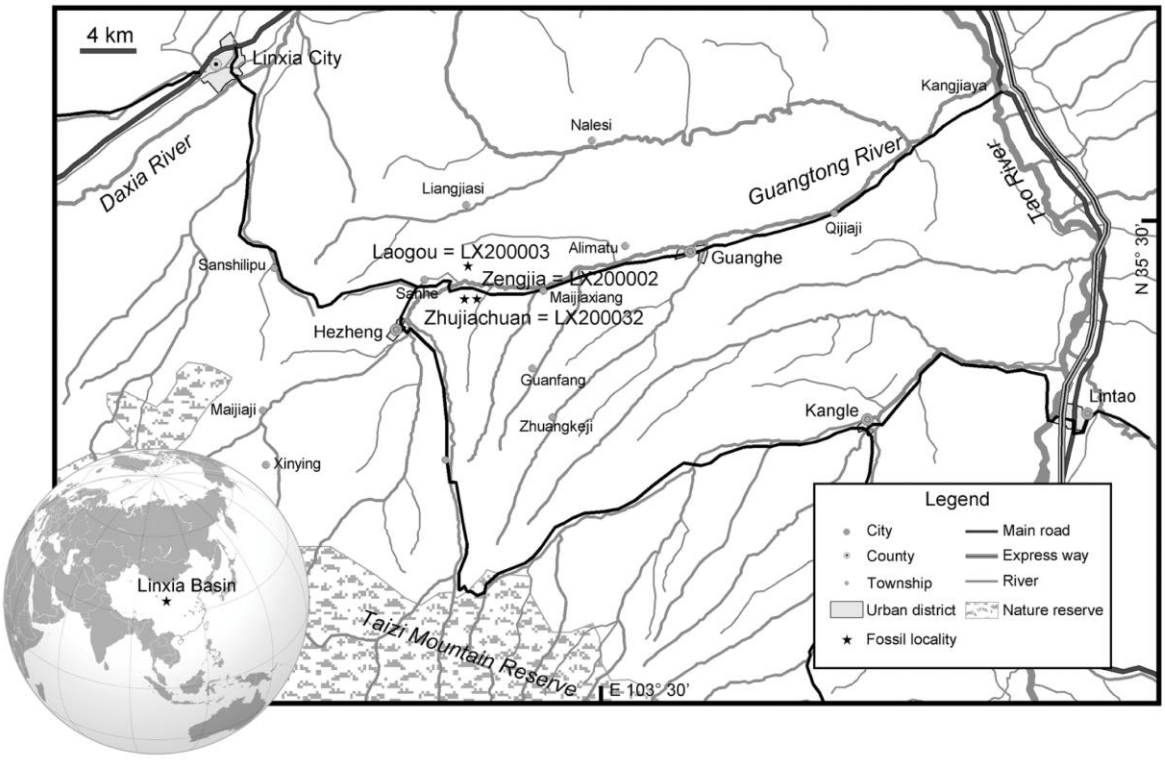

FIGURE 1. Geographic map indicating the fossil sites yielding *Gomphotherium tassyi*, sp. nov., in the Linxia Basin. Globe image from www.wikipedia.com.

Vertebrate Paleontology and Paleoanthropology, Chinese Academy of Sciences, Beijing, China; **MNHN**, Muséum National d'Histoire Naturelle, Paris, France; **NHMW**, Naturhistorisches Museum Wien, Vienna, Austria.

Other Abbreviations—CI, consistency index; **MN**, the European Mammal Neogene zone; **MPT**, the most parsimonious tree; **RI**, retention index.

MATERIALS AND METHODS

Materials

The material of the new species is housed in HMV. The comparative materials of *G. mongoliense, G. browni*, and *G. productum* are housed in AMNH; of *G. annectens, G. sylvaticum*, and *G. angustidens* in MNHN; of *G. subtapiroideum* in NHMW; and of *G. connexum, G. wimani*, and *G.* cf. *subtapiroideum* in IVPP. Information regarding other material was obtained from previous publications (Andrews, 1906; Schlesinger, 1917; Osborn, 1924, 1926, 1932; Borissiak and Belyaeva, 1928; Hopwood, 1935; Tassy, 1977a, 1985, 1986, 1994, 2013, 2014; Welcomme, 1994; Göhlich, 1998, 2007, 2010; Shoshani et al., 2006; Wang et al., 2013b, 2015; Wang, 2014; Yang et al., in press; for details, see Appendix 1).

Measurements, Terminology, and Explanation of Some Tooth Characters

Cranial and mandibular measurements follow Tassy (2013). All measurements were taken using calipers (in mm). The terminology used to describe the occlusal structures of gomphotheriid cheek teeth follows Tassy (1996b) (Fig. 2A), whereas cranial and mandibular terminology is after Tassy (2013) and Ferretti (2010). Dental age determination of *Gomphotherium* follows Tassy (2013).

It has long been known that some gomphotheriid taxa, such as *G. subtapiroideum*, show combined characters of bunodont and zygodont teeth (Schlesinger, 1917; Mazo, 1996; Göhlich, 2010); this is also the case for the new species. Wang et al. (2016) defined four levels to semiquantify the degree of tooth zygodonty (levels 0–3, for which larger numbers indicate higher degrees of zygodonty). For example, *G. subtapiroideum* was scored as level 1, characterized by moderate subdivision and anteroposterior compression of posttrite half-loph(id)s, moderate subdivision and alignment of the anterior and posterior pretrite central conules, and wide anteroposterior interloph(id)s. The new species has similar tooth morphology to *G. subtapiroideum*. Therefore, it was also scored as zygodont degree level 1. The detailed morphological features of each crown element for the four levels of semiquantification are shown in Wang et al. (2016).

Some tooth features should be further explained: (1) The anterior convexity of the first posttrite half-loph in occlusal view is clearly present in the new species. The wear figure of this loph shows a clear crescentic pattern that is anteriorly convex (Fig. 2B). This feature is also present in some taxa such as *Sinomastodon praeintermedium* (Fig. 2A; see also Wang et al., 2016). In most other gomphotheriid taxa, such as *G. subtapiroideum*, this loph is straight and the wear figure has a simple ring pattern (Fig. 2C). (2) There is anteroposterior compression of the interloph(id)s. Generally, a tooth with a higher degree of

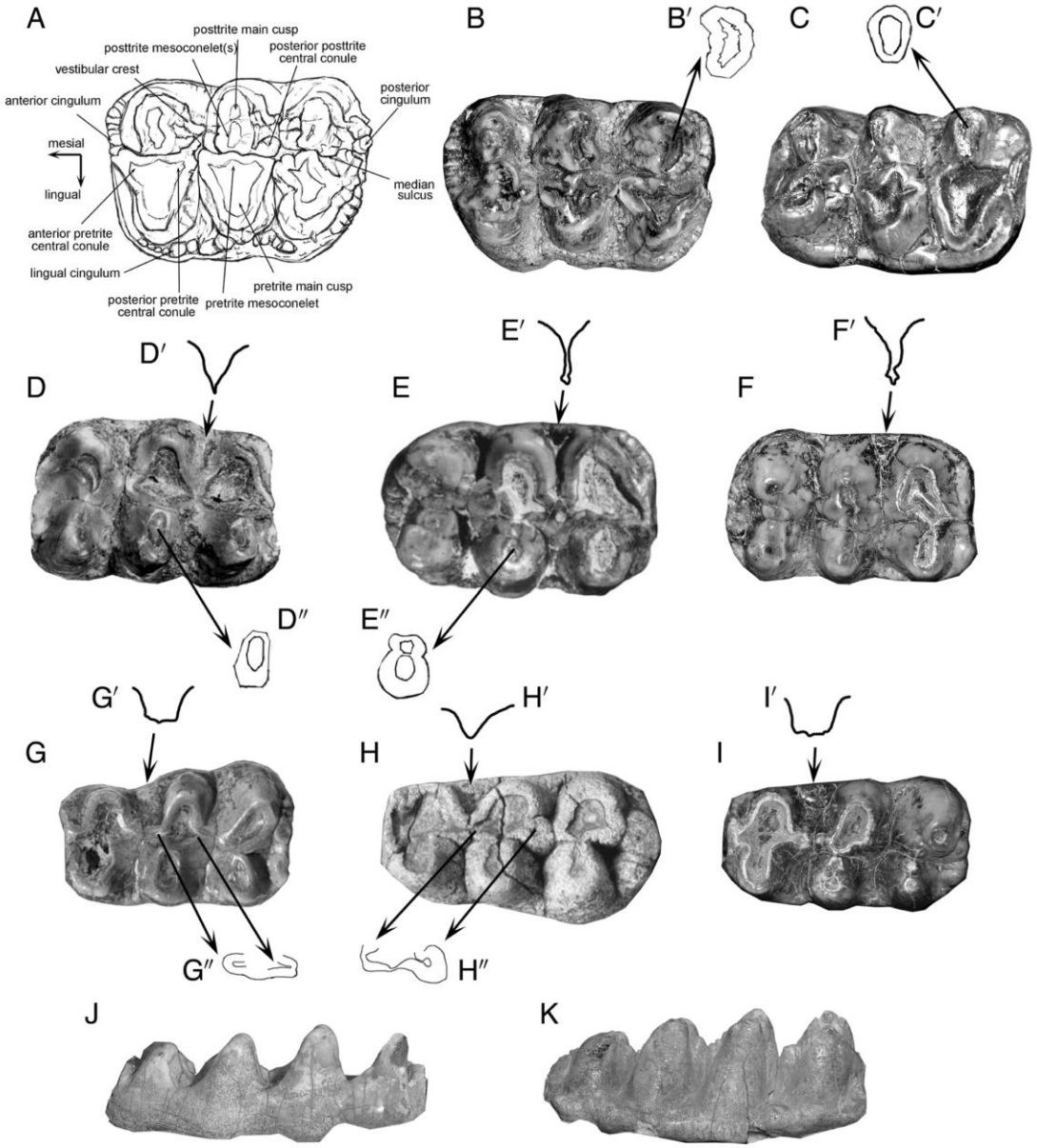

FIGURE 2. Tooth nomenclature and some important tooth features of *Gomphotherium*. **A**, nomenclature of a proboscidean tooth (*Sinomastodon praeintermedius*). After Wang et al. (2016:fig. 2). **B**, the anterior convex first loph in HMV 0028, type specimen of *Gomphotherium tassyi*, sp. nov., from Zhujiachuan, China. **C**, the straight first loph in the type specimen of *Gomphotherium subtapiroideum*, NHMW 3870 ex 1882 (A4135), from Vordersdorf near Eibiswald, Austria. Note the crescentic wear figure in **B′**, compared with the ring-shaped wear figure in **C′**. **D–I**, comparison of features of **D–F**, upper and **G–I**, lower molars among *G. subtapiroideum, G. angustidens*, and *G. sylvaticum*. **D**, **G**, *G. subtapiroideum*, from Sandelzhausen, Germany; after Göhlich (2010:figs. 8e, 10f). **E**, **H**, *G. angustidens*, from En Péjouan, France; after Tassy (2014, figs. 39g, 54a). **F**, **I**, *G. sylvaticum*, MNHN Ar 1487 and 1491, Artenay, France. Note the wide interloph in **D′** ('V'-shaped entoflexus), compared with the compressed interloph in **E′** and **F′** ('Y'-shaped entoflexus); the wide interlophid in **G′** and **I′** ('U'-shaped ectoflexid), compared with the compressed interlophid in **H′** ('V'-shaped ectoflexid); the compressed posttrite half-loph(id) in **D″** (narrow ring wear figure), compared with bulky posttrite half-loph(id) in **E″** (pear-shaped wear figure with a constriction); and the crest-like anterior and posterior central conules in **G″**, compared with the inflated anterior and posterior central conules in **H″**. **J**, **K**, m3 in *Gomphotherium tassyi*, sp. nov., and *G. wimani* in lingual view. **J**, low crowned m3 in *G. tassyi*, sp. nov. (HMV 1810, Laogou, China), compared with **K**, relatively high crowned m3 in *G. wimani* (IVPP V18795, Daoheigou, China). Not to scale.

zygodonty tends to display anteroposteriorly wide interloph(id)s. However, the upper and lower molars show distinct patterns. The upper molars of *G. subtapiroideum* possess wide anteroposterior interlophs and the first entoflexus shows a clear 'V' shape (Fig. 2D). In contrast, in upper molars of *G. angustidens*, the interlophs are compressed and the first entoflexus shows a clear 'Y' shape (Fig. 2E). Note that we only compared the first entoflexus, which is the most typical of all interlophs. In lower molars, the first ectoflexid in *G. subtapiroideum* (wide interlophid) is 'U'-shaped (Fig. 2G), and that in *G. angustidens* (compressed interlophid) is 'V'-shaped (Fig. 2H). It can be seen that the interlophs of upper molars are usually more compressed than the interlophids of lower molars in the same taxon. It should also be noted that in some taxa, such as *G. sylvaticum*, the interloph of upper molars is 'Y'-shaped (anteroposteriorly compressed) (Fig. 2F), whereas the interlophid of lower molars is 'U'-shaped (anteroposteriorly wide) (Fig. 2I). (3) In taxa with a high degree of zygodonty, such as *G. subtapiroideum*, the posttrite half-loph (id)s are anteroposteriorly compressed, showing an oval ring figure (Fig. 2D). Alternatively, in taxa with a low degree of zygodonty, such as *G. angustidens*, the posttrite half-loph(id)s are bulky and pear-shaped, with a constriction in the middle that separates into the main conelet and mesoconelet (Fig. 2E). (4) As in feature 3, crest-like pretrite central conules are usually observed in taxa with a high degree of zygodonty, such as *G. subtapiroideum*; this feature is caused by the slight wear on the subdivided and aligned central conules in these taxa (Fig. 2G). However, inflated pretrite central conules are usually displayed in taxa with a low degree of zygodonty, such as *G. angustidens* (Fig. 2H). In some cases, the central conules of the taxa with a low degree of zygodonty, such as *G. angustidens* and *G. connexum* (Tassy, 2014; Wang et al., 2015), are also subdivided, but they are seldom subdivided into more than two small conules, and each element is inflated and not crest-like. (5) Most *Gomphotherium* species typically have low crowns, including *G. tassyi* (Fig. 2J). However, some *Gomphotherium* species also develop relatively higher tooth crowns, such as *G. wimani* (Fig. 2K).

Cladistic Analysis

A cladistic analysis was performed to investigate the possible phylogenetic relationships among *Gomphotherium* species. The data matrix contains 50 binary characters and 19 taxa, including three outgroups (Appendices 1 and 2). The three outgroups are *Phiomia serridens* from the early Oligocene of Fayûm, Egypt (Andrews, 1906), *Eritreum melakeghebrekristosi* from the late Oligocene of Dogali, Eritrea (Shoshani et al., 2006), and *Gomphotherium* sp. from the early Miocene of Mwiti, Kenya (Tassy, 1986). Some characters used follow those of Tassy (1985), and some were unique for this study. Cladograms were obtained from a parsimony analysis carried out using the program TNT 1.1 with the 'traditional search' option (Goloboff et al., 2003). The reported results were based on a strict consensus tree. Node supports were calculated from a bootstrap analysis (10,000 replicates).

SYSTEMATIC PALEONTOLOGY

Order PROBOSCIDEA Illiger, 1811
Family GOMPHOTHERIIDAE Hay, 1922
Genus *GOMPHOTHERIUM* Burmeister, 1837

Type Species—*Gomphotherium angustidens* (Cuvier, 1817).
Type Locality and Horizon—Simorre, France, middle Miocene (Tassy and Göhlich, 2012).

GOMPHOTHERIUM TASSYI, sp. nov.
(Figs. 3–5; Tables 1, 2, S1, S2)

Gomphotherium subtapiroideum Schlesinger, 1917: Wang et al., 2013a.
Gomphotherium subtapiroideum Schlesinger, 1917: Wang, 2014.

Etymology—Dedicated to Professor Pascal Tassy, who has greatly contributed to the study of fossil proboscideans, especially *Gomphotherium*.

Holotype—HMV 0028, a complete cranium with functional M1 and M2, and erupting M3.

Type Locality—Zhujiachuan (LX 200023; Fig. 1), Hujialiang Formation, Linxia Basin, China; MN7/8 (Deng et al., 2013).

Paratypes—HMV 1805 and 1376, middle segments of right I2, Zhujiachuan; HMV 1375 and 1806, anterior segment of right i2, Zhujiachuan.

Referred Material—HMV 1824, an incomplete mandible with functional m2 and m3, and broken anterior part of the symphysis, Zengjia (LX 200002) (Fig. 1); HMV 1807, right dentary with m2 and m3, Laogou (LX 200003) (Fig. 1); HMV 1810, left dentary with m2 and m3, Laogou; HMV 1867, 1868, and 1869, anterior segments of right i2, Laogou; HMV 1947, right dp4; HMV 1948, left m2; HMV 1940, right m2; HMV 1949, left M3; HMV 1945, right m3; HMV 1944-1, segment of right i2; HMV 1944-2, tip of right i2 (the precise localities of the latter seven specimens are unknown, but they are all from the Hujialiang Formation of Linxia Basin).

Occurrences—Late middle Miocene, MN7/8, China.

Diagnosis—Medium- to large-sized *Gomphotherium*; brain case moderately arched, and, consequently, basicranium slightly erect; facial part short; perinasal fossa moderately broad; mandibular symphysis distant from the anterior end of the cheek tooth row; angular process moderately positioned; loph(id)s of cheek teeth anteroposteriorly compressed and, consequently, interloph(id)s anteroposteriorly wide; anterior and posterior pretrite central conules subdivided and linearly aligned (crest-like); the first posttrite half-lophs of the upper molar anteriorly convex in occlusal view.

Differential Diagnosis—Differs from the members of the '*G. annectens* group' (*G. annectens, G. cooperi, G. sylvaticum*, and *G. hannibali*) and *G. mongoliense* in the anteroposteriorly compressed loph(id)s, the crest-like pretrite central conules, and the complete fourth loph in M3; differs additionally from *G. annectens* in the presence of a perinasal fossa and the higher position of the mandibular angular process; differs from *G. inopinatum* in the anteroposteriorly compressed loph(id)s, the crest-like pretrite central conules, and the higher position of the mandibular angular process; differs from *G. angustidens* and *G. connexum* in the anteroposteriorly compressed loph(id)s, the crest-like pretrite central conules, the shorter facial part, the lower position of the mandibular angular process, and the flat dorsal wear facet of the lower tusks; differs from *G. steinheimense, G. browni*, and *G. productum* in the anteroposteriorly compressed loph(id)s, the crest-like pretrite central conules, and the curved, twisted, and pyriform– or semipyriform–cross-sectioned mandibular tusks; differs from *G. wimani* in the absence of posttrite central conules; differs from *G. subtapiroideum* in the larger size, the anterior convexity of the first posttrite half-loph of upper molars in occlusal view, and the higher position of the mandibular angular process; differs from *G.* cf. *subtapiroideum* (= *G. shensiensis*) in the anterior convexity of the first posttrite half-loph of upper molars in occlusal view, the more domed brain case, and the shorter facial part.

DESCRIPTION

Holotype

The type cranium, HMV 0028 (Fig. 3A–D), is almost complete except that it lacks both zygomatic processes. However, this specimen is mounted on an iron frame that cannot be taken

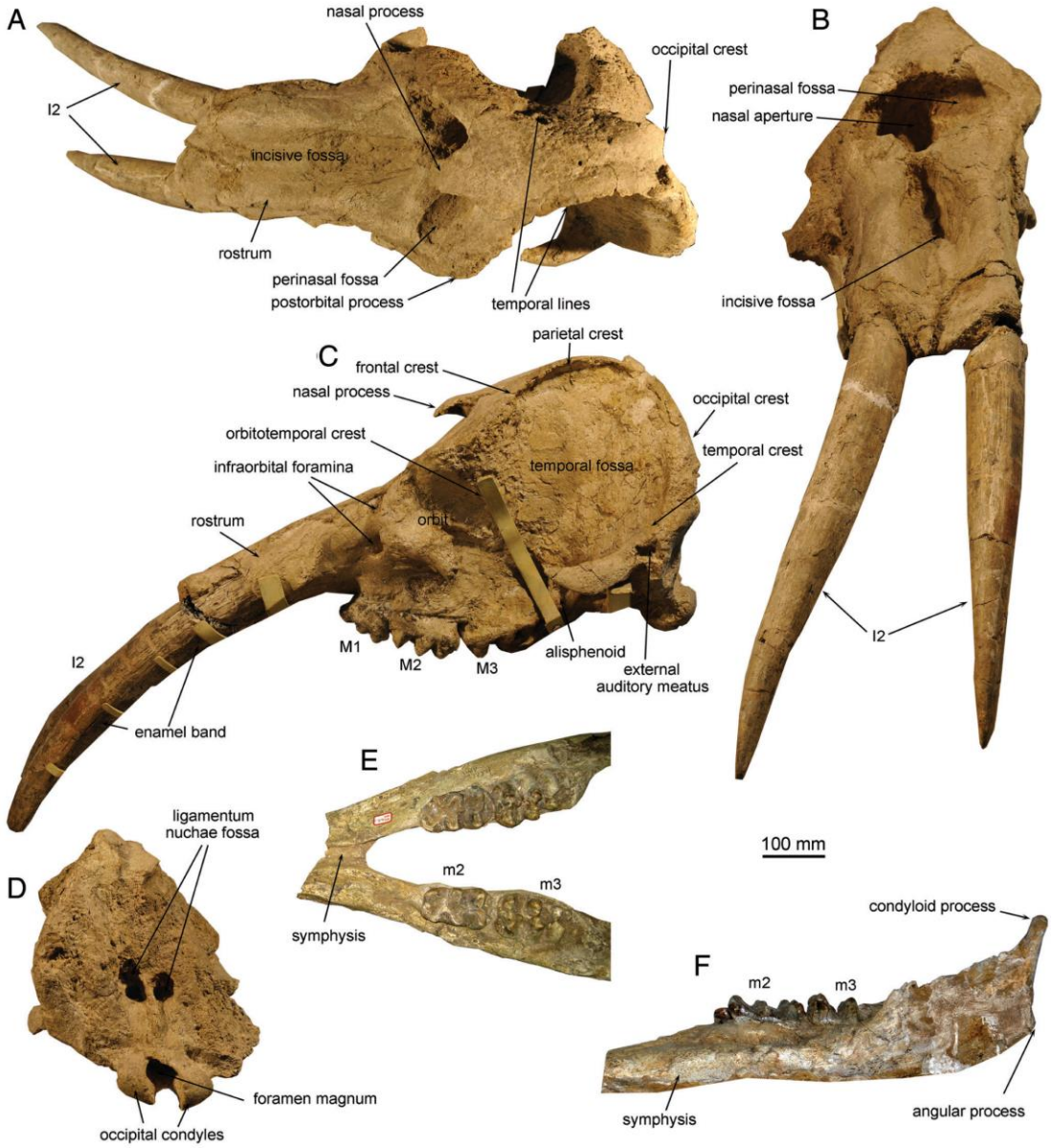

FIGURE 3. *Gomphotherium tassyi*, sp. nov., cranial skeleton. Cranium, HMV 0028 (holotype, Zhujiachuan, China), in **A**, dorsal, **B**, anterodorsal, **C**, lateral, and **D**, occipital views. Mandible, HMV 1824 (Zengjia, China), in **E**, dorsal and **F**, lateral views.

down, so that the ventral view cannot be observed. The M3 with erupted first loph indicates a nearly adult ontogenetic age (dental age XVII).

In dorsal view (Fig. 3A), the cranium is slightly deformed, showing a slightly rightward bent brain case. The occipital part is as wide as the orbital part. The occipital crest is almost straight, not anteriorly concave. The two temporal lines converge from the posterolateral flanges of the two temporal fossae, then turn anteriorly and extend parallel along both sides of the brain case, and gradually diverge until they reach the postorbital processes. The distance between the two temporal lines is relatively small, resulting in a narrow and quadratic brain case (partly due to lateral compression). The nasal process is strongly protruded. The nasal aperture is relatively wide, with two laterally extending

perinasal fossae. The superior-most rim of the nasal aperture posteriorly slightly exceeds the level of the two postorbital processes. The two postorbital processes are moderately laterally protruded. The rostrum is strongly anteriorly elongated, and it has almost equal width throughout its length. In the basal part, the incisive fossa has a deep median part and two shallow lateral steps, and it then extends anteriorly along the rostrum, resulting in a median trough. However, no constriction is present in the basal part of the incisive fossa. At the distal edge of the rostrum, the distance between the two alveolar sockets is relatively small.

In anterodorsal view (Fig. 3B), the right side of the specimen is deformed. The dorsal plate of the brain case is flat without bulges. The nasal aperture is transversely oval. The midline suture of the two premaxillae is clear, and the subnasal fossa seems to be absent. The rostrum is well developed in this view and shows two strong alveolar sockets. The incisive fossa is narrow and deep, especially in the basal part.

In lateral view (Fig. 3C), the brain case is strongly arched. The nasal process is greatly protruded in this view. The temporal fossa is almost circular, and the dorsal–ventral dimension of the fossa is large. The frontal and parietal crests (= temporal line) dorsally, occipital crest posteriorly, and temporal crest ventrally enclose the temporal fossa. The large and circular external auditory meatus is just posterior to the zygomatic process of the squamosal bone, and the ventral border of the external auditory meatus is closed by a bony plate. The occipital condyle is rounded and moderately protruded. The orbitotemporal crest, which is derived from the postorbital process, extends posteroventrally to reach the anterior edge of the alisphenoid. The anterior edge of the alisphenoid extends ventrally and wraps around the posterior end of the bulged maxillary process. The orbit is relatively small, and the anterior rim is located at the level of the middle part of the M2. The postorbital process is just at the level of the boundary of M2 and M3. The jugal bone of the zygomatic arch is broken. The facial part of the maxilla is not anteriorly elongated, and the area ventral to the zygomatic process is low. The lower infraorbital foramen is large and just anterior to the zygomatic process of the maxilla, and the upper infraorbital foramen is small and anterior to the orbit. The rostrum is thick; it is strongly anteriorly elongated and slightly ventrally bent.

In occipital view (Fig. 3D), despite the deformation, the brain case is relatively strongly arched. The ligamentum nuchae fossa is very deep, and the median crest is thick. Each half of the fossa is relatively rounded. The occipital condyle is bean-shaped and strongly extends ventrally, producing a relatively rounded (although deformed) foramen magnum.

The upper tusks are very strong. In anterior view (Fig. 3B), the two tusks extend almost parallel at the base, then moderately diverge in the middle (the left tusk is somewhat deformed; we can only observe this feature from the right tusk), and finally converge distally. In lateral view (Fig. 3C), the tusk bends ventrally. An enamel band is present on the lateroventral surface of the tusk and forms a ventral cutting edge. This enamel band turns slightly more ventrally where it extends apically, but it is not strongly helical as in *G. angustidens* (Tassy, 2014). Measurements (in mm, left/right): exposed length, 587/684; dorsoventral diameter at the opening of the alveolus, 103/107; transverse diameter at the opening of the alveolus, 91/91.

The deeply worn M1 (Fig. 4A) is composed of three lophs. The pretrite and posttrite half-lophs are connected to each other, producing three diamond-shaped wear figures.

The M2 (Fig. 4A) is moderately worn with three lophs. The tooth is bunodont with slightly anteroposterior compression of each loph. Furrows are developed on the walls of the lophs. Cingula are relatively strong and surround the anterior, posterior, and lingual sides of the tooth. Cementum is weak. The first pretrite half-loph is trifoliate with symmetric anterior and posterior central conules. The central conules are anteroposteriorly elongated and therefore somewhat crest-like. The first interloph is entirely blocked by the first posterior and the second anterior pretrite central conule; this interloph is anteroposteriorly wide, producing a 'V'-shaped entoflexus. The first posttrite half-loph is crescentic; it is anteroposteriorly compressed and anteriorly convex. Two grooves extend along the posterior wall of the first posttrite half-loph and divide this enamel wall into three crests. The buccal crest corresponds to the vestibular crest. The second pretrite half-loph is likewise trifoliate with slightly weaker anterior and posterior central conules than those of the first loph. The second interloph is also blocked by adjacent pretrite central conules. The second posttrite half-loph is also anteroposteriorly compressed, but anteriorly concave. A weak vestibular crest is present on the posterior wall. The third pretrite half-loph has only an enlarged mesoconelet and a single anterior central conule and lacks the posterior central conule. The third posttrite half-loph is anteroposteriorly compressed; it is subdivided into three conelets. A weak vestibular crest is present on the anterior wall. A series of enamel conelets composes the posterior cingulum that gradually rises in the lingual direction and attaches the posterior wall of the third pretrite half-loph.

Only the first posttrite half-loph of the M3 (Fig. 4A) can be observed; it is composed of four or five conelets that are arranged in an anteriorly convex arch. The buccal two larger conelets represent the main conelet, and the lingual small conelets represent the mesoconelet(s).

Referred Tusks

Specimen HMV 1376 (Fig. 5A, B) is a middle segment of a right upper tusk from the type locality. This segment shows an obviously ventral bend in lateral view. There is a wide enamel band present on the lateroventral surface of the tusk. The cross-section of the tusk (Fig. 5B) is oval, composed of approximately six to seven dentine layers that enclose the pulp cavity. This tusk is very similar to that of the type specimen; we therefore identified it as belonging to the same species.

Specimen HMV 1805 (Fig. 5C) is a short segment of a right upper tusk from the type locality; it also shows a ventral bend in lateral view. The enamel band is relatively narrow and positioned higher than that of the type specimen and HMV 1376. Because the formation of the enamel band decreases when the animal ages and finally ceases (Tassy, 2014), this tusk segment probably corresponds to a posterior tusk part and potentially belonged to an old animal. We tentatively attribute this to *G. tassyi*, because no other proboscidean taxa have been discovered so far from this locality.

Specimen HMV 1375 (Fig. 5D, E) is an anterior segment of a right lower tusk from the type locality. It is slightly right twisted (clockwise twisted in basal view) and tapers anteriorly, producing a sharp anteromedial angle. The dorsal wear facet is broad and long and is almost flat and not concave. A shallow dorsal groove runs throughout the tooth, but a ventral groove is not clear; thus, the cross-section is semipyriform.

Specimen HMV 1806 (Fig. 5F, G) is another anterior segment of a right lower tusk from the type locality. This tusk is smaller than HMV 1375 (Table 2), which indicates a younger ontogenetic age than HMV 1375, but has an identical morphology, such as slight right-hand twisting, anterior tapering, possessing a dorsal groove, and the flat dorsal wear facet. The ventral groove is not clear. The morphology of these lower tusks is typical for *Gomphotherium*. It should be noted that no other proboscidean taxa have been discovered so far from the type locality, Zhujiachuan; therefore, their attribution to *G. tassyi* is plausible.

There are some tusk fragments from other sites of the Hujialiang Formation other than the type locality. For example, HMV 1867, 1868, and 1869 are three anterior segments of right i2 that originated from the Laogou locality; HMV 1944-1 (Fig. 5H, I)

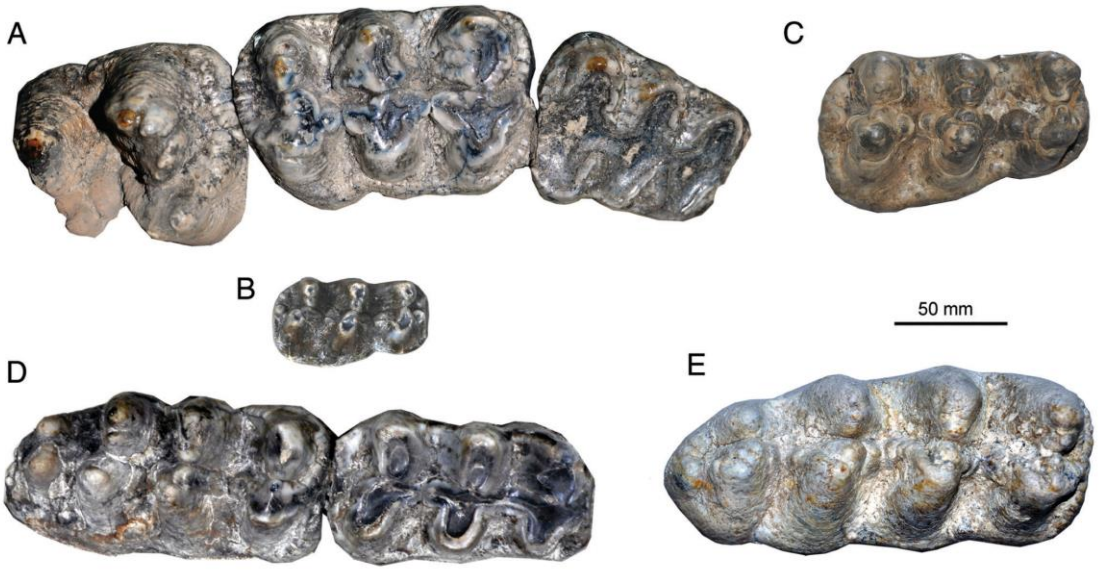

FIGURE 4. *Gomphotherium tassyi*, sp. nov., cheek teeth in occlusal view. **A**, right M1–M3 tooth row, HMV 0028 (holotype, Zhujiachuan); **B**, right dp4, HMV 1947 (unknown locality); **C**, left m2, HMV 1948, horizontally reversed (unknown locality); **D**, right m2 and m3, HMV 1807 (Laogou); **E**, right m3, HMV 1945 (unknown locality); mesial side to right.

and 1944-2 are segments of right i2 and a tip of right i2, respectively, but are from an unknown locality. These segments have almost identical morphology to those from the type locality. The dimensions of these tusks are similar to those of HMV 1375 and smaller than those of HMV 1806 (Table 1). All these tusks show a flat dorsal wear facet (if present), a gradually tapering distal end, slightly right-hand-twisted shaft, and a dorsal groove. Except for HMV 1944-1, which has a clear ventral groove (Fig. 5H), other specimens show a faint ventral groove; this is also a variable feature in *Gomphotherium* (Tobien, 1973; Tassy,

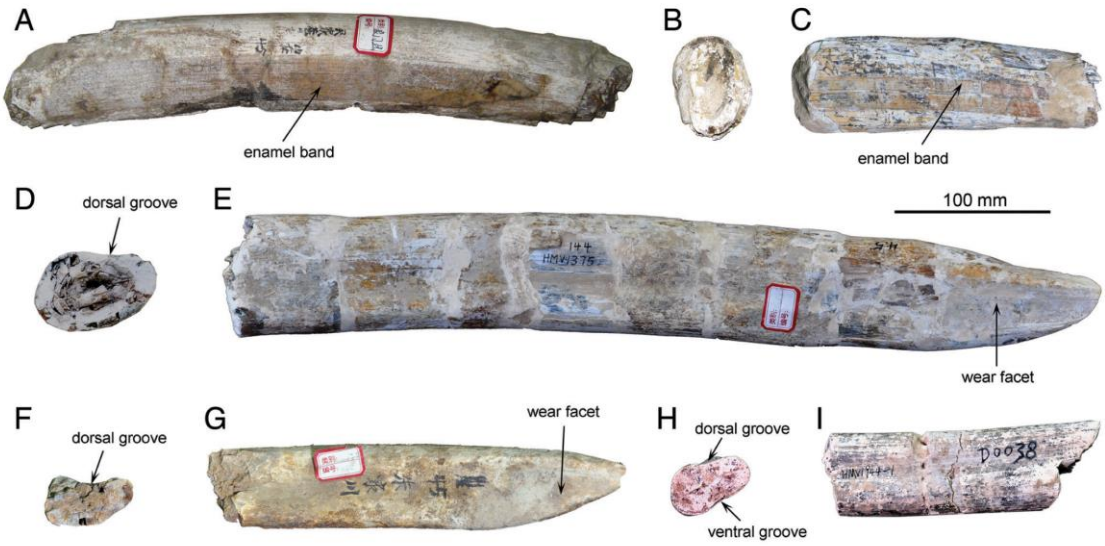

FIGURE 5. *Gomphotherium tassyi*, sp. nov., tusks. **A–B**, right upper tusk, HMV 1376 (Zhujiachuan), in lateral view and **B**, distal cross-section. **C**, right upper tusk, HMV 1805 (Zhujiachuan), in lateral view. **D–E**, right lower tusk, HMV 1375 (Zhujiachuan), in **D**, proximal cross-section and **E**, in dorsal view. **F–G**, right lower tusk, HMV 1806 (Zhujiachuan), in **F**, proximal cross-section and **G**, in dorsal view; **H–I**, right lower tusk, HMV 1944-1 (unknown locality), in **H**, proximal cross-section and **I**, in dorsal view.

TABLE 1. Cheek tooth measurements (in mm) of *Gomphotherium tassyi*, sp. nov., from the Linxia Basin.

Specimen	Locus	L	W	W1	W2	W3	W4	Hpo	I = W/L
HMV 0028	l. M1	103	73	63.5	67	73	—	—	0.71
HMV 0028	r. M1	100	75.5	61	67	75.5	—	—	0.76
HMV 0028	l. M2	130.5	87	84.5	87	86	—	$50+^{(2)}$	0.67
HMV 0028	r. M2	134	89	83	83	89	—	$50+^{(2)}$	0.66
HMV 1949	l. M3	151	83	83	80	79	60	$45.5+^{(3)}$	0.55
HMV 1947	r. dp4	69.5	40.5	34	40.5	39	—	$27^{(2)}$	0.58
HMV 1807	r. m2	114.5	69.5	57.5	61.5	69.5	—	—	0.61
HMV 1940	r. m2	114	71	55.5	61.5	71	—	$47.5^{(3)}$	0.62
HMV 1948	l. m2	120	73.5	57	66	73.5	—	$50^{(2)}$	0.61
HMV 1824	l. m2	116	66	56	60	66	—	—	0.57
HMV 1945	r. m3	188.5	86	77	86	82	66	$65^{(2)}$	0.46
HMV 1807	r. m3	165	75.5	71	74.5	75.5	55	$62^{(2)}$	0.46
HMV 1810	l. m3	171	80	75	80	80	70	$64+^{(3)}$	0.47

Parameters after Tassy (2014). **Abbreviations**: **Hpo**, height of the posttrite side (numbers in parentheses indicate the loph(id) from which the measurement was made); **I**, index; **L**, length; **W**, maximal width; **W1, W2, W3**, and **W4**, width at the first, second, third, and fourth loph(id)s.

2014). Because no other *Gomphotherium* species has been identified from the Hujialiang Formation, we tentatively attribute all these tusks to *G. tassyi*.

Mandibles and Lower Cheek Teeth

Mandibles and lower cheek teeth are unknown to date from the type locality Zhujiachuan. However, we found mandibular and lower cheek tooth remains of *Gomphotherium* from other localities of the Hujialiang Formation. The dimensions of these remains are very similar to those of the type material (Tables 1, S1, S2; also see below). The lower molars share important morphological features with the upper ones, including anteroposterior compression of posttrite half-loph(id)s, anteroposteriorly wide interloph(id)s, and subdivision of the posttrite half-loph(id)s and the pretrite central conules. Therefore, we attribute these mandibular and lower cheek tooth remains to *G. tassyi* (for details, see below).

Specimen HMV 1824 (Fig. 3E, F) is an incomplete mandible (dental age XVIII) from the Zengjia locality. The anterior part of the symphysis, the right ramus, and the left coronoid process are missing. The right mandibular condyloid process is present. In lateral view (Fig. 3F), the symphysis is not strongly ventrally inclined, and the angular process reaches nearly the level of the occlusal surface. The condyloid process is small. In dorsal view (Fig. 3E), there is a considerable distance between the posterior end of the symphysis and the anterior end of the tooth row. The tooth row is approximately 290 mm in length, which is close to the tooth row length of the type cranium (ca. 295 mm).

The dp4 (Fig. 4C) is composed of three lophids, with a constriction at the first interlophid. The interlophids are anteroposteriorly open with a 'U'-shaped ectoflexid. Furrows are developed on the enamel walls, and tiny conules are present in the interlophids. Cingulids are developed on the anterior and posterior ends, and cementum is absent. The first pretrite trefoil is complete; however, the anterior and posterior central conules are isolated. The posterior conule is distant from the main conelet and connected to it by a weak enamel crest. The first posttrite half-lophid has a large, anterobuccally–posterolingually oblique main conelet, and a small mesoconelet. The main conelet shows a tendency to subdivide as in deciduous premolars in many other proboscidean taxa. The second pretrite trefoil has two low anterior and posterior central conules; however, they are anteroposteriorly elongated (crest-like) and are in line with the median axis of the tooth. The third pretrite half-lophid has an anteriorly displaced mesoconelet and an anteriorly elongated anterior pretrite central conule, but the posterior central conule is almost absent. The second and third posttrite half-lophids are simply composed of a main conelet and a mesoconelet. The third lophid is slightly chevroned. Attribution of this tooth to *G. tassyi* is tentative because of the anteroposteriorly narrow molar crown apices and the elongation of the accessory conules.

The m2 (Fig. 4C, D) is composed of three lophids, of which the third is the widest. Cingulids are developed on the anterior and posterior ends of the tooth. The elements are clearly bunodont; however, the posttrite half-lophids are somewhat anteroposteriorly compressed, and the interlophids are anteroposteriorly wide. The first pretrite half-lophid is trifoliate. The pretrite mesoconelet is small and divided into two conelets. The first anterior pretrite central conule is subdivided into small conules that are arranged in line. The first posterior pretrite central conule is also subdivided and arranged in a line; however, the distal conule is inflated. The first posttrite half-lophid is composed of a large main conelet and a mesoconelet; additionally, the middle of the half-lophid is anteriorly convex, which means that this lophid is somewhat triangular in crown view. The first interlophid is blocked by adjacent pretrite central conules, and the first extoflexid is 'U'-shaped. The second pretrite half-lophid also has a crest-like anterior central conule; a small, undivided mesoconelet; and a crest-like posterior central conule with distal inflation. The second posttrite half-lophid is also composed of a large main conelet and a small mesoconelet, but it is slightly sub-

TABLE 2. Lower tusk measurements (in mm) of *Gomphotherium tassyi*, sp. nov., from the Linxia Basin.

Specimen	Locus	Remaining length	Width	Median thickness	Lateral thickness	Length of wear facet	Width of wear facet
HMV 1375	Right	562	80.94	55.47	34.66	102.18	45.97
HMV 1944-1	Left	179	57.00	37.00	28.50	—	—
HMV 1806	Right	260	57.12	28.74	19.60	89.46	47.36
HMV 1869	Right	309	54.85	31.58	17.18	93.49	42.11
HMV 1867	Right	210	43.10	33.69	22.57	63.69	40.37
HMV 1868	Right	204	50.814	33.47	23.65	—	—

Width and thickness are taken at the posterior end of the tusk fragments.

divided. The second interlophid is blocked by the adjacent pretrite central conules. The third pretrite half-lophid has a relatively large and undivided anterior central conule and mesoconelet, but the posterior pretrite central conule is weak and crest-like. The third posttrite half-lophid is also simple and shows a slight tendency to subdivision.

The m3 (Fig. 4D, E) is composed of four lophids, and the anterior two lophids are of equal width. Cingulids are developed on the anterior and posterior ends of the tooth. The elements are basically bunodont with somewhat anteroposteriorly compressed posttrite half-lophids and anteroposteriorly wide interlophids ('U'-shaped first extoflexid). In the first two lophids, the anterior and posterior central conules are subdivided into a line of conules, and the posterior central conule is larger than the anterior central conule. The distal ends of the posterior central conules are somewhat inflated. The first and second posttrite half-lophids are composed of a large main conelet and a small mesoconelet, with tendency to subdivide. The third pretrite mesoconelet is anteriorly located, and the anterior pretrite central conule is anterior to the mesoconelet, but not connected to the main conelet. The posterior pretrite central conule is small. The third posttrite half-lophid is indistinctly subdivided into three conelets. This lophid is slightly chevroned. The chevroned fourth lophid is composed of a tri-subdivided pretrite half-lophid and a single posttrite half-lophid. Cementum is weak in some cases (Fig. 4E), but relatively strong in other cases (Fig. 4D).

COMPARISONS AND DISCUSSION

Attribution of the New Material to *Gomphotherium*

The material from the late middle Miocene Hujialiang Formation of Linxia Basin undoubtedly belongs to a *Gomphotherium* species. We recognized several gomphotheriid features in the cranium, the mandibles, and the teeth: (1) The brain case is domed (although somewhat exaggerated in the type cranium because of lateral compression), which is also observed in other derived species of *Gomphotherium*. (2) The facial part of the cranium is greatly retreated so that the anterior end of the tooth row is only slightly anterior to the orbit. This feature clearly differs from that of members of the Amebelodontidae (except *Konobelodon*). (3) A step-like perinasal fossa is clearly developed. This feature is characteristic of the '*G. angustidens* group' but is missing in *G. annectens*. (4) In the Linxia specimens, the mandibular angular process is moderately elevated. The elevated angular process is common in *Gomphotherium*; in *Zygolophodon*, the mandibular angular process is rather low. (5) In the Linxia specimens, as in most other *Gomphotherium* species (except *G. annectens*), the posterior edge of the mandibular symphysis is distant from the tooth row. By contrast, in *Zygolophodon gobiensis*, the posterior edge of the mandibular symphysis and the anterior end of the tooth row (including the alveolus if it was not resorbed) are almost at the same level (Tobien et al., 1988: fig. 39). (6) The presence of a lateral enamel band on the upper tusks of the Linxia specimens is a common feature of Elephantiformes. The two upper tusks diverge more in the middle; this feature is also observed in *G. angustidens* (Tassy, 1977b), but with variation. (7) In the Linxia specimens, the lower tusks are peglike with a semipyriform (ventral groove is not well developed) or pyriform cross-section. This morphology is typical of *Gomphotherium* and shared with the early Miocene mammutid *Eozygodon morotoensis* (Tassy and Pickford, 1983), but it differs from the flattened cross-sections of amebelodontids and distally flattened cross-sections of *Phiomia*. (8) Although the cheek teeth have compressed posttrite half-loph(id)s (Wang et al., 2016), they are mainly bunodont with clear boundaries between crown elements. The cheek teeth also do not display amebelodontid or choerolophodont features, such as narrowness of the contour, secondary trefoils, pseudoanancoidy, choerodonty, and ptychodonty. Based on this information, attribution of the material to *Gomphotherium* is warranted.

Comparisons of the New Material with Other *Gomphotherium* Species

Crania of *Gomphotherium* are relatively rare. The cranium of the primitive *G. annectens* from the early Miocene of Banjôburo, Japan, is incomplete; however, this is the only known cranium in which the perinasal fossa is not developed (Tassy, 1994). On the other hand, *G. tassyi* displays a well-developed perinasal fossa. Tassy (2013) reported *G. angustidens* from the middle Miocene of En Péjouan, France. In these specimens, the perinasal fossa is well developed as in *G. tassyi*, and the braincase is likewise arched (Tassy, 2013:figs. 12B, 15A); however, the facial part is more anteriorly elongated than that of *G. tassyi*.

The North American *G. productum* should be further divided because there are distinguishable morphotypes. Nevertheless, *G. productum* (e.g., AMNH 10582, from the late Miocene of Clarendon, U.S.A.; see Osborn, 1936:fig. 370) possesses a slightly anteriorly elongated facial part and a relatively short rostrum, which differ from the significantly retreated facial part and relatively long rostrum of *G. tassyi*.

Chang and Zhai (1978) reported a gomphotheriid cranium from the middle Miocene of Lengshuigou, China, under the name '*G. shensiensis*,' which has been attributed to *G.* cf. *subtapiroideum* by Wang et al. (2015). This specimen also has an anteriorly elongated facial part relative to *G. tassyi*. Therefore, a shortened facial segment appears to represent an advanced feature of *G. tassyi* in this genus. Furthermore, *G.* cf. *subtapiroideum* shows a less arched braincase than that of *G. tassyi*. It is possible that *G. tassyi* (MN7/8) directly evolved from *G.* cf. *subtapiroideum* (MN6), and that both belong to the same lineage of *G. subtapiroideum*.

None of the mandibles of *G. tassyi* are complete. We found that the angular process of *G. tassyi* is relatively prominent and moderately elevated. In *G. angustidens*, the angular process is even higher and reaches the occlusal surface (Tassy, 2013); conversely, in *G. subtapiroideum, G. inopinatum, G.* aff. *steinheimense*, and *G. productum*, the angular process is low (Borissiak and Belyaeva, 1928; Osborn, 1936; Tassy, 1985; Göhlich, 1998, 2010; Wang, 2014). Furthermore, the mandibular corpus of *G. tassyi* is relatively low and the ramus is relatively posteriorly oblique, as in *G. angustidens*. However, in *G. subtapiroideum, G. inopinatum, G.* aff. *steinheimense*, and *G. productum*, the mandibular corpus is relatively high and the anterior and posterior borders of the ramus are nearly perpendicular to the occlusal surface (Borissiak and Belyaeva, 1928; Osborn, 1936; Tassy, 1985; Göhlich, 1998, 2010).

The lower tusks of *G. tassyi* are typical of *Gomphotherium*. The paratype shows a semipyriform cross-section without a ventral groove, but a ventral groove was present in some of the referred material. Lower tusk ventral grooves are present in *G. inopinatum, G. angustidens*, and *G. subtapiroideum* (Tassy, 1985; Göhlich, 2010) and absent in the more primitive *G. sylvaticum* and more derived *G. productum, G. browni*, and *G. steinheimense* (Tassy, 1985). However, the presence of a ventral groove on lower tusks is highly variable (Tobien, 1973; Tassy, 2014). The dorsal wear facet on the tip is polished and almost flat, which is distinct from the concave facet in *G. angustidens* (Tassy, 2014).

The dimensions of the *G. tassyi* cheek teeth are medium to large (Fig. 6). The M2 and m2 are larger than in most of the other species and have the same dimensions or are slightly smaller than those of *G. steinheimense*. The M3 and m3 are smaller than those of *G. steinheimense*; however, the dimensions of all teeth are larger than those of the type specimen of *G. subtapiroideum* (Vordersdorf near Eibiswald, Austria) and *G.*

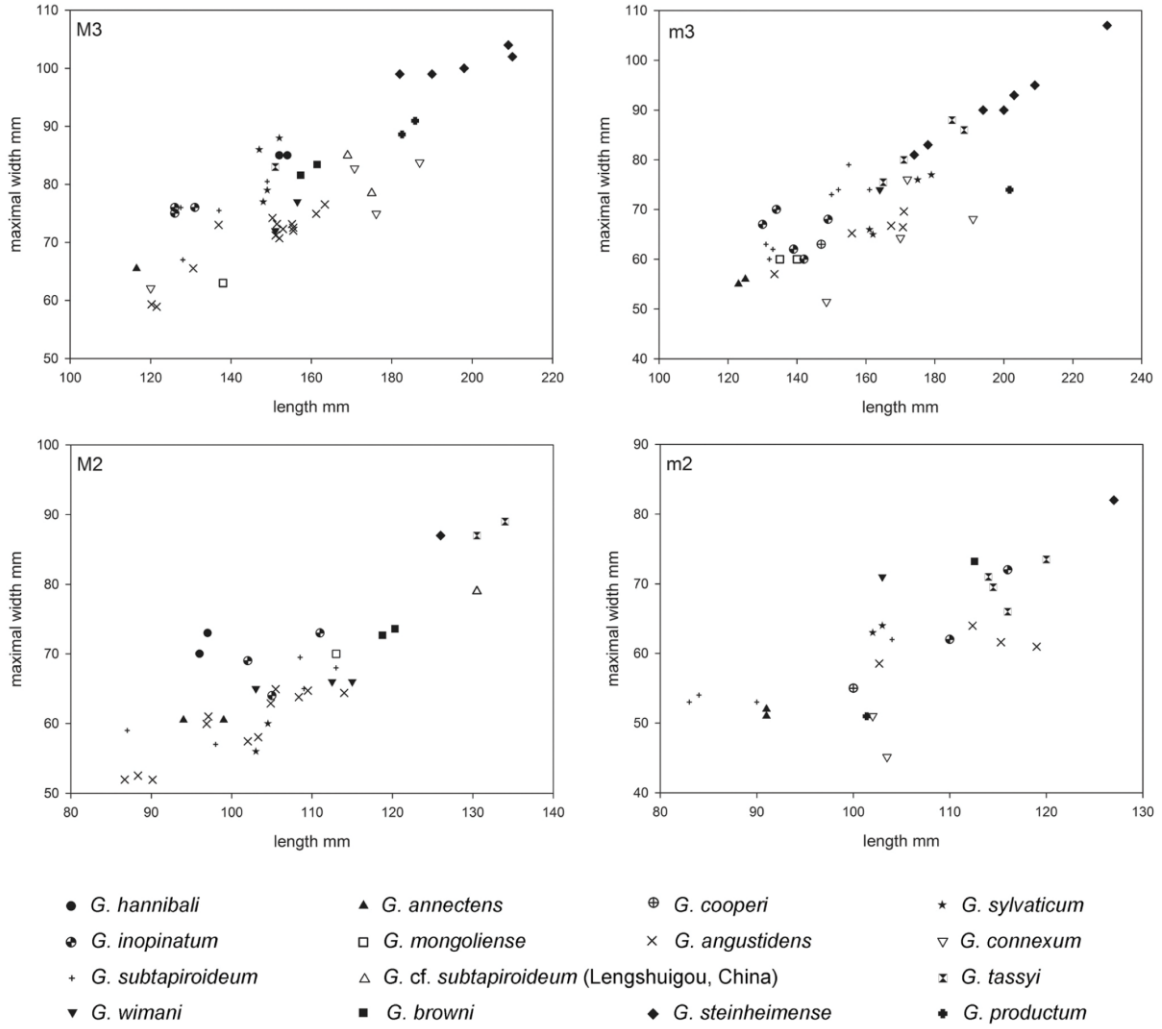

FIGURE 6. Bivariate plots of cheek tooth measurements of *Gomphotherium*. Data source: *G. hannibali*, Le Mazet, France (Welcomme, 1994); *G. annectens*, Banjöburo, Japan (cast in MNHN); *G. cooperi*, Dera Bugti, Pakistan (Osborn, 1932); *G. mongoliense*, Loh, Mongolia (AMNH and Göhlich, 2007); *G. sylvaticum*, Artenay, France (AMNH); *G. angustidens*, En Péjouan, France (Tassy, 2014); *G. connexum*, Diaogou and Junggar Basin, China (Hopwood, 1935; Wang et al., 2015); *G. inopinatum*, Turgai, Kazakhstan, and Ganchiliang, China (Borissiak and Belyaeva, 1928; Wang, 2014); *G. subtapiroideum*, Vordersdorf near Eibiswald, Austria, and Sandelzhausen, Germany (Schlesinger, 1917; Göhlich, 2010); *G.* cf. *subtapiroideum*, Lengshuigou, China (Wang et al., 2015); *G. wimani*, Bapanshan, Quantougou, and Zhengjiaping, China (Hopwood, 1935; Yang et al., in press); *G. browni*, Chinji Bungalow, Pakistan (AMNH); *G. steinheimense*, Massenhausen, Germany (Göhlich, 1999); *G. productum*, Clarendon, U.S.A. (AMNH).

subtapiroideum from Sandelzhausen, Germany (Schlesinger, 1917; Göhlich, 2010). The teeth of *G. tassyi* are also wider than those of *G. angustidens* and *G. connexum* (Fig. 6).

The cheek teeth of *G. tassyi* are subtapiroid-like; that is, they have zygodont-like features (Wang et al., 2016) that are similar to those of *G. subtapiroideum* from Europe and *G.* cf. *subtapiroideum* from Lengshuigou, China (Wang et al., 2015). Therefore, we did not compare the cheek teeth of *G. tassyi* with those of species for which the teeth only display bunodont features, such as *G. annectens, G. cooperi, G. sylvaticum, G. hannibali, G. mongoliense, G. angustidens, G. connexum, G. browni, G. productum*, and *G. steinheimense*. In *G. inopinatum*, although the interlophids are anteroposteriorly wide, the posttrite loph(id)s and pretrite central conules are almost undivided (Borissiak and Belyaeva, 1928; Wang, 2014), which is distinct from the strongly subdivided crown elements in *G. tassyi*. In *G. wimani* (Hopwood, 1935; Wang et al., 2013b), although the crown elements are subdivided, the contour of the teeth is narrower than that of *G. tassyi* and posterior posttrite central conules are present, which are never observed in *G. tassyi*. Furthermore, the tooth morphology of *G. tassyi* is very similar to that of *G. subtapiroideum* from Europe and *G.* cf. *subtapiroideum* from China, except that the first posttrite lophs of the upper molars are unchangeably

anteriorly convex. This feature has never been observed in *G. subtapiroideum* (Schlesinger, 1917; Göhlich, 1998, 2010) and is absent from *G.* cf. *subtapiroideum* (Wang et al., 2015).

Phylogeny of *Gomphotherium*

A cladistic analysis was carried out to elucidate the phylogeny within *Gomphotherium*. Three MPTs were obtained, and the topologies of the three MPTs differ with regard to the positions of *G. browni, G. productum*, and *G. steinheimense*: (*G. browni* (*G. productum, G. steinheimense*)), (*G. productum* (*G. browni, G. steinheimense*)), and (*G. steinheimense* (*G. productum, G. browni*)). The three species form a terminal trichotomy (Node M) in the strict consensus tree (Fig. 7).

There are three major monophyletic groups in the strict consensus tree. One group, (*G. libycum, G. pygmaeus*), includes the African species. The second group, (*G. inopinatum* (*G. mongoliense* (*G. connexum, G. angustidens*))), corresponds to the '*G. angustidens* group.' *Gomphotherium subtapiroideum* is not clustered within the '*G. angustidens* group,' as was proposed by Tassy (1985), but in the third group: ((*G. subtapiroideum, G. tassyi*) (*G. wimani* (*G. browni, G. productum, G. steinheimense*))), which is hereafter referred to as the 'derived *Gomphotherium* group.' This group appears to correspond to '*Serridentinus* Osborn, 1923.' The '*G. annectens* group' is a paraphyletic group and includes the other species that are stem taxa of *Gomphotherium*: *G. hannibali, G.*

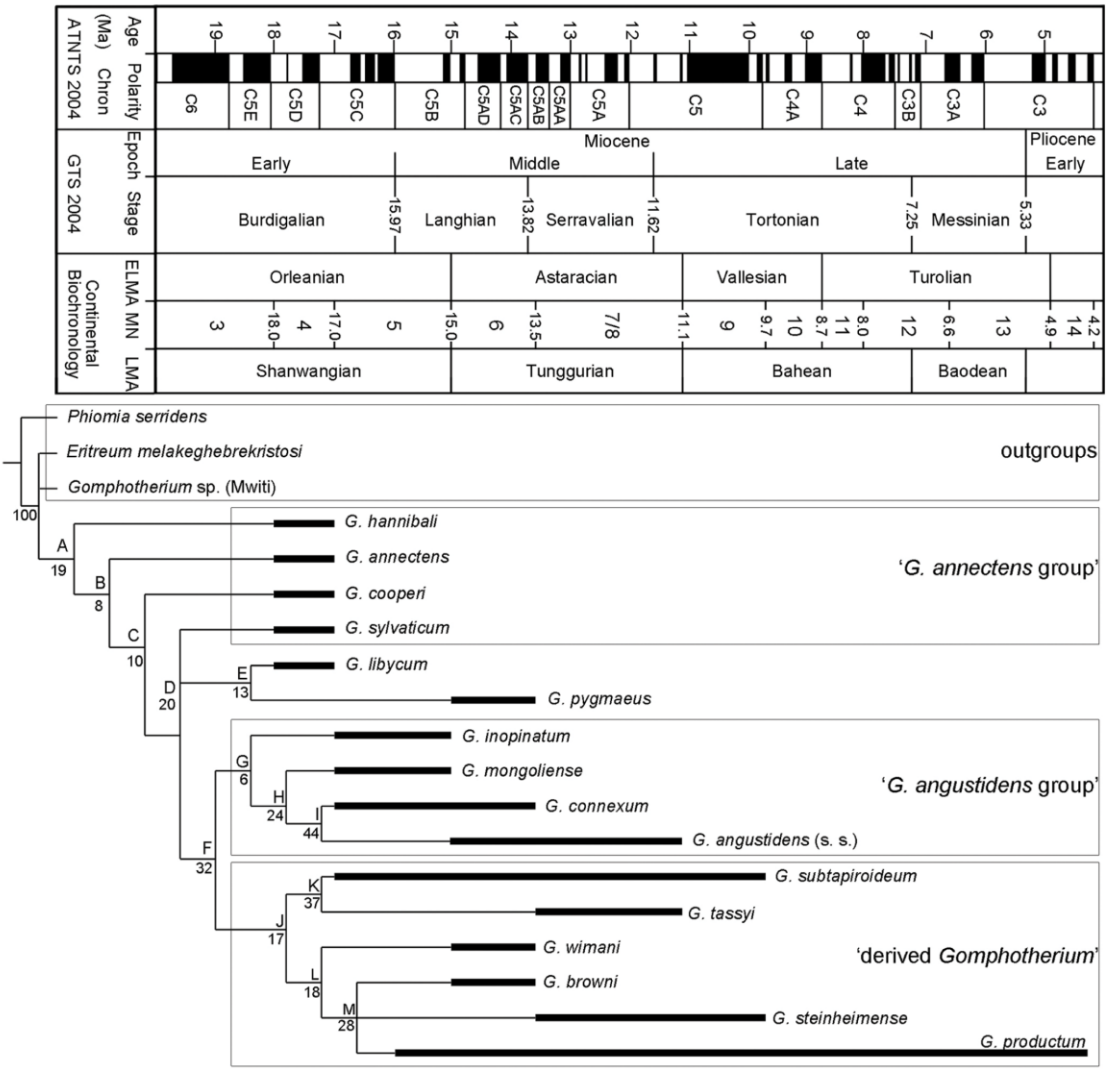

FIGURE 7. The strict consensus tree from three MPTs showing the phylogenetic reconstruction of the *Gomphotherium* species (tree length = 77, CI = 0.636, RI = 0.708). The number at each node represents the bootstrap support. See text for detailed explanation of each node and species.

annectens, G. cooperi, and *G. sylvaticum*. Detailed explanations of the important nodes are as follows.

Node A—This node represents the divergence of the most primitive known Eurasian *Gomphotherium, G. hannibali*. The type locality of this species is Le Mazet, France, and is correlated with the beginning of MN4 (Welcomme, 1994). Unfortunately, the tooth rows are so deeply worn that the molar pattern is unclear. This node is supported by one synapomorphy: presence of an incomplete fourth loph in the M3 (Character 26 in Appendix 1, CI = 1, RI = 1; simplified as 26 [1, 1]). *Gomphotherium hannibali* had a primitive feature of Elephantiformes: presence of the postpalatine spine. This feature is observed in Mammutidae but is not seen in any other species of *Gomphotherium*.

Node B—*Gomphotherium annectens* from Hiramaki Formation, Banjôburo, Japan (mainly MN4) (Tomida et al., 2013), displays numerous plesiomorphies of *Gomphotherium*. This node is supported by one synapomorphy: loss of the postpalatine spine (5 [1, 1]).

Node C—*Gomphotherium cooperi* occurs in Dera Bugti, Pakistan. Based on the updated chronostratigraphy, the first local appearance of *Gomphotherium* was in horizon 'Q = 4' of the upper member of the Chitarwata Formation (Antoine et al., 2013), which is correlated with the early Burdigalian (MN4) (Welcomme et al., 2001). One synapomorphy, anteroposterior enlargement of the interlophids of the lower molars (37 [0.333, 0.667]), supports this node. However, this character state is reversed several times in the more derived groups (e.g., in *G. angustidens* and *G. steinheimense*).

Node D—This node shows a trichotomy that indicates monophyly of the other *Gomphotherium* species. The supporting synapomorphy is the development of an individualized anterior pretrite central conule in the second lophid of the lower molars (24 [1, 1]). The most basal taxon on this node, *G. sylvaticum*, occurs in Artenay, France (MN4) (Göhlich, 2010).

Node E—This node indicates the sister relationship between the African *G. libycum* and *G. pygmaeus*. Originally, *Gomphotherium libycum* was referred to as *G. angustidens libycum*, and the type material of *G. angustidens libycum* comes from the early Miocene (ca. 18.0–17.0 Ma) Moghara Formation, Egypt (Sanders and Miller, 2002). Similar to *G. angustidens* s.s. from Europe, *G. libycum* has relatively narrow molar contours (34 [0.5, 0.5]). However, in the upper molars, the posterior pretrite central conules are smaller than the corresponding anterior pretrite central conules; this feature is distinct from that of *G. angustidens* s.s. Furthermore, as Tassy (2013, 2014) demonstrated, the specific epithet '*angustidens*' was overused, and it is reasonable to change *G. angustidens libycum* to *G. libycum*. The validity of *G. pygmaeus* is still debated (Sanders et al., 2010; Tassy et al., 2013). As Sanders et al. (2010) demonstrated, small species of *Gomphotherium* (the 'pygmy *Gomphotherium* group') were widely distributed during the early to middle Miocene in Afro-Arabian areas and the small size is likely a homoplastic character. At the present stage, we follow Sanders et al. (2010) and regard *G. pygmaeus* as a valid species that includes, for example, the Kabylie and Ngenyin specimens (Depéret, 1897; Pickford, 2004; Sanders et al., 2010). This node is supported by one synapomorphy: narrowness of the interlophs of upper molars (38 [0.333, 0.714]). This character state is repeated at Node L; therefore, this node seems not to be very strong. Possibly, discovery of more material, especially cranial and mandibular material, would be helpful for resolving this problem.

Node F—This node indicates the sister relationship between the '*G. angustidens* group' and the 'derived *Gomphotherium* group.' This node is supported by two synapomorphies: development of an individualized posterior pretrite central conule in the second loph of the upper molars (23 [1, 1]) and reduction and erection of the median flange of the astragalus (tarsus) (43 [1, 1]).

Node G—This node indicates monophyly of the '*G. angustidens* group' and is supported by three synapomorphies: strong torsion of the upper tusks (12 [1, 1]), spiral of the enamel band on the upper tusks (13 [1, 1]), and narrowness of the interlophids of lower molars (37 [0.33, 0.5]). As mentioned in the discussion of Node C, this character is reversed in the '*G. angustidens* group,' because interlophid enlargement is observed in *G. cooperi* and *G. sylvaticum*. The most basal taxon, *G. inopinatum*, occurs in the Jilančik Beds, Turgai, Kazakhstan, and in the Dongxiang Formation, Linxia, China (MN5) (Wang, 2014).

Node H—This node indicates monophyly of *G. mongoliense, G. connexum*, and *G. angustidens*. The supporting synapomorphies include the posterior pretrite central conule larger than the corresponding anterior pretrite central conule in the second loph of the upper molars (31 [1, 1]) and the narrowness of the interlophs of upper molars (38 [0.5, 0.8]). *Gomphotherium mongoliense* occurs in biozone D1/2 of the Loh Formation, Mongolia (MN5) (Daxner-Höck et al., 2013); this taxon has one autapomorphy: very large anterior pretrite central conules in the first lophs (32)

Node I—This node represents a sister relationship between *G. angustidens* s.s. and *G. connexum* and is supported by two synapomorphies: narrowness of the contour of the molars (29 [1, 1]) and reduction of cingulum(id) (31 [0.39, 0.44]). The latter character is also convergent with *G. browni* and *G. steinheimense. Gomphotherium connexum* occurs in Diaogou (possibly MN5) and the Halamagai Formation (MN6), China (Wang et al., 2015). *Gomphotherium angustidens* s.s. occurs from MN6 to MN7/8 in Europe (Tassy, 1985).

Node J—This node represents divergence within the 'derived *Gomphotherium* group,' which is supported by three synapomorphies: four or more lophs of M3 (27 [0.5, 0.833]), subdivision of posttrite half-loph(id)s (40 [1, 1]), and subdivision of pretrite central conules (41 [1, 1]). The species of this group are generally medium to large species that were distributed throughout Eurasia and North America during the middle to late Miocene.

Node K—This node indicates the close relationship between *G. subtapiroideum* and *G. tassyi*. This node is supported by one synapomorphy: anteroposteriorly compressed posttrite half-loph (id)s (35 [1, 1]). We noted several dental and mandibular differences between the two species, and several cranial differences between *G.* cf. *subtapiroideum* and *G. tassyi*. However, no cranium of *G. subtapiroideum* has been reported so far. *Gomphotherium subtapiroideum* occurs in several localities of Central Europe from MN5 to MN8/9 (Göhlich, 2010).

Node L—This node represents divergence of the '*G. productum* group' (Wang, 2014) and is supported by one synapomorphy: relatively high molar crown (39 [1, 1]). As the most primitive member in this group, *G. wimani* is from several localities of northern China during the MN6 biozone (Wang et al., 2013b).

Node M—This node represents a trichotomy between *G. browni, G. productum*, and *G. steinheimense* and is supported by two synapomorphies: narrowness of interlophs of upper molars (37 [0.5, 0.8]) and of interlophids of lower molars (38 [0.33, 0.5]). *Gomphotherium browni* occurs in the Lower Chinji horizon (locality B 51), Pakistan (mainly MN6) (Barry et al., 2013), and *G. steinheimense* is from several localities of Central Europe (MN7/8–MN9) (Göhlich, 1999). *Gomphotherium productum* represents the complex of North American species; further subdivision of this complex should be carried out.

CONCLUSIONS

In this work, we described a new *Gomphotherium* species, *G. tassyi*, from the late middle Miocene Hujialiang Formation, Linxia Basin, China. The molar morphology shows a slightly zygodont-like pattern, which is very similar to that of *G.*

subtapiroideum. The cranium and mandible of *G. tassyi* display some derived features of *Gomphotherium*, such as a domed and slightly erect braincase and retreated facial part. Based on a cladistic analysis of *Gomphotherium* species, four groups were recognized: the most basal '*G. annectens* group' is a paraphyletic group that includes *G. annectens, G. cooperi, G. sylvaticum*, and *G. hannibali*; *G. libycum* and *G. pygmaeus* composed an unnamed monophyletic group that is distributed in Afro-Arabia; the '*G. angustidens* group' is a monophyletic group that includes *G. inopinatum, G. mongoliense, G. connexum*, and *G. angustidens*; *G. subtapiroideum, G. tassyi, G. wimani, G. browni, G. productum*, and *G. steinheimense* constitute the 'derived *Gomphotherium* group' that was widely distributed in the middle to late Miocene of Eurasia and North America. This work is an updated synthesized study of the genus *Gomphotherium*, which played an important role in the evolution of Elephantida.

ACKNOWLEDGMENTS

We thank P. Tassy (MNHN, France) who read the initial manuscript and provided much advice to improve the manuscript. We thank G. Konidaris (Greece) and W. Sanders (U.S.A.) for their great suggestions in their review of this paper. We thank T. Deng, Z.-X. Qiu, S.-K. Hou, Q.-Q. Shi, and B.-Y. Sun (IVPP, China); U. Göhlich (NMHW, Austria); and J. Meng (AMNH, U.S.A.) for discussions and advice on this work. This work was supported by the National Basic Research Program of China (grant no. 2012CB821900), the Chinese Academy of Sciences (grant no. XDB03020104), the National Natural Science Foundation of China (grant nos. 41372001, 41430102), and the Special Research Program of Basic Science and Technology of the Ministry of Science and Technology (grant no. 2015FY310100-14).

LITERATURE CITED

Andrews, C. W. 1906. A Descriptive Catalogue of the Tertiary Vertebrata of the Fayûm, Egypt. British Museum (Natural History), London, 324 pp.

Antoine, P.-O., G. Métais, M. J. Orliac, J.-Y. Crochet, L. J. Flynn, L. Marivaux, A. R. Rajpar, G. Roohi, and J.-L. Welcomme. 2013. Mammalian Neogene biostratigraphy of the Sulaiman Province, Pakistan; pp. 400–422 in X.-M. Wang, L. J. Flynn, and M. Fortelius (eds.), Fossil Mammals of Asia: Neogene Biostratigraphy and Chronology of Asia. Columbia University Press, New York.

Barry, J. C., A. K. Behrensmeyer, C. E. Badgley, L. J. Flynn, H. Peltonen, I. U. Cheema, D. Pilbeam, E. H. Lindsay, S. M. Raza, A. R. Rajpar, and M. E. Morgan. 2013. The Neogene Siwaliks of the Potwar Plateau, Pakistan; pp. 373–399 in X.-M. Wang, L. J. Flynn, and M. Fortelius (eds.), Fossil Mammals of Asia: Neogene Biostratigraphy and Chronology of Asia. Columbia University Press, New York.

Burmeister, H. 1837. Handbuch der Naturgeschichte. Zum Gebrauch bei Vorlesungen. Enslin, Berlin, 526 pp.

Borissiak, A. A., and E. Belyaeva. 1928. *Trilophodon* (*Serridentinus*?) *inopinatus* n. sp. from the Jilančik Beds of the Turgai Region. Bulletin de l'Académie des Sciences de l'URSS, Classe des Sciences Physico-Mathématiques, Leningrad:241–252.

Chang, H.-T., and R.-J. Zhai. 1978. Miocene mastodonts of Lantian and Lintung, Shensi. Professional Papers of Stratigraphy and Palaeontology 7:136–142. [Chinese 136–141; English 141–142]

Cuvier, G. 1817. Le règne animal. Vol. 1. Déterville, Paris, 540 pp.

Daxner-Höck, G., D. Badamgarav, M. Erbajeva, and U. B. Göhlich. 2013. Miocene mammal biostratigraphy of Central Mongolia (Valley of Lakes): new results; pp. 477–494 in X.-M. Wang, L. J. Flynn, and M. Fortelius (eds.), Fossil Mammals of Asia: Neogene Biostratigraphy and Chronology of Asia. Columbia University Press, New York.

Deng, T., Z.-Y. Qiu, B.-Y. Wang, X.-M. Wang, and S.-K. Hou. 2013. Late Cenozoic biostratigraphy of the Linxia Basin, northwestern China; pp. 243–273 in X.-M. Wang, L. J. Flynn, and M. Fortelius (eds.), Fossil Mammals of Asia: Neogene Biostratigraphy and Chronology of Asia. Columbia University Press, New York.

Depéret, C. 1897. Découverte du *Mastodon angustidens* dans l'étage cartennein de Kabylie. Bulletin de la Société géologique de France 3:518–521.

Ferretti, M. P. 2010. Anatomy of *Haplomastodon chimborazi* (Mammalia, Proboscidea) from the Late Pleistocene of Ecuador and its bearing on the phylogeny and systematics of South American gomphotheres. Geodiversitas 32:663–721.

Fisher, D. C. 1996. Extinction of proboscideans in North America; pp. 296–315 in J. Shoshani and P. Tassy (eds.), The Proboscidea: Evolution and Palaeoecology of Elephants and Their Relatives. Oxford University Press, Oxford, U.K.

Göhlich, U. B. 1998. Elephantoidea (Proboscidea, Mammalia) aus dem Mittel- und Obermiozän der oberen Süßwassermolasse Süddeutschlands: Odontologie und Osteologie. Münchner Geowissenschaftliche Abhandlungen 36:1–245.

Göhlich, U. B. 1999. Order Proboscidea; pp. 157–168 in G. E. Rössner and K. Heissig (eds.), The Miocene Land Mammals of Europe. Verlag Dr. Friedrich Pfeil, Munich.

Göhlich, U. B. 2007. Gomphotheres (Proboscidea, Mammalia) from the Early-Middle Miocene of Central Mongolia; in G. Daxner-Höck (ed.), Oligocene-Miocene vertebrates from the Valley of Lakes (Central Mongolia): morphology, phylogenetic and stratigraphic implications. Annalen des Naturhistorischen Museums in Wien 108A:271–289.

Göhlich, U. B. 2010. The Proboscidea (Mammalia) from the Miocene of Sandelzhausen (southern Germany). Paläontologische Zeitschrift 84:163–204.

Goloboff, P. A., J. S. Farris, and K. C. Nixon. 2003. T.N.T.: Tree Analysis Using New Technology. Program and documentation. Available at www.zmuc.dk/public/phylogeny. Accessed May 1, 2016.

Hay, O. P. 1922. Further observations on some extinct elephants. Proceedings of the Biological Society of Washington 35:97–101.

Hopwood, A. T. 1935. Fossil Proboscidea from China. Palaeontologia Sinica, Series C 9:1–108.

Illiger, C. D. 1811. Prodromus systematis mammalium et avium additis terminis zoographicis uttriusque classis. Salfeld, Berlin, 301 pp.

Mazo, A. V. 1996. Gomphotheres and mammutids from the Iberian Peninsula; pp. 136–142 in J. Shoshani and P. Tassy (eds.), The Proboscidea: Evolution and Palaeoecology of Elephants and Their Relatives. Oxford University Press, Oxford, U.K.

Osborn, H. F. 1923. New subfamily, generic, and specific stage in the evolution of the Proboscidea. American Museum Novitates 99:1–4.

Osborn, H. F. 1924. *Serridentinus* and *Baluchitherium*, Loh Formation, Mongolia. American Museum Novitates 148:1–5.

Osborn, H. F. 1926. Additional new genera and species of the mastodontoid Proboscidea. American Museum Novitates 238:1–16.

Osborn, H. F. 1932. *Trilophodon cooperi* n. sp. of Dera Bugti, Baluchistan. American Museum Novitates 393:1–6.

Osborn, H. F. 1936. Proboscidea: A Monograph of the Discovery, Evolution, Migration and Extinction of the Mastodonts and Elephants of the World, Volume I. The American Museum Press, New York, 802 pp.

Pickford, M. 2004. Partial dentition and skeleton of *Choerolophodon pygmaeus* (Depéret) from Ngenyin, 13 Ma, Tugen Hills, Kenya: resolution of a century old enigma. Zona Arqueologica: Miscelánea en Homenaje a Emiliano Aguirre, Paleontologia. Madrid, Museo Arqueologico Regional 4:428–463.

Sanders, W. J., and E. R. Miller. 2002. New proboscideans from the early Miocene of Wadi Moghara, Egypt. Journal of Vertebrate Paleontology 22:388–404.

Sanders, W. J., E. Gheerbrant, J. M. Harris, H. Saegusa, and C. Delmer. 2010. Proboscidea; pp. 161–251 in L. Werdelin and W. J. Sanders (eds.), Cenozoic Mammals of Africa. University of California Press, Berkeley, California.

Schlesinger, G. 1917. Die Mastodonten des K. K. Naturhistorischen Hofmuseums. Denkschriften des K. K. Naturhistorischen Hofmuseums, Geologisch-paläontologische Reihe 1:1–231.

Shoshani, J. 1996. Para- or monophyly of the gomphotheres and their position within Proboscidea; pp. 149–177 in J. Shoshani and P. Tassy (eds.), The Proboscidea: Evolution and Palaeoecology of Elephants and Their Relatives. Oxford University Press, Oxford, U.K.

Shoshani, J., and P. Tassy (eds.). 1996. The Proboscidea: Evolution and Palaeoecology of Elephants and Their Relatives. Oxford University Press, Oxford, U.K., 472 pp.

Shoshani, J., R. C. Walter, M. Abraha, S. Berhe, P. Tassy, W. J. Sanders, G. H. Marchant, Y. Libsekal, T. Ghirmai, and D. Zinner. 2006. A proboscidean from the late Oligocene of Eritrea, a "missing link" between early Elephantiformes and Elephantimorpha, and biogeographic implications. Proceedings of the National Academy of Sciences of the United States of America 103:17296–17301.

Tassy, P. 1977a. Le plus ancien squelette de gomphothère (Proboscidea, Mammalia) dans la Formation Burdigalienne des sables de l'Orléanais France. Mémoires du Muséum National d'Histoire Naturelle (Série C) C 37:1–51.

Tassy, P. 1977b. Découverte de *Zygolophodon turicensis* (Schinz) (Proboscidea, Mammalia) au lieu-dit Malartic a Simorre, Gers (Vindobonien moyen): implications paléoécologiques et biostratigraphiques. Geobios 10:655–669.

Tassy, P. 1985. La place des mastodontes Miocènes de l'ancien monde dans la phylogénie des Proboscidea (Mammalia): hypothèses et conjectures. Ph.D. dissertation, Doctorat ès Sciences, Université Pierre et Marie Curie, Paris, 861 pp.

Tassy, P. 1986. Nouveaux Elephantoidea (Proboscidea, Mammalia) dans le Miocène du Kenya. Cahiers de Paléontologie. Éditions du Centre National de la Recherche Scientifique (CNRS), Paris, 135 pp.

Tassy, P. 1994. Gaps, parsimony, and early Miocene elephantoids (Mammalia), with a re-evaluation of *Gomphotherium annectens* (Matsumoto, 1925). Zoological Journal of the Linnean Society 112:101–117.

Tassy, P. 1996a. Who is who among the Proboscidea; pp. 39–48 in J. Shoshani and P. Tassy (eds.), The Proboscidea: Evolution and Palaeoecology of Elephants and Their Relatives. Oxford University Press, Oxford, U.K.

Tassy, P. 1996b. Dental homologies and nomenclature in the Proboscidea; pp. 21–25 in J. Shoshani and P. Tassy (eds.), The Proboscidea: Evolution and Palaeoecology of Elephants and Their Relatives. Oxford University Press, Oxford, U.K.

Tassy, P. 2013. L'anatomie cranio-mandibulaire de *Gomphotherium angustidens* (Cuvier, 1817) (Proboscidea, Mammalia): données issues du gisement d'En Péjouan (Miocène moyen du Gers, France). Geodiversitas 35:377–445.

Tassy, P. 2014. L'odontologie de *Gomphotherium angustidens* (Cuvier, 1817) (Proboscidea, Mammalia): données issues du gisement d'En Péjouan (Miocène moyen du Gers, France). Geodiversitas 36:35–115.

Tassy, P., and U. B. Göhlich. 2012. Retour sur la série type de *Gomphotherium angustidens* (Proboscidea, Mammalia): de Daubenton à Cuvier, et après. Estudios Geológicos 67:321–332.

Tassy, P., and M. Pickford. 1983. Un nouveau mastodonte zygolophodonte (Proboscidea, Mammalia) dans le Miocène inférieur d'Afrique orientale: systématique et paléoenvironnement. Géobios 16:53–77.

Tassy, P., F. Goussard, and M. G. Sanz. 2013. The status of *Mastodon angustidens pygmaeus* Depéret, 1897 (Proboscidea, Mammalia): the contribution of X-ray tomography. Géobios 46:329–334.

Tobien, H. 1973. On the evolution of mastodonts (Proboscidea, Mammalia), part 1: the bunodont trilophodont groups. Notizblatt des Hessischen Landesamtes für Bodenforschung zu Wiesbaden 101:202–276.

Tobien, H., G.-F. Chen, and Y.-Q. Li. 1988. Mastodonts (Proboscidea, Mammalia) from the Late Neogene and Early Pleistocene of the People's Republic of China, part II: the genera *Tetralophodon, Anancus, Stegotetrabelodon, Zygolophodon, Mammut, Stegolophodon*. Mainzer Geowissenschaftliche Mitteilungen 17:95–220.

Wang, S.-Q. 2014. *Gomphotherium inopinatum*, a basal *Gomphotherium* species from the Linxia Basin, China, and other Chinese members of the genus. Vertebrata PalAsiatica 52:183–200.

Wang, S.-Q., J. Duangkrayom, and X.-W. Yang. 2015. Occurrence of the *Gomphotherium angustidens* group in China, based on a revision of *Gomphotherium connexum* (Hopwood, 1935) and *Gomphotherium shensiensis* Chang and Zhai, 1978: continental correlation of *Gomphotherium* species across the Palearctic. Paläontologische Zeitschrift 89:1073–1086.

Wang, S.-Q., T. Deng, W. He, S.-Q. Chen, and J. Duangkrayom. 2013a. Gomphotheriidae and Mammutidae (Proboscidea, Mammalia) from the Miocene of the Linxia Basin. Acta Geologica Sinica (Supplement) 87:873–874.

Wang, S.-Q., S.-P. Liu, G.-P. Xie, J. Liu, T.-J. Peng, and S.-K. Hou. 2013b. *Gomphotherium wimani* from Wushan County, China and its implications for the Miocene stratigraphy of the Tianshui Area. Vertebrata PalAsiatica 51:71–84.

Wang, S.-Q., X.-P. Ji, N. G. Jablonski, D. F. Su, J.-Y. Ge, C.-F. Ding, T.-S. Yu, W.-Q. Li, and J. Duangkrayom. 2016. The oldest cranium of *Sinomastodon* (Proboscidea, Gomphotheriidae), discovered in the uppermost Miocene of southwestern China: implications for the origin and migration of this taxon. Journal of Mammalian Evolution 23:155–173.

Welcomme, J.-L. 1994. Le plus ancien crâne de proboscidien d'Europe, *Gomphotherium hannibali* nov. sp. (Proboscidea, Mammalia), du Miocène inférieur du Languedoc (France). Comptes rendus de l'Académie des sciences Paris, Série II 319:135–140.

Welcomme, J.-L., M. Benammi, J.-Y. Crochet, L. Marivaux, G. Métais, P.-O. Antoine, and I. Baloch. 2001. Himalayan Forelands: palaeontological evidence for Oligocene detrital deposits in the Bugti Hills (Balochistan, Pakistan). Geological Magazine 138:397–405.

Yang, X.-W., Y. Li, and S.-Q. Wang. in press. Cranial and dental material of Gomphotherium wimani (Gomphotheriidae, Proboscidea) from the Middle Miocene of the Linxia Basin, northwestern China. Vertebrata PalAsiatica http://www.ivpp.cas.cn/cbw/gjzdwxb/press online/201705/P020170511538126191371.pdf

Submitted December 5, 2016; revisions received January 30, 2017; accepted January 30, 2017.
Handling editor: Blaire Van Valkenburgh.

APPENDIX 1. Characters used in the cladistic analysis of *Gomphotherium*.

(1) Cranium, lateral view: flat (0); slightly arched (1).
(2) Basicranium: not erected (0); slightly erected (1).
(3) Facial part, in lateral view: relatively long (anteriorly extended) (0); relatively short (posteriorly retreated) (1).
(4) Rostrum (alveolar socket): relatively short (0); relatively long (1).
(5) Nasal aperture, perinasal fossa: absent (0); present (1).
(6) Palate, postpalatal spine: present (0); absent (1).
(7) Mandibular symphysis, posterior border: close to the anterior end of the cheek tooth row (0); distant from the anterior end of the cheek tooth row (1).
(8) Angular process, position: low (0); high (1).
(9) Symphysis: elongated (0); relatively short (retreated) (1).
(10) Symphysis, degree of ventral deflection: relatively small (0); relatively large (1).
(11) Symphysis, anterior border in dorsal view: anteriorly oblique from both lateral sides to median axis (showing an anteriorly apex) (0); almost straight (1).
(12) Ascending ramus, posterior inclination: almost vertical (0); posteriorly inclined (1).
(13) Upper tusks: without torsion (0); with torsion (1).
(14) Upper tusks, enamel band: not helical (0); helical (1).
(15) Upper tusks, lateral view: strongly bent ventrally (0); relatively straight (1).
(16) Lower tusks, shape of cross-section: flattened (0); not flattened (1).
(17) Lower tusks, shape of cross-section: pyriform or semipyriform (0); oval or subcircular (1).
(18) Lower tusks, dorsal wear facet: flat (0); concave (1).
(19) Lower tusks, lateral view: dorsally bent (0); almost straight (1).
(20) Lower tusks, ventral groove along the tooth: present (0); absent (1).
(21) Cheek teeth, succession: P4/p4 present when M3/m3 in function (0); P4/p4 absent when M3/m3 in function (1).
(22) Cheek teeth: entirely bunodont (0); showing slight zygodont-like pattern (1).
(23) Molar size: relatively large (i.e., M3 and m3 larger than ~100 mm in length and ~80 mm in width) (0); very small

(i.e., M3 and m3 smaller than ~100 mm in length and ~80 mm in width) (Sanders et al., 2010:fig. 15.7) (1).
(24) Upper molars, posterior pretrite central conule (in the second lophs): absent or very weak (0); at least individualized (1).
(25) Lower molars, anterior pretrite central conule (in the second lophids): absent or very weak (0); at least individualized (1).
(26) Molars, M2/m2: third loph(id) incomplete (0); third loph (id) complete (1).
(27) Upper molars, M3: fourth loph not present (0); fourth loph developed (1).
(28) Upper molars, M3: fourth loph incomplete in most cases (0); fourth loph complete in most cases (1).
(29) Upper molars, M3: fifth loph not developed (0); fifth loph developed (1).
(30) Lower molars, m3: fourth lophid incomplete (0); fourth lophid complete (1).
(31) Lower molars, m3: fifth lophid incomplete in most cases (0); fifth loph complete in most cases (1).
(32) Upper molars, pretrite central conules in the second lophs: posterior one equivalent to or smaller than the anterior one (0); posterior one larger than the anterior one (1).
(33) Upper molars, anterior pretrite central conule in the first lophs: not very large (0); very large (1).
(34) Lower molars, posttrite mesoconelet in the second lophids: present (0); nearly absent (1).
(35) Molars, contour: relatively wide (0); relatively narrow (1).
(36) Molars, posttrite half-loph(id)s: not compressed (0); anteroposteriorly compressed (1).
(37) Upper molars, cingulum: relatively developed (0); relatively reduced in most individuals (1).
(38) Lower molars, interlophids: moderate wide ('V'-shaped first ectoflexid) (0); anteroposteriorly widened ('U'-shaped first ectoflexid) (1).
(39) Upper molars, interlophs: moderately wide ('V'-shaped first entoflexus) (0); anteroposteriorly compressed ('Y'-shaped first entoflexus) (1).
(40) Molars, crown: low crowned (0); relatively high crowned (1).
(41) Molars, posttrite half-loph(id)s: not subdivided (0); subdivided (1).
(42) Molars, pretrite central conules in the first two loph(id)s: not subdivided in most cases (0); subdivided (1).
(43) Molars, posttrite central conules: absent (0); slightly developed (1).
(44) Molars, posttrite half-lophs in the first lophs of upper molars: not anteriorly convex (0); anteriorly convex (1).
(45) Upper molars, M3: widest part at the first loph (0); widest part moved posteriorly (1).
(46) Upper premolars, P4: with two roots (0); with three roots (1).
(47) Upper deciduous premolars, DP3: central conules not enlarged (0); central conule enlarged (1).
(48) Deciduous premolars, DP3/dp3: central conules without alternated contact (0); central conules with alternated contact (1).
(49) Astragulus, trochlea: median flange strong and inclined (0); median ledge reduced and erected (1).
(50) Tarsus, articulation between calcaneum and navicular: present (0); absent (1).

APPENDIX 2. Character states used in the cladistic analysis of *Gomphotherium*. Data source: *Phiomia serridens* (Andrews, 1906); *Eritreum melakeghebrekristosi* (Shoshani et al., 2006); *Gomphotherium* sp. from Mwiti (Tassy, 1986); *G. hannibali* (Welcomme, 1994); *G. annectens* (Tassy, 1994); *G. cooperi* (Osborn, 1932); *G. sylvaticum* (Tassy, 1977a); *G. libycum* (Sanders and Miller, 2002); *G. pygmaeus* (Depéret, 1897; Pickford, 2004; Sanders et al., 2010); *G. inopinatum* (Borissiak and Belyaeva, 1928; Wang, 2014); *G. mongoliense* (Osborn, 1924; Göhlich, 2007); *G. angustidens* s.s. (Tassy, 2013, 2014); *G. connexum* (Hopwood, 1935; Wang et al., 2015); *G. subtapiroideum* (Schlesinger, 1917; Göhlich, 2010; Wang et al., 2015); *G. wimani* (Hopwood, 1935; Wang et al., 2013b); *G. browni* (Osborn, 1926); *G. steinheimense* (Göhlich, 1999); *G. productum* (AMNH).

Taxon	0	10	20	30	40
Phiomia	0000000000	0000000000	0000000000	0000000000	000000??00
Eritreum	????????00	??????10?0?	000?01???1	0??00000?0	0000??????
Mwiti *Gomphotherium*	?????0????	??????????	0000?1000?	?000000?00	0000000???
G. hannibali	??00?0????	??????????	0000?11001	?000000000	0000000???
G. annectens	??0?010000	10???10000	0000011001	0000000000	0000000???
G. cooperi	??????????	??????????	0000011001	0000000100	0000000???
G. sylvaticum	??????????	??00110010	?000111001	0000000100	0000000000
G. libycum	??????????	??????????	?000111001	0000100110	0000000???
G. pygmaeus	??????????	??????????	?010111001	0000000110	0000000???
G. inopinatum	???????000	?011110001	?001111001	0000000000	0000000???
G. mongoliense	??????????	?????10???	0001111001	0110000010	0000100???
G. angustidens s.s.	1111111101	1111010101	1001111101	0100101010	0000111111
G. connexum	???????1?01	??????1?1??	1001111001	0101101010	0000000???
G. subtapiroideum	0001111000	1000110001	1101111101	0000010100	1100001???
G. tassyi	1111111100	?100010001	1101111101	0000010100	1101000???
G. wimani	???????1???	??????1????	1101111101	0000000101	1110100???
G. browni	?????11?11	1?00111010	1001111101	?000001011	1110000???
G. steinheimense	?????11001	0000111010	1001111111	1000000011	1110100???
G. productum	1100111001	0000011000	1001111101	0000001011	1100100???

PLOS | ONE

RESEARCH ARTICLE

Freshwater Fossil Pearls from the Nihewan Basin, Early Early Pleistocene

Su-Ping Li[1,2]*, Pei-Yi Yao[1], Jin-Feng Li[3], David Kay Ferguson[4], Long-Rui Min[1], Zhen-Qing Chi[1], Yong Wang[1], Jian-Xin Yao[1,2], Jin-Geng Sha[5]

1 Institute of Geology, Chinese Academy of Geological Sciences, Beijing, P. R. China, **2** Key Laboratory of Stratigraphy and Paleontology, Ministry of Land and Resources of China, Beijing, P. R. China, **3** State Key Laboratory of Systematics and Evolution, Institute of Botany, Chinese Academy of Sciences, Beijing, P. R. China, **4** University of Vienna, Institute of Palaeontology, Vienna, Austria, **5** Nanjing Institute of Geology and Palaeontology, Chinese Academy of Sciences, Nanjing, P. R. China

* lisuping@cags.ac.cn

Citation: Li S-P, Yao P-Y, Li J-F, Ferguson DK, Min L-R, Chi Z-Q, et al. (2016) Freshwater Fossil Pearls from the Nihewan Basin, Early Early Pleistocene. PLoS ONE 11(10): e0164083. doi:10.1371/journal.pone.0164083

Editor: Daniel Rittschof, Duke University Marine Laboratory, UNITED STATES

Received: July 27, 2016

Accepted: September 19, 2016

Published: October 19, 2016

Data Availability Statement: All relevant data are within the paper.

Funding: This research was supported by the Ministry of Science and Technology of the People's Republic of China (No. 2015FY310100), the National Natural Science Foundation of China (Nos. 41172150, 31500183, 41472030, 31300186), the Ministry of Land and Resources of China (No. 201211005-1), the China Geological Survey (Nos. DD20160120-04, DD20160345, 121201140 26701) and the Basic Research Fund of the Chinese Academy of Geological Sciences (No. YYWF201501). The funders had no role in study

Abstract

Fossil blister pearls attached to the shells of an *Anodonta* mollusk from China, early Early Pleistocene, are reported here for the first time. The pearls were investigated in detail using a variety of methods. Micro-CT scanning of the fossil pearls was carried out to discover the inner structure and the pearl nucleus. Using CTAn software, changes in the gray levels of the biggest pearl, which reflect the changing density of the material, were investigated. The results provide us with some clues on how these pearls were formed. Sand grains, shell debris or material with a similar density could have stimulated the development of these pearls. X-ray diffraction analysis of one fossil pearl and the shell to which it was attached reveals that only aragonite exists in both samples. The internal structures of our fossil shells and pearls were investigated using a Scanning Electron Microscope. These investigations throw some light on pearl development in the past.

Introduction

The Nihewan beds, located in Hebei Province, northern China, are famous for their continuous deposition and complete set of Quaternary strata. Numerous studies were carried out after the "Nihewan Layer" was chosen as the Standard Stratum for the early Pleistocene of northern China (e.g. [1–4]). Fossils excavated in the Nihewan area are both numerous and highly diverse, including human remains (e.g. [1], [4], [5]), pollen and spores (e.g. [6–7]), mammalian fossils (e.g. [8–10]) and mollusks [11]. In the course of collecting mollusk fossils in the Taier-gou section, Nihewan area, the fossil pearls studied in this contribution were found by chance.

Pearl is traditionally and commonly used as a decorative element in jewelry. We are familiar with pearls extracted from living mollusks, but fossil pearls are seldom encountered. Various studies on mollusk fossils, as the producers of pearls, have been carried out in the past few years (e.g. [12–14]). However, reports on fossil pearls are comparatively rare. Some occurrences of fossil pearls have been reported since the first mention of them by Woodward in 1723 [15]. Boucot and Poinar Jr [16] have provided us with a comprehensive survey of most of the

design, data collection and analysis, decision to publish, or preparation of the manuscript.

Competing Interests: The authors have declared that no competing interests exist.

previously published records of fossil pearls. The oldest structures that are possible blister pearls occur in some Silurian *Nuculodonta* from Gotland [17], while similar "pearl-like" structures were also discovered in a Late Silurian cardiolid bivalve [18]. In addition, pearl pits from early Devonian ammonoids were reported by De Baets et al. [19]. The oldest free pearls of bivalves are from the Late Triassic [20]. The richest findings of fossil pearls are from the Cretaceous, with most of the shells to which they were attached being identified as *Inoceramus* (e.g. [21–24];). Cenozoic occurrences of fossil pearls are also common, except for the Paleocene (e.g. [22], [23], [25–32]). The youngest findings of fossil pearls are from the Pleistocene. According to Boucot and Poinar Jr [16], five occurrences of fossil pearls in the Pleistocene have been published: "*Modiolus modiolus*, Scotland [29]; *Mytilus edulis*, Sweden [29], *Anadara transversa*, Maryland [33]; *Arca transversa*, Maryland [34] and *Volsella modiolus*, Scotland [25]". Actually, *Modiolus modiolus* (Syn. *Volsella modiolus*) mentioned in [29] is just referring to [25], and *Anadara transversa* (Syn. *Arca transversa*) in [33] is referring to [34]. The first description of Pleistocene pearls from *Mytilus edulis* in Scotland was by Jackson [22]. In addition, there are two records of Pleistocene *Mytilus edulis* from Ontario, Canada [30], which were missed by Boucot and Poinar Jr [16]. To conclude, Pleistocene pearls have so far only been found in Europe and North America from three mollusk species, viz.: *Modiolus modiolus*, Scotland [25]; *Mytilus edulis*, Sweden [22] and Canada [30]; *Anadara transversa*, Maryland [34]. The present paper reports the first occurrence of fossil pearls from the Pleistocene of Asia. Although ancient freshwater mollusks also produced pearls, most fossil pearls come from saltwater species of mollusks.

Because fossil pearls, especially those from freshwater, are rare, any new discovery deserves to be made public. The present material provides us with an opportunity to study the microstructure of the fossil pearls in detail.

Locality, Material and Methods

No permits were required for the described study, which complied with all relevant regulations. Our fossil site is not a protected area and the collections are considered to be sporadic collections. Based on relevant legislation in China, no administrative approval is necessary for sporadic collections of fossils. Sporadic collections refer to activities using hand-held rather than mechanical tools to excavate a small number of fossils at the surface, involving no changes to the earth's surface or other resources.

The fossil material was collected in the east of the Taiergou Section, Nihewan Basin (Fig 1). The latitude and longitude of the sampling site are N40°12′24.46″ and E114°38′11.35″ respectively. The geological age of the Taiergou Section ranges from 3.6 Ma to 0.11 Ma based on paleomagnetic and thermoluminescence studies [35], and is further divided into three formations including the Pliocene Yuxian Formation, the Pleistocene Nihewan Formation and the Xiaodukou Formation [35–36]. Our fossil site is located at the bottom of the Nihewan Formation, i.e. early Early Pleistocene. The Nihewan Formation is mainly composed by yellowish sand, silty sand and clayey silt of fluvio-lacustrine origin. The outcrop near our fossil site is rich in sand (Fig 2). The underlying stratum, the Yuxian Formation, lies in conformable contact with the Nihewan Formation.

In total 18 pieces of mollusk fossils were collected, 3 of which are whole shells (Fig 3A–3C). Fossil pearls were found on 6 pieces of fragments (Fig 4). However, some of the tiny bumps, which might be pearls, are difficult to recognize. Therefore, the number of pearls is somewhat uncertain, about sixty grains. Of these, the biggest one (red arrow in Fig 4E) measured 3.06 mm×4.11 mm. Another five pearls have diameters between 1 mm to 2 mm. The diameters of all the remaining pearls are less than or about 1 mm. All the measurements of fossil mollusks (length, height and width) and pearls (diameter) were obtained using a vernier caliper.

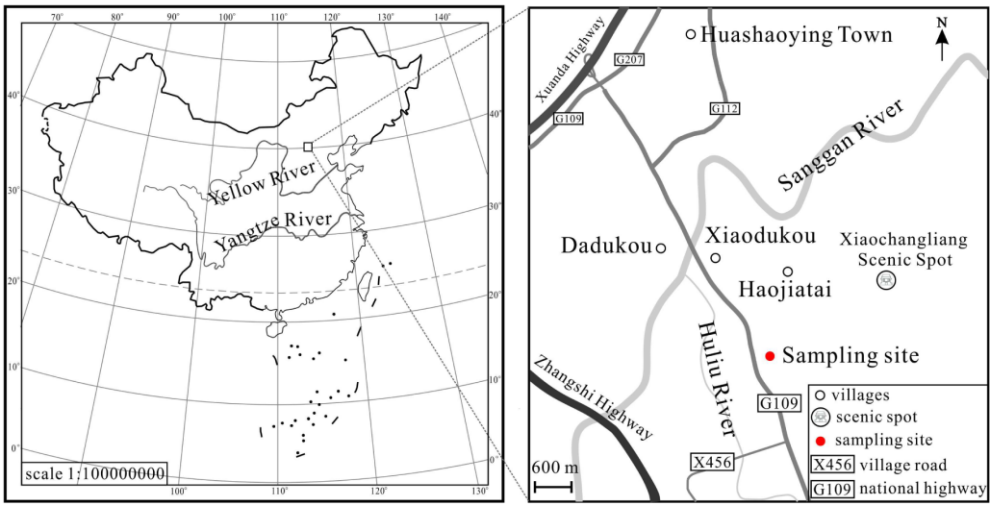

Fig 1. Sketch map showing the location of the fossil site. Map of the People's Republic of China (No. GS(2008)1826) downloaded from the website of the National Administration of Surveying, Mapping and Geoinformation (http://219.238.166.215/mcp/Default.html).

doi:10.1371/journal.pone.0164083.g001

The photographs of our specimens were taken with a Nikon D300s. One shell specimen with fossil pearls was scanned under a Sky scan 1172 X-Ray micro-CT machine (source voltage 80 kV, source current 112 microamperes). Analyses of these CT photos, such as measuring the size of the nucleus, the curve of gray levels, were carried out using a CTAn program. One pearl was manually detached from the shell and together with some pieces of the shell, was milled into a fine powder for X-ray diffraction (XRD) (Y2000 machine, Cu-Ni, 30kV, 20 mA, 0.1°/S). Using a tweezer, another grain of pearl was broken into small pieces, some of which were picked out and observed under a JEOL 6701F Scanning Electron Microscope (SEM), after they had been coated with white gold. All the remaining specimens (identification numbers: NHW16-01~NHW16-24) are deposited in the Institute of Geology, Chinese Academy of Geological Sciences, No. 26 Baiwanzhuang Road, Xicheng District, Beijing, P. R. China. All these specimens are accessible in a permanent repository.

Results and Discussion

The fossil mollusks

Photographs of the fossil shells are shown in Fig 3. Based on the features below, we assign our fossil mollusk to *Anodonta* sp., Unionidae.

Outline is oval or rounded rectangular. The shell is thin and fragile with a relatively smooth surface. The length ranges from 8.7 cm to 11.4 cm based on three well-preserved specimens, and the height and width vary from 6.9 cm to 8.8 cm and 3.1 cm to 4.8 cm respectively. Umbo is slightly projecting beyond the hinge margin and lies at slightly less than 1/3 of the valve length close to the anterior end. The maximum convexity is not within the umbonal region. The posteroventral angle is distinct. Concentric rings are obvious on the shell surface, being stronger near the valve margin. The hinge margin is narrow and the hinge teeth are weak on the hinge plate (see Fig 3D and 3E).

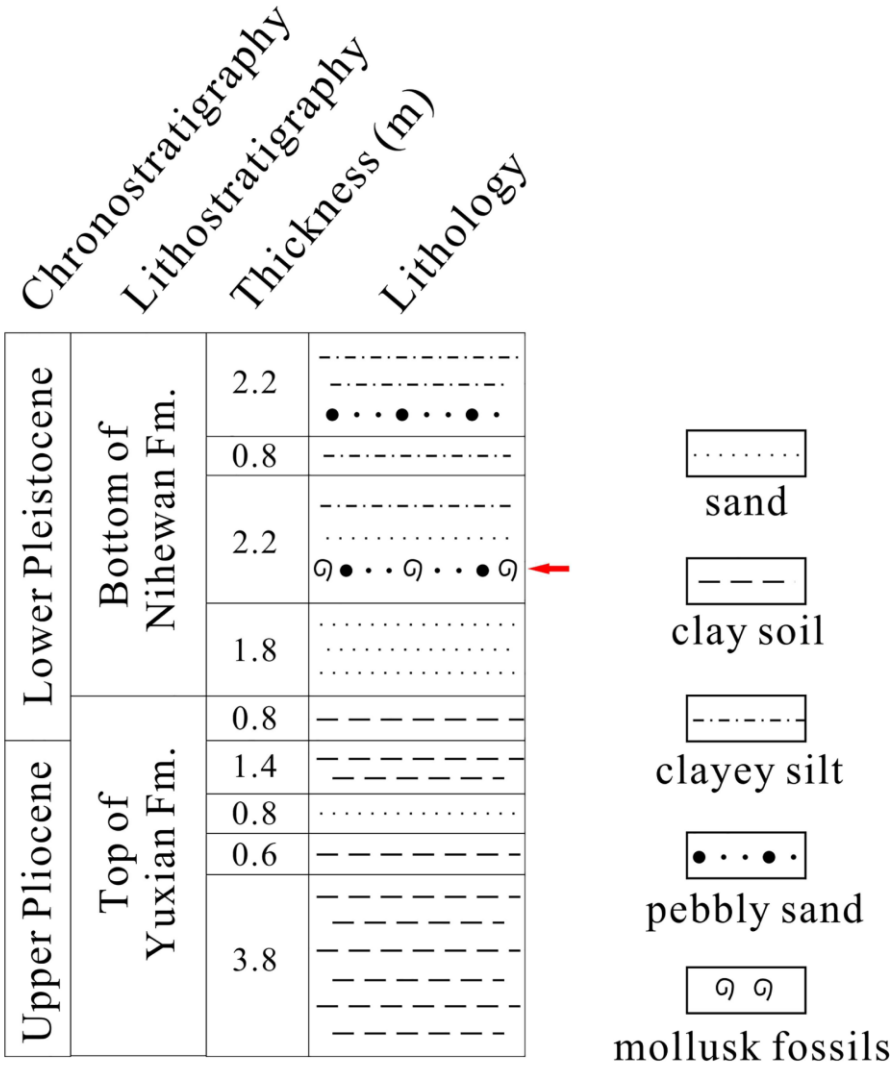

Fig 2. Sedimentary succession at the fossil site (Based on [35]). The red arrow indicates the fossil horizon.

doi:10.1371/journal.pone.0164083.g002

Although many other species of living pelecypods produce pearls, the ones for commercial use are taken almost entirely from bivalve mollusks of which the most important families are Pteriidae, Aviculidae, Mytilidae and Unionidae [27]. Our mollusk fossils with their numerous pearls belong to the Unionidae.

Fossil pearls

About sixty blister pearls were found on six shell fragments (Fig 4). They are solidly attached to the inner surface of the shells. The pearls are almost spherical or flattened spherical with a well-developed pearly lustre. The biggest pearl is about 3.06 mm×4.11 mm.

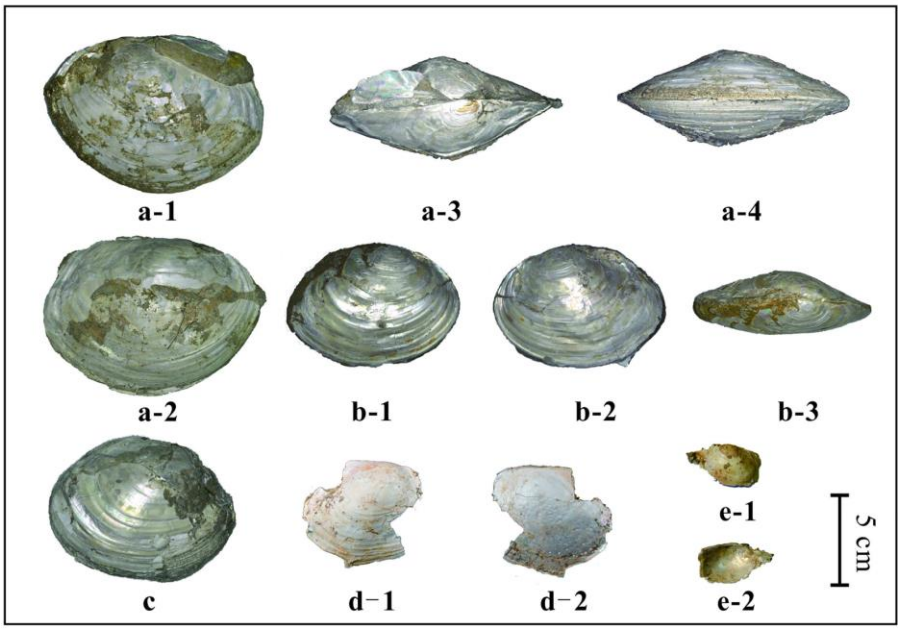

Fig 3. Photographs of mollusk fossils found in the Nihewan Basin. Fig 3a-1, 3a-2, 3a-3 and 3a-4 show the same specimen from different angles, as do Fig 3b-1, 3b-2 and 3b-3. Fig 3d-1 and 3e-1 display the morphology of the left valve and the right valve of different specimens, while Fig 3d-2 and 3e-2 are of their inner surface.

doi:10.1371/journal.pone.0164083.g003

How the fossil pearls formed. In response to an injury or stimulation of the mantle tissue, mollusks can secrete shelly material and pearls to protect the soft body tissues. The process of pearl development has been termed biomineralization [37–39]. It is commonly considered that

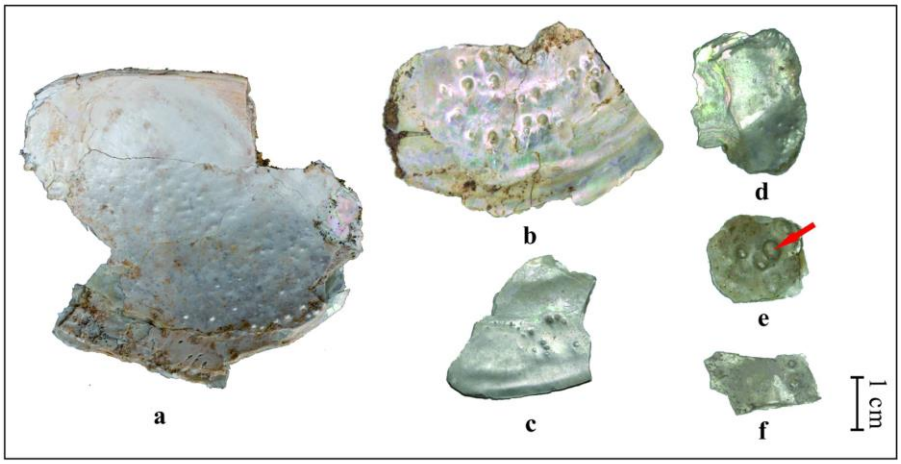

Fig 4. Photographs of fossil pearls found in the Nihewan Basin. The red arrow points to the biggest pearl we found.

doi:10.1371/journal.pone.0164083.g004

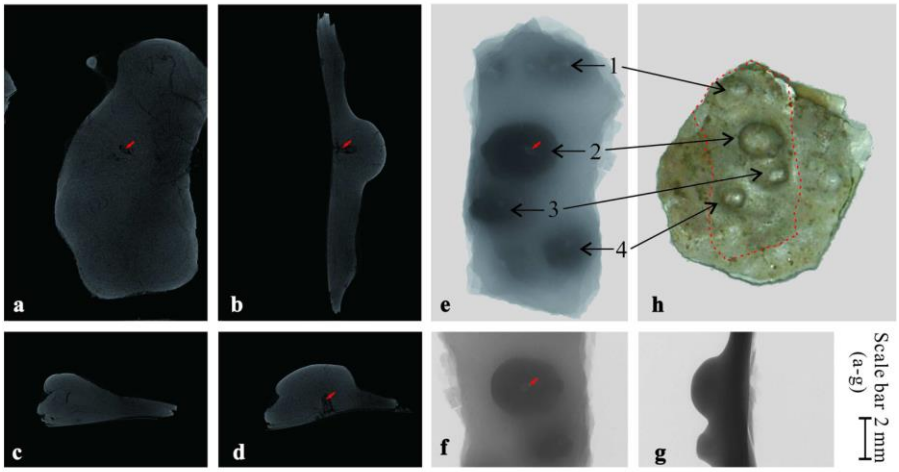

Fig 5. Photographs showing the pearls under micro-CT scan machine. Fig 5a to 5d are scanning photos, while Fig 5e to 5g are shadow projections. Four pearls on one specimen were scanned, among which the pearl of No. 2 is the biggest. Fig 5b, 5d and 5f also show this pearl. The red arrows point to the nucleus.

doi:10.1371/journal.pone.0164083.g005

foreign objects, such as sand grains or parasites etc., which invade between the mantle and the shell, can cause the secretion of shelly material which encapsulates the irritant in a cyst to protect the soft body tissues of the mantle. In due course, a pearl sac is formed. Some evidence also suggests that natural pearls are the result of an oyster's response to mantle tissue injury only. But, in this case, there is no pearl nucleus.

As the development of pearls can have different causes, it is necessary to find some evidence as to how our pearls were formed. The shell with fossil pearls in Fig 4E was scanned under the micro-CT (Fig 5). For the convenience of scanning, the original shell was cut to a smaller piece to fit the specimen chamber, as shown with the dashed line in Fig 5H. In Fig 5A to 5D, changes in the gray level reflect differences in the density of the material, a lighter color, reflects a greater density. Only in the biggest pearl, a nucleus was found as shown by the red arrows in Fig 5A, 5B, 5D, 5E and 5F. It was found to measure about 0.3 mm×0.8 mm using the CTAn program.

The curve on the right hand side of Fig 6 shows the gray level changes of the biggest pearl along the red line on the left. Abrupt decreases in gray level (getting darker) at a and b indicate the low density of material at these two points. Based on the structure of pearls, the thin layer

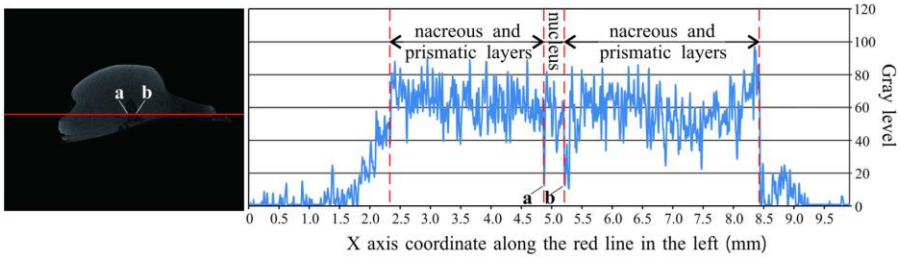

Fig 6. Changing curve showing the gray levels of each pixel along the red line on the left. Labels a and b show the amorphous matrix layer.

doi:10.1371/journal.pone.0164083.g006

should be an amorphous matrix layer (mainly organic matter). The thickness of the amorphous matrix layer varies greatly among different species. In our specimen, the maximum thickness is about 1 mm. The gray intensities of the pearl nucleus and the nacreous layer, based on the curve in Fig 6, are comparable. That is, the densities of the material from the nacreous layer and the nucleus are similar. In this case, we assume that materials with a density close to that of the pearl, such as sand grains or small pieces of broken shell, stimulated the development of these pearls.

The formation of a pearl is the result of a rather accidental occurrence within the normal life cycle of a mollusk [40] and *Anodonta* is a genus with a strong tendency to produce pearls. But why should so many pearls be formed in the shell? It must have some connection with the environment in which the mollusk lived. A flowing, turbid waterbody, even of limited duration, might have caused a single formation of so many pearls, because in this way, more alien matter such as sand grains will enter the mollusks in the course of feeding.

Analysis of XRD patterns. No matter whether one is dealing with freshwater or seawater, natural or cultured pearls, $CaCO_3$ is the main constituent. But different kinds of pearls possess different crystalline phases of $CaCO_3$. The earliest study on pearl structure stated that only calcite and aragonite exist in pearls and shells [41]. Calcite constitutes the prismatic layer while the nacreous layer is composed of aragonite and sometimes a little calcite. In recent years, it has become apparent that the calcium carbonate can occur as aragonite, calcite and vaterite or mixtures of two of these components, depending on differences in the pearl's texture and living environment [42–43]. Vaterite is rare in nature because it is an unstable crystalline form of calcium carbonate, which is only found in cultured pearls [44]. In most of the mollusk shells, the main $CaCO_3$ configuration existing in the shell is aragonite. This crystalline phase is also commonly encountered in pearls. Aragonite is known to be less stable than calcite. During diagenesis, the aragonite is converted into calcite. Fossil shells composed of aragonite become increasingly rare in successively older geological deposits [45]. Therefore, it is necessary to investigate the exact composition of our fossils.

X-ray diffraction (XRD) is usually used to distinguish the crystal polymorphs and it was applied to our fossil samples to check their composition. For comparison, the XRD patterns of the fossil pearl and the shell to which it was attached are shown in Fig 7, while the detailed diffraction data are shown in Table 1. XRD patterns of the fossil pearl (CT-1) and shell (CT-2) are quite similar. All the standard X-ray diffraction peaks of calcite, aragonite and vaterite are taken from GDNU [46]. No diffraction peaks of either calcite (3.030) or vaterite (3.289, 2.732 and 1.821) were detected in these two patterns, which indicate that calcite and vaterite are both absent in our fossil samples. The five strongest peaks in the fossil sample (3.382, 3.261, 2.694, 2.365 and 1.973) approximate the standard XRD spectra for aragonite (3.396, 3.273, 2.700, 2.372 and 1.977). The XRD results reveal that our fossils have undergone little diagenesis.

Microstructures under SEM. During diagenesis the pearl's mineral components may change, but the fossil pearl should retain its original concentric layering. In modern pearls, there are two essential layers, viz. the nacreous layer and the prismatic layer. In order to study the internal structure of our fossil pearl and shell in detail, some broken pieces were investigated under a Scanning Electron Microscope (Fig 8). Their microstructures show great differences, with only nacreous layers being observed in the shell while more complicated structures were encountered in the pearl.

Studies on modern shells of *Anodonta cygnea* and *A. anatina* show great differences in microstructure [47–48], especially in the ratios of prism to nacre thickness in these two species. The prism to nacre ratios values in the *A. anatina* shell are: 0.7:3.8 mm in the marginal region and 1.1:3.9 mm in the central part. In the species *A. cygnea*, these ratios are 0.23:0.14 mm in the marginal region and 0.22:0.85 mm near the central part. The dominance of prism at the

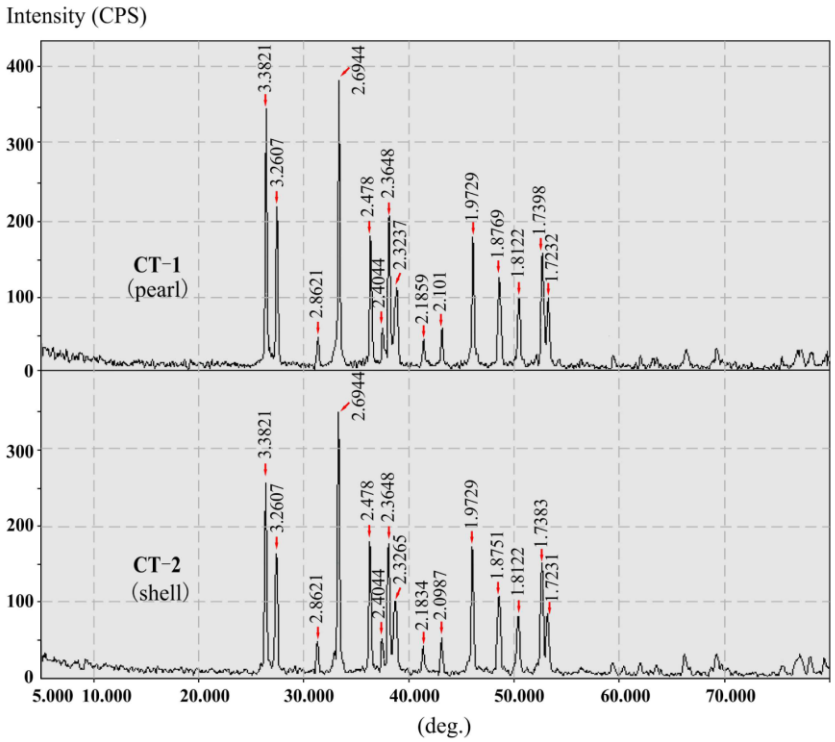

Fig 7. XRD patterns of one fossil pearl and the shell to which it was attached.

doi:10.1371/journal.pone.0164083.g007

margin of *A*. *cygnea* might explain the apparent fragility at the gape where pieces are easily broken from this very thin area [47]. In addition, nacre is considered to withstand compression and bending (e.g. [49–51]). These microstructure features of the two species are presumed to be results of their adaptation to the habitats in which they live: *A*. *cygnea* prefers quiet water bodies with muddy but not oozy bottoms, while *A*. *anatina* is commonly observed in flowing water with a sandy substrate [47]. In our mollusk fossils, only nacreous layers can be found in specimens from both central and marginal parts as shown in Fig 8A–8C. Although the prismatic layer must have been present, we assume that our fossil shell belonged to the thin outer prismatic layer type. Undoubtedly, a thick organic interprismatic envelope completely covered the external surface of the prisms [47]. With the decomposition of the organic material, the thin prismatic layer might flake off during fossilization. The presence of short prisms growing in a dense organic matrix was also observed in the shell of modern *Entodesma navicula* [52]. Although somewhat speculative, the microstructure of our mollusk fossils suggests that the waterbody in which our mollusks lived was flowing and turbid during early Early Pleistocene. This paleoecological interpretation confirms the sedimentological interpretation.

On the pearl surface shown in Fig 8D, irregular polygonal shapes can be observed. These should represent the single lamella of aragonite tablets. We measured the thickness of the aragonite tablets based on the two detached pieces (labels 1 and 2) in Fig 8E. These are 0.34 μm and 0.37 μm respectively with an average of 0.36 μm. In Fig 8F the growing surface of the aragonite crystal layer is shown. The spherical structures shown in Fig 8G and 8H seem to be

Table 1. X-ray powder diffraction data of fossil pearl and shell and calcium carbonate minerals.

CT-1 (pearl)		CT-2 (shell)		Standard X-ray powder diffraction data of calcium carbonate minerals [46]					
				Vaterite 33–268		Aragonite 5–0453		Calcite 24–27	
d	I/I0	d	I/I0	d	I/I0	d	I/I0	d	I/I0
-	-	-	-	4.219	25	4.212	2	-	-
3.382	90	3.382	73	3.571	60	3.396	100	3.582	29
3.261	56	3.261	46	3.289	100	3.273	52	-	-
-	-	-	-	-	-	-	-	3.03	100
2.862	12	2.862	14	-	-	2.871	4	2.834	2
-	-	-	-	-	-	2.73	9	-	-
2.694	100	2.694	100	2.732	90	2.7	46	-	-
2.478	46	2.478	50	-	-	2.481	33	2.495	7
2.404	15	2.404	15	-	-	2.409	14	-	-
2.365	53	2.365	50	-	-	2.372	38	-	-
-	-	-	-	-	-	2.341	31	-	-
2.324	29	2.326	28	2.32	5	2.328	6	2.284	18
2.186	11	2.183	12	-	-	2.188	11	-	-
2.101	15	2.099	15	2.061	60	2.106	23	2.094	27
1.973	45	1.973	48	-	-	1.977	65	1.926	4
1.877	31	1.875	30	1.855	30	1.877	25	1.907	17
1.812	25	1.812	23	1.821	70	1.814	23	1.872	34
1.757	6	-	-	-	-	-	-	-	-
1.74	40	1.738	42	-	-	1.742	25	-	-
1.723	25	1.723	23	-	-	1.728	15	-	-
1.694	4	1.695	3	-	-	-	-	-	-
1.635	4	1.635	3	1.644	30	-	-	1.625	2
1.557	5	1.557	5	-	-	1.557	4	1.604	15
-	-	1.532	4	-	-	-	-	-	-
1.499	5	1.498	6	-	-	-	-	-	-
1.473	4	-	-	1.477	10	-	-	-	-
1.465	5	1.464	5	-	-	-	-	-	-
1.41	7	1.412	9	-	-	1.411	5	-	-
1.358	7	1.357	9	1.366	10	1.358	3	-	-
1.261	5	1.258	4	-	-	-	-	-	-
1.24	7	-	-	-	-	-	-	-	-
1.236	10	1.236	9	-	-	-	-	-	-
1.224	6	1.223	8	-	-	-	-	-	-
1.205	6	1.206	7	-	-	-	-	-	-

doi:10.1371/journal.pone.0164083.t001

attached to the fibrous prism of the outer layer. Fig 8I shows the junction area of the sperulitic structures. They are also composed of fibrous aragonite with concentric growth. Perhaps, because of the competitive growth of the fibrous aragonite or deformation during fossilization, the shapes shown in Fig 8G are not all spherical. The nature of the outer prismatic layer has been slightly altered during fossilization, since some of the individual prisms are no longer easy to distinguish (Fig 8J). The structure of the prismatic layer is not simple as in modern pearls [43]. Aragonite tablets exist not only in the nacreous layer, but also in the prismatic layer. Banding can be observed because of the interlacing and parallel distribution of prisms and tablet zones (Fig 8J and 8K). However, the thickness of the tablets in Fig 8I (label 5) is about 0.31 μm thicker (with a mean thickness of 0.67 μm) than that of the nacreous layer. Two

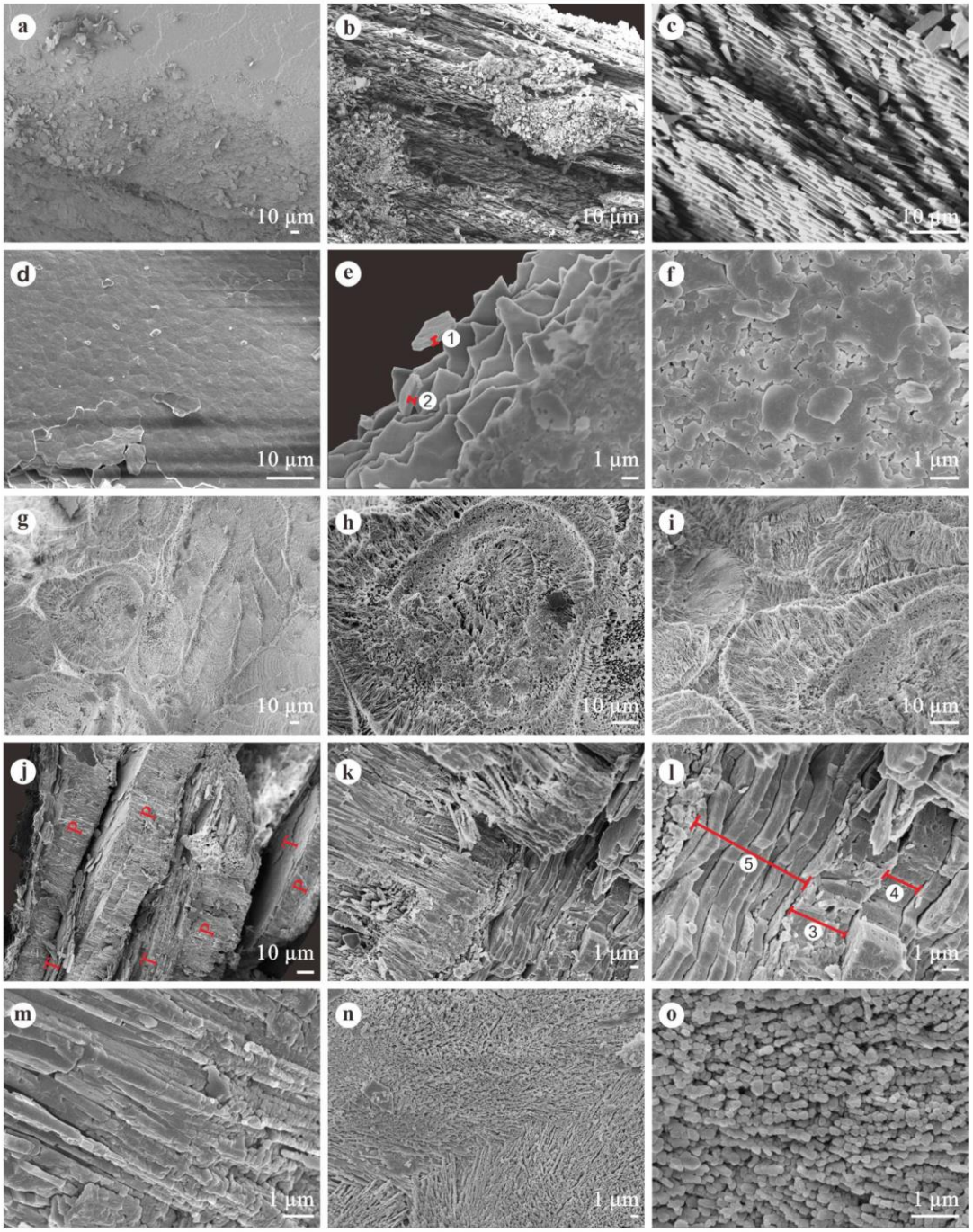

Fig 8. SEM photographs showing the internal structure of the fossil shells (a-c) and pearls (d-o). (Fig 8a-8c) Nacreous layers of the fossil shell. (Fig 8d) The pearl surface. (Fig 8e) Nacreous layer of the fossil pearl. (Fig 8f) Growing surface of the aragonite crystals. (Fig 8g

and 8h) Spherulitic structure formed by fibrous aragonite. (Fig 8i) Junction area of the spherulitic structures. (Fig 8j and 8k) Interlacing aragonitic prisms and tablets. (Fig 8l) Thickness variations of different layers among the tablets interlayer. (Fig 8m and 8o) Longitudinal and transverse sections of the fibrous aragonite crystals. (Fig 8n) Junction between two fibrous prisms. Labels 1–4 indicate the thicknesses of each layer, 1 = 0.34 μm; 2 = 0.37 μm; 3 = 3.23 μm; 4 = 2.3 μm; 5, the thickness of the 11 tablet layers is 7.32 μm (0.67 μm on average). P and T in Fig 8j indicate prism layers and tablet layers respectively.

doi:10.1371/journal.pone.0164083.g008

abnormally thick layers (labels 3 and 4) are also observed among the tablet layers as shown in Fig 8I. These are much thicker (with thicknesses of about 3.23 μm and 2.3 μm respectively) than those of the tablets. How these were formed is unclear. The prisms in the prismatic layer are composed of long and thin aragonitic fibers as shown in Fig 8M, 8N and 8O. The diameters of these fibers range from 0.08 μm to 0.29 μm. The junction between two fibrous prisms, with a typical structure of diverging fibers, is shown in Fig 8N.

Conclusions

1. Fossil pearls, dating from the early Early Pleistocene, were found attached to shells of *Anodonta* in the Nihewan Basin, northern China. Although a few fossil pearls have been reported from other parts of the world, this is the first record from the Pleistocene of Asia.
2. CT scans indicate the presence of a pearl nucleus. The density of the nucleus is similar to that of the nacreous and prismatic layers, which indicates that sand grains, shell debris or material with a similar density caused the fossil pearls to develop.
3. X-ray Diffraction analysis reveals that the fossil shells and pearls are aragonitic.
4. Microstructures of fossil shell and pearl were observed under a Scanning Electron Microscope. Only nacreous layers were found in the fossil shell, while both prismatic and nacreous layers are present in the fossil pearl.
5. The results shown here represent essential and critical information for a proper understanding of the development of pearls.

Acknowledgments

The authors would like to express their gratitude to the anonymous reviewers for their comments. Sincere thanks to Prof. Antonio Checa and Dr. Ana Vasiliu from the University of Granada, Dr. Michio Suzuki from the University of Tokyo, Prof. Du Xiao-Dong and Prof. Tong Yin-Hong from the Guangdong Ocean University for their help with the understanding of the microstructures of modern shells and pearls.

Author Contributions

Conceptualization: SPL PYY.

Investigation: SPL PYY JFL.

Resources: PYY LRM ZQC YW.

Validation: SPL JFL.

Writing – original draft: SPL JFL DKF.

Writing – review & editing: JXY JGS.

References

1. Zhu RX, Potts R, Xie F, Hoffman KA, Deng CL, Shi CD, et al. New evidence on the earliest human presence at high northern latitudes in northeast Asia. Nature. 2004; 431: 559–562. doi: 10.1038/nature02829 PMID: 15457258
2. Wang H, Deng C, Zhu R, Wei Q, Hou Y, Boëda E. Magnetostratigraphic dating of the Donggutuo and Maliang paleolithic sites in the Nihewan Basin, North China. Quat Res. 2005; 64: 1–11. doi: 10.1016/j.yqres.2005.04.001
3. Ao H, Deng C, Dekkers MJ, Sun Y, Liu Q, Zhu R. Pleistocene environmental evolution in the Nihewan Basin and implication for early human colonization of North China. Quat Int. 2010; 223: 472–478. doi: 10.1016/j.quaint.2010.02.002
4. Keates SG. Evidence for the earliest Pleistocene hominid activity in the Nihewan Basin of northern China. Quat Int. 2010; 223, 408–417. doi: 10.1016/j.quaint.2010.01.017
5. Liu Y, Hou YM, Ao H. Analysis of lithic technology of Lower Pleistocene sites and environmental information in the Nihewan Basin, North China. Quat Int. 2013; 295: 215–222. doi: 10.1016/j.quaint.2012.09.024
6. Liu X, Chi Z, Herzschuh U, Wang Y, Ni J, Xu Q. A MIS 3 charcoal and pollen record and quantitative precipitation inferences from the Jingerwa section of the Nihewan Basin, north-central China. J Paleolimnol. 2014; 51: 211–221. doi: 10.1007/s10933-013-9716-8
7. Mu H, Xu Q, Zhang S, Hun L, Li M, Li Y, et al. Pollen-based quantitative reconstruction of the paleoclimate during the formation process of Houjiayao Relic Site in Nihewan Basin of China. Quat Int. 2015; 374: 76–84. doi: 10.1016/j.quaint.2015.02.019
8. Qiu ZX. Nihewan fauna and Q/N boundary in China. Quaternary Sciences. 2000; 20: 142–154.
9. Deng C, Zhu R, Zhang R, Ao H, Pan Y. Timing of the Nihewan formation and faunas. Quat Res. 2008; 69: 77–90. doi: 10.1016/j.yqres.2007.10.006
10. Tong HW, Chen X. On newborn calf skulls of Early Pleistocene *Mammuthus trogontherii* from Shanshenmiaozui in Nihewan Basin, China. Quat Int. 2015; 406: 57–69. doi: 10.1016/j.quaint.2015.02.026
11. Huang BY, Guo SY. Freshwater fauna of lamellibranch from Nihewan area, Hebei province in early Pleistocene. Bull. Nanjing Inst. Geol. & Palaeont., Acad. Sinica. 1982; 5: 231–252.
12. Foote M, Crampton JS, Beu AG, Marshall BA, Cooper RA, Maxwell PA, et al. Rise and fall of species occupancy in Cenozoic fossil mollusks. Science. 2007; 318: 1131–1134. doi: 10.1126/science.1146303 PMID: 18006744
13. Amano K, Jenkins RG, Ohara M, Kiel S. Miocene vesicomyid species (Bivalvia) from Wakayama in southern Honshu, Japan. Nautilus. 2014; 128: 9–17.
14. Kusworo A, Reich S, Wesselingh FP, Santodomingo N, Johnson KG, Todd JA, et al. Diversity and paleoecology of Miocene coral-associated mollusks from East Kalimantan (Indonesia). Palaios. 2015; 30: 116–127. doi: 10.2110/palo.2013.124
15. Woodward J. An essay toward a natural history of the Earth, and terrestrial bodyes, especially minerals. London; 1723.
16. Boucot AJ, Poinar GO Jr. Fossil behavior compendium. Boca Raton: CRC Press; 2010.
17. Liljedahl L. Silurian nuculoid and modiomorphid bivalves from Sweden. Fossil and Strata. 1994; 33: 1–89.
18. Kříž J. Silurian Cardiolidae (Bivalvia). Sborník Geologických věd, Paleontologie. 1979; 22: 1–160.
19. De Baets K, Klug C, Korn D. Devonian pearls and ammonoid-endoparasite co-evolution. Acta Palaeontol Pol. 2011; 56: 159–180. doi: 10.4202/app.2010.0044
20. Kutassy E. Die älteste fossile Perle und Verletzungsspuren an einem triadischen Megalodus. Math. Naturwiss. Anz. Ung. Akad. Wiss. 1937; 55: 1005–1023.
21. Newton RB. Fossil pearl-growths. J Molluscan Stud. 1908; 8: 128–139.
22. Jackson JW. On some fossil pearl-growths. J Molluscan Stud. 1909; 8: 318–320.
23. Russell RD. Fossil pearls from the Chico formation of Shasta County, California. American Journal of Science. 1929; 18: 416–428. doi: 10.2475/ajs.s5-18.107.416
24. Brown R. Fossil pearls from the Colorado Group of western Kansas. J Wash Acad Sci. 1940; 30: 365–374.
25. Robertson DI. On the Post-tertiary Beds of Garvel Park, Greenock. Transactions of the Geological Society of Glasgow. 1883; 7: 1–37. doi: 10.1144/transglas.7.1.1
26. Marwick J, Hamilton A. Fossil pearls in New Zealand. N Z J Sci Technol. 1922; 5: 202.
27. Jackson JF. Fossil Pearls. Proc. Isle of Wight Nat. Hist. Soc. 1926; 1: 466.

28. Berry CT. A Miocene pearl. Am. Midl. Nat. 1936; 17: 464–470. doi: 10.2307/2419973
29. Zilch A. Unsre (sic. Unsere) Kenntnis von fossilen Perlen. Archiv für Molluskenkunde. 1936; 68: 238–252.
30. Wagner FJ. Unusual Pleistocene Fossils from Southeastern Ontario. In: Transactions Royal Society of Canada, 1957; Vol. II, Series III, Section four: 5–11.
31. Bachmayer F, Binder H. Fossile Perlen aus dem Wiener Becken. Annalen des Naturhistorischen Museums in Wien. 1967; 71: 1–12.
32. Isaji S, Kato H. A Fossil Pearl from the Upper Miocene Kubota Formation in the Higashitanagura Area, Fukushima Prefecture, Northeastern Japan. Venus. 2011; 69(3–4): 195–201.
33. Vokes HE. Cenozoic pearls from the Atlantic coastal plain. J Wash Acad Sci. 1955; 45(8): 260–262.
34. Brown RW. A Pleistocene pearl from southern Maryland. J Wash Acad Sci. 1946; 36: 75–76.
35. Min LR, Zhang ZH, Wang XS, Zheng SH, Zhu GX. The basal boundary of the Nihewan Formation at the Tai'ergou Section of Yangyuan, Hebei province. Journal of Stratigraphy. 2006; 30: 103–108.
36. Chen X, Chi Z, Dong S, Yan Z, Yang J, Shi W, et al. Late Cenozoic sedimentation of Nihewan Basin, central North China and its tectonic significance. Journal of Asian Earth Sciences. 2015; 114: 242–257. doi: 10.1016/j.jseaes.2015.06.020
37. Comps M, Herbaut C, Fougerouse A. Abnormal periostracum secretion during the mineralization process of the pearl in the blacklip pearl oyster *Pinctada margaritifera*. Aquat. Living Resour. 2000; 13: 49–55. doi: 10.1016/s0990-7440(00)00134-0
38. Che LM, Golubic S, Le Campion-Alsumard T, Payri C. Developmental aspects of biomineralisation in the Polynesian pearl oyster *Pinctada margaritifera* var. *cumingii*. Oceanologica Acta. 2001; 24: 37–49. doi: 10.1016/s0399-1784(01)00100-1
39. Southgate P, Lucas J. The pearl oyster. Oxford: Elsevier; 2011.
40. Taylor J, Strack E. Pearl production. Amsterdam: Elsevier; 2008.
41. Arajirou K. The study of pearls. Japan: The Skill Report Hall; 1960.
42. Jackson A, Vincent J, Turner R. The mechanical design of nacre. Proceedings of the Royal Society of London B: Biological Sciences. 1988; 234: 415–440. doi: 10.1098/rspb.1988.0056
43. Yan J, Deng XQ, Hu DJ, Fang SB, Liu PJ, Fang B, et al. Microscopic morphology of prismatic layers of freshwater cultured pearl. South China Fisheries Science. 2013; 9: 49–52.
44. Qiao L, Feng QL. Study on twin stacking faults in vaterite tablets of freshwater lacklustre pearls. J Cryst Growth. 2007; 304: 253–256. doi: 10.1016/j.jcrysgro.2007.02.001
45. Buchardt B, Weiner S. Diagenesis of aragonite from Upper Cretaceous ammonites: a geochemical case-study. Sedimentology. 1981; 28: 423–438. doi: 10.1111/j.1365-3091.1981.tb01691.x
46. GDNU (Geology Department of Nanjing University). Phase analysis of X-ray powder diffraction. Beijing: Geological Publishing House; 1980.
47. Freer A, Greenwood D, Chung P, Pannell CL, Cusack M. Aragonite Prism – Nacre Interface in Freshwater Mussels *Anodonta anatina* (Linnaeus, 1758) and *Anodonta cygnea* (L. 1758). Cryst Growth Des. 2009; 10(1): 344–347. doi: 10.1021/cg901265x
48. Lopes-Lima M, Rocha A, Gonçalves F, Andrade J, Machado J. Microstructural characterization of inner shell layers in the freshwater bivalve *Anodonta Cygnea*. J. Shellfish Res. 2010; 29(4): 969–973. doi: 10.2983/035.029.0431
49. Taylor JD, Layman M. The mechanical properties of bivalve (Mollusca) shell structures. Palaeontology. 1972; 15: 73–87.
50. Lin AY, Chen PY, Meyers A. The growth of nacre in the abalone shell. Acta Biomateralia. 2008; 4: 131–138. doi: 10.1016/j.actbio.2007.05.005 PMID: 17616487
51. Barthelat F. Nacre from mollusk shells: a model for high-performance structural materials. Bioinspir Biomim. 2010; 5: 1–8.
52. Harper EM, Checa AG, Rodríguez-Navarro AB. Organization and mode of secretion of the granular prismatic microstructure of *Entodesma navicula* (Bivalvia: Mollusca). Acta Zool (Stockholm). 2009; 90: 132–141. doi: 10.1111/j.1463-6395.2008.00338.x

第55卷 第3期 古 脊 椎 动 物 学 报 pp. 233–256
2017年7月 VERTEBRATA PALASIATICA figs. 1–7

Early *Mammut* from the Upper Miocene of northern China, and its implications for the evolution and differentiation of Mammutidae

WANG Shi-Qi[1,2] LI Yu[1,3] Jaroon DUANGKRAYOM[1,3,4] CHEN Shao-Kun[5]
HE Wen[6] CHEN Shan-Qin[6]

(1 *Key Laboratory of Vertebrate Evolution and Human Origins of Chinese Academy of Sciences*, *Institute of Vertebrate Paleontology and Paleoanthropology*, *Chinese Academy of Sciences* Beijing 100044, China wangshiqi@ivpp.ac.cn)
(2 *CAS Center for Excellence in Tibetan Plateau Earth Sciences* Beijing 100101, China)
(3 *University of Chinese Academy of Sciences* Beijing 100049, China)
(4 *Northeastern Research Institute of Petrified Wood and Mineral Resources*, *Nakhon Ratchasima Rajabhat University* Nakhon Ratchasima 30000, Thailand)
(5 *Three Gorges Institute of Paleoanthropology*, *China Three Gorges Museum* Chongqing 400015, China)
(6 *Hezheng Paleozoological Museum* Hezheng, Gansu 731200, China)

Abstract *Mammut* is the terminal taxon of the proboscidean group Mammutidae, which survived to the Late Pleistocene. Although this genus was widely distributed in the Pliocene of Eurasia and the Pleistocene of North America, little is known about its early evolution. Here, we report on *Mammut* cf. *M. obliquelophus* from the Upper Miocene of northern China based on new fossil material, including an almost complete juvenile cranium and other remains, which show many primitive features within Mammutidae and clearly demonstrate the morphological evolution of *Mammut*. The strongly laterally expanded lateral wing of the occiput and the presence of basal constriction of the incisive fossa display cranial similarity between *Mammut* cf. *M. obliquelophus* and both *Eozygodon morotoensis* and *Choerolophodon guangheensis*, early representatives of the Mammutidae and Choerolophodontidae, respectively, indicating the close relationship between these two groups: both of them are located at the basal phylogenetic positions in Elephantimorpha. This result is further confirmed by a cladistic analysis.

Key words northern China, Upper Miocene, Mammutidae, Choerolophodontidae, Elephantimorpha

Citation Wang S Q, Li Y, Duangkrayom J et al., 2017. Early *Mammut* from the Upper Miocene of northern China, and its implications for the evolution and differentiation of Mammutidae. Vertebrata PalAsiatica, 55(3): 233–256

Since Vacek (1877) divided mastodont molars into “bunodont” and “zygodont” patterns, this guiding concept has remained prominent in the minds of researchers for almost 150 years. In the current phylogenetic taxonomy system, the two patterns correspond to Elephantida and Mammutida, respectively, which constitute the two basic branches of Elephantimorpha during

国家重点基础研究发展计划项目(编号：2012CB821900)、中国科学院战略性科技先导专项(编号：XDB03020104)、国家自然科学基金(批准号：41372001, 41430102)和科学技术部基础性工作专项(编号：2015FY310100-14)资助。
收稿日期：2016-11-15

the entire Neogene (Tassy, 1982, 1994a; Shoshani and Tassy, 2005; Gheerbrant and Tassy, 2009). The earliest recognized member of Mammutidae is *Losodokodon losodokius* from Losodok, Kenya, in the Late Oligocene, dated to ~27.0–24.0 Ma (Rasmussen and Gutierrez, 2009), followed by the Early Miocene *Eozygodon morotoensis* from Meswa Bridge, dated to ~22.0 Ma (Tassy and Pickford, 1983; Tassy, 1986). The earliest example of *Zygolophodon* (*Z. aegyptensis*) was found in Wadi Moghara, Egypt, from the Early Miocene, dated to ~18.0–17.0 Ma (Sanders and Miller, 2002). Possibly during the same period, *Zygolophodon* invaded Eurasia, accompanied by the early *Gomphotherium* (Tassy, 1990a), represented by members of the "*Zygolophodon turicensis* group" (i.e., *Z. turicensis*, *Z. metachinjiensis*, *Z. atavus*, and *Z. gobiensis*; see Tassy, 1996a, and Tobien, 1996). In Europe, *Mammut* appeared during the early Turolian (~8 Ma), in the form of the species *M. obliquelophus* (= *M. praetypicum*) (Göhlich, 1999; Markov, 2008). *M. obliquelophus* has a longer mandibular symphysis than the subsequent widely known species, *M. borsoni* from the Pliocene of Eurasia and *M. americanum* from the Pleistocene of North America. Unlike the abundant and diverse material from gomphotheres (including Gomphotheriidae, Choerolophodontidae, and Amebelodontidae), unfortunately, material from mammutids is relatively rare and less differentiated during the entire Miocene. This has led to uncertainty among researchers over the evolution of Mammutidae.

In China, Hopwood (1935) reported *Mastodon americanus* from the Baode region (e.g., Jijiagou = Chi Chia Kou, Loc. 49), including a juvenile mandible; these remains were later attributed to *Mammut borsoni* by Tobien et al. (1988). This locality is correlated to MN12 (e.g., ~7.2 Ma of Loc. 49; see Kaakinen et al., 2013, and Yue et al., 2004). Markov (2008) compared this juvenile mandible with two known juvenile *Mammut* mandibles from Pikermi, which he referred to as *M. obliquelophus* (but see Konidaris and Koufos, 2013; in the current paper, we refer to the Pikermi material as *Mammut* sp.), and proposed that the mammutids from the Baode region could represent a new species due to their more primitive features. Recently, a complete mammutid cranium was discovered in the Hualinsanshe locality of the Upper Miocene Liushu Formation in the Linxia Basin (Fig. 1). This new cranium is slightly ontogenetically older than the cranium of *Mammut* sp. from Pikermi, and possesses some more primitive features. However, this new specimen shows an evolutionary grade similar to that of *Mammut obliquelophus*, and thus here we attribute the new specimen and the juvenile mandible from Baode to *Mammut* cf. *M. obliquelophus*. The accompanying fauna includes *Struthio linxiaensis*, *Plesiogulo brachygnathus*, *Adcrocuta eximia*, *Ictitherium* sp., *Metailurus minor*, *Hipparion* sp., *Chilotherium* sp., *Chleuastochoerus stehlini*, *C. linxiaensis*, and *Samotherium* sp., indicating a correlation to MN12 (Deng et al., 2013; Hou, 2012; Hou and Deng, 2014). This is a critical time in the evolution of *Mammut*, so the new material provides us with substantial information on the cranial anatomy and transition from *Zygolophodon* to *Mammut*. Furthermore, because this cranium retains some primitive features of Elephantimorpha, it is also an important specimen to discuss the early differentiation of the following main families of Elephantimorpha: Mammutidae, Gomphotheriidae, Choerolophodontidae, and Amebelodontidae.

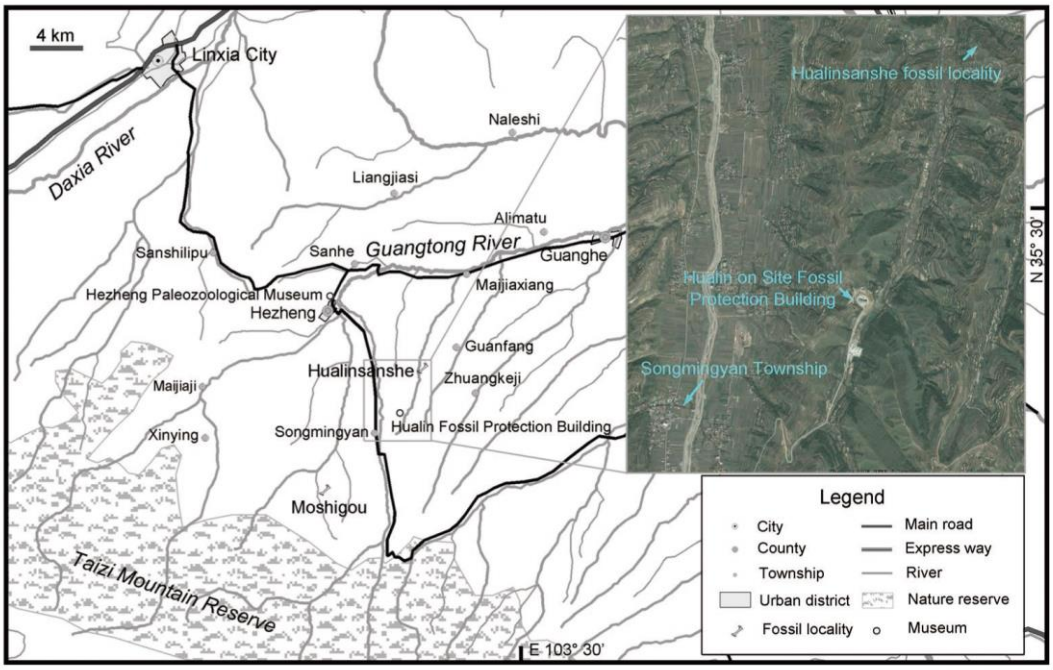

Fig. 1 Map indicating fossil sites yielding *Mammut* cf. *M. obliquelophus* in the Linxia Basin
The insert panel is the satellite map showing the type locality and the Hualin on site Fossil Protection Building (taken from Google Earth)

Abbreviations AMNH, American Museum of Natural History, New York, USA; HMV, Hezheng Paleozoological Museum, Hezheng, China; IVPP, Institute of Vertebrate Paleontology and Paleoanthropology, Chinese Academy of Sciences, Beijing, China; MN, European Neogene mammal zone; MNHN, Muséum National d'Histoire Naturelle, Paris, France; MPT, the most parsimonious tree; NHMUK, the Natural History Museum of London, United Kingdom.

1 Materials and methods

Materials The materials of *Mammut* cf. *M. obliquelophus* and *Platybelodon grangeri* are housed in HMV. The comparative materials of *Mammut americanum* is housed in AMNH, and that of *Gomphotherium annectens* in MNHN. The comparative material of *Gomphotherium* cf. *G. subtapiroideum*, *Choerolophodon guangheensis*, and *Protanancus brevirostris* are housed in IVPP. For the other materials, images and data were obtained from previous publications (Andrews, 1906; Matsumoto, 1925; Osborn, 1929; Tassy, 1977, 1982, 1983, 1986, 1994a,b, 1996a, 2013, 2014; Tassy and Pickford, 1983; Shoshani, 1996; Tobien, 1996; Pickford, 2003; Prado and Alberdi, 2008; Sanders et al., 2010; Wang and Deng, 2011; Wang et al., 2013, 2015a,b; Konidaris et al., 2016; for details, see Appendix 1).

Measurements and terminology Cranial and mandibular measurements follow Tassy (2013). All measurements were performed using calipers (in mm). The terminology of the occlusal structures of mammutid cheek teeth follows Tassy (1996b) (Fig. 2), and the dental age of trilophodont proboscideans follows Tassy (2013). The terminology of the cranium and mandible

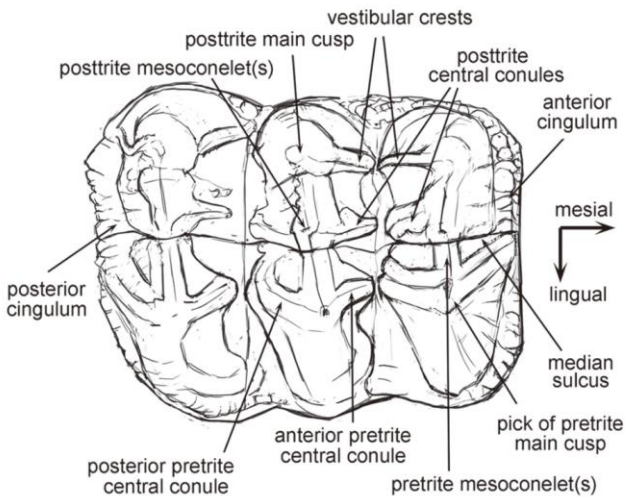

Fig. 2 Terminology used to describe zygodont teeth (a right M2 of *Mammut americanum*)

follows Tassy (2013) and Ferretti (2010).

Cladistic analysis A cladistic analysis was performed to investigate the possible phylogenetic relationships within the primitive groups of Elephantimorpha. The data matrix contains 30 unordered characters and 12 taxa, in which *Phiomia serridens* serves as the outgroup (see Appendices 1 and 2). Characters selected are explained in detail in Appendix 1. Cladograms were obtained from a parsimony analysis carried out using the TNT1.1 program (Goloboff et al., 2003). The reported results were based on MPTs.

2 Systematic paleontology

Order Proboscidea Illiger, 1811

Unranked group Elephantimorpha Tassy & Shoshani, 1997

Family Mammutidae Hay, 1922

Genus *Mammut* Blumenbach, 1799

Type species *Mammut americanum* (Kerr, 1792)

***Mammut* cf. *M. obliquelophus* (Mucha, 1980)**

(Figs. 3–5; Tables 1–3)

Mastodon americanus (Kerr, 1792): Hopwood, 1935, p. 43–46, pl. 6.5

pr. min. p. *Mammut borsoni* (Hays, 1834): Tobien et al., 1988, p. 165–168, figs. 57, 58

Referred material HMV 1428, an almost complete cranium of a juvenile with deeply worn DP3, slight worn DP4, and erupting M1, dental age V, locality Hualinsanshe (= LX 200045, 35°23′37.2″N, 103°25′47.3″E, Fig. 1). HMV 0009, a fragmentary facial part and left upper palate of a juvenile with deeply worn DP2 and DP3, and slightly worn DP4, dental age III, locality Moshigou (= LX 200013, Fig. 1). Both fossiliferous horizons belong to the Upper Miocene Liushu Formation of the Linxia Basin, MN12. Teeth and mandible remains reported by Hopwood (1935:43–46, pl. 6.5). A cast of a left hemimandible (NHMUK-M14825) is stored at NHMUK and another cast (IVPP RV 35020) of the same specimen is housed in IVPP, locality Jijiagou = Chi Chia Kou, Loc. 49, Baode region.

Occurrence Late Miocene, ~ MN12, China.

Description The cranium of HMV 1428 (Fig. 3) is almost complete except for breakage of the left one-third of the occipital surface and two occipital condyles, as well as the middle part of both zygomatic arches (these parts are reconstructed using plaster in the specimen and shaded in Fig. 3).

In dorsal view (Fig. 3A), the cranium is characterized by its wide occipital part relative to the orbital part. The occipital crest is almost straight, not anteriorly concave. The temporal fossa is strongly posterolaterally expanded, which can be observed in the dorsal view. The two temporal lines converge from the posterolateral flanges of the two temporal fossae, and diverge until reach the postorbital processes. The two temporal lines are far apart, resulting in a wide

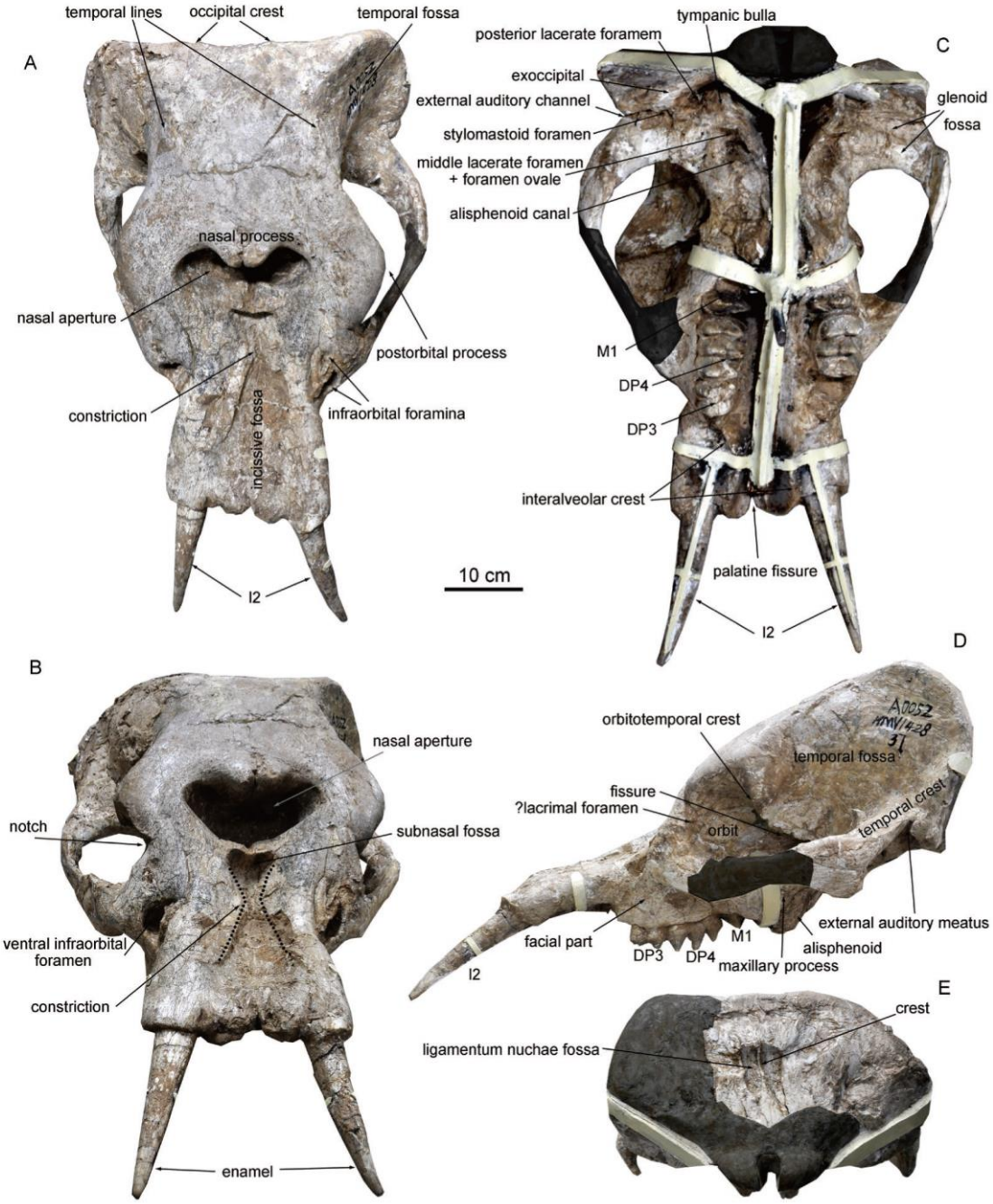

Fig. 3 Cranium of *Mammut* cf. *M. obliquelophus* (HMV 1428) in dorsal (A), anterodorsal (B), ventral (C), lateral (D) and occipital (E) views
Shadowed parts are reconstructed by plaster

brain case. The nasal process is relatively blunt and the median suture between the two nasal bones is clear. The nasal aperture is relatively narrow, and the superior-most rim of the nasal aperture slightly posteriorly exceeds the level of the two postorbital processes. In this view, the tip of the nasal bones and the prominent symphysis of the two premaxillae are close to each other in the middle, forming a dumbbell-shaped nasal aperture. The two postorbital processes are not strongly laterally protruded, leaving a relatively narrow orbital part; however, the zygomatic arch is relatively laterally expanded, mainly contributed to by the laterally expanded zygomatic process of the squamosal bone. Both the dorsal infraorbital foramen and the ventral infraorbital foramen can be observed in dorsal view, and they are close to each other. The former is small and slit-like, and the latter is large. The rostrum is narrow at the base (between the left and right ventral infraorbital foramina) and largely expanded at the distal part. The incisive fossa is distinct and strongly constricted at the proximal one-quarter, dividing the incisive fossa into a small basal subnasal fossa and a tubaeform distal part. At the distal edge of the rostrum, the distance between the two alveolar sockets is large.

In anterodorsal view (Fig. 3B), the dorsal plate of the brain case forms a flat surface that is oblique anteroventrally, without bulges. The nasal aperture is invertedly trapezoidal with two rounded dorsolateral angles. The subnasal fossa that excavates the proximal end of the incisive fossa is invertedly triangular and is dorsally separated by a thin bony plate of the symphysis of the two premaxillae (Ferretti, 2010). The nasal aperture is narrow and no step-like perinasal fossa is present. The zygomatic process of the maxilla is huge and strongly laterally expanded, forming a prominent notch between the zygomatic arch and the orbital part of the frontal bone. The ventral infraorbital foramen anterior to the zygomatic arch is very large, dorsoventrally elongated, and has a sharp dorsal angle that turns slightly medially.

In ventral view (Fig. 3C), the cranium is tightly locked on an iron frame so that some critical features are invisible, including the post-palatine spine. The tympanic bulla is laterally expanded. It is triangular with a prominent anteromedial angle. A fossa lateral to the tympanic bulla represents the channel for stylomastoid foramen and the tympanohyal, and another fossa posterior to the tympanic bulla represents the posterior lacerate foramen (*foramen metoticum*). The middle lacerate foramen and *foramen ovale* are confluent and located beneath the anterolateral margin of the bulla. A rounded posterior opening of the alisphenoid canal is anterior to the anterior edge of the bulla. The glenoid area is transversely elongated and is composed of an anterior ventrally convex temporal condyle for the normal position of the mandibular condyle, and a posteriorly dorsally concave groove for containing the posteriorly shifted mandibular condyle when the mouth is open. The exoccipital bone is crest-like; it is laterally and slightly anteriorly elongated. The lateral part of the occipital plane turns slightly anteroventrally, which can be seen in the ventral view. Between the glenoid area and the exoccipital bone, there is a long slit in which the external auditory channel is concealed. The zygomatic process of the maxilla is strongly expanded from the brain case. The pterygoid process lateral to the choanae is enlarged and the pterygoid crest extends posteriorly to the tympanic bulla. The palate is

Table 1 Cranial measurements of *Mammut* cf. *M. obliquelophus* (HMV 1428) (mm)

Maximal length measured from the occipital border	618
Length of cerebral part	260
Length of premaxilla	331
Length of incisive fossa	294
Length of nasal bones from the tip to the upper border of the nasal fossa	39
Maximal supraorbital width	347
Posterior rostral width (as measured between the infraorbital foramina)	197
Anterior rostral width	237
Width of nasal bones at the upper border of the nasal fossa	92
Width of nasal fossa	186
Minimal cerebral width between temporal lines	196
Length of zygomatic arch measured from the processus zygomaticus of the maxilla to the posterior Border of the glenoid fossa	285
Length of orbitotemporal fossa measured at the level of the zygomatic arch	180
Palatal length from the anterior grinding tooth to the choanae	345
Thickness of processus zygomaticus of the maxilla	101
Maximal cranial width across the zygomatic arches	475
Width of basicranium between the lateral borders of the glenoid fossae	389
Maximal width of choanae	63
Internal maximal width of the palate	70
External maximal width of the palate	216
Internal width of the palate measured at the anterior grinding teeth	85
Minimal palatal width between the inter-alveolar cristae (maxillary ridges)	71
Occipital width	ca. 436
Height of premaxilla	63
Facial height measured at the anterior grinding tooth	96
Height of the maxilla ventral to the processus zygomaticus	ca. 40
Height of the orbit	90
Cranial height measured from the top of the cranium to the pterygoid process	344
Facial length measured from the tip of the rostrum to the pterygoid process	382
Length of the orbitotemporal fossa measured from the squamosal to the anterior border of the orbit	212
Mid-cranial length measured from the external auditory meatus to the ventral border of the orbit	262
Mid-cranial height measured from the pterygoid process to the dorsal border of the orbit	255

Note: measures after Tassy (2013).

relatively wide and the tooth rows are laterally convex. The zygomatic process of the maxilla is triangular, slightly dorsally concave, and not strongly laterally expanded. The interalveolar crest extends anteriorly along the rostrum. The two crests converge in the middle. At the anterior margin of the rostrum, there is a palatine fissure (= anterior palatine foramina).

In lateral view (Fig. 3D), the braincase is very low, flat, and anteroposteriorly elongated with an anteroposteriorly expanded temporal fossa. The occipital surface is posteriorly convex with a strongly anteriorly extending temporal crest. The basicranium is slightly erected. A notch for the external auditory meatus is posterior to the zygomatic arch. The orbitotemporal crest originates from the postorbital process; it first extends ventrally and then runs posteroventrally to reach the anterior edge of the alisphenoid. A large fissure is located beneath the anterior margin of the alisphenoid, in which the optic foramen, the anterior lacerate foramen (*foramen orbitale*), and the *foramen rotundum* are present. The anterior edge of the alisphenoid turns anteroinferiorly, reaches the pterygoid process, and wraps around the posterior end of the

bulged maxillary process. The orbit is large and the anterior rim is located at the level of the middle part of the DP4, and the postorbital process is just at the level of the pterygoid process. A lacrimal foramen may be present, although the finding is ambiguous. The facial part of the maxilla is slightly anteriorly elongated and that ventral to the zygomatic process is shallow. The rostrum is anteriorly elongated and slightly ventrally bent.

In occipital view (Fig. 3E), the left one-third of the occipital bone is broken, and the occipital condyles are reconstructed using plaster. Nevertheless, the brain case in this view appears very compressed. The ligamentum nuchae fossa is dorsoventrally elongated and divided into two parts by a thin crest in the middle. The ventrolateral part of the occipital bone is anteriorly inclined.

The upper tusk of HMV 1428 (Fig. 3A–D) appears relatively slender and short. The tusk is circular in the basal cross section and tapers apically. Enamel covers the distal part of the tusks. In anterior view of the cranium, the two tusks are divergent; in the lateral view, they bend ventrally. Measurements (exposed length/maximal diameter/minimal diameter at alveolus, in mm): 176/42/36 (left); 196/46/31 (right).

The right DP3 has been shed and the left DP3 is deeply worn (Fig. 4A). The latter is rectangular and composed of two lophs, with the posterior one being slightly wider.

Table 2 Cheek teeth measurements of *Mammut* cf. *M. obliquelophus* (mm)

No.	Locus	L	W	W1	W2	W3	Hpo	I=W/L
HMV 0009	l. DP2	28	26	25	26	–	–	0.929
HMV 1428	l. DP3	48	52.5	48	45	–	–	1.094
HMV 1428	l. DP4	82	65	56.5	65	63	38(2)	0.793
HMV 1428	l. DP4	79.5	65	60	63.5	65	39(2)	0.818
HMV 0009	l. DP4	75	61.5	53	61.5	59.5	37(2)	0.820
IVPP RV 35020	r. dp2	22.89	16.89	16.89	–	–	–	0.738
IVPP RV 35020	r. dp3	55.65	–	36.38	–	–	24.58(2)	–

Abbreviations: L. length; W. maximal width; W1, 2, and 3. width at the first, second, and third loph(id); Hpo. height of the posttrite side; I. index. Numbers in parentheses indicate the loph(id) from which the measurement was made.

DP4 is moderately worn in the first loph and slightly worn in the posterior two lophs (Fig. 4A). The tooth is typically zygodont with a high degree of zygodonty (level 3; see Wang et al., 2016). Furrows have developed on the anterior and posterior walls of the lophs and the cingula are relatively strong, surrounding the entire tooth. Cementum is not present. The first pretrite half-loph is trifoliate, with crest-like anterior and posterior central conules. The first posttrite half-loph is transversely elongated and the dentinal figures of the first pre- and posttrites are in connection with each other. A vestibular crest (zygodont crest) is present on the posterior wall of the first posterior half-loph. The second pretrite half-loph is trifoliate with sharp, crest-like anterior and posterior central conules and mesoconelet. The second posttrite half-loph is transversely elongated, especially for the posttrite mesoconelet. The second pre- and posttrite half-lophs are well separated by a median sulcus. Vestibular crests are present on both anterior and posterior walls of the second half-loph. The third pretrite half-loph is also trifoliate with relatively slim and crest-like, anterior and posterior central conules. The mesoconelet is

also crest-like, but with a slightly inflated distal end. The second posttrite half-loph is also transversely elongated, without a definite boundary between the main cusp and the mesoconelet. The third pre- and posttrite half-lophs are well separated by a median sulcus. A vestibular crest is not clearly present on the third half-loph; however, a small crest is present on the posterior wall of the posttrite mesoconelet, the homologue of the third posterior posttrite central conule.

Only the first loph of M1 has erupted (Fig. 4A). The first pretrite half-loph is trifoliate with sharp, crest-like anterior and posterior central conules and mesoconelet. The first posttrite half-loph is transversely elongated. The posttrite main cusp is relatively inflated with a subdivided summit. It is slightly posterolaterally positioned. The posttrite mesoconelet is subdivided into a row (4–5) of conelets. The first pre- and posttrite half-lophs are well separated by a median sulcus and a weak vestibular crest is present on the posterior wall of the posttrite half-loph. Cingula are present on the anterior end and buccal and lingual sides of the first loph.

HMV 0009 (Fig. 4B–D) is the left palate and facial part of a juvenile individual. DP2 and DP3 are deeply worn and DP4 is moderately worn. The upper tusk is present.

In the anterior view (Fig. 4C), the upper tusk runs ventrally and slightly laterally. Enamel covers the entire tooth. There are clearly two infraorbital foramina that are close to each other. The dorsal one is small and the ventral one is large; however, both are rounded. In the lateral view (Fig. 4D), the facial part is relatively developed. The premaxilla is ventrally inclined, but the alveolar socket is broken. The upper tusk is straight. The zygomatic arch begins at the

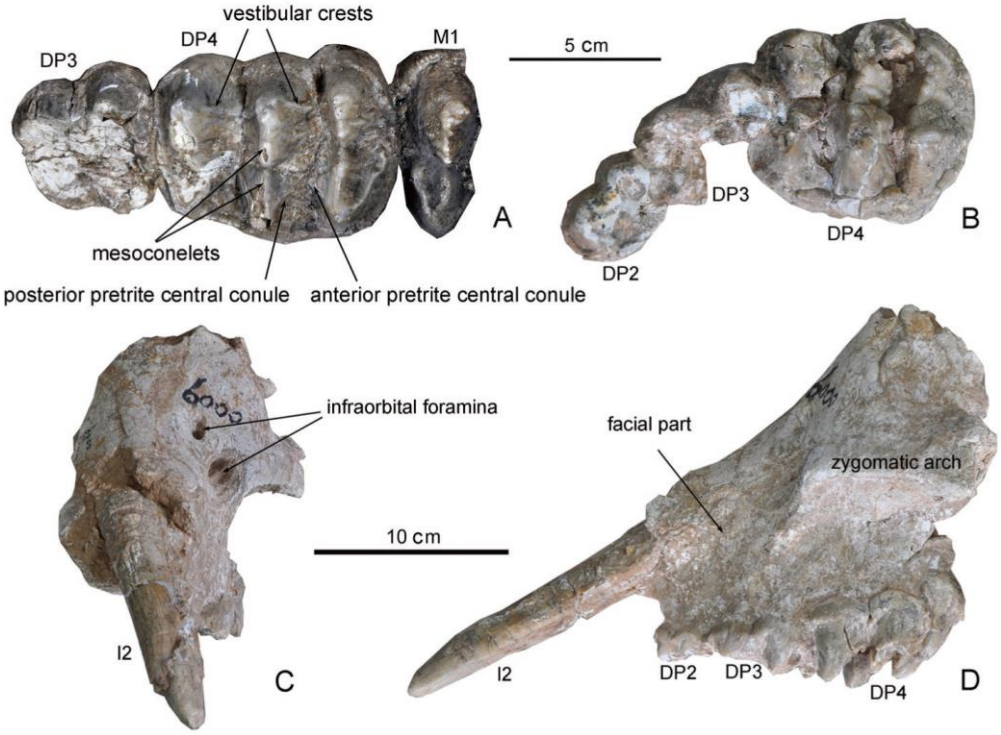

Fig. 4 Teeth and cranial fragment of *Mammut* cf. *M. obliquelophus*
A. DP3–M1 tooth row of HMV 1428 in crown view; B. DP2–DP4 tooth row of HMV 0009 in crown view; C. anterior view of HMV 0009; D. lateral view of HMV 0009

level of the boundary between DP3 and DP4, and the anterior rim of the orbit is at the level of the middle part of DP4. The lophs of DP4 are somehow anteriorly oblique. In the ventral view, the tooth row is laterally convex with a relatively wide half-palate. The zygomatic process is triangular. Measurements of the tusk (exposed length/maximal diameter/minimal diameter at alveolus, in mm): 151/41.5/36.

DP2 (Fig. 4B) is small and sub-oval. There is a large anterior cusp representing the fused protocone and paracone. The hypocone and the metacone are deeply worn, and clearly distinct. Except for the buccal margin, most of DP3 is broken. It appears to be composed of two lophs.

DP4 is quadrate and composed of three lophs (Fig. 4B). It is partially damaged and shows a zygodont pattern. The component elements are crest-like and furrows have developed on the anterior and posterior walls of the lophs. The cingula surround the entire tooth, and cementum is not developed. The first pretrite half-loph is moderately worn. This loph is compressed by DP3, and the anterior pretrite central conule and mesoconelet pretrite are broken. The posterior central conule seems to be crest-like. The first half-loph is relatively narrow. The posttrite mesoconelet and the main cusp are separated by a shallow groove and the median sulcus is clear. A vestibular crest is present on the posterior wall of the first posttrite half-loph. The second pretrite trefoil is incomplete, in which the anterior pretrite central conule is missing and the posterior central conule and mesoconelet are small and nodule-like. The main cusp of the second posttrite half-loph is broken and the second posttrite mesoconelet is crest-like with a crest-like posterior posttrite central conule. The third loph is narrower and less well developed than the former two lophs and the second interloph is anteroposteriorly narrow. The third anterior pretrite central conule is almost completely missing and the mesoconelet and posterior central conule are weak and crest-like. The third posttrite half-loph is crest-like and is slightly posteriorly convex. The main posttrite cusp and mesoconelet are not separated and a crest-like posterior central conule is present.

IVPP RV 35020 (Fig. 5; Table 2, 3) is a left hemimandible preserving the mandibular symphysis. Most of the left ascending ramus is missing, as well as the right hemimandible. The mandibular corpus is relatively narrow in dorsal view and relatively low in lateral view. Although considerably broken, the ascending ramus appears to be very low, with a strongly posteriorly oblique anterior ramal border. The position of the mandibular angular process is relatively high.

The mandibular symphysis is distant from the tooth row, despite the anterior part of the mandibular corpus being broken and reconstructed. The mandibular symphysis is triangular in the dorsal view. There is a posterior spine at the posterior edge of the symphysis. This feature is rarely found in Elephantida, but is observed in *Phiomia* (Andrews, 1906). Both lateral sides of the alveolar sheath are broken and the right mandibular tusk is absent, so the deeply excavated alveolus can be clearly observed. The proximal end of the left incisive alveolus extends to the level of dp2. At the anterior end of the mandibular symphysis, the two alveoli are only separated by a thin bony plate.

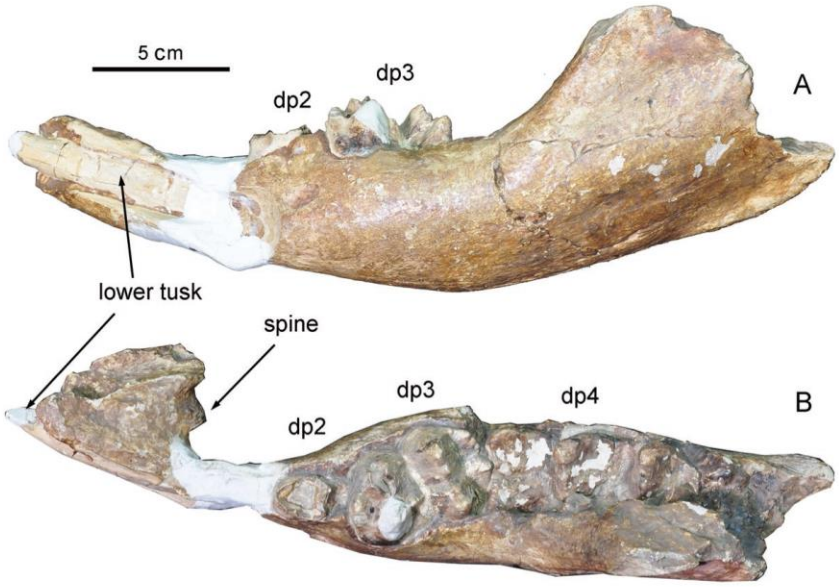

Fig. 5 Left hemimandible of *Mammut* cf. *M. obliquelophus* from Baode (IVPP RV 35020) in lateral (A) and dorsal (B) views, a cast
The original specimen was published by Hopwood (1935: pl. 6.5)

The left mandibular tusk is long and cylindrical (Fig. 5). It is strongly medially bent and the two tusks must have been convergent anterior to the symphysis. The tip of the left tusk is reconstructed using plaster and the shape of the wear facet is unknown.

Most of the crown of dp2 (Fig. 5) is broken. The dp2 is oval with a relatively strong posterior cingulid.

Table 3 Mandibular measurements of *Mammut* cf. *M. obliquelophus* (IVPP RV 35020) (mm)

Symphyseal length	68
Alveolar distance (from the most salient point of the trigonum retromolare to the symphyseal border of the corpus)	ca. 166
Ventral length measured from the gonion (angulus mandibular) to the tip of the symphysis	292
Width of corpus measured at the root of the ramus	61.5
Width of corpus measured at the anterior alveolus (or the grinding tooth if the alveolus is entirely resorbed)	33
Posterior symphyseal width	61.5
Maximum symphyseal width	61.5
Height of corpus measured at the anterior end of the cheek tooth alveolus (measurement taken perpendicular to the ventral border of the corpus)	41
Height of corpus measured at the root of the ramus (measurement as above)	50
Rostral height measured at the symphyseal border (measurement taken perpendicular to the ventral border of the symphyseal rostrum)	31
Mid-alveolar length measured on the buccal side between the anterior alveolus (or grinding tooth if the alveolus is resorbed) and the root of the ramus	90

Note: measures after Tassy (2013).

The dp3 (Fig. 5) is quadrate and composed of two lophids. The interlophid is wide and open, and the anterior and posterior cingulids are strong. The first pretrite half-lophid (protoconid) is broken, and the posterior pretrite central conule is thin and crest-like. The summit of the first posttrite half-lophid is also broken. It is strongly anteroposteriorly compressed and shows clear anterior and posterior vestibular crests. The second lophid is

transversely wider than the first one. The summit of the pretrite half-lophid is composed of fine conelets. The anterior and posterior central conules are thin and crest-like, and they run from the pretrite mesoconelet to the valley. The second posttrite half-lophid is also anteroposteriorly compressed; however, the main cuspid and the mesoconelets are distinguishable. Vestibular crests are not developed on this half-lophid, but a small, crest-like anterior posttrite central conule is developed.

The dp4 (Fig. 5B) has not erupted yet. However, some of the bones on the medial side of the mandibule ramus are removed. The dp4 is composed of three lophids with very wide interlophids. Most features of the pretrite half-lophids cannot be observed, except the crest-like pretrite central conules on the first and second half-lophids. The three posttrite half-lophids are strongly anteroposteriorly compressed. The main cuspid and the mesoconelets of the posttrite half-lophids are distinguishable. However, vestibular crests are weak or absent.

3 Comparisons and discussion

Generic assignment of the new material The new material is undoubtedly a member of the Mammutidae because of the clear zygodonty of the cheek teeth. These teeth show high zygodonty with sharp and highly crest-like pretrite central conules and posttrite half-lophs (zygodont degree 3 in Wang et al., 2016). Except for *Mammut*, other mammutids (i.e., *Losodokodon*, *Eozygodon*, and *Zygolophodon*) show a somewhat lower degree of zygodonty (zygodont degree 2 in Wang et al., 2016); that is, posttrite half-lophs are divided into main cusps and mesoconelets (although each of them is crest-like), and pretrite mesoconelets and central conules are sometimes not very crest-like, especially in lower molars. Therefore, the new material can be attributed to the genus *Mammut*. However, as asserted by Tobien (1996), *Mammut* differs from the other mammutids (especially *Zygolophodon*) in having either straight or upturned tusks (see also Kubiak, 1972), but the new material contradicts this by showing upper tusks that are downwardly oriented. Here, we believe that the direction of the upper tusks is due to the young ontogenetic age (dental ages V and III). The tusks are even covered by enamel. If this is true, the upper tusks would eventually curve upwards once the animal reaches adulthood.

Comparison of the mandible of *Mammut* cf. *M. obliquelophus* with those of the other species of *Mammut* As has been demonstrated, *Mammut obliquelophus* is a primitive Turolian *Mammut* that differs from the other two species in this genus, *M. borsoni* and *M. americanum*, in possessing a longer mandibular symphysis and mandibular tusks. Markov (2008) stated that the juvenile mandible from Jijiagou of Baode (*Mammut* cf. *M. obliquelophus*, Fig. 5) represents a different taxon based on a comparison with the juvenile mandible of *Mammut* sp. from Pikermi (see Tassy, 1985: fig. 216). Here, we further emphasize these differences. The mandibular corpus of the Baode material is narrower (indicating a possibly more elongated symphysis). The two tusk alveoli are closer to each other. It should also be noted that there is a small spine posterior to the mandibular symphysis (a plesiomorphy inherited from *Phiomia*) and the symphysis is distant from the anterior end of the cheek teeth row. However, the Baode material is from a

juvenile individual and these features might not be very stable. Therefore, here, we refer to the Baode material as *Mammut* cf. *M. obliquelophus*. It is clearly the case that the Baode material is more primitive than *M. borsoni* and *M. americanum*. Moveover, Mothé et al. (2016) reported *Sinomammut tobieni* (Mammutidae) based on a specimen that Wang et al. (2014) attributed to Sinomastodontinae. The age of *S. tobieni* is postulated to be Baodean, possibly the same as *Mammut* cf. *M. obliquelophus*. *S. tobieni* possesses a relatively long symphysis, but lacks lower tusks. It shows a distinct course of evolution compared with *Mammut*.

Comparison of the cranium of *Mammut* cf. *M. obliquelophus* with other mammutids

Mammut americanum is very common in the Pleistocene of North America. From this cranium (HMV 1428), we can observe that many of the plesiomorphies in *M. americanum* are also preserved in the present material, including the low and flat brain case, the slightly erected basicranium, the narrow nasal aperture without step-like perinasal fossa, and the presence of the dorsal infraorbital foramen (Fig. 3). Unfortunately, the presence of lacrimal foramen and post-palatine spine is not clear in this specimen. These two features are important plesiomorphies in *M. americanum* that are inherited from the ancestral *Phiomia* (Andrews, 1906; Tassy, 1994b). In the cranium of *Mammut* cf. *M. obliquelophus*, the brain case is lower, the nasal aperture is narrower, and the facial part is lower and more anteriorly elongated than those of *M. americanum* (Figs. 3, 6A, B), indicating a more primitive evolutionary stage.

There are two particular features of the cranium of *Mammut* cf. *M. obliquelophus*. First, the contour of the nasal aperture is invertedly trapezoidal. In contrast, in *M. americanum*, the nasal aperture is simply oval (Fig. 6A). Second, the basal end of the incisive fossa shows a pronounced constriction. In *M. americanum*, although the basal end of the incisive fossa is also deeply excavated in the rostrum, no strong proximal constriction is present (Fig. 6A, B). However, these two features appear to be present in the more primitive species *Mammut* sp. from Pikermi and even to be traced back to the Early Miocene *Eozygodon morotoensis* (Pickford, 2003; see below). Therefore, they are possibly plesiomorphies of Mammutidae.

Crania of *Mammut* from Eurasia have rarely been discovered. The cranium of *Mammut* sp. from Pikermi (see Tassy, 1985: fig. 215) provides perfect material for comparison with the Hualin material (HMV 1428). DP2 of the Pikermi cranium is present, indicating a younger ontogenetic age than that of the cranium HMV 1428 (and the same as HMV 0009). As we mentioned above, in anterior view, the Pikermi *Mammut* sp. possesses a nearly invertedly trapezoidal nasal aperture and a basal constriction in the incisive fossa, although these two features in *Mammut* sp. are not as conspicuous as those in the Hualin material. In dorsal view, the occipital part is almost equal in width to the orbital part. However, in the Hualin material, the occipital part is strongly laterally expanded, being much wider than the orbital part. The strongly laterally expanded occipital part is also observed in the primitive *Eozygodon morotoensis* (see below). All of these cranial features indicate that the Hualin material well demonstrates the early evolution of the cranial features within the genus *Mammut*. As with the Baode material (RV 35020), the Hualin material is a juvenile cranium and its features might not

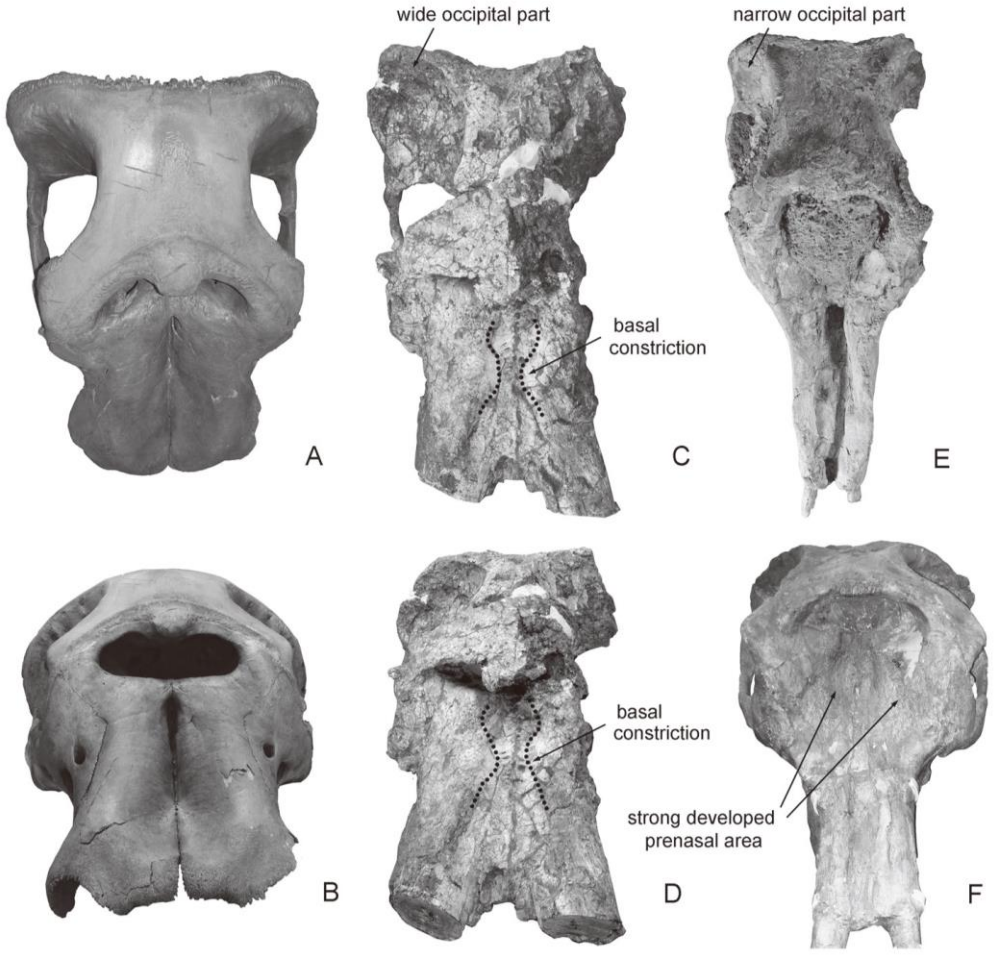

Fig. 6 Cranial comparison of *Mammut americanum* AMNH 14535 (A, B), *Choerolophodon guangheensis* IVPP V 17685 (C, D), *Platybelodon grangeri* HMV 0023 (E) and HMV 0024 (F)
A, C, and E are in dorsal view; B, D, and F are in anterodorsal view. Not to Scale

be very stable. However, both the Hualin and the Baode materials show slightly more primitive features than the Pikermi material. At least these features represent the primitive stage in *Mammut* (juvenile individuals often show primitive features (Gould, 1977)). Considering the high morphological conservation of Mammutidae in its evolution, we attributed the Hualin and the Baode materials to *Mammut* cf. *M. obliquelophus*.

Zygolophodon represents the intermediate evolutionary stage between *Eozygodon* and *Mammut* during the late Early to early Late Miocene (Göhlich, 1999). The only known cranium of *Zygolophodon* is possibly *Z. turicensis* from Villafranche d'Astarac, France (see Tassy, 1985: fig. 208). However, only the lateral view can be observed in this figure. Although the occipital part of the specimen is broken, the cranium is low and the basicranium does not seem to be erected, which is similar to the Hualin specimen. However, the orbit is very anteriorly positioned (even the posterior edge of the orbit is anterior to the tooth row) and the facial part is very anteriorly elongated. This morphology, as primitive features preserved in *Zygolophodon*, is distinct from *Mammut* cf. *M. obliquelophus* from Hualin.

Eozygodon morotoensis from the Early Miocene of Africa is an early representative of mammutids. Pickford (2003) reported two adult crania of *E. morotoensis* from the lower Orange River Valley, Namibia. In the dorsal view, the cranium of *E. morotoensis* shows a significantly wide occipital part (wider than that of *Mammut* cf. *M. obliquelophus*), and the remaining left zygomatic arch is strongly laterally expanded. In anterior view, the basal constriction in the incisive fossa also appears to be present (Pickford, 2003: fig. 4.2); however, this is not very clear. The two lateral wings of the nasal aperture extend slightly dorsally. This feature is also comparable to that of *Mammut* cf. *M. obliquelophus*. The above cranial features are similar to those of *Mammut* cf. *M. obliquelophus* and also indicate a common cranial morphology of Mammutidae. However, the nasal aperture is low and wide, distinct from the high and narrow nasal aperture in *Mammut* cf. *M. obliquelophus*. The cranium of *E. morotoensis* is highly arched and the basicranium is strongly erected (Pickford, 2003). The latter two features are often expressed in derived taxa, such as *Anancus*. It is possible that *Eozygodon* was an early offshoot of Mammutidae.

Comparisons of crania of *Mammut* cf. *M. obliquelophus* with other crania of Elephantimorpha and implications for early phylogenetic differentiation and evolution in Elephantimorpha *Choerolophodon guangheensis* (Fig. 6C, D) from the Early Miocene of the Linxia Basin is the earliest complete cranium known in this genus. Konidaris et al. (2016) mentioned that *C. guangheensis* presents a combination of primitive and more advanced features; we consider this species to be a very primitive representative of Choerolophodontidae based on the very low brain case, the very anteriorly positioned orbit, and the presence of P4. In *C. guangheensis*, although the nasal aperture is broad, no step-like perinasal fossa is present. This feature persists in the Middle Miocene *C. chioticus* and the Late Miocene *C. pentelici* and *C. corrugatus*. This character state is also very similar to that of *Zygolophodon* and *Mammut*. In *C. guangheensis*, the incisive fossa has a basal constriction and the distal part of the incisive fossa is tubaeform (Fig. 6C, D). These features are very similar to that of *Mammut* cf. *M. obliquelophus* and even developed in the Late Miocene *Choerolophodon corrugatus* (but seem to have been lost in *C. pentelici*; see Schlesinger, 1917: pls. 24, 27). In *C. guangheensis*, the occipital part is strongly laterally expanded in a character state similar to that in *Mammut* cf. *M. obliquelophus* (Fig. 6C, D). In *Mammut americanum*, the lateral expansion of the occiput is not pronounced as in *Mammut* cf. *M. obliquelophus*, but is still more pronounced than in extant elephants. Therefore, Choerolophodontidae and Mammutidae may have a closer phylogenetic relationship than we previously thought.

Gomphotherium angustidens, a representative of Gomphotheriidae, is a common species in the Middle Miocene of Western Europe, for which several crania have been reported (Tassy, 2013) and can be compared with *Mammut* cf. *M. obliquelophus*. In *G. angustidens*, a step-like perinasal fossa is well developed (Tassy, 1994b, 2013). This feature is also considered a synapomorphy of higher Elephantida (Tassy, 1994b) including *Gomphotherim* cf. *G. subtapiroideum*, but is missing in primitive *G. annectens*. We have already mentioned that

this structure is also missing in Mammutidae and Choerolophodontidae. In *G. angustidens*, especially in males (Tassy, 2013: fig. 9), no strong constriction is developed in the proximal part of the incisive fossa, in contrast to the presence of a strong proximal constriction in the incisive fossa of *Mammut* cf. *M. obliquelophus*. Furthermore, in *G. angustidens*, the lateral expansion of the occiput is weaker than that in *Mammut* cf. *M. obliquelophus* (Tassy, 2013: figs. 13, 14).

The cranium of *Archaeobelodon* aff. *A. filholi* from Buluk, Kenya, is a typical primitive cranium of Amebelodontidae (Tassy, 1986: pls. 3, 4). The facial part is strongly anteriorly elongated, regarded as a synapomorphy of Amebelodontidae (Sanders et al., 2010). The step-like perinasal fossa is developed and no strong proximal constriction in the incisive fossa is present. These features are closer to Gomphotheriidae than to Mammutidae and Choerolophodontidae. However, in the specialized amebelodontid, *Platybelodon grangeri* (Fig. 6E, F), the proximal constriction in the incisive fossa is also absent, but the perinasal fossa is not developed. Alternatively, there are two enlarged slopes between the nasal aperture and the rostrum along the lateral side of the incisive fossa; here, we describe this feature as "broad prenasal area." This feature also appears to be present in *Protanancus brevirostris* (Wang et al., 2015b: fig. 4a), a primitive member of *Protanancus*. It seems that the loss of perinasal fossa and alternatively developed prenasal area is a synapomorphy of Amebelodontidae above the level of *Protanancus* and *Platybelodon*. Otherwise, we have to consider the polyphyletic state of Amebelodontidae.

Phylogeny Phylogenetic analyses of proboscideans based on cladistic analysis have been carried out by Tassy (1990b, 1996a) and Shoshani (1996), further developed by Shoshani et al. (2006), and modified and extended by Cozzuol et al. (2012). In these analyses, Mammutidae and Amebelodontidae were identified as monophyletic groups and *Choerolophodon* as a sister group of the other Elephantida. However, there are also some debates among these groups. For example, Shoshani (1996) stated that the phylogenetic position of *Choerolophodon* is possibly inserted within gomphotheres and that the monophyletic state of Mammutidae is not supported by the parsimony rule. In addition, Tassy (1996a) considered that the monophyletic state of Amebelodontidae is one of the least robust among the elephantoid groups. One important reason for this is the incompleteness of the data on the early members of Mammutidae, Choerolophodontidae, and Amebelodontidae.

A cladistic analysis was carried out to clarify the phylogenetic positions of the early branches of Elephantimorpha, since our knowledge of cranial and mandibular features of the early members of Elephantimorpha has increased. For simplicity, we only include the most typical representatives of Mammutidae, Choerolophodontidae, Gomphotheriidae, and Amebelodontidae, because the purpose of this cladistic analysis is to test the mono- or paraphyletic states of these groups and to search for the differentiation sequence of these main groups in Elephantimorpha. The most crown groups, such as Stegodontidae, Elephantidae, and some taxa of Gomphotheriidae and Amebelodontidae, are not included in this analysis. We either do not include the genera *Eritreum*, *Hemimastodon*, and *Losodokodon* because only dental remains are known from

these taxa. The representative taxa and characters are given in Appendices 1 and 2. Two MPTs were obtained (Fig. 7A, B). Both of them (Fig. 7A, B) support the monophyly of Mammutidae and Choerolophodontidae, and the differentiation of Choerolophodontidae is prior to that of Amebelodontidae and Gomphotheriidae, indicating the more stem position of Choerolophodontidae, as we hypothesized. However, the topologies of the two MPTs conflict in terms of the differentiation of Amebelodontidae and Gomphotheriidae. In one MPT (Fig. 7A), the Amebelodontidae is a monophyletic group that differentiated from *Gomphotherium* in a fairly distal position, whereas *Gomphotherium* cf. *G. subtapiroideum* and *G. angustidens* are sequentially differentiated after *G. annectens*, and the Gomphotheriidae is a paraphyletic group. In the other MPT (Fig. 7B), *Gomphotherium annectens* constitutes the sister group of the others, and *Archaeobelodon* serves as the sister group of *Gomphotherium angustidens* and *Gomphotherium* cf. *G. subtapiroideum*; in this case, neither Amebelodontidae nor Gomphotheriidae is monophyletic. Although a more detailed discussion of this issue is beyond the scope of this work, it should be noted that the early differentiation of Elephantida may be much more complex than we ever considered. Although disagreements persist, we confirm a certain close relationship between Mammutidae and Choerolophodontidae in Elephantimorpha, which was not well resolved prior to this work.

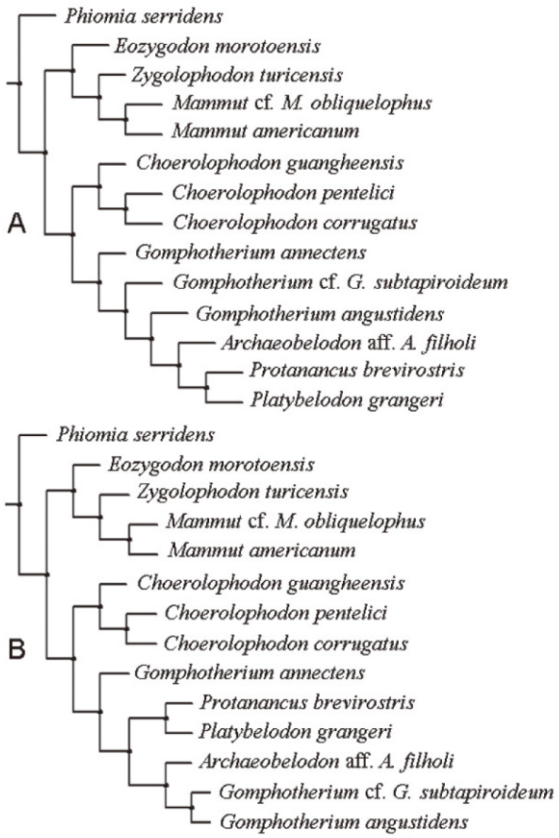

Fig. 7 The phylogeny of the Elephantimorpha
Two most parsimony trees calculated from the cladistic analysis of the proboscideans, based on the characters provided in Appendix 1 (A) and the data matrix in Appendix 2 (B). Tree length = 59, CI (consistency index) = 0.644; RI (retention index) = 0.767

4 Conclusions

In this work, we describe a primitive cranium and other remains of *Mammut* from the Upper Miocene of the Linxia Basin and the Baode region, China, which roughly corresponds to MN12. The new material displays derived dental features like the other members of *Mammut*, and possesses many primitive features within Mammutidae, which provides substantial new information about the morphological development of *Mammut*. We attributed the new material to *Mammut* cf. *M. obliquelophus*. *Mammut* cf. *M. obliquelophus* also provides important information on the differentiation of Mammutidae from the primitive Elephantimorpha. The cranial features also suggest a certain close relationship between

the primitive members of Mammutidae and Choerolophodontidae, indicating the early differentiation of Choerolophodontidae from the basal Elephantida.

Acknowledgements We thank T. Deng, Z. X. Qiu, S. K. Hou, Q. Q. Shi, B. Y. Sun, IVPP, China; P. Tassy, Muséum National d'Histoire Naturelle, France; U. Göhlich, Naturhistorisches Museum Wien, Austria; G. Markov, National Museum of Natural History, Bulgaria; and J. Meng, American Museum of Natural History, New York, USA for discussions and advice on this work. We thank G. F. Chen, IVPP, China, and G. Konidaris, Aristotle University of Thessaloniki, Greece, for very important opinion in the review of the work. This work was supported by the National Basic Research Program of China (Grant No. 2012CB821900), the Chinese Academy of Sciences (Grant No. XDB03020104), the National Natural Science Foundation of China (Grant Nos. 41372001, 41430102), and the Special Research Program of Basic Science and Technology of the Ministry of Science and Technology (Grant No. 2015FY310100-14).

中国北方上中新统的早期玛姆象属(*Mammut*)及其在玛姆象科(Mammutidae)分化和演化中的意义

王世骐[1,2]　李　雨[1,3]　董佳荣[1,3,4]　陈少坤[5]　何　文[6]　陈善勤[6]

(1 中国科学院古脊椎动物与古人类研究所，中国科学院脊椎动物演化与人类起源重点实验室 北京 100044)

(2 中国科学院青藏高原地球科学卓越创新中心 北京 100101)

(3 中国科学院大学 北京 100049)

(4 泰国那空叻差是玛皇家大学东北木化石与矿产资源研究所 那空叻差是玛 30000)

(5 重庆三峡古人类研究所，重庆中国三峡博物馆 重庆 400015)

(6 和政古动物化石博物馆 和政 731200)

摘要：玛姆象属是长鼻类玛姆象科这一重要类群的最终成员。虽然这一属在上新世的欧亚大陆和更新世的北美大陆广泛分布，它早期的进化历史却鲜为人知。报道了中国北方上中新统发现的斜脊玛姆象(相似种) (*Mammut* cf. *M. obliquelophus*)的新材料，包括一个几乎完整的幼年头骨，这些材料显示了玛姆象科的许多原始特征，因此很好地解释了玛姆象属形态特征的形成过程。斜脊玛姆象(相似种)具有强烈向两侧扩展的枕部，在门齿窝的基部具有收缩，这些特征与莫罗托始轭齿象(*Eozygodon morotoensis*)和广河豕脊齿象(*Choerolophodon guangheensis*)均具有相似性，后两者分别为玛姆象科与豕脊齿象科的早期代表。因此，玛姆象科与豕脊齿象科(Choerolophodontidae)具有近的亲缘关系，二者同位于象形类(Elephantimorpha)系统发育中的基部。支序分析支持了这一结论。

关键词：中国北方，上中新统，玛姆象科，豕脊齿象科，象形类

中图法分类号：Q915.878　　**文献标识码**：A　　**文章编号**：1000–3118(2017)03–0233–24

References

Andrews C W, 1906. A Descriptive Catalogue of the Tertiary Vertebrata of the Fayûm, Egypt. London: British Museum (Natural History). 1–324

Cozzuol M A, Mothé D, Avilla L S, 2012. A critical appraisal of the phylogenetic proposals from the South American Gomphotheriidae (Proboscidea: Mammalia). Quatern Int, 255: 36–41

Deng T, Qiu Z X, Wang B Y et al., 2013. Late Cenozoic biostratigraphy of the Linxia Basin, northwestern China. In: Wang X M, Flynn L J, Fortelius M eds. Fossil Mammals of Asia: Neogene Biostratigraphy and Chronology of Asia. New York: Columbia University Press. 243–273

Ferretti M P, 2010. Anatomy of *Haplomastodon chimborazi* (Mammalia, Proboscidea) from the Late Pleistocene of Ecuador and its bearing on the phylogeny and systematics of South American gomphotheres. Geodiversitas, 32(4): 663–721

Gheerbrant E, Tassy P, 2009. L'origine et l'évolution des éléphants. C R Palevol, 8: 281–294

Göhlich U B, 1999. Order Proboscidea. In: Rössner G E, Heissig K eds. The Miocene Land Mammals of Europe. München: Verlag Dr. Friedrich Pfeil. 157–168

Goloboff P A, Farris J S, Nixon K C, 2003. T.N.T.: tree analysis using new technology. Program and documentation, available from the authors, and at www.zmuc.dk/public/phylogeny

Gould S J, 1977. Ontogeny and Phylogeny. London: The Belknap Press of Harvard University Press. 1–520

Hopwood A T, 1935. Fossil Proboscidea from China. Palaeont Sin, Ser C, 9: 1–108

Hou S K, 2012. A survey of *Chleuastochoerus* (Suidae, Artiodactyla) from Linxia Basin, Gansu Province, China. Ph.D Dissertation. Beijing: Graduate University of Chinese Academy of Sciences. 1–162

Hou S K, Deng T, 2014. A new species of *Chleuastochoerus* (Artiodactyla: Suidae) from the Linxia Basin, Gansu Province, China. Zootaxa, 3872(5): 401–439

Kaakinen A, Passey B H, Zhang Z Q et al., 2013. Straitigraphy and paleoecology of the classical dragon bone localities of Baode County, Shanxi Province. In: Wang X M, Flynn L J, Fortelius M eds. Fossil Mammals of Asia: Neogene Biostratigraphy and Chronology of Asia. New York: Columbia University Press. 203–217

Konidaris G E, Koufos G D, 2013. Late Miocene Proboscidea (Mammalia) from Macedonia and Samos Island, Greece: preliminary results. Paläont Z, 87(1): 121–140

Konidaris G E, Koufos G D, Kostopoulos D S et al., 2016. Taxonomy, biostratigraphy and palaeoecology of *Choerolophodon* (Proboscidea, Mammalia) in the Miocene of SE Europe-SW Asia: implications for phylogeny and biogeography. J Syst Palaeont, 14(1): 1–27

Kubiak H, 1972. The skull of *Mammut praetypicum* (Proboscidea, Mammalia) from the collection of the Jagiellonian University in Cracow, Poland. Acta Zool Cracov, 17: 305–324

Lehmann U, 1950. Über Mastodontenreste in der Bayerischen Staatssammlung in München. Palaeontographica, 99: 121–228

Markov G N, 2008. The Turolian proboscideans (Mammalia) of Europe: preliminary observations. Hist Nat Bulg, 19: 153–178

Matsumoto H, 1925. Preliminary notes on two new species of fossil mastodon from Japan. J Geol Soc Tokyo, 31: 395–414

Mothé D, Avilla L S, Zhao D S et al., 2016. A new Mammutidae (Proboscidea, Mammalia) from the Late Miocene of Gansu

Province, China. An Acad Bras Ciênc, 88(1): 65–74

Osborn H F, 1929. New Eurasiatic and American proboscideans. Am Mus Novit, 393: 1–28

Osborn H F, 1936. Proboscidea: a Monograph of the Discovery, Evolution, Migration and Extinction of the Mastodonts and Elephants of the World. New York: The American Museum Press. 1–802

Pickford M, 2003. New Proboscidea from the Miocene strata in the lower Orange River Valley, Namibia. Mem Geol Surv Nam, 19: 207–256

Prado J L, Alberdi M T, 2008. A cladistic analysis among trilophodont gomphotheres (Mammalia, Proboscidea) with special attention to the South American genera. Palaeontology, 51(4): 903–915

Rasmussen D T, Gutierrez M, 2009. A mammalian fauna from the Late Oligocene of northwestern Kenya. Palaeontogr Abt A: Paläozool Stratigr, 288(1-3): 1–52

Sanders W J, Miller E R, 2002. New proboscideans from the Early Miocene of Wadi Moghara, Egypt. J Vert Paleont, 22(2): 388–404

Sanders W J, Gheerbrant E, Harris J M et al., 2010. Proboscidea. In: Werdelin L, Sanders W J eds. Cenozoic Mammals of Africa. Berkeley: University of California Press. 161–251

Schlesinger G, 1917. Die Mastodonten des K. K. naturhistorischen Hofmuseums. Denkschr K K Naturhist Hofmus 1, Geol-Paläont Reihe, 1: 1–231

Shoshani J, 1996. Para- or monophyly of the gomphotheres and their position within Proboscidea. In: Shoshani J, Tassy P eds. The Proboscidea: Evolution and Palaeoecology of Elephants and Their Relatives. Oxford: Oxford University Press. 149–177

Shoshani J, Tassy P, 2005. Advances in proboscidean taxonomy and classification, anatomy and physiology, and ecology and behavior. Quatern Int, 126-128: 5–20

Shoshani J, Walter R C, Abraha M et al., 2006. A proboscidean from the Late Oligocene of Eritrea, a “missing link” between early Elephantiformes and Elephantimorpha, and biogeographic implications. Proc Nat Acad Sci, 103: 17296–17301

Tassy P, 1977. Découverte de *Zygolophodon turicensis* (Schinz) (Proboscidea, Mammalia) au lieu-dit Malartic a Simorre, Gers (Vindobonien moyen): implications paléoécologiques et biostratigraphiques. Geobios, 10(5): 655–669

Tassy P, 1982. Les principales dichotomies dans l'histoire des Proboscidea (Mammalia): une approche phylogénétique. Geobios (Mém Spéc), 6: 225–245

Tassy P, 1983. Les Elephantoidea Miocènes du Plateau du Potwar, Groups de Siwalik, Pakistan. Ann Paléont, 69(2-4): 99–136, 235–297, 317–354

Tassy P, 1985. La place des mastodontes Miocènes de l’ancien monde dans la phylogénie des Proboscidea (Mammalia): hypothèses et conjectures. Unpublished Thèse. Paris: Doctorat ès Sciences UPMC. 1–861

Tassy P, 1986. Nouveaux Elephantoidea (Proboscidea, Mammalia) dans le Miocène du Kenya: essai de réévaluation systématique. Paris: Cahiers de Paléontologie. E'ditions du Centre National de la Recherche Scientifique (CNRS). 1–135

Tassy P, 1990a. The “proboscidean datum event:” how many proboscideans and how many events? In: Lindsay E H, Fahlbusch V, Mein P eds. European Neogene Mammal Chronology. New York: Plenum Press. 237–252

Tassy P, 1990b. Phylogénie et classification des Proboscidea (Mammalia): historique et actualité. Ann Paléont, 76: 159–224

Tassy P, 1994a. Origin and differentiation of the Elephantiformes (Mammalia, Proboscidea). Verh Naturwiss Ver Hamburg,

34: 73–94

Tassy P, 1994b. Gaps, parsimony, and Early Miocene elephantoids (Mammalia), with a re-evaluation of *Gomphotherium annectens* (Matsumoto, 1925). Zool J Linn Soc, 112: 101–117

Tassy P, 1996a. Who is who among the Proboscidea. In: Shoshani J, Tassy P eds. The Proboscidea: Evolution and Palaeoecology of Elephants and Their Relatives. Oxford: Oxford University Press. 39–48

Tassy P, 1996b. Dental homologies and nomenclature in the Proboscidea. In: Shoshani J, Tassy P eds. The Proboscidea: Evolution and Palaeoecology of Elephants and Their Relatives. Oxford: Oxford University Press. 21–25

Tassy P, 2013. L'anatomie cranio-mandibulaire de *Gomphotherium angustidens* (Cuvier, 1817) (Proboscidea, Mammalia): données issues du gisement d'En Péjouan (Miocène moyen du Gers, France). Geodiversitas, 35(2): 377–445

Tassy P, 2014. L'odontologie de *Gomphotherium angustidens* (Cuvier, 1817) (Proboscidea, Mammalia): données issues du gisement d'En Péjouan (Miocène moyen du Gers, France). Geodiversitas, 36(1): 35–115

Tassy P, Pickford M, 1983. Un nouveau mastodonte zygolophodonte (Proboscidea, Mammalia) dans le Miocène inférieur d'Afrique orientale: Systématique et paléoenvironnement. Geobios, 16(1): 53–77

Tobien H, 1996. Evolution of zygodons with emphasis on dentition. In: Shoshani J, Tassy P eds. The Proboscidea: Evolution and Palaeoecology of Elephants and Their Relatives. Oxford: Oxford University Press. 76–88

Tobien H, Chen G F, Li Y Q, 1988. Mastodonts (Proboscidea, Mammalia) from the late Neogene and Early Pleistocene of the People's Republic of China, part II: the genera *Tetralophodon*, *Anancus*, *Stegotetrabelodon*, *Zygolophodon*, *Mammut*, *Stegolophodon*. Mainzer Geowiss Mitt, 17: 95–220

Vacek V M, 1877. Über österreichische Mastodonten und ihre Beziehungen zu den Mastodon-Arten Europas. Abh Kaiserlich-Königlichen Geol Reichsanstalt, 7: 1–45

Wang S Q, Deng T, 2011. The first *Choerolophodon* (Proboscidea, Gomphotheriidae) skull from China. Sci China Earth Sci, 54(9): 1326–1337

Wang S Q, He W, Chen S Q, 2013. Gomphotheriid mammal *Platybelodon* from the Middle Miocene of Linxia Basin, Gansu, China. Acta Palaeont Pol, 58(2): 221–240

Wang S Q, Zhao D S, Xie G P et al., 2014. An Asian origin for *Sinomastodon* (Proboscidea, Gomphotheriidae) inferred from a new Upper Miocene specimen from Gansu of China. Sci China Earth Sci, 57(10): 2522–2531

Wang S Q, Deng T, Tang T et al., 2015a. Evolution of *Protanancus* (Proboscidea, Mammalia) in East Asia. J Vert Paleont, e881830, doi:10.1080/02724634.2014.881830

Wang S Q, Duangkrayom J, Yang X W, 2015b. Occurrence of the *Gomphotherium angustidens* group in China, based on a revision of *Gomphotherium connexum* (Hopwood, 1935) and *Gomphotherium shensiensis* Chang and Zhai, 1978: continental correlation of *Gomphotherium* species across the Palearctic. Paläont Z, 89: 1073–1086

Wang S Q, Ji X P, Jablonski N G et al., 2016. The oldest cranium of *Sinomastodon* (Proboscidea, Gomphotheriidae), discovered in the uppermost Miocene of southwestern China: implications for the origin and migration of this taxon. J Mammal Evol, 23: 155–173

Yue L P, Deng T, Zhang Y X et al., 2004. Magnetostratigraphy of stratotype section of the Baode stage. J Stratigr, 28(1): 48–63

Appendix 1 Characters in Elephantimorpha

In this study, for simplicity, we only include the most typical representatives of Mammutidae, Choerolophodontidae, Gomphotheriidae, and Amebelodontidae, because the purpose of this cladistic analysis is to test the mono- or paraphyletic states and to search for the sequence of differentiation of these main groups in Elephantimorpha. The most crown groups, such as Stegodontidae, Elephantidae, and some taxa of Gomphotheriidae and Amebelodontidae, are not included in this analysis (see Appendix 2). The selected characters are mainly related to the cranial features, which can be well extracted based on previous and newly discovered specimens. We also do not include some stem taxa only represented by teeth or mandible fragments, namely, *Eritreum*, *Hemimastodon* and *Losodokodon*. *Phiomia serridens* was served as the outgroup. All characters are treated as unordered.

Characters:

0. Brain case: lateral view. States: 0 = low and flat; 1 = relatively domed. Interpretation: in primitive Elephantimorpha, the brain case is very low and flat and, in almost all derived taxa in various clades, the brain case rises (even in *Mammut americanum*, the brain case shows a slightly domed appearance) (Prado and Alberdi, 2008).
1. Basicranium: States: 0 = not erected; 1 = slightly erected. Interpretation: accompanied by character 0, the erected basicranium is observed in almost all derived taxa in various clades of Elephantimorpha, except in Mammutidae (Tassy, 1996a; Shoshani, 1996).
2. Facial part: lateral view. States: 0 = in the primitive position (as in *Phiomia*); 1 = anteriorly elongated (as in amebelodontids); 2 = anteriorly and ventrally elongated (as in choerolophodontids); 3 = retreated to some degree (as in derived gomphotheres and *Mammut*). Interpretation: anterior elongation of the facial part is regarded as a synapomorphy of Amebelodontidae (Sanders et al., 2010). In derived taxa of Choerolophodontidae, the facial part is strongly ventrally extended, but this feature is not observed in *C. guangheensis*. In the derived groups, namely, taxa of Stegodontidae, Elephantidae, and *Mammut americanum*, the facial part is strongly retreated (the anterior end of the cheek tooth row and the anterior rim of the orbit are on the same level).
3. Incisive fossa: dorsal view. States: 0 = without strong constriction; 1 = with strong constriction. Interpretation: see the text.
4. Palate: post-palatal spine. States: 0 = present; 1 = absent. Interpretation: as a plesiomorphy seen in *Phiomia*, the post-palatal spine is also retained in *Mammut americanum* (more tuberosity-like rather than spine-like in *Mammut americanum*), but is absent in the taxa of Elephantida.
5. Nasal aperture: perinasal fossa. States: 0 = absent; 1 = present. Interpretation: see the text.
6. Nasal aperture: broad prenasal area. States: 0 = absent; 1 = present. Interpretation: see the text.
7. Occipital part: dorsal view. States: 0 = narrow; 1 = wide. Interpretation: see the text.
8. Orbit: lateral view. States: 0 = low position; 1 = high position. In derived taxa of Choerolophodontidae, the orbit is strongly dorsally moved to near the roof of the cranium, but this feature is not observed in *C. guangheensis* (Wang and Deng, 2011).
9. Orbit: lacrimal foramen. States: 0 = present; 1 = absent. Interpretation: as in character 4, lacrimal foramen is present in *Phiomia* and in *Mammut americanum*, but is absent in the other Elephantidae (Tassy, 1994b).
10. Mandibular symphysis: posterior border. States: 0 = close to the anterior end of the cheek tooth row; 1 = distant from the anterior end of the cheek tooth row. Interpretation: except in typical longirostrine taxa such as *Gomphotherium* and members of Amebelodontidae, the posterior mandibular symphyseal border is distant from the anterior end of the cheek tooth row. Otherwise, they are close together, as in *Phiomia*.
11. Angular process: position. States: 0 = low; 1 = high. Interpretation: the mandibular angular process has a low position in *Phiomia* and is also observed in *Mammut* (Tassy, 1994a; Tobien, 1996), but it has a high position in the taxa of Elephantida (Tassy, 1994a).
12. Symphysis: States: 0 = elongated; 1 = relatively short. Interpretation: elongated symphysis is a plesiomorphy of Elephantimorpha, but it has been largely reduced in all of the derived groups (Tassy, 1996a; Shoshani, 1996).
13. Symphyseal trough: States: 0 = shallow; 1 = deep. Interpretation: deep symphyseal trough is considered a synapomorphy of Choerolophodontidae (accompanied by the loss of lower tusks) (Tassy, 1996a; Shoshani, 1996).
14. Ascending ramus: posterior inclination. States: 0 = almost vertical; 1 = posteriorly inclined. Interpretation: posteriorly

inclined ascending ramus is observed in some longirostrine taxa such as in *Gomphotherium* and in *Platybelodon*, and is possibly functionally related.

15. Upper tusks: lateral view. States: 0 = ventrally bent; 1 = dorsally bent. Interpretation: the plesiomorphy of upper tusks is ventrally bent; however, they are dorsally bent in all derived groups, accompanied by the loss of lower tusks (Tassy, 1996a; Shoshani, 1996).
16. Upper tusks: enamel band. States: 0 = present; 1 = absent. Interpretation: the presence of enamel bands is a plesiomorphy of Elephantimorpha; however, enamel bands are lost in most derived taxa (Tassy, 1996a; Shoshani, 1996).
17. Upper tusks: anterodorsal view. States: 0 = simply divergent; 1 = secondarily divergent in the medial part. Interpretation: secondary divergence in the medial part of the upper tusks is considered a feature distinguishing *Gomphotherium* and *Zygolophodon* (Tassy, 1977). Secondary divergence of the upper tusks is also observed in Choerolophodontidae, which might have developed independently from Gomphotheriidae
18. Lower tusks: States: 0 = present; 1 = absent. Interpretation: the absence of lower tusks is common in all derived taxa of Elephantimorpha (Tassy, 1996a; Shoshani, 1996).
19. Lower tusks: cross section: States: 0 = flattish pyriform; 1 = pyriform; 2 = rounded; 3 = flattened. Interpretation: the term flattish pyriform is particularly used to describe the shape of the lower tusk cross section of *Phiomia*. A similar shape is also observed in *Archaeobelodon filholi*. In other members of Amebelodontidae, the cross section is even more flattened. In primitive *Gomphotherium* and *Eozygodon*, the lower tusk cross section is pyriform, whereas in derived members of *Gomphotherium* and Mammutidae, this cross section is rounded.
20. Lower tusks: lateral view. States: 0 = dorsally bent; 1 = almost straight. Interpretation: straight lower tusks are common in those derived taxa including *Mammut*, if present. However, in primitive forms, lower tusks are always slightly dorsally bent (Tassy, 1996a; Shoshani, 1996).
21. Lower tusks: dorsal wear facet. States: 0 = flat; 1 = concave. Interpretation: a concave dorsal wear facet of lower tusks is characteristic of *Gomphotherium angustidens* (Tassy, 2014).
22. Lower tusks: inner structure. States: 0 = concentric lamination; 1 = dentinal tubules. Interpretation: dentinal tubules are found in the cross section of the lower tusks in some amebelodontid taxa, for example, *Platybelodon*, in contrast to normally concentric lamination (Wang et al., 2013, 2015a).
23. Lower tusks: basal end. States: 0 = separated; 1 = close to each other. Interpretation: in those forms with regressive lower tusks, for example, *Mammut*, lower tusks are close to each other in their basal part. In contrast, in forms having developed lower tusks, alveoli of lower tusks are separated basally.
24. Cheek teeth succession: degree of horizontal succession. States: 0 = vertical succession; 1 = partially horizontal succession; 2 = entirely horizontal succession (premolar absent). Interpretation: vertical succession as in most other mammals occurs in the outgroup *Phiomia*. Partially horizontal succession is represented by primitive Elephantimorpha, such as *Gomphotherium*, *Zygolophodon*, and members of Amebelodontidae, in which premolars, although highly regressive, are not missing; this contrasts with the complete loss of premolars in the derived taxa (Tassy, 1996a; Shoshani, 1996).
25. Cheek teeth: cingulum/cingulid. States: 0 = strong; 1 = weak. Interpretation: strong cingulum/cingulid is a plesiomorphy still preserved in Mammutidae (Tassy, 1996a; Shoshani, 1996).
26. Cheek teeth: pattern. States: 0 = bunodont; 1 = zygodont. Interpretation: see the text.
27. Cheek teeth: bunodont pattern. States: 0 = typical bunodont; 1 = bunodont with strong development of posterior pretrite central conules; 2 = bunodont with rudimentary anancoidy and rudimentary secondary trefoils; 3 = choerolophodonty. Interpretation: state 1 is characteristic of *Gomphotherium angustidens* (Tassy, 2014). States 2 and 3 are synapomorphies of amebelodontids and choerolopodontids (Tassy, 1983, 1986), respectively.
28. Cheek teeth: cementum. States: 0 = weak; 2 = heavy. Interpretation: heavy cementum is developed in some taxa, such as in *Platybelodon*, and members of Choerolophodontidae (Tassy, 1996a; Shoshani, 1996).
29. Molars: States: 0 = moderate; 1 = relatively wide; 2 = relatively narrow. Interpretation: relatively wide molar is a synapomorphy of Mammutidae, whereas relatively narrow molar is a synapomorphy of Amebelodontidae (Tassy, 1982).

Appendix 2 Data matrix for cladistic analysis

		1	2
Taxon	0	0	0
Phiomia serridens[1)]	0000000000	0000000000	0000000000
Gomphotherium annectens[2)]	??00100?0?	1100100?01	0000100010
Gomphotherium cf. *G. subtapiroideum*[3)]	1030110001	1100100101	0000100010
Gomphotherium angustidens[4)]	1030110001	1100100101	0100110112
Eozygodon morotoensis[5)]	110110010?	??00?00001	000??01-01
Zygolophodon turicensis[6)]	001??????0?	0000000002	1001101-01
Mammut cf. *M. obliquelophus*	0001000100	001001?002	?000?01-01
Mammut americanum[7)]	0031000100	0010011002	1001201-01
Choerolophodon guangheensis[8)]	0001100101	0?0101111-	----110310
Choerolophodon pentelici[9)]	0120100111	011111111-	----210310
Choerolophodon corrugatus[10)]	1121100111	010101111-	----210310
Archaeobelodon aff. *A. filholi*[11)]	1010110001	1100100100	0000110012
Protanancus brevirostris[12)]	0010101001	1100100003	0000110012
Platybelodon grangeri[13)]	0010101001	1100101003	0010110212

1) Scoring of the outgroup *Phiomia serridens* is based on the complete cranium and mandibles reported by Andrews (1906: figs. 48–50, 53, 54). 2) *Gomphotherium annectens* is from the Early Miocene of Japan (Matsumoto, 1925), represented by a palate and the associated mandible. Scoring of this taxon is based on a cast of the holotype preserved in MNHN; see also Tassy (1994b). 3) *Gomphotherium* cf. *G. subtapiroideum* is from Lengshuigou, China (= *G. shensiensis*, Wang et al., 2015b), represented by an incomplete cranium. The tooth morphology is similar to that of the holotype of *Gomphotherium subtapiroideum* from Austria; in contrast, no cranium of the latter has been discovered. In the type locality of *Gomphotherium* cf. *G. subtapiroideum*, no material of the mandible has been discovered. Scoring of the mandible is based on unpublished material from two other localities, Linxia and Zhongning. It should be noted that the cranium of *Gomphotherium* cf. *G. subtapiroideum* from the Lengshuigou locality shows some primitive features; for example, the facial part of the Lengshuigou specimen is to some extent anteriorly elongated (Wang et al., 2015b: fig. 5), but the new materials from Linxia and Zhongning show a relatively retreated facial part, and character 2 is scored as "3" in our matrix. It is possible that the new materials from Linxia and Zhongning represent a more derived species than *Gomphotherium* cf. *G. subtapiroideum* from the Lengshuigou, and they are closely related to *G. subtapiroideum*. 4) *Gomphotherium angustidens* s.s. is from Simorre and En Péjouan, France. Scoring of this taxon is based on crania and mandibles reported by Tassy (2013: figs. 5–12, 21–24). 5) *Eozygodon morotoensis* is from Meswa Bridge, Kenya, and lower Orange River Valley, Namibia. Scoring of this taxon is based on crania reported by Pickford (2003: pls. 2–5) and teeth reported by Tassy and Pickford (1983: figs. 4–9, 14–16). 6) Scoring of *Zygolophodon turicensis* is based on the cranium from Villafranche d'Astarac, which was reported by Tassy (1985: fig. 208), and mandibles reported by Osborn (1936: fig. 657), Lehmann (1950: pl. 14, fig. 26), and Tassy (1985: fig. 210). 7) Scoring of *Mammut americanum* is based on complete crania and mandibles housed in AMNH, for example, AM 2595, 14535, 17727, and 17771A. 8) *Choerolophodon guangheensis* is from the Linxia Basin, China, represented by a nearly complete cranium (Wang and Deng, 2011, see Fig. 6C, D). Although some researchers considered the evolutionary state of this species to be intermediate, showing a mixture of primitive and more advanced features (Konidaris et al., 2016), we believe that this species is a typical primitive form of the genus. Scoring of mandibular features is based on unpublished new material from the same locality. 9) Scoring of *Choerolophodon pentelici* is based on the material reported by Konidaris and Koufos (2013: figs. 2, 3) and Konidaris et al. (2016: fig. 6). 10) *Choerolophodon corrugatus* is from Siwalik, Pakistan. Scoring of this taxon is based on the complete cranium and mandible reported by Osborn (1929: figs. 10–13), and Tassy (1983: figs. 13–16). 11) Scoring of *Archaeobelodon* aff. *A. filholi*, from Buluk, Kenya, is based on the nearly complete cranium with the associated mandible reported by Tassy (1986: pls 2, 3). 12) *Protanancus brevirostris* is from the Linxia Basin, China, represented by a nearly complete cranium with an associated mandible (Wang et al., 2015a: fig. 4). It is the most primitive species of this genus. However, this specimen is badly preserved. Scoring of this taxon is further based on unpublished new material from the same locality. 13) Scoring of *Platybelodon grangeri* is based on the crania and mandibles from the Linxia Basin reported by Wang et al. (2013).

+Model
PALWOR-488; No. of Pages 33
ARTICLE IN PRESS

Available online at www.sciencedirect.com

ScienceDirect

Palaeoworld xxx (2019) xxx–xxx

Palaeoworld

www.elsevier.com/locate/palwor

Correlating the global Cambrian–Ordovician boundary: Precise comparison of the Xiaoyangqiao section, Dayangcha, North China with the Green Point GSSP section, Newfoundland, Canada

Xiao-Feng Wang [a], Svend Stouge [b,*], Jörg Maletz [c], Gabriella Bagnoli [d], Yu-Ping Qi [e,f], Elena G. Raevskaya [g], Chuan-Shang Wang [a], Chun-Bo Yan [a]

[a] *Wuhan Center of China Geological Survey (Wuhan Institute of Geology and Mineral Resources), Wuhan, China*
[b] *Natural History Museum of Denmark, University of Copenhagen, Copenhagen, Denmark*
[c] *Institute of Geology, Free University of Berlin, Germany*
[d] *Dipartimento di Scienze della Terra, Via S. Maria 53, I-56126 Pisa, Italy*
[e] *State Key Laboratory of Palaeobiology and Stratigraphy, Nanjing Institute of Geology and Palaeontology, Chinese Academy of Sciences, 39 East Beijing Road, Nanjing 210008, China*
[f] *Center for Excellence in Life and Palaeoenvironment, Nanjing Institute of Geology and Palaeontology, Chinese Academy of Sciences, 39 East Beijing Road, Nanjing 210008, China*
[g] *AO 'Geologorazvedka', Fayansovaya Street 20, Building 2A, Saint Petersburg 192019, Russia*

Received 14 July 2018; received in revised form 29 November 2018; accepted 22 January 2019

Abstract

The Cambrian–Ordovician boundary interval exposed at the Xiaoyangqiao section, North China is presented. The distribution of stratigraphically important fossils in the Xiaoyangqiao section revealed several nearly coeval graptolite, conodont, trilobite, and acritarch bioevents in the uppermost Cambrian–lowermost Ordovician carbonate-siliciclastic sedimentary sequence. The precise correlation to the Green Point GSSP section, western Newfoundland, Canada allows for the identification of the corresponding GSSP level in the Xiaoyangqiao section. The combined data from the Xiaoyangqiao section and the Green Point GSSP section provide a series of events that all can be applied as proxies for identification of the Cambrian–Ordovician boundary horizon outside the GSSP. Based on this, the Xiaoyangqiao section, Dayangcha, is here strongly recommended as a candidate for an Auxiliary Boundary Stratigraphic Section and Point section (ASSP) for the base of the Ordovician System, because it provides one of the best and most complete Cambrian–Ordovician transitions in the world and because the first planktic graptolites are from the Xiaoyangqiao section.

Keywords: Dayangcha ASSP section; Green Point GSSP section; Cambrian–Ordovician boundary; Acritarchs; Conodonts; Graptolites

1. Introduction

Recognition of the boundary between the Cambrian and Ordovician systems is a matter of global scale discussions. During the last couple of decades, several integrated studies of Cambrian–Ordovician boundary sections from different regions were published with the objective to show the presence of the chosen biological marker in these sections and the potential for correlation of the Cambrian–Ordovician boundary (e.g., Albanesi et al., 2015; Zhen et al., 2017). The latest Cambrian to Early Ordovician transition (ca. 485.4 Ma; based on the International Chronostratigraphic Chart 2017/2), representing an important episode in Earth History, is excellently displayed in the Xiaoyangqiao section (=lower part of the Xiaoyangqiao composite section (XCS) of Chen et al. (1985,

* Corresponding author.
E-mail addresses: ycwangxiaofeng@163.com (X.F. Wang), svends@snm.ku.dk (S. Stouge), yorge@zedat.fu-berlin.de (J. Maletz), gabriella.bagnoli@unipi.it (G. Bagnoli), ypqi@nigpas.ac.cn (Y.P. Qi), lena.raevskaya@mail.ru (E.G. Raevskaya), wangchuanshang@163.com (C.S. Wang), yanchunbo123@163.com (C.B. Yan).

https://doi.org/10.1016/j.palwor.2019.01.003
1871-174X/

Please cite this article in press as: Wang, X.F., et al., Correlating the global Cambrian–Ordovician boundary: Precise comparison of the Xiaoyangqiao section, Dayangcha, North China with the Green Point GSSP section, Newfoundland, Canada. Palaeoworld (2019), https://doi.org/10.1016/j.palwor.2019.01.003

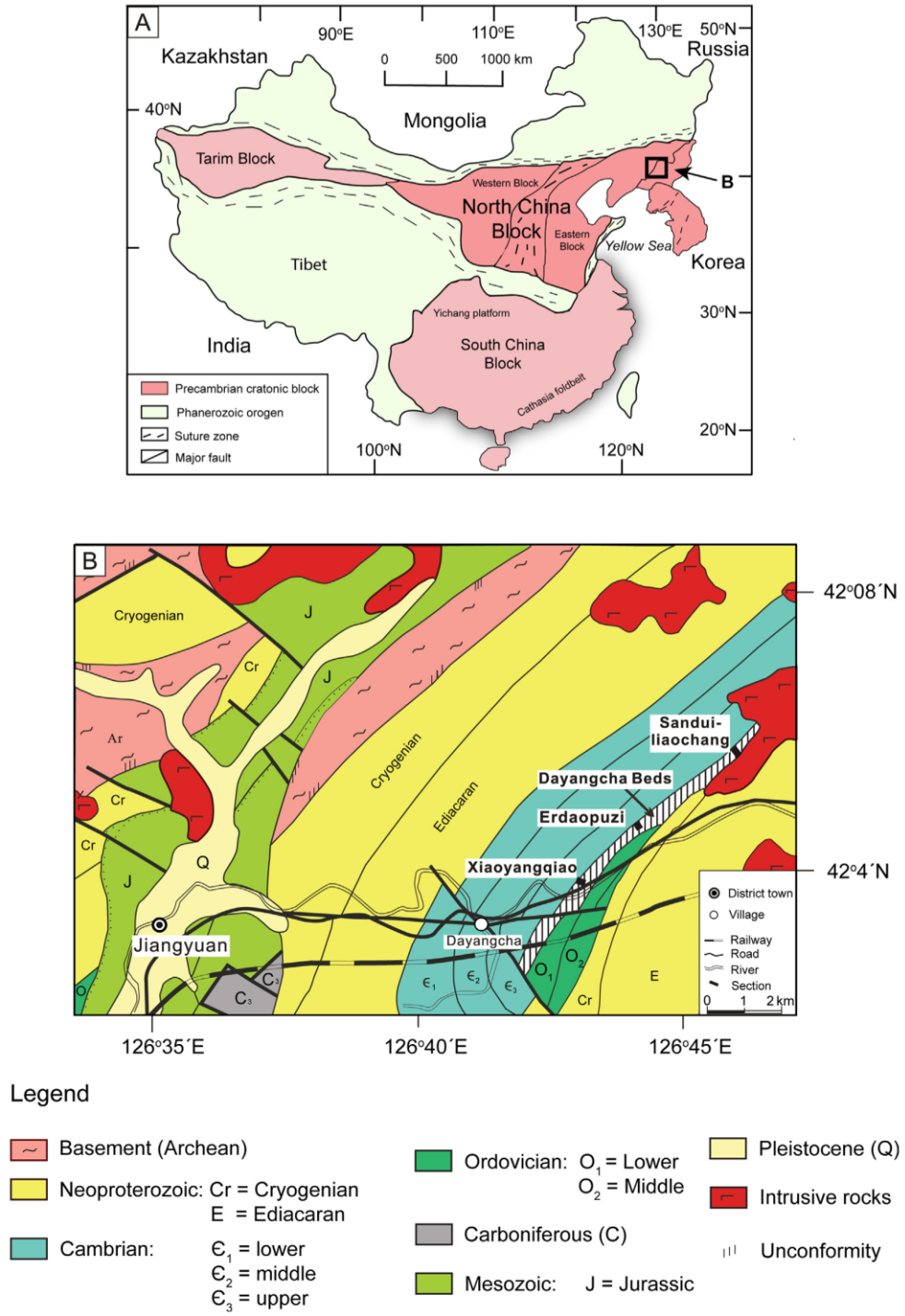

Fig. 1. (A) Simplified tectonic map of the three main China plates (Tarim, North China and South China). (B) Geological and location map of the study area. The location of the significant Xiaoyangqiao, Erdaopuzi and Sanduiliaochang sections that are situated to the northeast of Dayangcha village is shown. The Baishan City, the main city of the Jiangyuan District, is located ca. 20 km southwest of Dayangcha (and outside (B)).

Please cite this article in press as: Wang, X.F., et al., Correlating the global Cambrian–Ordovician boundary: Precise comparison of the Xiaoyangqiao section, Dayangcha, North China with the Green Point GSSP section, Newfoundland, Canada. Palaeoworld (2019), https://doi.org/10.1016/j.palwor.2019.01.003

1986, 1988), Dayangcha, North China. In comparison with coeval successions from Europe and Asia, the stratigraphically continuous Cambrian–Ordovician limestone-shale succession at the Xiaoyangqiao section offers one of the best possibilities to document the Cambrian–Ordovician transition over a wide area and on a global scale. The Xiaoyangqiao section, close to the township Dayangcha (Fig. 1), is here recommended as a global Auxiliary Boundary Stratigraphic Section and Point (ASSP) because it comprises a complete conodont, graptolite, acritarch and trilobite succession; moreover, the $\delta^{13}C_{carb}$ isotope data, the sequence stratigraphy, and magnetostratigraphy provide additional and important results, enabling precise comparison with known key and widely separated sections spanning the Cambrian–Ordovician boundary in the world.

This paper discusses the results of the new integrated study using two macrofossil groups (graptolites, trilobites) and two microfossil groups, i.e., conodonts and acritarchs, as well as stable isotope data ($\delta^{13}C_{carb}$, $\delta^{18}O$), sea-level changes and sequence stratigraphy in the Xiaoyangqiao section and the comparison with the Green Point GSSP section in Newfoundland, Canada.

1.1. The Cambrian–Ordovician line: a historical review

The International Working Group on the Cambrian–Ordovician Boundary (COBWG I) was established in 1974. In this period, members of the Working Group visited several proposed candidate boundary sections, which were widely distributed in the world (Australia, China, Great Britain, Kazakhstan, North America and Scandinavia). The Working Group arranged many workshops, field meetings and conferences that all were devoted towards the Cambrian–Ordovician boundary. The working group documented these activities, discussions and the decisions/results in numerous reports and publications (e.g., Norford, 1991).

The extensive list of publications includes the volumes of papers on candidate boundary sections published in Bassett and Dean (1982) and Norford and Webby (1988). Chen et al. (1985) and Chen (1986) published two special volumes of papers, specifically on the Dayangcha section, covering a wide range of disciplines. Additional papers concerning issues on the Cambrian–Ordovician boundary appeared in Barnes and Williams (1991) and Webby and Laurie (1992).

The first working group also discussed the principles, procedures, candidate sections, and discussed the boundary definition, and various potential levels for the boundary. One main activity of the Working Group was the selection of the level for the boundary and subsequently, the choice of the marker taxon became important. After 19 years and replacement of three chairmens, this first working group and the executive and voting members stepped down in 1993. The second working group (COBWG II) was established in 1993. In this period, the members visited and investigated in detail the Dayangcha, Green Point, and Lawson Cove candidate sections.

At the working meeting held in Canada in 1985 the COBWG I proposed that the Cambrian–Ordovician boundary should be drawn at the level below but close to the appearance of first planktic graptolites and marked by the FAD (First Appearance Datum) of a species of the complete evolutionary succession of the conodont genus *Cordylodus* Pander (Barnes, 1988; Nicoll, 1990, 1992).

However, due to systematic problems with the originally proposed conodont marker *Cordylodus lindstromi* (i.e., Barnes, 1988) this taxon was abandoned and instead the conodont species *Iapetognathus fluctivagus* Nicoll et al., 1999 was introduced as the primary marker for the Cambrian–Ordovician boundary (Nicoll et al., 1999). Accordingly, the Green Point section, Newfoundland, Canada, became the only candidate for the GSSP section for the base of the Ordovician System, because both the marker species and planktic graptolites are present in the section.

Succeeding the selection of Green Point as the GSSP section several problems remained and new ones arose. One of the remaining problems is the difficulty in correlating shallow-water deposits to the deep-water Green Point section. A second problem was the assumption that the conodont succession at the Green Point section was dominated by reworked taxa (e.g., Miller and Flokstra, 1999; Miller et al., 2003). An additional problem arose when Terfelt et al. (2012) demonstrated that the selected biomarker *Iapetognathus fluctivagus* appeared higher in the Green Point section and above the appearance of planktic graptolites. Terfelt et al. (2012) also proposed additional horizons that could serve as boundary levels, but did point out that currently, the Cambrian–Ordovician boundary is fixed by the first appearance of *Iapetognathus preaengensis*. Miller et al. (2014) however rejected this interpretation and maintained that *Iapetognathus fluctivagus* is the correct marker species for the base of the Ordovician.

Zhou et al. (1984) were the first to propose the Xiaoyangqiao section, Dayangcha, as stratotype section for the Cambrian–Ordovician system boundary. It was recommended as a GSSP candidate for the base of the Ordovician System at the Calgary Plenary Session (Chen et al., 1985). At the Sixth International Symposium on the Ordovician System held in Sydney, Australia, in 1991, the Xiaoyangqiao section was accepted as the only candidate section for Global Cambrian–Ordovician Boundary Stratotype by the International Cambrian–Ordovician Working Group (ICOBWG I). However, the selection of *Iapetognathus fluctivagus* as marker for the base of Ordovician by the Working Group became crucial, because the taxon has not been recorded from the Xiaoyangqiao section and the ICOBWG II selected the Green Point section, Newfoundland, Canada, as the Global Stratotype Section and Point (GSSP) for the base of the Ordovician System in January 1999. The decision was approved by the International Subcommission on Ordovician Stratigraphy (ISOS) in September 1999 and the Commission on Stratigraphy (ICS) in November 1999, and finally ratified by the International Union of Geological Sciences (IUGS) in January 2000 (Cooper et al., 2001).

2. The Xiaoyangqiao section

The Xiaoyangqiao section (42°3′24″N, 126°42′21″E), Dayangcha, Hunjiang, Jilin Province, NE China is situated along

Please cite this article in press as: Wang, X.F., et al., Correlating the global Cambrian–Ordovician boundary: Precise comparison of the Xiaoyangqiao section, Dayangcha, North China with the Green Point GSSP section, Newfoundland, Canada. Palaeoworld (2019), https://doi.org/10.1016/j.palwor.2019.01.003

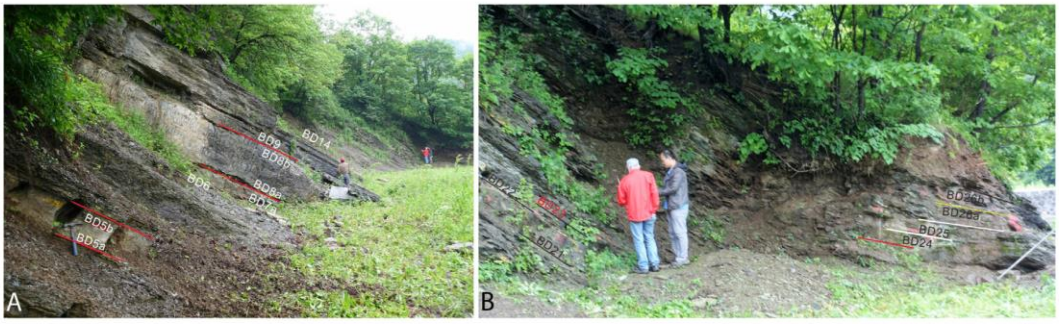

Fig. 2. Photos from the Xiaoyangqiao section (persons for scale). (A) Top of lithological units I and II. The base of lithological unit II is at BD 7a. Lithological unit II comprises BD 7a and extends to just above BD 14. The higher beds belong to lithological unit III. (B) Upper part of lithological unit III. The FAD of planktic graptolites is just above BD 26a at 20.9 m (to the right on the photo).

the NW side of a small rivulet — a tributary of the Hunjiang River — 2.5 km NNE of the town of Dayangcha (Fig. 1). Access by car is approximately 40 min from Baishan, and ca. 10 min from Jiangyuan, and 5 min drive from the town of Dayangcha; alternatively, the train from Baishan takes about 30 min.

The lithology, fossil record and stratigraphy of the upper Cambrian (Stage 10, Furongian Series) and Lower Ordovician (Tremadocian) succession of the Xiaoyangqiao section were studied by Kuo et al. (1982), Zhou et al. (1984), Chen et al. (1983, 1985, 1988, 1995), Chen (1986), and Zhang et al. (1996). The fauna comprises acritarchs, conodonts, graptolites and trilobites in high variety and abundance. Erdtmann (1986), Lin (1986), Wang and Erdtmann (1987), and Zhang and Erdtmann (2004) studied the graptolites from the section. The conodonts have been documented by Chen et al. (1985) followed by Chen and Gong (1986) with additional information by Nowlan and Nicoll (1995) and Nicoll et al. (1999). Yin (1985, 1986, 1995) described the acritarch assemblages, and Qian (1986) described the trilobite fauna. Chen and Zhang (1986), Zhang (1986), and Zhang and Chen (1986) provided details on the succession and the depositional environment and Wang and Yang (1986) investigated the clay composition of the sediments. Chen et al. (1986) described the distribution of rare earth elements in the succession. Yang et al. (1986) estimated an uppermost Cambrian horizon (HBA 9B1) within the section to 500.7 ± 7.4 Ma based on Rb-Sr method. Ripperdan and Kirschvink (1992), Ripperdan et al. (1992), and Chen et al. (1995), independently, presented quite similar $\delta^{13}C$-isotope curves from the Xiaoyangqiao section. Ripperdan and Kirschvink (1992) and Ripperdan et al. (1992, 1993) introduced the magnetostratigraphy of the Cambrian–Ordovician beds and correlated the magnetostratigraphy to the biostratigraphy data.

2.1. Restudy of the Xiaoyangqiao section

In the past four years an international research group, consisting of seven geologists from China, Denmark and Germany re-sampled and re-studied the Xiaoyangqiao section and other relevant sections in the Dayangcha area. Three additional participants joined the project and expanded the international working group with one geologist from China and two geologists from Italy and Russia, respectively.

2.2. Material and methods

The Xiaoyangqiao section was measured between 2014 and 2016. Bed thicknesses (terminology after Tucker, 2003), colours, lithologies, textures, sedimentary structures, macrofossils and the stacking pattern of the strata were recorded in the field. Carbonates are described according to the classification scheme of Dunham (1962), mixed siliciclastic-carbonate deposits are classified after Mount (1985) and siliciclastic sediments are classified after Wentworth (1922). The section was studied using an integrated litho-, bio-, sequence- and isotope stratigraphy approach.

The upper Cambrian–lowermost Ordovician succession (Fig. 2) was collected in detail or nearly bed-by-bed for conodont research. Two sample series (BH and DC) were collected, giving a total of 115 conodont-yielding samples. In addition, the original material described and published by Chen and Gong (1986) has been inspected and used for this investigation. The conodonts were studied under light stereomicroscope and some specimens are documented using the light microscope and Scanning Electron Microscope (SEM).

The new palynological data are obtained from 46 new samples (series DA) collected from either the same beds as for the conodonts, close to them, or just in-between the levels collected by Yin (1986). Some of the additional sampled levels yielded rich acritarch assemblages, allowing for the expansion of the previously known palynological characteristics of the studied strata.

Graptolite faunas are known from three levels/intervals in the Xiaoyangqiao section. In connection with the investigation of the faunas from the Xiaoyangqiao section, material from various localities (e.g., Quebec, Canada; western Newfoundland, Canada; Victoria, Australia) have been investigated and biostratigraphically compared with the Chinese faunas. This provided a better understanding of the preservation aspects and led to more precise biostratigraphical correlation of the earliest planktic graptolite faunas worldwide.

Please cite this article in press as: Wang, X.F., et al., Correlating the global Cambrian–Ordovician boundary: Precise comparison of the Xiaoyangqiao section, Dayangcha, North China with the Green Point GSSP section, Newfoundland, Canada. Palaeoworld (2019), https://doi.org/10.1016/j.palwor.2019.01.003

Carbon isotope analysis was carried out on the bulk carbonate fraction of 96 samples in the Cambrian–Ordovician interval from the Xiaoyangqiao section. The geochemical analysis was prepared and analyzed at the Isotopic Geochemistry Laboratory of the Wuhan Center of China Geological Survey, Wuhan, China. The carbon isotope ratios were measured using Gasbench II and ThermoFisher MAT253 mass spectrometer. The C-isotope values are reported in the standard δ notation in per mil (‰) relative to the PDB standard with a precision of 0.1‰.

The transgressive-regressive (T-R) sequence approach introduced by Embry and Johannessen (1992) is adopted here for the sequence stratigraphy approach. The transgressive-regressive approach uses the subaerial unconformity as the unconformable portion of the boundary, and the maximum regressive surface (MRS) as the correlative conformity. The T-R sequence approach is used due to the absence of subaerial unconformities in the section, which might otherwise be used as sequence boundaries. The individual T-R sequences are bound by MRSs, not sequence boundaries of the traditional Exxon sequence stratigraphic model (cf. Catuneanu et al., 2009, 2011).

A single T-R sequence can be further divided into a fining-upward transgressive systems tract (TST) below, and a coarsening-upward regressive systems tract (RST) above, with the maximum flooding surface (MFS) being the mutual boundary. These are distinctive surfaces of non-deposition, sediment starvation and condensation that tend to cap the finest grained sediments of the TSTs and precede the onset of coarsening-upward cycles (RSTs).

All data provide the basis for the sequence stratigraphic arrangement introduced here and the T-R approach works well in more distal sections, which lack a subaerial erosional unconformity.

3. Geological context of the Xiaoyangqiao section of Dayangcha, Hunjiang, Jilin Province

3.1. Geological setting

The upper Cambrian–Lower Ordovician sedimentary successions accumulated on the stable North China Craton (NCC or Sino–Korean Craton, SKC; Fig. 1), which comprises most of North China and parts of the Korean Peninsula (Fig. 1; Zhu et al., 2012). The craton forms the core of the North China plate, which is one of the three Chinese peri-Gondwana terranes (i.e., North China, South China, and Tarim blocks; Meyerhoff et al., 1991; Torsvik and Cocks, 2016). Today, the North China Craton is bounded to the north by the Central Asian Orogenic belt (Altaids) (Meng et al., 1997; Zheng et al., 2013), to the west by the western Tethyan subdomain, and to the south by the Qinling–Tongbai–Hong'an–Dabie–Sulu Orogenic Belt (Li and Powell, 2001; Kusky et al., 2007; Xiao et al., 2009; Zhai and Santosh, 2013). The eastern margin is delineated by the Pacific subduction zone, which was formed by the collision with South China (Lee and Chough, 2011). Thus today, the North China block covers an area of about 1500 km from east to west and 1000 km from north to south (Meng et al., 1997).

The basement of the North China Craton is composed of Archean (Eastern block), with the oldest dated at 3800 Ma, and Palaeoproterozoic rocks (Western Block). A thick succession of Neoproterozoic to Palaeozoic sedimentary deposits unconformably overlies the basement (Zhao and Zhai, 2013; Zheng et al., 2013). The Cambrian–Ordovician platform succession, about 500–1000 m thick, is composed of carbonate shallow marine water deposits with intervals of extensive biostromal microbialites (Lee et al., 2012), some mixed carbonate and siliciclastic and evaporites (gypsum), oolites and lime breccias that accumulated on the craton (Feng and Jin, 1994). A thicker package composed of mixed carbonates and siliciclastics was deposited in the median to outer shelf to slope setting of the southeastern margin of the North China (Fig. 1). The carbonate platform of eastern North China settled on a ramp-like margin during the late Cambrian–Early Ordovician. The median shelf siliciclastic-carbonate belt was in places rimmed seaward by a low stromatolite reef and the outer shelf carbonate platform was flanked seaward by a shale-rich outer detrital belt of the platform margin.

During the late Cambrian and Early Ordovician the North China plate occupied a tropical position and the sedimentary succession was deposited in an extensive epeiric sea (Meyerhoff et al., 1991; Fu, 1996, pp. 37–38; Fu and Lai, 1996, pp. 37–40; Meng et al., 1997). The North China Block drifted northward and was situated near the equator during the early Palaeozoic (Fu, 1996; Fu and Lai, 1996; Li and Powell, 2001; Burrett et al., 2014; Torsvik and Cocks, 2016). In the late Cambrian the palaeogeographical position of the North China block was within 10° of the equator, but in the latest Cambrian to earliest Ordovician it changed to the subaequatorial belt with hurricanes. This is seen in the increase of storm deposits, evaporites (gypsum), oolites and lime breccias in the uppermost Cambrian to lowermost Ordovician successions of the North China block (Liu and Zheng, 1998; Kwon et al., 2006). It was tectonically stable during most of the Cambrian, but a hiatus of variable magnitude across the Cambrian–Ordovician boundary is developed at many sites on the North China platform, which is interpreted as being caused by an uplift that occurred on the western margin of the North China plate. The Ordovician succession is interrupted due to the 'Huaiyuan Movement' forming a hiatus extending from the mid-late Floian (Early Ordovician) into the early Darriwilian (Liu et al., 1997; Wang et al., 2016; Zhen et al., 2016). Sedimentation on the North China plate returned in the Middle Ordovician and persisted into the early Late Ordovician. A second uplift caused the formation of a great hiatus and lower Upper Ordovician sedimentary rocks are disconformably overlain by an upper Carboniferous to lower Permian succession composed of marine and terrestrial deposits (Zheng et al., 2013).

3.2. Stratigraphy and succession

The Ordovician sedimentary rocks of the Dayangcha area form a succession characterized by marine mixed siliciclastic-carbonate, upward-deepening and upward shallowing cyclic sedimentation. These upper Cambrian to Lower Ordovician sedimentary rocks, very well exposed at the Xiaoyangqiao section,

Please cite this article in press as: Wang, X.F., et al., Correlating the global Cambrian–Ordovician boundary: Precise comparison of the Xiaoyangqiao section, Dayangcha, North China with the Green Point GSSP section, Newfoundland, Canada. Palaeoworld (2019), https://doi.org/10.1016/j.palwor.2019.01.003

are here referred — informally — to the Dayangcha beds (cf. Erdtmann, 1986; Fig. 1B). The underlying, mainly sedimentary carbonates and subordinate shales, exposed along the road in the Xiaoyangqiao lower section (XLS), immediately to the south of the Xiaoyangqiao composite section (XCS) (Fig. 1B), are referred to the Furongian Fengshan Formation (Zhang, 1962). The Lower Ordovician (Tremadocian) strata of the Yeli (or Yehli) Formation (Grabau, 1922) overlie the Dayangcha beds (Zhang, 1962; Wang et al., 1996). The Yeli strata are composed mainly of carbonate sedimentary rocks with only subordinate calcareous shale. The Yeli Formation is exposed in the other small rivulet immediately to the south of the Xiaoyangqiao section and along the new main road (Zhang and Erdtmann, 2004; Fig. 1B). The Xiaoyangqiao section and the westerly facing section with exposures of the Yeli Formation and situated just to the south of the Xiaoyangqiao section are together named the Xiaoyangqiao composite section (XCS) (Chen, 1986; Zhang, 1986; Fig. 1B).

3.2.1. Lithostratigraphy

The Dayangcha beds exposed at the Xiaoyangqiao section consist of mixed carbonate-siliciclastic sedimentary rocks, composed primarily of limestone, siltstone and shale, subordinate conglomerates and strata bound breccias that dip evenly from 21° to 48° to the northeast (Fig. 2).

The Dayangcha beds can be subdivided into four lithostratigraphic informal units (I–IV; Fig. 3).

3.2.1.1. Unit I

Unit I is composed of mixed shale, shale with thin limestone lenses and limestone beds. Unit I, ca. 11 m thick, comprises a series of upward deepening one metre-scale cycles but shows an increasing abundance of siltstone in the uppermost part of the unit and just below the capping limestone. In the unit the ratio carbonate: siliciclastic is about 1:1 with an increase upsection of the siliciclastic content. Unit I starts from middle of the Xiaoyangqiao low section (XLS), exposed along the road to Dayangcha (Fig. 1), and continues upwards from the base of the Xiaoyangqiao section; it terminates just below the reference level of the Xiaoyangqiao section (i.e., at 0.0 on Fig. 3). Trilobites, associated with some brachiopods, are present to common in the shale.

3.2.1.2. Unit II

This unit is dominated by carbonate deposition starting with shallow water carbonate into gradually increasing deeper water carbonates, commonly nodular, and minor interbedded shale (parted and ribbon limestone). This unit includes the prominent columnar stromatolite marker bed (1.4–1.6 m thick) slightly above the reference level. Unit II begins at −0.2 m and extends up to +7.1 m in the section (Figs. 2, 3). Trilobites are present in the unit.

Unit II represents a brief recovery of the carbonate factory on the platform with little input of siliciclastic material.

3.2.1.3. Unit III

Unit III is predominantly siliciclastic shale and siltstone interbedded with minor thin argillaceous, commonly nodular, limestone beds. Input of carbonate conglomerate and imbricated limebreccia horizons is recorded in the middle of the unit and a series of strata bound limebreccia beds characterizes the top of the unit. Glauconite becomes a characteristic component in the middle to upper part of unit III. Trilobites are frequent in unit III and the first planktic graptolite appears at the top of the unit (Figs. 2, 3). Unit III starts at +7.1 m and extends to +21.4 m and thus it is 14.3 m thick. Sponge spicules are common in the limestone.

The limebreccias are interpreted as storm generated deposits or tempestites produced by hurricanes (e.g., Kwon et al., 2006; Chen and Lee, 2013; Chen, 2014). The conglomerate bed probably was deposited by a debris flow. The presence of glauconite in the upper unit III signifies a depth of 150–200 m (e.g., Porrenga, 1967) and low deposition rate (Odin, 1988).

3.2.1.4. Unit IV

Unit IV comprises almost exclusively siliciclastic sedimentary rocks, composed of green, light grey shale to black shale, and grey to light grey siltstone and few fine-grained sandstone beds. Thin, flat lenticular carbonate beds may occur in the dark grey to black shale; a few beds of limestone are recorded at the top of the unit. Except for the black shale, glauconite is a common mineral in this member. The most significant macrofossils in unit IV are planktic graptolite assemblages. This unit extends from +21.4 m and up to the top of the exposed section (Fig. 3). Unit IV is at least 9.8 m thick: it is most likely thicker as the upper boundary of the unit has not been reached in the Xiaoyangqiao section.

3.2.2. Biostratigraphy

The biostratigraphy of conodonts and graptolites from the Xiaoyangqiao section is outlined below. The acritarchs are in an early stage of revision and biostratigraphic units are presented informally. The trilobite succession, described by Chen et al. (1983, 1985, 1986, 1988), is presented here in abbreviated form.

3.2.3. Conodonts

The conodont fauna comprises eu- and paraconodonts, which are moderately to relatively abundant and the fauna is moderately diverse. In this investigation only the euconodonts are discussed. The specimens are only mildly altered showing a CAI of 1.5–2 suggesting that the host rocks were heated to a maximum of 140 °C (Epstein et al., 1977). The specimens are generally well preserved, but at times the specimens have broken cups and some are preserved with silt attached to the specimens.

3.2.3.1. Conodont evolutionary lineages

The investigated Cambrian–Ordovician interval in the Xiaoyangqiao section preserves the evolutionary succession of the conodont genus *Cordylodus* Pander, 1856 that derived from *Eoconodontus notchpeakensis* (Miller, 1969) (Figs. 4A, 5A). The *Cordylodus* lineage starts with *Cordylodus primitivus* Bagnoli, Barnes and Stevens, 1987 (Figs. 4B, 5B) succeeded

Please cite this article in press as: Wang, X.F., et al., Correlating the global Cambrian–Ordovician boundary: Precise comparison of the Xiaoyangqiao section, Dayangcha, North China with the Green Point GSSP section, Newfoundland, Canada. Palaeoworld (2019), https://doi.org/10.1016/j.palwor.2019.01.003

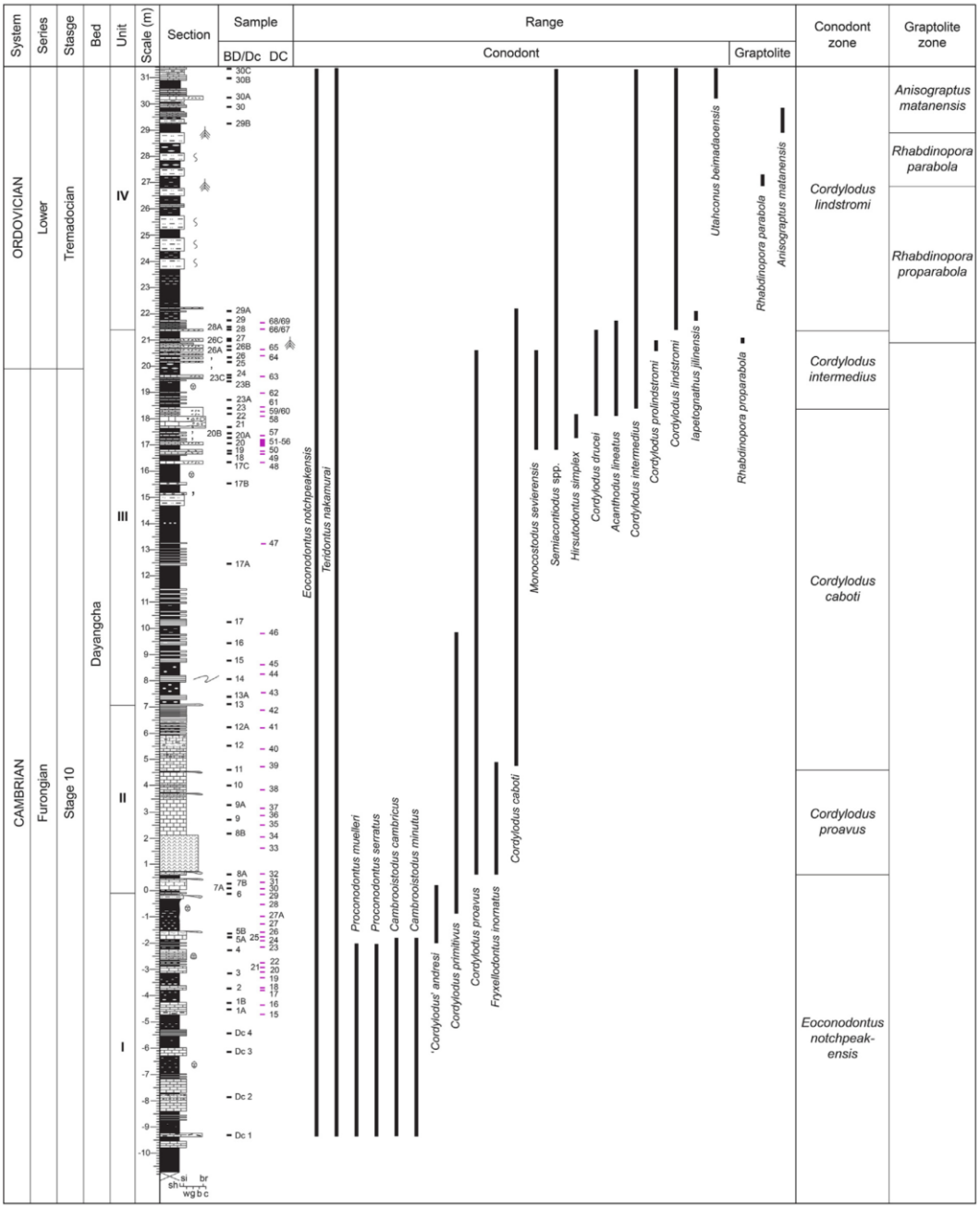

Fig. 3. Upper Cambrian to Lower Ordovician (Tremadocian) stratigraphy of the Xiaoyangqiao section and ranges of selected conodont and graptolite species. For legend, see Fig. 10. Abbreviations used for grainsize: sh = shale; si = siltstone; br = breccia; w = wackestone; g = grainstone; b = boundstone; c = conglomerate.

by *C. proavus* Müller, 1959 (Figs. 4C, D, 5C, D), *C. caboti* Bagnoli, Barnes and Stevens, 1987 (Figs. 4E, F, 5E, F), *C. intermedius* Furnish, 1938 (Figs. 4I, J, 5I, J) and *C. lindstromi* Druce and Jones, 1971 (Figs. 4K–M, 5K–M). '*Cordylodus*' *andresi* Viira and Sergeeva in Kaljo et al., 1986 (see Viira et al., 1987) is recorded first at −2.4 m in the section and just below the appearance of *C. primitivus*. However, '*Cordylodus*' *andresi* is not phylogenetically connected with the genus *Cordylodus s.s.* (Bagnoli and Stouge, 2014).

In the Xiaoyangqiao section *Iapetognathus jilinensis* Nicoll, Miller, Nowlan, Repetski and Ethington, 1999 (Fig. 4O, P) represents a segment of the evolutionary lineage that yet has to be

Please cite this article in press as: Wang, X.F., et al., Correlating the global Cambrian–Ordovician boundary: Precise comparison of the Xiaoyangqiao section, Dayangcha, North China with the Green Point GSSP section, Newfoundland, Canada. Palaeoworld (2019), https://doi.org/10.1016/j.palwor.2019.01.003

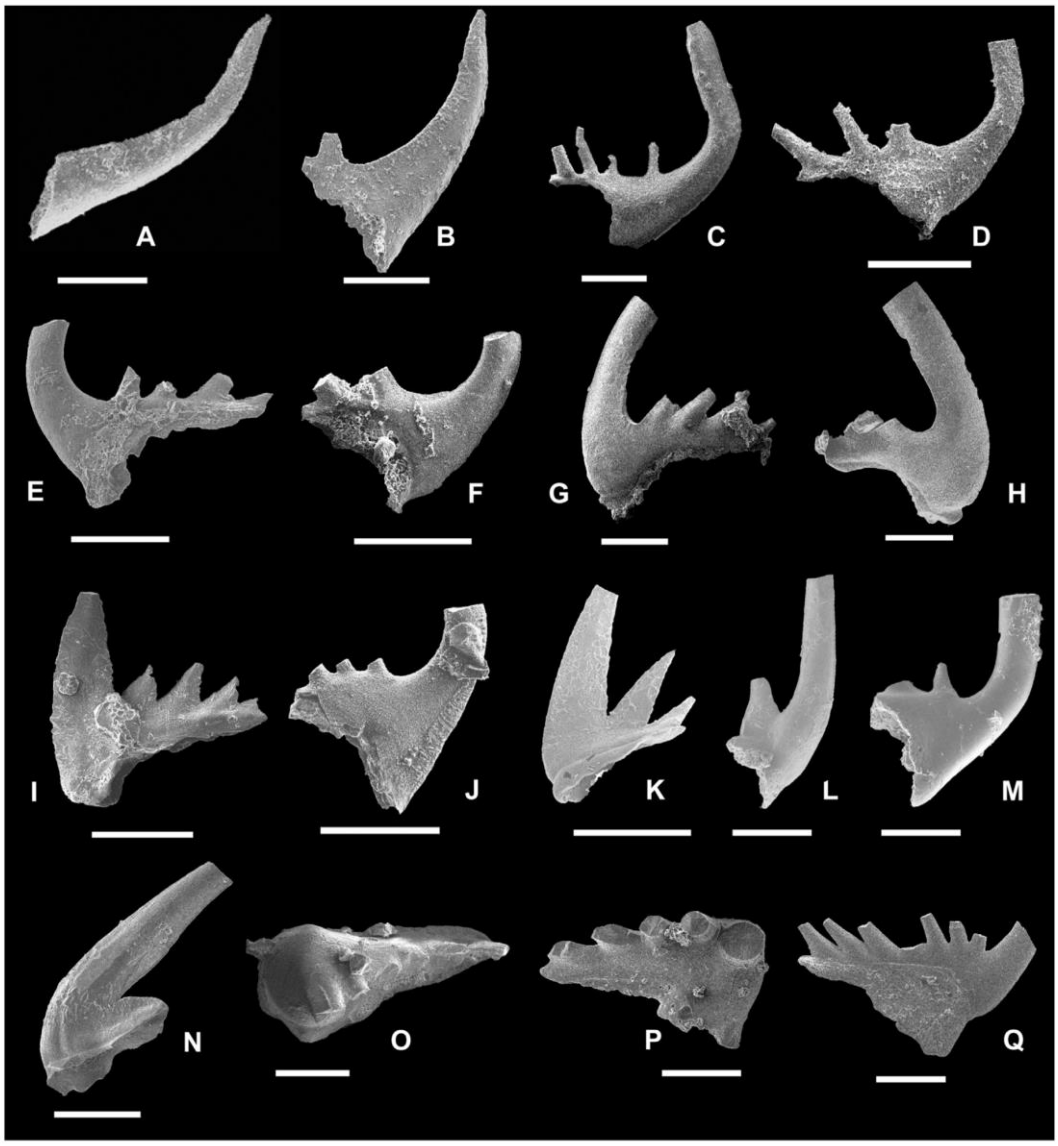

Fig. 4. Representative conodont species from the Xiaoyangqiao section. (A) *Eoconodontus notchpeakensis* (Miller, 1969), lateral view, BD 15, NIGP 174030. (B) *Cordylodus primitivus* Bagnoli, Barnes and Stevens, 1987, lateral view, BD 15, NIGP 174044. (C, D) *Cordylodus proavus* Müller, 1959, rounded elements, lateral view, BD 8B, NIGP 8B001 and, BD 15, NIGP 174034. (E, F) *Cordylodus caboti* Bagnoli, Barnes and Stevens, 1987, rounded elements, lateral view; (E) BD 23A, NIGP 23A001; (F) BD 22, NIGP 174017. (G, H) *Cordylodus drucei* Miller, 1980, outer lateral view, BD 22; (G) NIGP 174015; (H) NIGP 174016. (I, J) *Cordylodus intermedius* Furnish, 1938, lateral view; (I) compressed element, BD 23A, NIGP 23A002; (J) rounded element, BD 24, NIGP 174011. (K–M) *Cordylodus lindstromi* Druce and Jones, 1971, lateral view; (K) compressed element, BD 30, NIGP 182033; (L) rounded element, BD 30, NIGP 182032; (M) rounded element, BD 28B, NIGP 182030. (N) *Utahconus beimadaoensis* Chui and Zhang in An et al., 1983, lateral view, BD 30A, NIGP 30A002. (O, P) *Iapetognathus jilinensis* Nicoll, Miller, Nowlan, Repetski and Ethington, 1999, left and right elements, upper view, BD 29, NIGP 173046 and NIGP 29002. (Q) *Cordylodus prion* Lindström, 1955, *sensu* Nicoll (1991), rounded element, outer lateral view, BD 19, NGIP 19001. Scale bars represent 200 μm. All figured specimens are housed in Nanjing Institute of Geology and Palaeontology, Chinese Academy of Sciences, Nanjing, China (acronym: NIGP).

fully documented. It represents a derived taxon from its possible ancestor *Iapetognathus preaengensis* Landing in Fortey et al., 1982, which is the oldest known representative of the genus. Nowlan and Nicoll (1995) recorded 'an advanced species of *Iapetognathus*', from limestone beds in the upper Unit IV and exposed at top of the Xiaoyangqiao section, but these authors did not elaborate further on this occurrence. Here specimens of *Iapetognathus* have not been recorded from above the horizon with *Iapetognathus jilinensis*.

Please cite this article in press as: Wang, X.F., et al., Correlating the global Cambrian–Ordovician boundary: Precise comparison of the Xiaoyangqiao section, Dayangcha, North China with the Green Point GSSP section, Newfoundland, Canada. Palaeoworld (2019), https://doi.org/10.1016/j.palwor.2019.01.003

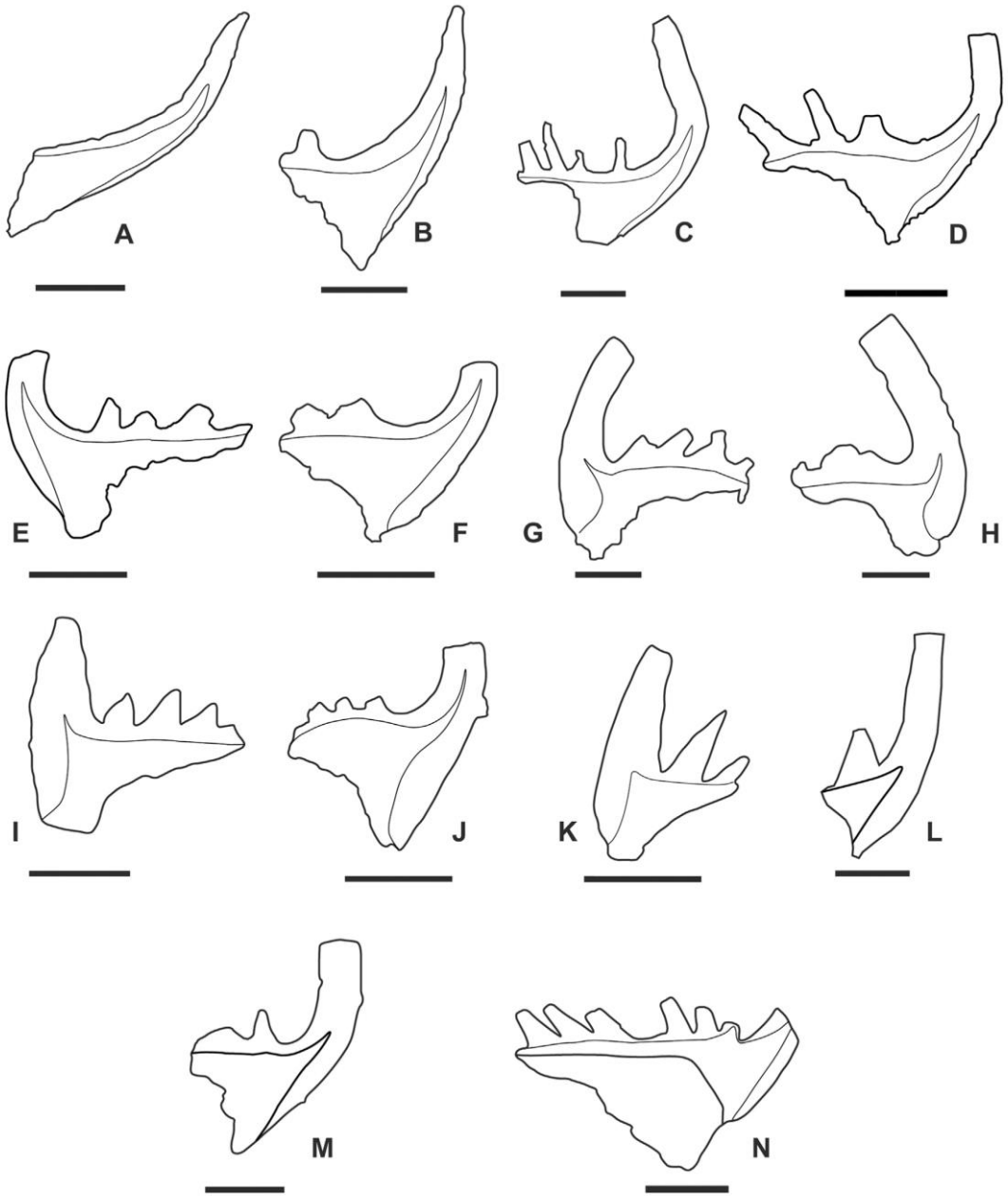

Fig. 5. Linedrawings of selected conodont species from Fig. 4 showing the outline of the basal cavity. (A) *Eoconodontus notchpeakensis* (Miller, 1969), lateral view, BD 15, NIGP 174030 (same specimen as Fig. 4A). (B) *Cordylodus primitivus* Bagnoli, Barnes and Stevens, 1987, lateral view, BD 15, NIGP 174044 (same specimen as Fig. 4B). (C, D) *Cordylodus proavus* Müller, 1959, rounded elements, lateral view, BD 8B, NIGP 8B001 and, BD 15, NIGP 174034 (same specimens as Fig. 4C, D). (E, F) *Cordylodus caboti* Bagnoli, Barnes and Stevens, 1987, rounded elements, lateral view; (E) BD 23A, NIGP 23A001; (F) BD 22, NIGP 174017 (same specimens as Fig. 4E, F). (G, H) *Cordylodus drucei* Miller, 1980, outer lateral view, BD 22; (G) NIGP 174015, (H) NIGP 174016 (same specimens as Fig. 4G, H). (I, J) *Cordylodus intermedius* Furnish, 1938, lateral view; (I) compressed element, BD 23A, NIGP 23A002; (J) rounded element, BD 24, NIGP 174011 (same specimens as Fig. 4I, J). (K–M) *Cordylodus lindstromi* Druce and Jones, 1971, lateral view; (K) compressed element, BD 30, NIGP 182033; (L) rounded element, BD 30, NIGP 182032; (M) rounded element, BD 28B, NIGP 182030 (same specimens as Fig. 4K–M). (N) *Cordylodus prion* Lindström, 1955, *sensu* Nicoll (1991), rounded element, outer lateral view, BD 19, NGIP 19001 (same specimen as Fig. 4Q). Scale bars represent 200 μm.

Please cite this article in press as: Wang, X.F., et al., Correlating the global Cambrian–Ordovician boundary: Precise comparison of the Xiaoyangqiao section, Dayangcha, North China with the Green Point GSSP section, Newfoundland, Canada. Palaeoworld (2019), https://doi.org/10.1016/j.palwor.2019.01.003

3.2.3.2. Conodont zonation

The complete evolutionary succession of *Eoconodontus–Cordylodus* allows for a precise biozonation in ascending order: the *Eoconodontus notchpeakensis*, *Cordylodus proavus*, *Cordylodus caboti*, *Cordylodus intermedius*, and *Cordylodus lindstromi* bio (lineage) zones (Fig. 3). The overlying *Cordylodus angulatus* Zone has not been reached in the investigated section, but has been recorded from a closely located succession (Chen and Gong, 1986). The lineage zones used here are briefly outlined:

Eoconodontus notchpeakensis Zone is based on the FAD of the nominate species and ranges upward to the FAD of *Cordylodus proavus*. *Cambroistodus cambricus* (Miller, 1969) and *C. minutus* (Miller, 1969) are characteristic and common associated species. The long-ranging *Teridontus nakamurai* (Nogami, 1967) is present throughout the zone. *Proconodontus muelleri* Miller, 1969 and *P. serratus* Miller, 1969 from below extend high into the zone. *Cordylodus primitivus* and '*Cordylodus*' *andresi* both appear in the upper to uppermost part of the zone; both range into the next zone.

The *Eoconodontus notchpeakensis* Zone is not completely developed in the Xiaoyangqiao section as the nominate taxon is already present in the basal beds of the section (Chen and Gong, 1986; this study). Chen and Gong (1986) defined the *Cambrooistodus* Zone for the same interval. *Cordylodus primitivus* is a potential taxon for the establishment of an additional zone or subzone (cf. Barnes, 1988) but is not introduced here.

The FAD of *Cordylodus proavus* defines the base of the *Cordylodus proavus* Zone in the Xiaoyanqgiao section. *Cordylodus proavus* first appears in samples BD 8A/DC 32 at 0.6 m, i.e., a level, which is just below the prominent and characteristic stromatolite marker bed in the lower part of the Xiaoyangqiao section (Fig. 3). The upper boundary is at the FAD of *Cordylodus caboti*. Associated species include *Teridontus nakamurai* and *Fryxellodontus inornatus* Miller, 1969. The *C. proavus* Zone is 4.1 m thick in the Xiaoyangqiao section.

The *Cordylodus caboti* Zone is marked by the FAD of *Cordylodus caboti* and the top of the zone is at the FAD of *Cordylodus intermedius.* In the Xiaoyangqiao section *Cordylodus caboti* is first recorded in sample BD 11 at +4.6 m above the reference level. The associated fauna includes the species known from the *C. proavus* Zone and with the presence of *Cordylodus prion* Lindström, 1955 *sensu* Nicoll (1991) (Figs. 4Q, 5N). New taxa appearing in the very top of the zone include *Monocostodus sevierensis* (Miller, 1969), *Semiacontiodus lavadamensis* (Miller, 1969), *Hirsutodontus simplex* (Druce and Jones, 1971) and *Cordylodus drucei*, Miller, 1980 (Figs. 4G, H, 5G, H). The *C. caboti* Zone is 13.8 m thick in the Xiaoyangqiao section.

The *Cordylodus intermedius* Zone is defined by the FAD of the nominate species. The top is at the base of the overlying zone. The first record of *C. intermedius* in the Xiaoyangqiao section is in samples BH 23/DC 61; both samples were collected at +18.4 m. The top of the zone is represented by sample, BD 28 at +21.4 m above the reference level and the zone is 3.0 m thick in the Xiaoyangqiao section. The zone includes several of the taxa from below, i.e., *Cordylodus drucei*, *Monocostodus sevierensis*, *Semiacontiodus* spp. and *Utahconus utahensis* (Miller, 1969). *Cordylodus prolindstromi* Nicoll, 1991 appears at +20.6 m (sample BD 26A) and is present with a short range within the uppermost part of the *C. intermedius* Zone (Fig. 3).

The *Cordylodus lindstromi* Zone is marked by the FAD of the eponymous species in sample BH 28 at +21.4 m above the reference level, which is ca. 50 cm above the FAD of *Rhabdinopora proparabola* (at +20.9 m). The upper boundary of the zone is not defined in the section as the marker species for the next zone, i.e., *Cordylodus angulatus*, has not been recorded in the section. *Cordylodus proavus*, *Cordylodus caboti*, and *Cordylodus intermedius* from below range into the zone.

In addition to the *Cordylodus* zonal species mentioned above the long-ranging *Teridontus nakamurai* is present; the characteristic *Iapetognathus jilinensis* appears in the lower part of the zone (in sample BD 29 at +21.7 m) and is present with a short range. *Utahconus beimadaoensis* Chui and Zhang in An et al., 1983 *sensu* Chen and Gong (1986) is a newcomer and appears in the uppermost part of the zone (i.e., at +30.2 m and within the *Anisograptus matanensis* graptolite Zone). This relatively unknown taxon may be useful for long distance correlation, as it has also been recorded from Laurentia (Landing et al., 1996; Landing and Westrop, 2006).

3.2.4. Graptolites

3.2.4.1. Graptolite evolutionary lineages

Rhabdinopora proparabola (Lin, 1986) (Fig. 6A–C) is the first planktic graptolite appearing in the succession of the Xiaoyangqiao section. It is recorded at +20.9 m above the base level (Fig. 3). This first planktic graptolite of the *Rhabdinopora* graptolite lineage appeared in the earliest Ordovician. Lin (1986) for the first time described the fauna of this level and differentiated nine species included in the three genera *Dictyonema*, *Heterograptus* and *Staurograptus*. All taxa are now interpreted to represent different growth stages and preservational aspects of a single species, *Rhabdinopora proparabola*. The species can be recognized by its three-vaned structure with an angle about 120° between them at the proximal end (Lin, 1986; Fig. 6A–C). None of the specimens can be shown to possess a nema and the three-vaned construction is directly attached to the tip of the sicula. The origin of this feature is unclear, but *R. proparabola* might not be termed a nematophorous graptolite (cf. Kozłowski, 1971; Erdtmann, 1982), but it was likely a planktic taxon. There is no indication of an attachment disc and the peculiar three-vaned feature cannot have served as one, as it is too regularly developed. These vanes show a fusellar construction that starts at the tip of the sicula and later encroaches onto the sides of the sicula, covering it in part (Fig. 6A–C).

The next representative of the graptolite lineage is the revised *Rhabdinopora parabola* (Bulman, 1954) (Fig. 6D–G). *Rhabdinopora praeparabola* Erdtmann, 1982 is interpreted to represent juveniles of *R. parabola* and thus regarded as a junior synonym. *R. parabola* has a well-developed nema starting from the tip of the sicula. All more complete specimens from the Xiaoyangqiao section show that this nema shows multiple branching divisions (Fig. 6E, F) and is not comparable in con-

Please cite this article in press as: Wang, X.F., et al., Correlating the global Cambrian–Ordovician boundary: Precise comparison of the Xiaoyangqiao section, Dayangcha, North China with the Green Point GSSP section, Newfoundland, Canada. Palaeoworld (2019), https://doi.org/10.1016/j.palwor.2019.01.003

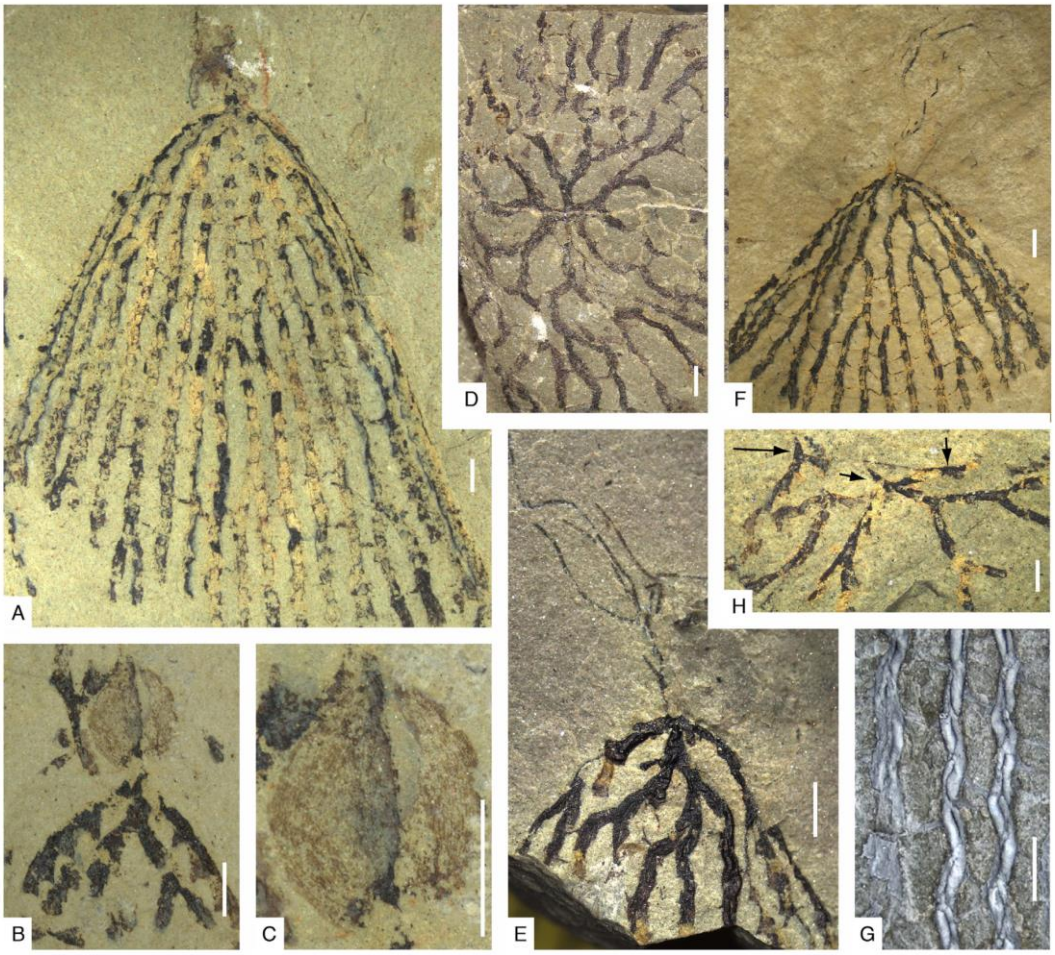

Fig. 6. (A–C) *Rhabdinopora proparabola* (Lin, 1986); (A) NIGP 98646, larger specimen with fragmented proximal structure showing colony shape; (B, C) NIGP 98605, small specimen showing three-vaned proximal structure, note fusellar construction in (C). (D–G) *Rhabdinopora parabola* (Bulman, 1954); (D) NIGP 168426, dorsal view showing quadriradiate development; (E, F) NIGP 168427 and NIGP 164496, laterally preserved specimens showing colony shape and branched nemata; (G) NIGP 168428, stipe fragment in relief, coated with ammonium chlorite. (H) *Anisograptus matanensis* Ruedemann, 1937, NIGP 168429, several small specimens showing sicula (arrows). Scale bars represent 1 mm. All figured specimens are housed in Nanjing Institute of Geology and Palaeontology, Chinese Academy of Sciences, Nanjing, China (acronym: NIGP).

struction to the vanes of *R. proparabola*. A number of taxa with branched nemata have been described from the Early Ordovician strata worldwide. As examples are here indicated *R. campanulatum* (Harris and Keble, 1928), *R. enigma* (Cooper and Stewart, 1979) and *R. scitulum* (Harris and Keble, 1928) from Australia and *R. flabelliformis belgica* (Bulman, 1970) from Belgium. It is currently unclear, whether these forms might be synonymous to *R. parabola* and a revision of these taxa is in progress. Previously, the density of stipes and dissepiments in the various species of the genus *Rhabdinopora* has been used to differentiate individual species statistically (Cooper et al., 1998), but this approach is problematic, because distortion and varying preservational aspects (Maletz et al., 2017). Thus, the identity of these, presumably earliest planktic graptoloids, has to be questioned in many cases.

3.2.4.2. Graptolite zonation

The *Rhabdinopora proparabola*, *R. parabola* and *Anisograptus matanensis* graptolite biozones are all well represented in the Xiaoyangqiao section.

The *R. proparabola* Zone is recorded at the appearance of *R. proparabola*, +20.9 m above the reference level. This is the only level at which the species has been recorded. All taxa described by Lin (1986) can be included in this single species as astogenetic variants or preservational aspects.

The *R. parabola* Zone is recorded 5.8 m above the appearance of *R. proparabola*. *R. parabola* is a common species in a short interval of about 10 cm in the Xiaoyangqiao section. All astogenetic stages from juveniles to mature and gerontic specimens have been described (Lin, 1986), but often specimens are fragmented. A number of specimens show enough relief to

Please cite this article in press as: Wang, X.F., et al., Correlating the global Cambrian–Ordovician boundary: Precise comparison of the Xiaoyangqiao section, Dayangcha, North China with the Green Point GSSP section, Newfoundland, Canada. Palaeoworld (2019), https://doi.org/10.1016/j.palwor.2019.01.003

investigate the thecal and proximal end construction of this taxon including the quadriradiate proximal development suggested by Cooper et al. (1998).

The *Anisograptus matanensis* Zone is marked by the appearance of the nominate species at +29.8 m (Figs. 3, 6H). A number of closely spaced horizons occur in which largely fragments of *Anisograptus matanensis* can be found. Specimens of *Rhabdinopora* have not been discovered in this interval. The top of the zone has not been recorded in the section.

3.2.5. Acritarchs

Early studies of acritarchs from the Xiaoyangqiao section demonstrated the occurrence of remarkably diverse and well-preserved palynomorphs of varying abundance throughout the sampled sedimentary succession (Yin, 1986). The palynological material was well described and illustrated and five acritarch assemblages were proposed from the latest Cambrian to earliest Ordovician (Yin, 1985, 1986, 1995). However, since 1995 significant taxonomical revisions and/or reconsiderations in acritarch taxonomy — especially of the Cambrian acritarch taxa — have been made. Therefore, comparison and correlation of the palynofloras described from the Xiaoyangqiao section with coeval assemblages from outside North China remained difficult.

This review revises some of taxonomical problems of the acritarch assemblages and also improves their distribution in the Cambrian–Ordovician interval recorded at the Xiaoyangqiao section (Fig. 7). The new study confirms that the distribution of acritarchs through the section is not homogeneous. Highly fossiliferous levels are followed by intervals with a gradual decrease in abundance and taxonomical diversity of the acritarchs. At some levels the acritarch assemblages are almost monospecific and represented predominantly by simple sphaeromorphs (*Leiosphaeridia*, *Granomarginata* (=*Annulum*), etc.). Probably the cyclic pattern, from favorable to poor, is one response to the repetitive changes of the depositional environment.

Three acritarch assemblages are distinguished in the upper Cambrian–Lower Ordovician succession of the Dayangcha beds (Fig. 7). Their correlation with the microflora described by Yin (1986) is shown in Fig. 9. Some of the suggested taxonomical changes concerning acanthomorph and diacrodian acritarchs (i.e., Dean and Martin, 1982; Moczydłowska, 1991; Raevskaya and Servais, 2009, with references) are adopted here.

3.2.5.1. Assemblage 1 (Timofeevia phosphoritica–Polygonium–Solisphaeridium)

Assemblage 1 is recorded in the lower part of the studied section, i.e., from −10.7 m to ca. −5.8 m (samples DA 1–DA 8) (Fig. 7). It is characterized by the association of simple acanthomorph acritarchs belonging to the *Polygonium–Solisphaeridium* (Fig. 8O) plexus together with *Timofeevia phosphoritica* Vanguestaine, 1978 (Fig. 8N) and less numerous representatives of the galeate taxa *Cymatiogalea* sp. and *Stelliferidium* sp. Some specimens of *Cristallinium*, *Multiplicisphaeridium* sp., ?*Comasphaeridium* sp., and *Granomarginata squamacea* Volkova, 1968 (=*Annulum squamaceum* (Volkova) Martin and Dean, 1983) are present in subordinate amount. Single fragments of ?*Retisphaeridium* sp., and possible *Eliasum* sp. are found in the sample DA 2, whereas representatives of?*Tectitheca* are present in samples DA 3 and DA 4. The latter sample is characterized by a sharp increase in number of acritarchs, especially of the two genera *Timofeevia* and *Polygonium*. The occurrence here of some rare diacrodians, such as *Actinotodissus*, is considered to be stratigraphically important, confirming a late Furongian age (Volkova, 1990; Volkova and Kir'janov, 1995; Raevskaya and Servais, 2009). Similarly, the appearance of *Cymatiogalea* and *Stelliferidium* is confined to the Furongian Series (Volkova, 1990; Volkova and Kir'janov, 1995), whereas *Retisphaeridium*, *Eliasum*, *Comasphaeridium*, *Cristallinium*, *Timofeevia* and *Granomarginata* range from strata below. The gradual decrease in the acritarch abundance, in the samples DA 5–DA 8, is replaced by a new peak in sample DA 9 at −5.6 m, in which the next assemblages can be distinguished.

3.2.5.2. Assemblage 2 (Vulcanisphaera africana–Ninadiacrodium)

Assemblage 2 comprises almost all of the previous listed taxa but in varying quantities at different levels (i.e., samples DA 9–DA 24), however diacrodian acritarchs become remarkably more diverse and numerous. Apart from *Actinotodissus*, other genera occur, including *Acanthodiacrodium*, *Dasydiacrodium*, *Ninadiacrodium*, and *Trunculumarium*. The most important late Furongian index species are *Ninadiacrodium caudatum* (Vanguestaine, 1973) Raevskaya and Servais, 2009 (Fig. 8I), *Dasydiacrodium obsonum* Martin in Martin and Dean, 1988 (in samples DA 11, DA 15, DA 15-1; Fig. 8L, M), *Ninadiacrodium dumontii* (Vanguestaine, 1973) Raevskaya and Servais, 2009 (samples DA 12 and DA 15; Fig. 8K), and *Trunculumarium* sp. (sample DA 14).

Acritarch diversity of the assemblage 2 is complemented by occurrence in the sample DA15 of some rare *Vulcanisphaera africana* (Deunff, 1961) Rasul, 1976 (Fig. 8H) and various galeates such as *Cymatiogalea* aff. *C. bouvardii* Martin, 1973 (Fig. 8E), *C. columellifera* (Deunff, 1961) Deunff et al., 1974, *C. cylindrata* Rasul, 1974, *Priscogalea* sp., *Stelliferidium stelligerum* (Gorka, 1967) Deunff et al., 1974 (Fig. 8D), and *Stelliferidium* sp. In addition, *Globosphaeridium*, *Micrhystridium*, ?*Priscoteca* sp., and *Tasmanites* sp. are also present. The very rich interval, from −1.3 to −0.5 m (samples DA 15 and DA 16), is followed by almost barren strata. This change is associated with the transition from lithological unit I (mainly shale) to unit II (mainly carbonates) and evidently, environmental and/or preservational conditions favourable for acritarchs changed. Only rare small acanthomorphs and simple sphaeromorphs are still present. *Timofeevia* has its upper range within this assemblage.

3.2.5.3. Assemblage 3 (Corollasphaeridium wilcoxianum)

Assemblage 3 is recognized from the sample DA 25 by the appearance of the very distinctive palynomorph *Corollasphaeridium wilcoxianum* Martin in Dean and Martin, 1982 (Fig. 8A–C). This taxon is accompanied by *Acanthodiacrodium*, *Actinotodissus*, *Cymatiogalea*, *Globosphaeridium*, *Polygonium* and *Solisphaeridium*. The change in composition is

Please cite this article in press as: Wang, X.F., et al., Correlating the global Cambrian–Ordovician boundary: Precise comparison of the Xiaoyangqiao section, Dayangcha, North China with the Green Point GSSP section, Newfoundland, Canada. Palaeoworld (2019), https://doi.org/10.1016/j.palwor.2019.01.003

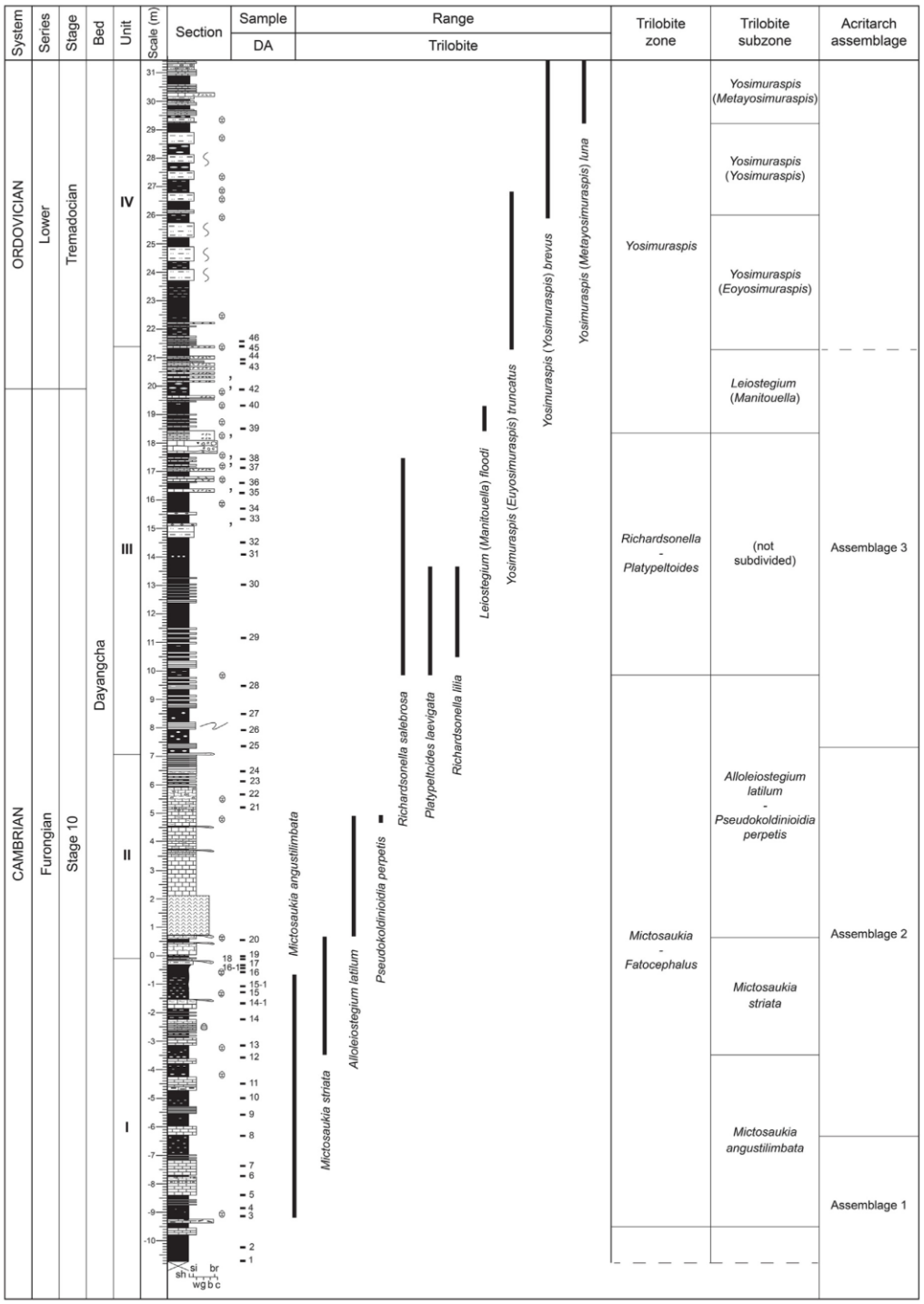

Fig. 7. Upper Cambrian to Lower Ordovician (Tremadocian) acritarch and trilobite biostratigraphy of the Xiaoyangqiao section. For legend, see Fig. 10. Abbreviations used for grainsize: sh = shale; si = siltstone; br = breccia; w = wackestone; g = grainstone; b = boundstone; c = conglomerate.

Please cite this article in press as: Wang, X.F., et al., Correlating the global Cambrian–Ordovician boundary: Precise comparison of the Xiaoyangqiao section, Dayangcha, North China with the Green Point GSSP section, Newfoundland, Canada. Palaeoworld (2019), https://doi.org/10.1016/j.palwor.2019.01.003

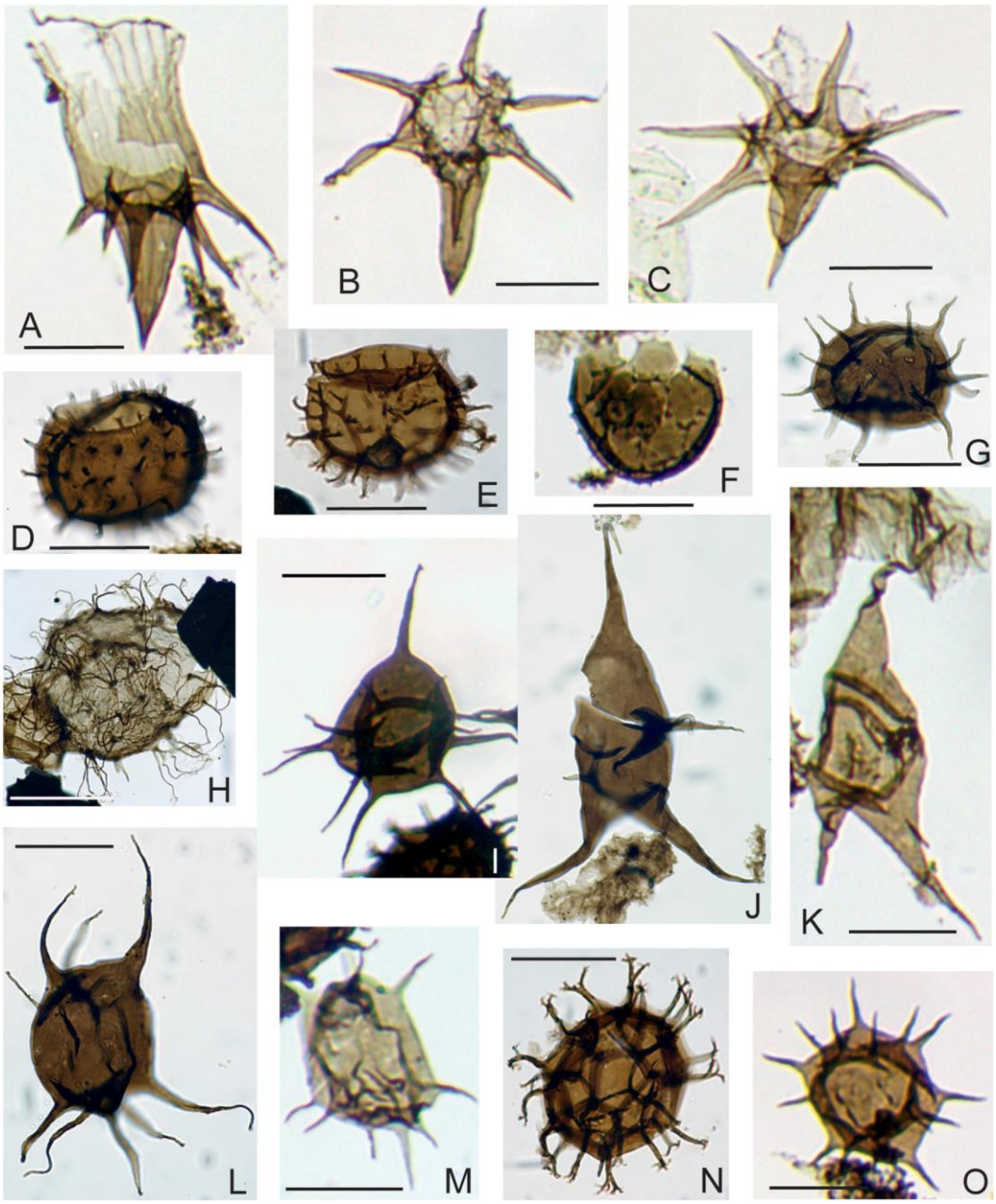

Fig. 8. Representative late Cambrian (Furongian) to Lower Ordovician acritarchs species from the Xiaoyangqiao section. The sample/slide number and England Finder coordinates are indicated for all specimens. (A–C) *Corollasphaeridium wilcoxianum* Martin in Martin and Dean, 1982; (A) specimen in lateral view, sample DA 36, E31/3; (B, C) specimens in compressed transverse view, sample DA 36, B51/1 (B), P55/1 (C). (D) *Stelliferidium stelligerum* (Gorka, 1967) Deunff et al., 1974, sample DA 15, T42/2. (E) *Cymatiogalea* aff. *C. bouvardii* Martin, 1973, sample DA 15, H27/1. (F) *Cymatiogalea cuvillieri* (Deunff, 1961) Deunff, 1964, sample DA 37, V39/2. (G) *Actinotodissus achrasi* (Martin, 1983) Martin and Dean, 1988, sample DA 15, F31/1,3. (H) *Vulcanisphaera africana* (Deunff, 1961) Rasul, 1976, sample DA 15, L23/3,4. (I) *Ninadiacrodium caudatum* (Vanguestaine, 1973) Raevskaya and Servais, 2009, sample DA 15, C42. (J) *Ninadiacrodium* sp. A, sample DA 15, F29/2,4. (K) *Ninadiacrodium dumontii* (Vanguestaine, 1973) Raevskaya and Servais, 2009, sample DA 15, S51/3. (L, M) *Dasydiacrodium obsonum* Martin in Martin and Dean, 1988; (L) sample DA 15, L47/3; (M) sample DA 15-1, L46/2. (N) *Timofeevia phosphoritica* Vanguestaine, 1978, sample DA 4, H34/2. (O) Acritarch ex. gr. *Polygonium–Solisphaeridium*, sample DA 4, K48. Scale bars represent 20 μm.

Please cite this article in press as: Wang, X.F., et al., Correlating the global Cambrian–Ordovician boundary: Precise comparison of the Xiaoyangqiao section, Dayangcha, North China with the Green Point GSSP section, Newfoundland, Canada. Palaeoworld (2019), https://doi.org/10.1016/j.palwor.2019.01.003

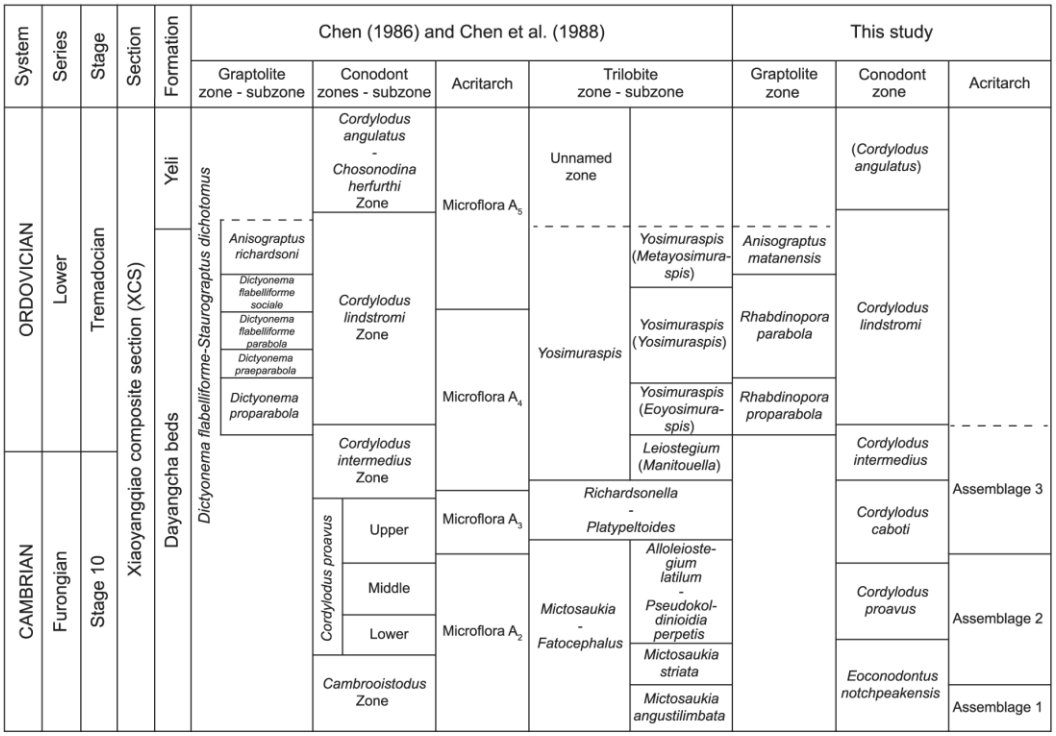

Fig. 9. Comparison between the integrated zonation systems of Chen (1986) and Chen et al. (1988) and this study. The trilobite zonation is the same for both studies.

clearly associated with the lithological change from unit II to unit III.

Several horizons within assemblage 3 are dominated by mainly one acritarch genus. *Granomarginata* is present in high numbers in samples DA 27, DA 30, DA 34, and DA 36; *Cymatiosphaera* in sample DA 28 and *Leiosphaeridia* is the predominant taxon in sample DA 39. The occurrence of *Cymatiogalea cuvillieri* (Deunff, 1961) Deunff, 1964 (Fig. 8F) in sample DA 37 confirms a proximity to the base of the Tremadocian (Raevskaya, 2000).

From sample DA 39 and to the top of the studied interval palynomorphs become very rare. Different morphotypes of *Corollasphaeridium* and related unidentified fragments occur together with few long-ranging taxa mentioned above (Section 3.2.5).

3.2.6. Trilobites

Trilobites in the Xiaoyangqiao section are present throughout the succession and found commonly in the shales (Fig. 7). Trilobites of the Dayangcha beds are of Asian–Australian affinity, but the fauna does share taxa with Laurentia. Among the taxa in the trilobite assemblage is the genus *Mictosaukia*, which is applied as zonal taxon in North, Northeast, and South China, and Western Australia for the uppermost Cambrian. *Leiostegium* is another widely distributed trilobite genus, which is known from Australia and North America and also useful for intercontinental correlation.

The biostratigraphic subdivision of the Dayangcha succession using trilobites is based on the zonation of Qian (1986) and summarized by Chen et al. (1988). Most of the zones were termed assemblage zones, but they are based on the first appearance and co-occurrences of several taxa (Fig. 7). Qian (1986) introduced three zones and seven subzones. According to this, the association of trilobites is referred to the Furongian *Mictosaukia–Fatocephalus* and *Richardsonella–Platypeltoides* zones and the *Yosimuraspis* Zone spanning the uppermost Furongian and lowermost Tremadocian (Fig. 7).

4. Integration of biozones and acritarch assemblages

In the Xiaoyangqiao succession the *Cordylodus* lineage is recorded mostly from units I, II and III, and the graptolite fauna mostly from unit IV. However, representatives of the two fossil groups overlap in upper unit III and the zonal conodont index *Cordylodus lindstromi* almost coincides with *Rhabdinopora proparabola* in the top of unit III. The appearance of *Rhabdinopora proparabola* is recorded in a thin green shale horizon at +20.9 m and *Cordylodus lindstromi* first appears at +21.4 m, i.e., 0.5 m above the first graptolite horizon. The fact that the appearances of these two important species are very close provides a significant tie for zonal integration of these two important fossil groups and for intercontinental correlation. The *R. parabola* Zone is constrained to the *Cordylodus lindstromi*

Please cite this article in press as: Wang, X.F., et al., Correlating the global Cambrian–Ordovician boundary: Precise comparison of the Xiaoyangqiao section, Dayangcha, North China with the Green Point GSSP section, Newfoundland, Canada. Palaeoworld (2019), https://doi.org/10.1016/j.palwor.2019.01.003

Zone, and the *Anisograptus matanensis* Zone begins within the *Cordylodus lindstromi* Zone.

Acritarch assemblage 1 is constrained to the *Eoconodontus notchpeakensis* Zone. Acritarch assemblage 2 initiates in the *E. notchpeakensis* Zone and extends upwards into the *Cordylodus caboti* Zone. Assemblage 3 from unit III coincides largely with the upper *Cordylodus caboti* Zone and all of the *C. intermedius* Zone.

The *Mictosaukia angustilimbata* and *Mictosaukia striata* trilobite subzones of the *Mictosaukia–Fatocephalus* Zone are recorded from the *Eoconodontus notchpeakensis* Zone. The *Alloleiostegium latilum–Pseudokoldiniodia perpetis* Subzone of the *Mictosaukia–Fatocephalus* Zone comprises all of the *Cordylodus proavus* Zone and extends into the lower *C. caboti* Zone. The *Richardsonella–Platypeltoides* Assemblage Zone is constrained to the upper *Cordylodus caboti* Zone. The following *Leiostegium* (*Manitouella*) Subzone of the *Yosimuraspis* Zone correlates clearly to the *Cordylodus intermedius* Zone and thus represents the top Cambrian. The *Yosimuraspis* (*Eoyosimuraspis*) and *Y.* (*Yosimuraspis*) subzones of the *Yosimuraspis* Zone are coeval to the *Cordylodus lindstromi* Zone, where the former is contained in the *R. proparabola* Zone and the latter is coeval to the *R. parabola* Zone. The base of the top *Yosimuraspis* (*Metayosimuraspis*) Subzone coincides closely with the appearance of *Utahconus beimadaoensis*, which is from the basal part of the *A. matanensis* graptolite Zone.

The integration of the biozones and acritarch assemblages is summarized in Fig. 9.

5. Sequence stratigraphy

The succession exposed at the Xiaoyangqiao section was deposited on a calm terrigenous-dominated mid to outer shelf of the ramp. The shallow to deep water marine sediments accumulated on the mid shelf to the margin and edge of the shelf, which is indicated by the sedimentary rocks and the diverse macroinvertebrate and conodont faunas, and acritarch microfloras. The mid shelf facies association includes wackestone and locally authochthonous buildups. With increasing water depth the trilobite constituents gradually increase in abundance and siliceous sponge spicules become more numerous. The carbonate content decreases upward and fine-grained siliciclastic sedimentary rocks dominate the upper part of the succession, suggesting a progressive uplift of the source area and decrease of the carbonate factory activity.

Occasionally intercalated, thin- to medium-bedded limestones (wackestones to grainstones, limebreccias) marked by coarse-grained debris from the middle and inner shelf zones are interpreted as debris flows (tempestites), reflecting the storm-related export of shallow-marine material into the most distal and deepest shelf zones.

5.1. Sequence analysis

The succession exposed at the Xiaoyangqiao section is composed of meter-scale 'parasequences' deposited in marine subtidal to deeper water marine settings. The Xiaoyangqiao sequence is here arranged into five low frequency (3rd or higher order) cycles expressed by an alternation of (1) shale-limestone, (2) limestone, (3) shale, limestone and lime breccias and (4) siltstone-shale. Each of the five depositional sequences recognized in the whole exposed succession is bounded by the MRS that caps a succession of regressive sediments that coarsen upward as a result of decreasing accommodation space. The lower and upper sequences are not fully developed in the section whereas the middle sequences are fully preserved.

The biostratigraphic zonal boundaries usually are recorded within the lower transgressive parts of the sequences, close to but clearly above the MRS surfaces. Some biozones (i.e., graptolite biozones) are established immediately above the maximum flooding surface in the sequence.

5.1.1. Sequence A

Sequence A comprises lithological unit I. This lower depositional sequence is represented by the cyclically developed beds from the base of the section and up to the first limestone bed just above the siltstone bed at the top of unit I. Sequence A includes all the lower parasequences (Fig. 10). It consists of cyclic deposition composed of grey to dark grey shale and limestone. Basal portions of the parasequences are typically shale although some sequence bases are nodular to lenticular shale in outcrop. Middle portion of the parasequences is typically shale with nodular to lenticular limestone and shale grading upwards into fine-bedded shale. The upper portion of the parasequences is composed of wavy bedded argillaceous wackestone. The upper surface of the limestone is sometimes developed as a discontinuity surface with burrows.

Unit I represents a deepening-upward succession and is part of the transgressive system tract of sequence A. The MFS is displayed in the thickest shale layer with minor intervals of thin elongated limestone and shale (Fig. 10), which represents the regressive system tract of sequence A. The maximum regressive surface is just above the top siltstone bed (at −0.2 m).

Sequence A comprises the upper *Eoconodontus notchpeakensis* conodont Zone.

5.1.2. Sequence B

The second depositional sequence is represented by all the carbonate beds of unit II and includes the lower grey to dark grey shales of unit III. It is composed mainly of increasing deepening carbonate deposits in the lower half with an upward increase of the siliciclastic component. The prominent stromatolite marker horizon near the base is contained in the sequence. The transgressive system tract of sequence B is composed of carbonates with the maximum flooding surface within the upper shale unit (Fig. 10). The regressive system tract is composed of stacks of upwards coarsening shale to silt deposits. The maximum regressive surface is placed at the top of the cyclic siliciclastic facies and above the siltstone horizon at +15.1 m.

Sequence B comprises the *Cordylodus proavus* Zone and the lower to middle part of the *Cordylodus caboti* Zone.

Please cite this article in press as: Wang, X.F., et al., Correlating the global Cambrian–Ordovician boundary: Precise comparison of the Xiaoyangqiao section, Dayangcha, North China with the Green Point GSSP section, Newfoundland, Canada. Palaeoworld (2019), https://doi.org/10.1016/j.palwor.2019.01.003

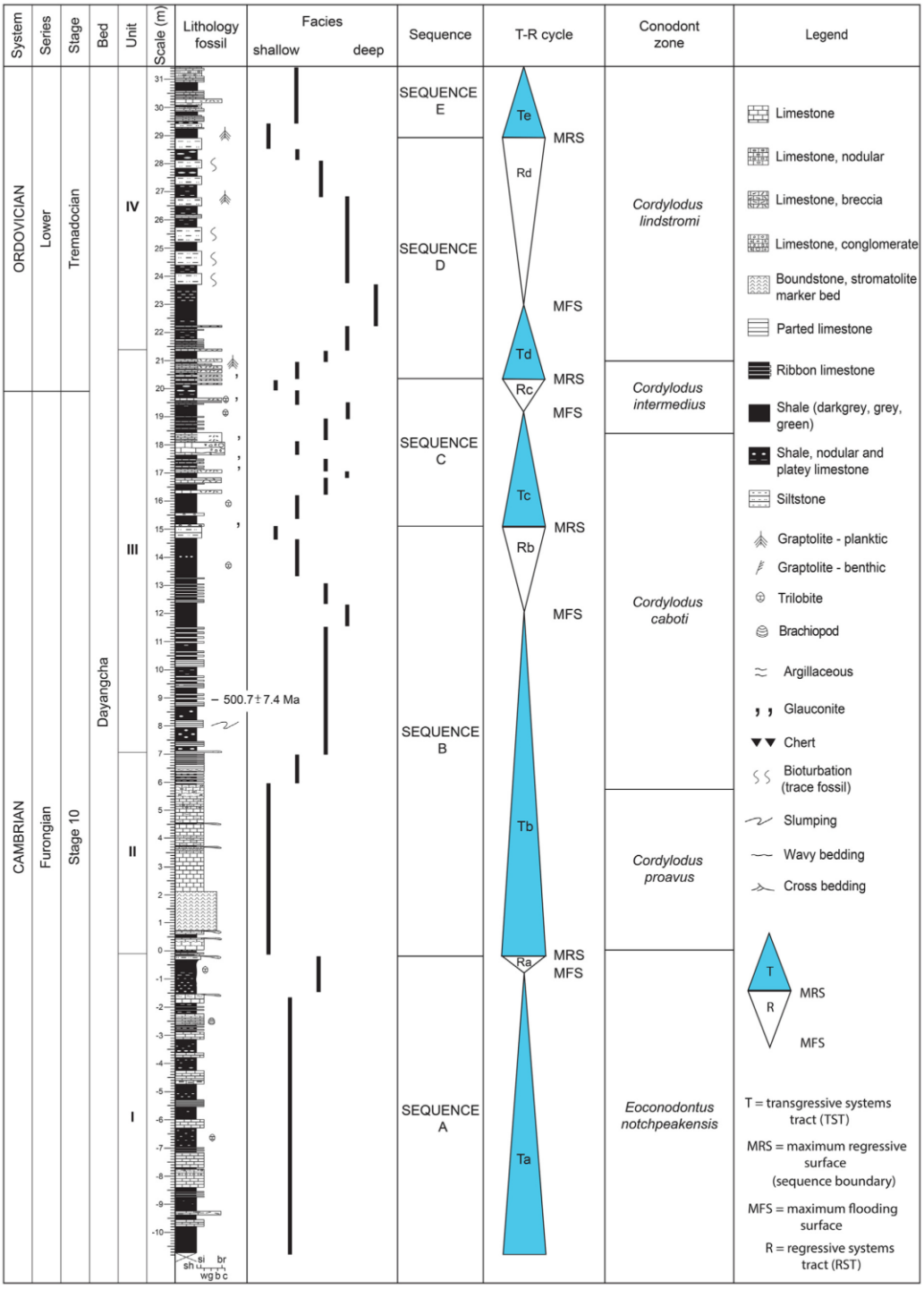

Fig. 10. T-R sequence stratigraphy of the Xiaoyangqiao section. The sequences are based on the T-R procedure promoted by Embry and Johannessen (1992). The sequences are of 3rd and higher order. Abbreviations used for grainsize: sh = shale; si = siltstone; br = breccia; w = wackestone; g = grainstone; b = boundstone; c = conglomerate.

Please cite this article in press as: Wang, X.F., et al., Correlating the global Cambrian–Ordovician boundary: Precise comparison of the Xiaoyangqiao section, Dayangcha, North China with the Green Point GSSP section, Newfoundland, Canada. Palaeoworld (2019), https://doi.org/10.1016/j.palwor.2019.01.003

5.1.3. Sequence C

Sequence C comprises the upper part of unit III. The basal part, composed of glauconite limemudstone and shale followed by increasing deepening deposits of shale-limestone, represents the trangressive system tract. The position of the MFS is here placed within the shale (ca. at +19.3 m) (Fig. 10). The following series of limebreccias (tempestites) in the shale dominated facies (i.e., the background deposition) marks the RST. The MRS is placed at ca. +20.4 m, which is near the top of the brecciated beds. Internally, sequence C is composed of two parasequences: the lower parasequence comprises the strata from +15.1 m to +18.1 m and is capped by a debris flow, and the second parasequence comprises the strata from +18.1 m to +20.4 m.

Sequence C comprises the top of the *Cordylodus caboti* Zone and most of the *Cordylodus intermedius* Zone.

5.1.4. Sequence D

Sequence D consists of cycles composed of dark grey shale, black shale with thin flat lenses of limestone and dull grey, light grey to green siltstone.

The transgressive system tract is characterized by cycles of black shale and black shale with one cm or less thin lenses of limestone. The maximum flooding surface is recorded ca. at +23.0 m within an interval of black shale. The following regressive system tract is composed of cyclic wavy bedded siltstone to fine-grained sandstone interbedded with grey, green shale and minor black shale and shale with thin and flat limestone lenses.

In the Xiaoyangqiao section, the first planktic graptolite horizon and the appearance of *Cordylodus lindstromi* are recorded near the base of the transgressive system tract. Sequence D comprises the *Cordylodus lindstromi* conodont Zone (*pars*), *Rhabdinopora proparabola* and *R. parabola* graptolite zones.

5.1.5. Sequence E

This sequence is composed of limestone beds, some with ripple marks, interbedded with light grey shale/siltstone. Sequence E is not completely preserved in the Xiaoyangqiao section and only the TST is exposed in the top of the section. The base is placed on the top of the uppermost siltstone of sequence D, i.e., at +28.9 m.

Sequence E is contained within the uppermost part of the *Cordylodus lindstromi* conodont Zone and closely associated with the base of the *Anisograptus matanensis* Zone. *Utahconus beimadaoensis* is also a good marker for the beginning of sequence E.

6. Sea-level changes

The deposits of the Xiaoyangqiao section display a series of sea-level changes, which are reflected in significant regressive events of global significance (cf. Haq and Schutter, 2008). Palaeoclimate played a significant role for the sea-level changes in the late Cambrian to Early Ordovician and a cooling stage interrupted the warm water carbonate deposition in the latest Cambrian (Stage 10, Furongian) (Frakes et al., 2005; Trotter et al., 2008; Runkel et al., 2010; Hearing et al., 2018). This caused a drop in the sea level, promoting a predominance of siliciclastic deposition in the latest Cambrian and earliest Ordovician.

The first significant sea-level lowstand or regressive event is recognized at the top of lithological unit I and just beneath the base of lithological unit II in the Xiaoyangqiao section. The top of unit I is upward coarsening from shale to siltstone and then changing into the overlying unit II composed of carbonate sedimentary rocks. Faunally, this regressive event corresponds to the end of the *Eoconodontus notchpeakensis* Zone and acritarch assemblage 3 followed by the *Cordylodus proavus* Zone.

The second regressive-transgressive transition is recognized within the lithological unit III. It is marked by the transition from the upward coarsening shale to siltstone regressive succession into the transgressive shale-limestone-conglomerate succession. This second regressive event occurs in the uppermost part of the *C. caboti* Zone preceeding the beginning of the *Cordylodus intermedius* conodont Zone.

The third regressive event in the section is seen in the upper unit III. It is marked by the upwards shallowing succession and characterized by condensed deposition. The regression event is displayed by a series of intraformational breccia beds, interpreted as tempestites, in the section. The regression event corresponds to the top of the *Cordylodus intermedius* (conodont) Zone.

The fourth regressive event is less prominent. It is seen in the higher part of unit IV. It is marked by the change from the upwards coarsening succession composed of the interbedded shale, shale with platey limestone and siltstone of the T-R sequence D and into the transgressive interbedded silt/shale and limestone beds of T-R sequence E. It is recorded within the upper *Cordylodus lindstromi* Zone, and contained within the lower *Anisograptus matanensis* Zone.

Internationally, the prominent regressive-transgressive sea-level change recorded at the top of unit I is coeval to the Lange Ranch lowstand or the global Lange Ranch Eustatic Event (LREE) of Miller (1992). The following regressive-transgressive event recognized in the section and found within unit III, correlates with the Basal House Lowstand of Miller (1984). The third regressive-transgressive event in the Xiaoyangqiao section corresponds to the 'Acerocare Regressive Event' of Erdtmann (1982, 1986) that is abbreviated ARE (cf. Cooper et al., 2001; Nicoll et al., 1992). The fourth regressive event recorded in the top of the Xiaoyangqiao section probably represents the Black Mountain Eustatic Event (BMEE) of Miller (1984) followed by the Stonehenge Transgression of Taylor et al. (1992); i.e., the T-R sequence E; but today most of these transgressive strata are covered at the Xiaoyangqiao section.

7. Chemostratigraphy

Three δ^{13}C-isotope curves have been prepared from the Xiaoyangqiao section (Ripperdan et al., 1993; Chen et al., 1995; this study, Fig. 11). Largely, the C-isotope curves resemble each other, although they diverge in detail (Fig. 11). Here the newly prepared C-isotope curve is used as reference.

Please cite this article in press as: Wang, X.F., et al., Correlating the global Cambrian–Ordovician boundary: Precise comparison of the Xiaoyangqiao section, Dayangcha, North China with the Green Point GSSP section, Newfoundland, Canada. Palaeoworld (2019), https://doi.org/10.1016/j.palwor.2019.01.003

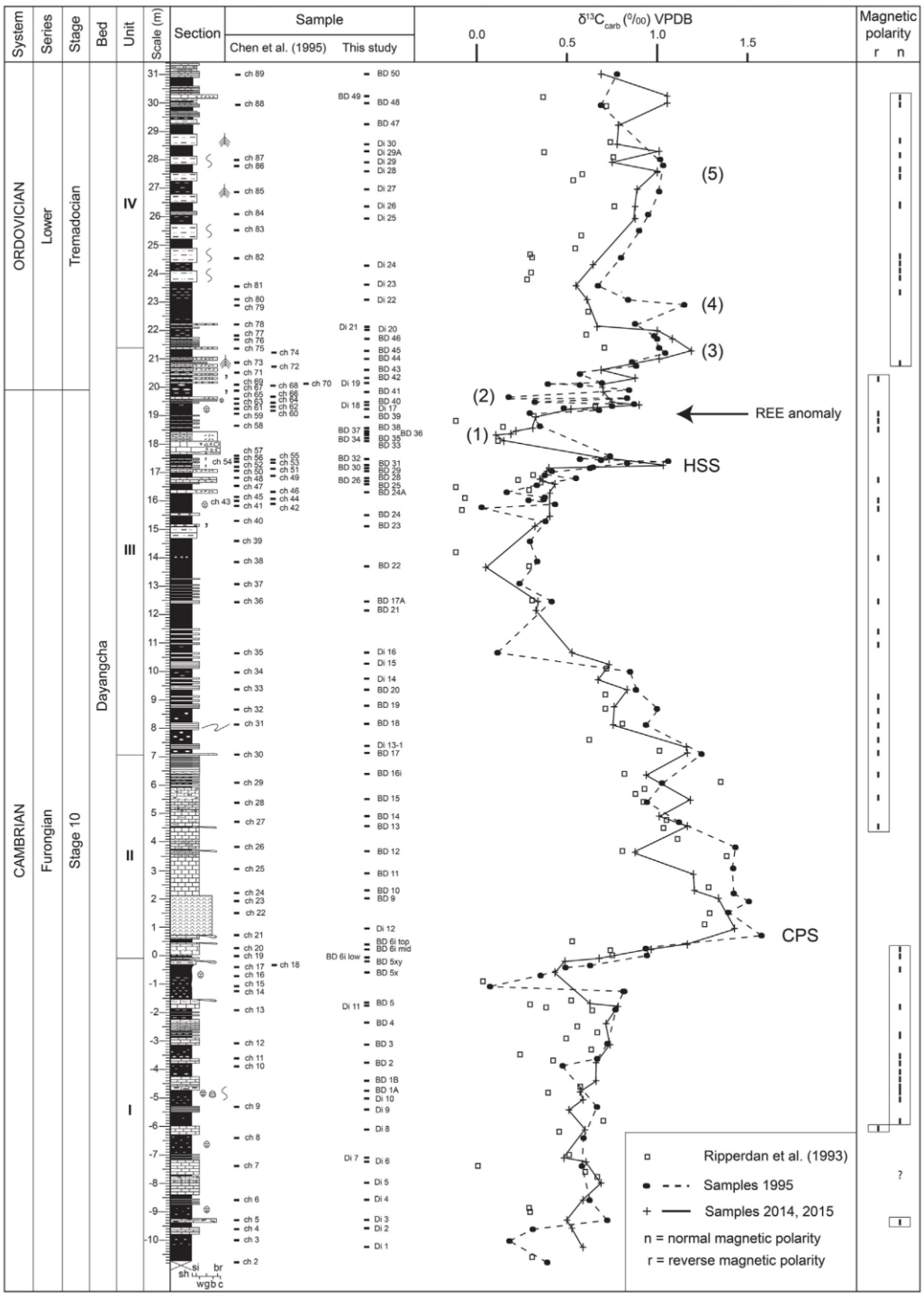

Fig. 11. C-isotope curves and magnetic polar reversals from the Xiaoyangqiao section. The C-isotope curves are respectively from Ripperdan et al. (1993), Chen et al. (1995), and this study (=+ and unbroken lines). The magnetic reversal data are from Ripperdan et al. (1993) and Chen et al. (1995, table 2). For details see text. For Legend, see Fig. 10. Abbreviations used for grainsize: sh = shale; si = siltstone; br = breccia; w = wackestone; g = grainstone; b = boundstone; c = conglomerate.

Please cite this article in press as: Wang, X.F., et al., Correlating the global Cambrian–Ordovician boundary: Precise comparison of the Xiaoyangqiao section, Dayangcha, North China with the Green Point GSSP section, Newfoundland, Canada. Palaeoworld (2019), https://doi.org/10.1016/j.palwor.2019.01.003

7.1. $\delta^{13}C_{carb}$-isotope curves

The C-isotope curve shows three prominent and two smaller positive peaks. The most prominent negative-positive shift is recorded at the base of lithological unit II, i.e., from −1.4 m to +0.5 m in the section, where the values from +0.60 abruptly drop to +0.01, and then shifts to above +1.50 (Fig. 11). Chen et al. (1995) named this prominent negative-positive excursion 'Pre-*Cambroistodus* minimum' (TCM), but this name is abandoned because the genus *Cambroistodus* ranges across the excursion. The prominent excursion is characterized by the FAD of *Cordylodus proavus*, and is here assigned to the '*Cordylodus proavus* spike' (CPS) (Figs. 3, 11).

The following upward trend from +0.6 m and up to +14.0 m is generally negative; this trend was named the '*Cordylodus proavus* decline' (CPD) by Chen et al. (1995). A negative-positive excursion from +4.9 m to +7.1 m coincides with the gradual facies change from limestone to shale within unit II.

The following long negative trend from above the '*Cordylodus proavus* spike' (CPS) positive spike extends up to ca. 14 m where a shift towards the positive at ca. +14.0 m coincides with the MRS surface of sequence B. The prominent positive rise from ca. +16.3 m to ca. +17.3 m is very characteristic as also observed by Ripperdan et al. (1993) and Chen et al. (1995); the latter authors named this positive peak 'the *Hirsutodontus simplex* spike' (HSS). This name is maintained and applied here, because the positive excursion is clearly associated with the presence of *Hirsutodontus simplex* in the section (Figs. 3, 11).

The $\delta^{13}C_{carb}$-isotope curve changes sharply towards the negative, forming a negative peak at ca. +18.4 m (= no. 1, Fig. 11) above which a series of closely spaced negative-positive C-isotope excursions is recorded (Fig. 11). Chen et al. (1995) named the short interval from +19.0 m to +19.7 m the 'Basal *Cordylodus lindstromi* fluctuations' (BCLF), a term that is abandoned here because the FAD of *C. lindstromi* is recorded above this excursion in the section (Figs. 3, 11). The negative termination of the 'zig-zag' pattern (no. 2, Fig. 11) is characteristic; it is followed by a positive trend culminating in the large positive spike above the first planktic graptolite at +21.30 m (no. 3, Fig. 11) and within the TST of sequence C. This positive spike represents the first large, positive C-isotope excursion in the Early Ordovician that corresponds to the 'Rise of Planktic Graptolites' (see Section 8.1.2). In the Xiaoyangqiao section, *Rhabdinopora proparabola* occurs at the positive rise towards the first large, positive C-isotope excursion (no. 3, Fig. 11) and the peak nearly coincides with the FAD of *Cordylodus lindstromi.* Upsection, the C-isotope curve displays a second but slightly smaller positive peak at +22.9 m (no. 4, Fig. 11), coinciding with the MFS of sequence D. A gentle positive trend is noted upwards with a culmination peak at ca. +27.6 m (no. 5, Fig. 11). This broad positive culmination is followed by the appearance of *Anisograptus matanensis* in the Xiaoyangqiao section.

7.2. REE geochemical anomaly

The analysis for REE and other trace elements using brachiopod apatite in the section recorded a prominent REE anomaly or positive spike peaking at +19.5 m (Chen et al., 1986). This peak is recorded in the upper part of lithological unit III slightly above the MFS of sequence C in the section. It also coincides with the characteristic 'zig-zag' pattern of the C-isotope curve recorded within the *Cordylodus intermedius* Zone (Chen et al., 1995; this study; Fig. 11).

7.3. Magnetostratigraphy

The magnetic polarity pattern for the Cambrian–Ordovician transition has been documented for the entire Xiaoyangqiao section (Fig. 11; Ripperdan and Kirschvink, 1992; Ripperdan et al., 1992, 1993; Chen et al., 1995). Two normal-polarity zones and one reversed-polarity zone are identified in the section. The lower period of normal polarity is represented by the strata referred to lithologic unit I, with one single short reversal-polarity at −6.1 m (Fig. 11). This period of normal polarity is assigned to the *Eoconodontus notchpeakensis* Zone although the interval from the base of the section to −6.2 m is mainly without data (cf. Ripperdan et al., 1993; Chen et al., 1995, table 2). A shift from the normal- to reversed-polarity zone is recorded at −5.9 m and the period with the reverse-polarity is represented by the strata of the lithologic units II and III. This reverse period corresponds to the *Cordylodus caboti* and *Cordylodus intermedius* zones. The return to a period with normal polarity at ca. +20.6 m in the Xiaoyangqiao section is abrupt and the shift to the normal polarity zone coincides closely with the sequence D boundary followed by the appearance of *Rhabdinopora proparabola* (i.e., at +20.9 m). The normal-polarity zone comprises the strata of lithologic unit IV and up to the top of the exposed strata in the Xiaoyangqiao section. This period comprises the *Cordylodus lindstromi* conodont Zone and the *Rhabdinopora proparabola*, *R. parabola* and *Anisograptus matanensis* graptolite zones (Figs. 3, 11; Chen et al., 1995, table 2).

8. Correlation with the Green Point GSSP section

One purpose here is to demonstrate that the detailed data obtained from the Xiaoyangqiao section allow for precise correlation, using multidisciplinary approach, with the Green Point GSSP section, Newfoundland, Canada.

8.1. The Green Point GSSP section

The information from Green Point GSSP section for the global Cambrian–Ordovician boundary includes biostratigraphy and geochemical data. The Green Point GSSP section was logged in detail by James and Stevens (1986), who referred the succession to the Green Point Formation (with two members) of the Cow Head Group (Figs. 12, 13). Smaller lithological units were referred to units 19–28 (also labelled 'beds' by some authors) in the section (Figs. 12, 13). Tripathy et al. (2014) provided a radiometric age at 484 ± 16 Ma, based on Re-Os isotopes, for the Green Point GSSP horizon, which is within unit 23.

The conodonts have been studied in great detail and fully described by Bagnoli et al. (1987) and Barnes (1988); additional

Please cite this article in press as: Wang, X.F., et al., Correlating the global Cambrian–Ordovician boundary: Precise comparison of the Xiaoyangqiao section, Dayangcha, North China with the Green Point GSSP section, Newfoundland, Canada. Palaeoworld (2019), https://doi.org/10.1016/j.palwor.2019.01.003

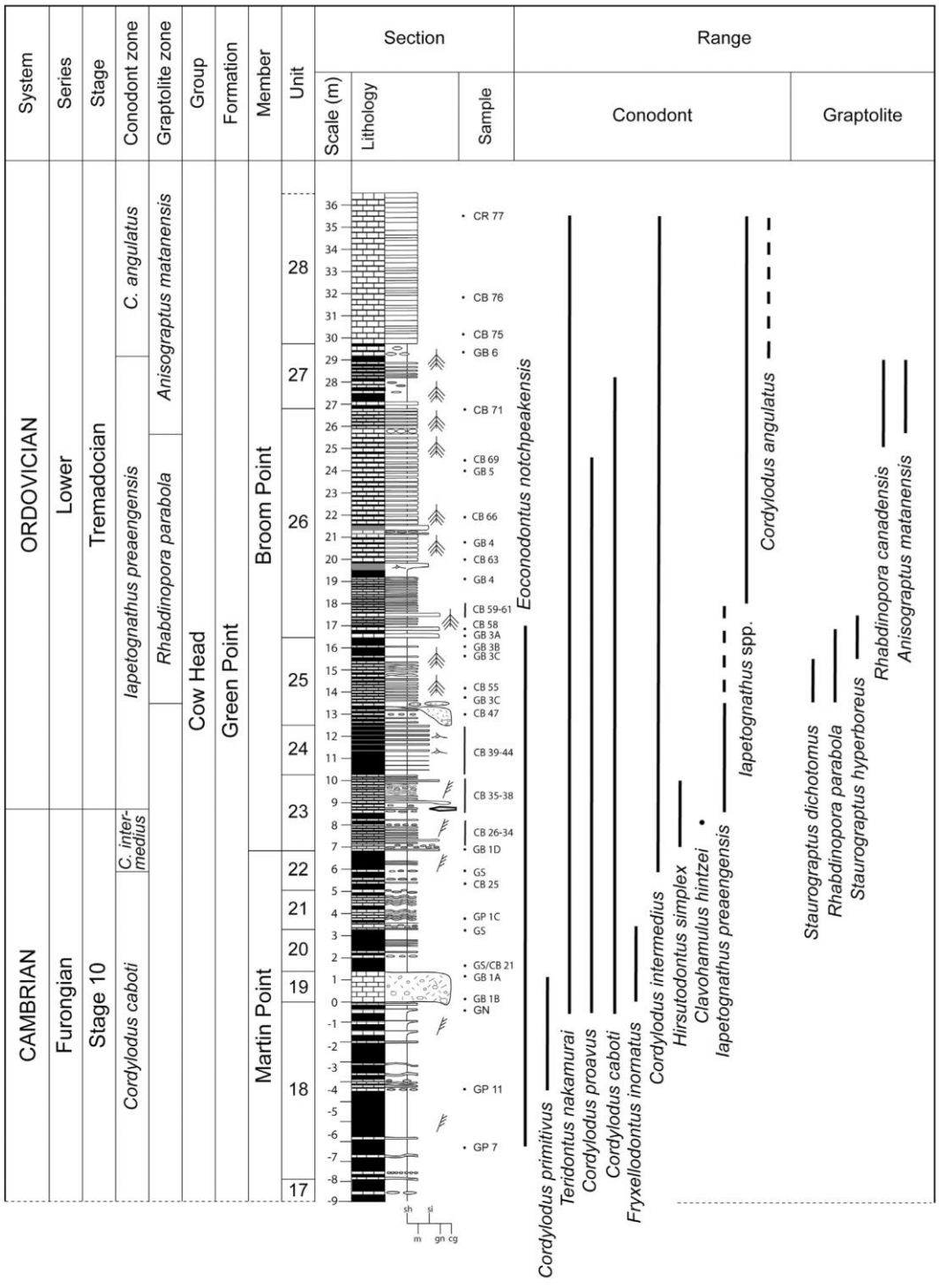

Fig. 12. Upper Cambrian to Lower Ordovician stratigraphy of the Green Point GSSP section with conodont and graptolite ranges and zones. The GSSP horizon is marked by a 'golden spike' in unit 23. The samples are from Barnes (1988, CB), (Bagnoli et al., 1987, GB) and own collection (GS, GN). For legend, see Fig. 10. Abbreviations used for grainsize: sh = shale; si = siltstone; m = mudstone; gn = grainstone; cg = conglomerate.

Please cite this article in press as: Wang, X.F., et al., Correlating the global Cambrian–Ordovician boundary: Precise comparison of the Xiaoyangqiao section, Dayangcha, North China with the Green Point GSSP section, Newfoundland, Canada. Palaeoworld (2019), https://doi.org/10.1016/j.palwor.2019.01.003

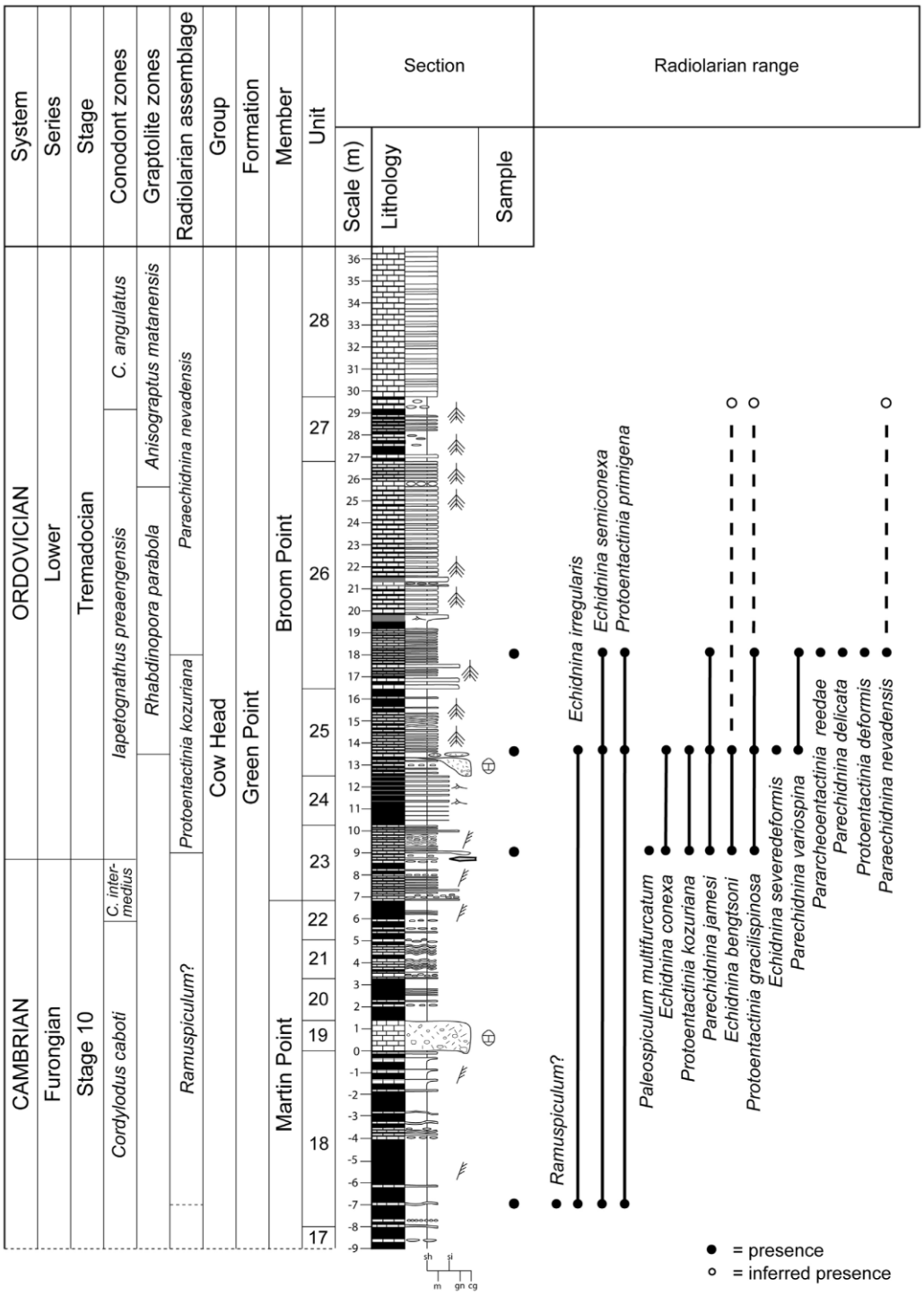

Fig. 13. Upper Cambrian to Lower Ordovician radiolarian biostratigraphy at Green Point (*Parechidina nevadensis* level of Kozur et al., 1996, *Cordylodus angulatus* conodont zone) from Nevada is added. The *Ramuspiculum* assemblage(?) from unit 18 correlates with the *C. caboti* Zone. The *Protoentactinia kozuriana* and *Paraechidnina nevadensis* radiolarian assemblages correlate with the *Iapetognathus preaengensis* Zone and the *R. parabola* Zone. Species of the latter radiolarian assemblage extends into the *C. angulatus* Zone (Kozur et al., 1996) and the *Anisograptus matanensis* Zone. For legend, see Fig. 10. Abbreviations used for grainsize: sh = shale; si = siltstone; m = mudstone; gn = grainstone; cg = conglomerate.

Please cite this article in press as: Wang, X.F., et al., Correlating the global Cambrian–Ordovician boundary: Precise comparison of the Xiaoyangqiao section, Dayangcha, North China with the Green Point GSSP section, Newfoundland, Canada. Palaeoworld (2019), https://doi.org/10.1016/j.palwor.2019.01.003

information is provided by Terfelt et al. (2012) and Stouge et al. (2017). The graptolites in the Green Point section were described by Erdtmann (1988) and Cooper et al. (1998) and summarized by Cooper et al. (2001).

8.1.1. Biostratigraphy and correlation

Here, the conodonts and graptolites are used for the biostratigraphical correlation of the Xiaoyangqiao section with the Green Point GSSP section. The *Cordylodus caboti*, *Cordylodus intermedius* and *Cordylodus angulatus* conodont zones are well constrained in the Cambrian–Ordovician transitional beds, exposed at the Green Point GSSP section (Bagnoli et al., 1987; Barnes, 1988; Cooper et al., 2001; Terfelt et al., 2012; Fig. 12). The base of the upper Cambrian *C. caboti* Zone at Green Point has not yet been defined in the section, whereas *Cordylodus intermedius*, i.e., the nominate species for the uppermost Cambrian conodont zone, is first recorded from unit 22. The *C. intermedius* Zone extends to the FAD of *Iapetognathus preaengensis* in unit 23. *Iapetognathus preaengensis* (previously *I. fluctivagus* in Cooper et al., 2001; cf. Terfelt et al., 2012) is the biomarker for the GSSP and its FAD defines the base of the Ordovician System (Terfelt et al., 2012). The *Cordylodus angulatus* conodont Zone is recorded from unit 27, ca. 11 m above the GSSP. *Cordylodus lindstromi* has not been positively identified from the Green Point GSSP section.

In the Green Point section the first record of planktic graptolites is from unit 25, where *Rhabdinopora parabola* is recorded, associated with *Staurograptus dichotomus* Emmons, 1855. Previously, the beds of unit 25 were subdivided into the *R. praeparabola* and *R. parabola* zones (Erdtmann, 1986; Cooper et al., 1998, 2001), but the two biozones are here reduced to one zone. The *Anisograptus matanensis* Zone is present in the upper part of unit 26 and the base of this zone is below the base of the *Cordylodus angulatus* conodont Zone (Bagnoli et al., 1987; Barnes, 1988; Cooper et al., 2001).

New biostratigraphical information from the Green Point GSSP section includes three radiolarian assemblages, which are recorded from the units 18, 23, 25 and 26 (Won et al., 2005; Maletz, 2011; Pouille et al., 2014) (Figs. 13, 14). The late Cambrian radiolarian assemblage recorded from unit 18 is referred to the *Ramuspiculum*? assemblage. The next *Protoentactinia kozuriana* assemblage appears high in unit 23 and extends into unit 25, thus marking the base of the Ordovician System (Pouille et al., 2014). New taxa appear in unit 26 and this fauna is referred to the *Paraechidnina nevadensis* assemblage, which extends into the *C. angulatus* Zone according to Kozur et al. (1996). The radiolarian assemblages can be tied to the conodont and graptolite zonation (Fig. 13). The characteristic distribution of the radiolarian assemblages in the Cambrian–Ordovician boundary interval shows that this microfossil group has a great potential for identification of the Cambrian–Ordovician boundary and for intercontinental correlation.

Trilobites and brachiopods are rare but occur in the conglomerate layers (i.e., *Symphysurina cleora* and *Nanorhis hamburgensis* in unit 19 and *Symphysurina* cf. *brevis* in unit 25; James and Stevens, 1986).

The interval from unit 18 and up to the upper unit 22 correlates with the *C. caboti* Zone of the Xiaoyangqiao section. The upper unit 22 to the lower part of unit 23 correlates with the *Cordylodus intermedius* Zone in the Xiaoyangqiao section. The graptolite zones including the revised *Rhabdinopora parabola* Zone in unit 25 and *Anisograptus matanensis* Zone in the uppermost part of unit 26 correlates with the two graptolite zones of the same names in the Xiaoyangqiao section.

The GSSP and the FAD of *Iapetognatus preaengensis* cannot be correlated biostratigraphically to the Xiaoyangqiao section due to the absence of the marker species in the Xiaoyangqiao section. The characteristic species *Iapetognathus jilinensis* from the Xiaoyangqiao section, occurring above the appearance of *Rhabdinopora proparabola* and in the *Cordylodus lindstromi* Zone, has not been recorded from Green Point section. Barnes (1988) and Cooper et al. (2001) noted that the GSSP level should be marked by the appearance of *Cordylodus lindstromi s.l.*, but this taxon has not been well documented and the presence of *C. lindstromi* (or *C. lindstromi s.l.*) at this level still awaits to be confirmed.

8.1.2. Chemostratigraphy and matching of the isotope chemostratigraphy

Three C-isotope curves have been prepared from the Green Point section (Magaritz, 1991; Nowlan, 1995; Azmy et al., 2014; Stouge et al., 2017). The C-isotope curve shown by Cooper et al. (2001, fig. 4) is a general curve that is not derived from the Green Point section.

The precise and high-resolution $\delta^{13}C_{carb}$ profile of the Green Point Section (Azmy et al., 2014; Stouge et al., 2017) is in detail very similar to that recorded from the Xiaoyangqiao section (Chen et al., 1995; this study) and the succession of spikes can be identified (Fig. 15). Among the most prominent common features of the two $\delta^{13}C_{carb}$ profiles is the positive trend from unit 21 with a broad positive peak in unit 22 in the Green Point section. This same trend and positive peak matches precisely the positive excursion recorded in the Xiaoyangqiao section and annotated HSS (i.e., '*Hirsutodontus simplex* spike' of Chen et al., 1995). The succeeding strong negative shift in the lower part of the overlying unit 23 and ca. 1.8 m below the GSSP level (no. 1, Fig. 15) matches the similar negative shift recognized at +18.4 m in the Xiaoyangqiao section (no. 1, Fig. 11; see also Chen et al., 1995). The 'zig-zag' pattern that characterizes the overlying interval from the lower to middle part of unit 23 and immediately below the GSSP horizon (Azmy et al., 2014; Stouge et al., 2017) also provides a precise match to the similar 'zig-zag' development observed in the Xiaoyangqiao section. In both sections this 'zig-zag' pattern is recognized from within the *C. intermedius* Zone. The maximum negative peak (no. 2, Figs. 11, 15) is the same for the two sections and characterizes the top of the Cambrian System in the Green Point GSSP section (Cooper et al., 2001; Azmy et al., 2014; Stouge et al., 2017) and accordingly also in the Xiaoyangqiao section.

In the Green Point section, the most prominent C-isotope positive peak, representing the largest positive isotope $\delta^{13}C_{carb}$ isotope excursion in the earliest Ordovician, is identified from the lower part of unit 25, at 4.5 m above the GSSP horizon (no. 3,

Please cite this article in press as: Wang, X.F., et al., Correlating the global Cambrian–Ordovician boundary: Precise comparison of the Xiaoyangqiao section, Dayangcha, North China with the Green Point GSSP section, Newfoundland, Canada. Palaeoworld (2019), https://doi.org/10.1016/j.palwor.2019.01.003

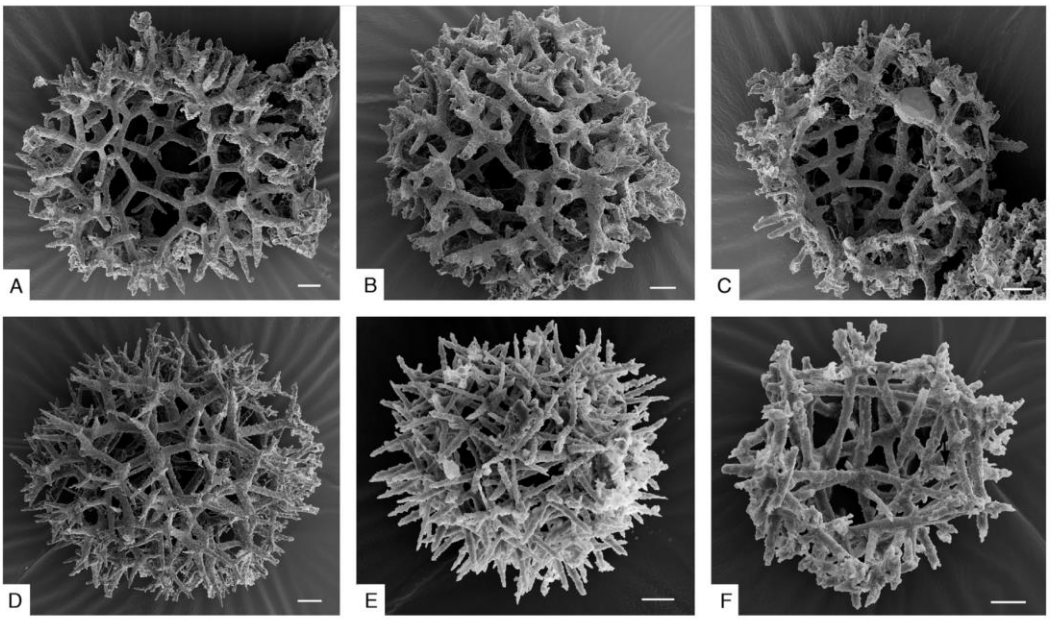

Fig. 14. Representative lowermost Ordovician radiolarian species from the *Protoentactinia kozuriana* assemblage, basal Tremadocian, Green Point GSSP section. (A, D) *Protoentactinia gracilispinosa*, GSC 140463 and GSC 140464. (B, C) *Protoentactinia kozuriana*, GSC 140465 and GSC 140466. (E, F) *Echidnina conexa*, GSC 140467 and GSC 139213 (*Subechidnina* sp. in Maletz, 2017, fig. 2.6). Scale bars represent 20 μm.

Fig. 15). It coincides precisely with the base of the revised *Rhabdinopora parabola* Zone (i.e., *R. praeparabola* Zone of Cooper et al., 2001) in the Green Point section. In the Xiaoyangqiao section, and above the appearance of *R. proparabola*, the matching C-isotope maximum peak is barren of graptolites. The next higher C-isotope positive peak marks the *R. parabola* Zone in the Green Point section (no. 4, Figs. 12, 15). Upsection follows the positive peak that appears below the base of the *Anisograptus matanensis* Zone (no. 5, Figs. 12, 15).

8.1.3. Geochemical anomalies

A geochemical REE anomaly has been detected in the Green Point GSSP section low within the 'zig-zag' excursions in unit 23 of the *Cordylodus intermedius* Zone (Azmy et al., 2014, fig. 6). This is identical and coeval to the Xiaoyangqiao section, where the REE geochemical anomaly is recorded from the *Cordylodus intermedius* Zone, as described above (Section 7.2). This REE geochemical anomaly, first recognized in the Xiaoyangqiao section (Chen et al., 1986), is similar and coeval to the REE anomaly documented from the Green Point section (Azmy et al., 2014). The REE anomaly of Green Point section is recorded below the GSSP in the Green Point section.

8.1.4. Sea-level changes

The interval preserving the GSSP horizon is contained between the Basal House lowstand, the base of which is marked by the prominent conglomerate named unit 19 (Figs. 12, 15) and the 'Acerocare Regressive Event', which is expressed by the prominent brown-weathering dolomitic siltstone/limestone of unit 24. Like in the Xiaoyangqiao section, the shift is from a broad negative C-isotope excursion to the initiation of the largest C-isotope positive excursion.

The precise correlation and matching between the two sections is shown in Fig. 16.

8.1.5. The Cambrian–Ordovician boundary in the Xiaoyangqiao section

The similarity between the $\delta^{13}C_{carb}$ curves from the two sections, and constrained by the precise biozonal correlation, demonstrates — with confidence — that these curves provide strong correlative potential. Based on the precise match of the pattern of the $\delta^{13}C_{carb}$ isotope curves between the Green Point GSSP section and the Xiaoyangqiao section it is possible to determine the precise level for the FAD of the planktic graptolite in the former and to identify the level equivalent to the Green Point GSSP horizon in the latter.

In the Green Point section, the first planktic graptolite species *Rhabdinopora proparabola* has not been recorded or positively identified. However, the first planktic graptolite *R. proparabola* should be found from the top of unit 24 extending into the base of unit 25 in the Green Point section, i.e., from the transgressive part of the prominent brown weathering siltstone horizon (= unit 24) that represents the 'Acerocare Regressive Event' and at the initiation of the largest positive $\delta^{13}C_{carb}$ isotope excursion. A further implication of this match is that unit 25, i.e., a level ca. 5 m above the GSSP horizon, represents the *Cordylodus lindstromi* conodont Zone as it is identified in the Xiaoyangqiao section. *Cordylodus lindstromi*, as mentioned above (Section 8.1.2), has not been recorded from the Green Point section. The genus is represented mainly by *Cordylodus proavus*, *Cordylodus*

Please cite this article in press as: Wang, X.F., et al., Correlating the global Cambrian–Ordovician boundary: Precise comparison of the Xiaoyangqiao section, Dayangcha, North China with the Green Point GSSP section, Newfoundland, Canada. Palaeoworld (2019), https://doi.org/10.1016/j.palwor.2019.01.003

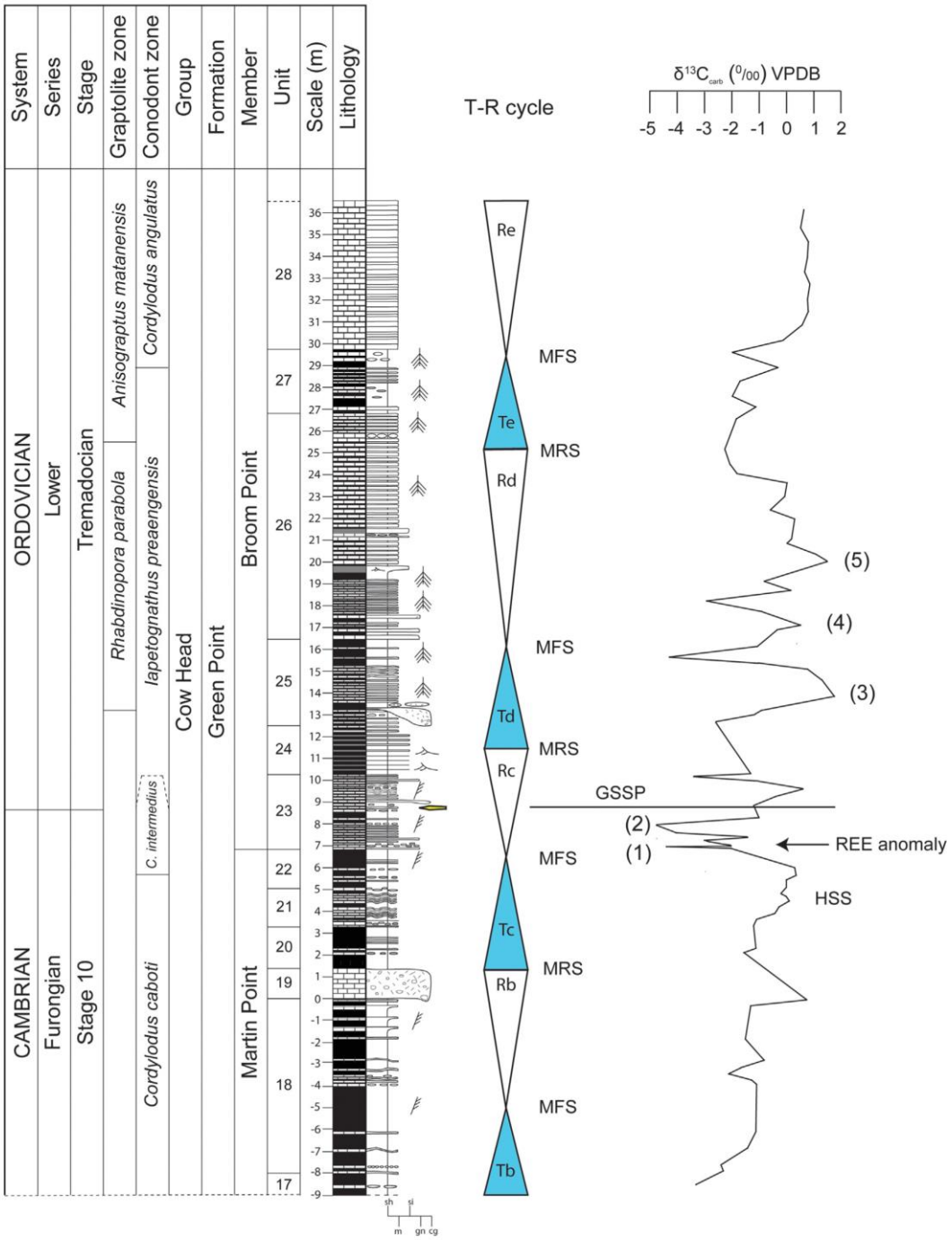

Fig. 15. Detailed sequence stratigraphy, C-isotope curve and geochemical anomaly of the Green Point GSSP Section. The numbered spikes are interpreted to represent the same spikes as for the Xiaoyangqiao section shown in Fig. 10. The GSSP horizon lies within the Regressive System Tract (Rc). The large C-isotope peak (3) coincides with the base of the *R. parabola* Zone in the Green Point section, (4) corresponds to the *Rhabdinopora parabola* Zone *sensu* Cooper et al. (2001), and the broad spike (5) is below the *Anisograptus matanensis* graptolite Zone. For legend, see Fig. 10. Abbreviations used for grainsize: sh = shale; si = siltstone; m = mudstone; gn = grainstone; cg = conglomerate.

Please cite this article in press as: Wang, X.F., et al., Correlating the global Cambrian–Ordovician boundary: Precise comparison of the Xiaoyangqiao section, Dayangcha, North China with the Green Point GSSP section, Newfoundland, Canada. Palaeoworld (2019), https://doi.org/10.1016/j.palwor.2019.01.003

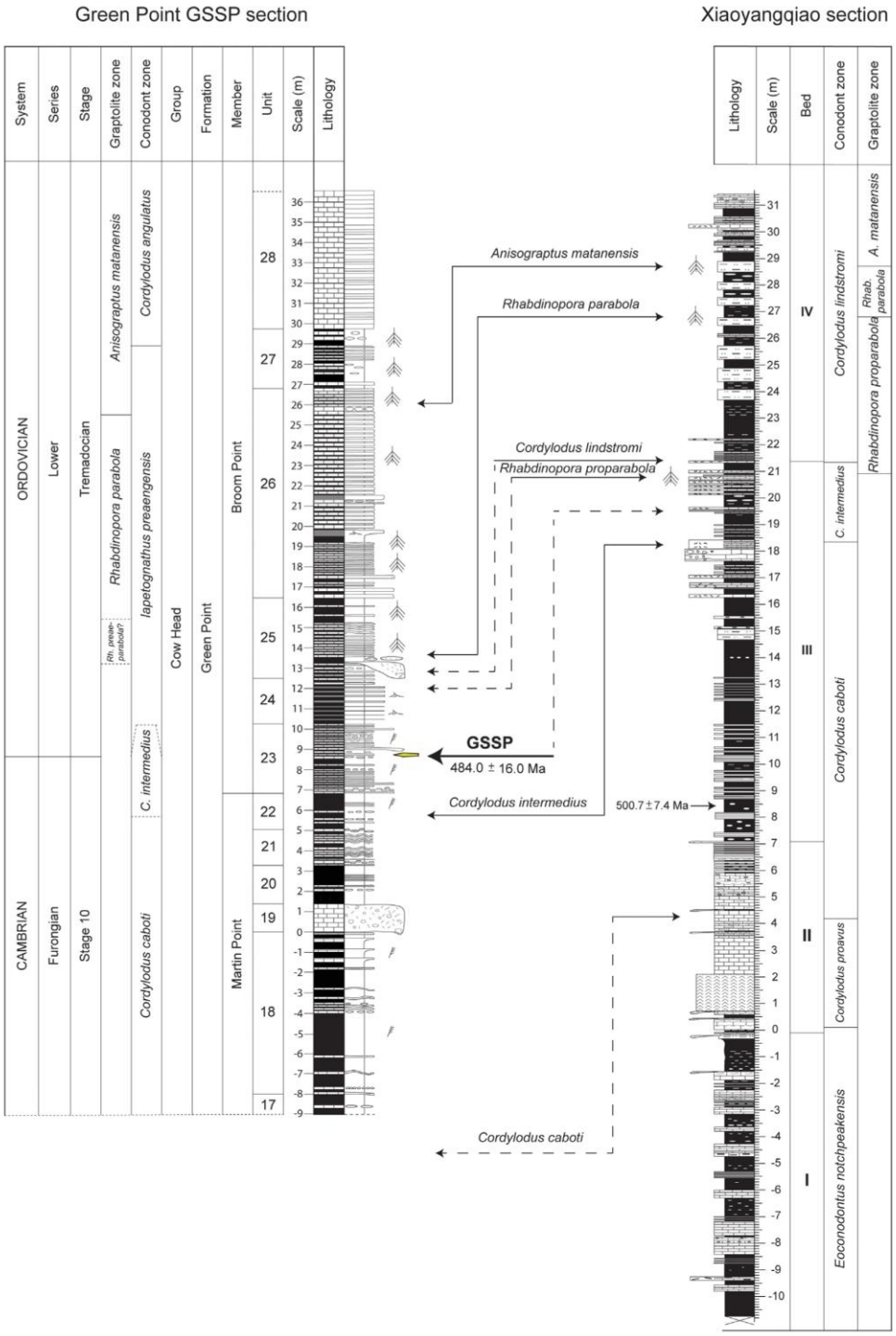

Fig. 16. Detailed biostratigraphic correlation of the Xiaoyangqiao section and the Green Point GSSP section. Unbroken lines and arrows point at direct evidence. The dashed lines represent the likely position and interpreted correlation of a taxon that is represented in only one of the sections. For legend, see Fig. 10 (for grainsize: see Figs. 12, 13 and 15).

Please cite this article in press as: Wang, X.F., et al., Correlating the global Cambrian–Ordovician boundary: Precise comparison of the Xiaoyangqiao section, Dayangcha, North China with the Green Point GSSP section, Newfoundland, Canada. Palaeoworld (2019), https://doi.org/10.1016/j.palwor.2019.01.003

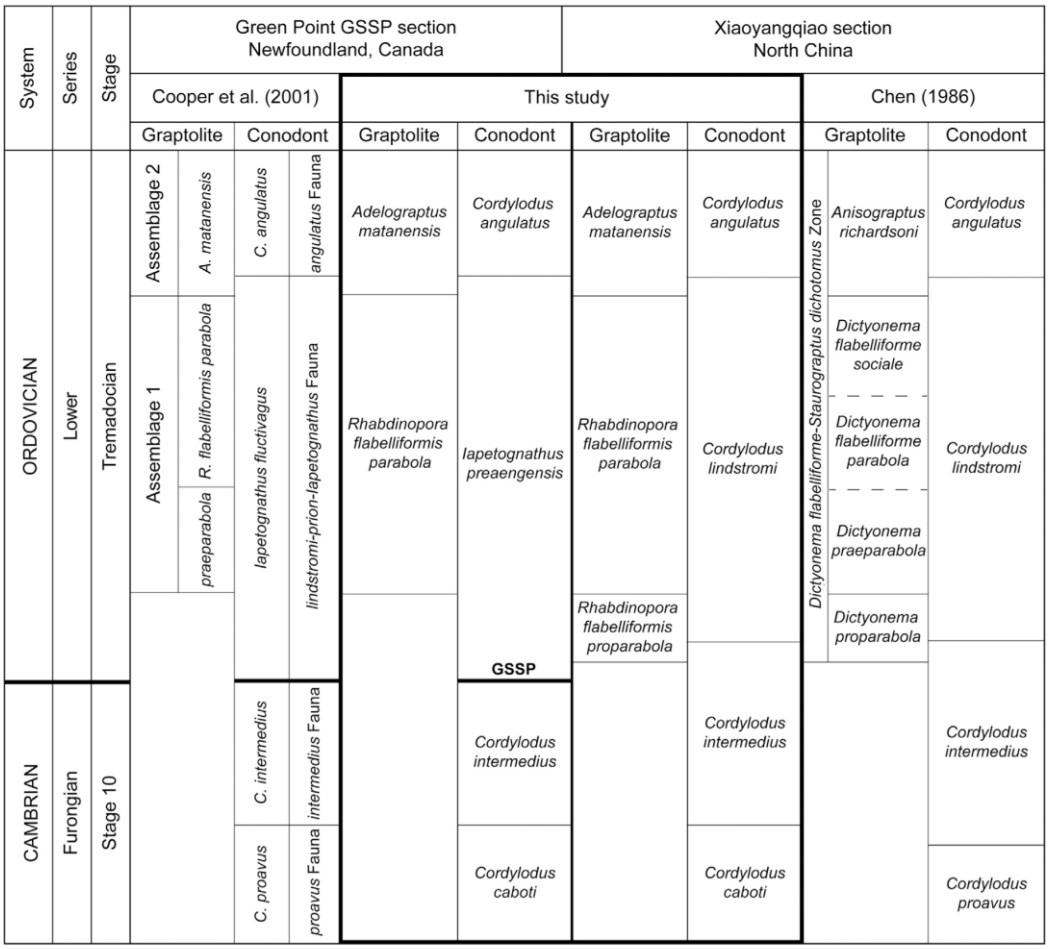

Fig. 17. Summary of the precise correlation and match of the Xiaoyangqiao section, North China and the Green Point GSSP section, western Newfoundland, Canada. The GSSP horizon lies within the upper *Cordylodus intermedius* conodont Zone and below the first appearance of planktic graptolites. The GSSP horizon is above the Lower House lowstand and below the 'Acerocare Regressive Event' in the Green Point succession.

caboti and *Cordylodus intermedius*, which all are long-ranging conodont species that have been recorded from unit 25 in the Green Point section (Fig. 12; Bagnoli et al., 1987; Barnes, 1988; Cooper et al., 2001; this study).

The position of the GSSP horizon in unit 23 is situated just above the prominent negative excursion (no. 2, Fig. 15) in the Green Point Section and above the REE geochemical anomaly in the *Cordylodus intermedius* Zone. In the Xiaoyangqiao section the Cambrian–Ordovician boundary horizon can be placed at ca. +19.9 m (±0.2 m), which is approximately 1 m below the appearance of the first planktic graptolite at +20.9 m in Xiaoyangqiao section (Fig. 3).

9. Proposal of the Xiaoyangqiao section as an ASSP section for the base of the Ordovician System

The correlation and precise match of C-isotope curves between the Xiaoyangqiao section and the Green Point GSSP section presented here demonstrates — for the first time — that accurate correlation and match of the GSSP horizon for the global Cambrian–Ordovician boundary outside the Green Point section, western Newfoundland, Canada is indeed possible. This fact alone strongly justifies the recommendation of the Xiaoyangqiao section as AASP for the global Cambrian–Ordovician boundary.

The Xiaoyangqiao section fully satisfies the requirements for a GSSP/ASSP section set out in the revised Guidelines for the establishment of global chronostratigraphic standards (Salvador, 1994; Remane et al., 1996).

9.1. The following requirements are fulfilled

1. The Xiaoyangqiao section is easily accessible.
2. The succession is well-exposed; it displays a continuous sedimentation, and the sedimentary rocks are nonmetamorphic and not affected by strong diagenesis.

Please cite this article in press as: Wang, X.F., et al., Correlating the global Cambrian–Ordovician boundary: Precise comparison of the Xiaoyangqiao section, Dayangcha, North China with the Green Point GSSP section, Newfoundland, Canada. Palaeoworld (2019), https://doi.org/10.1016/j.palwor.2019.01.003

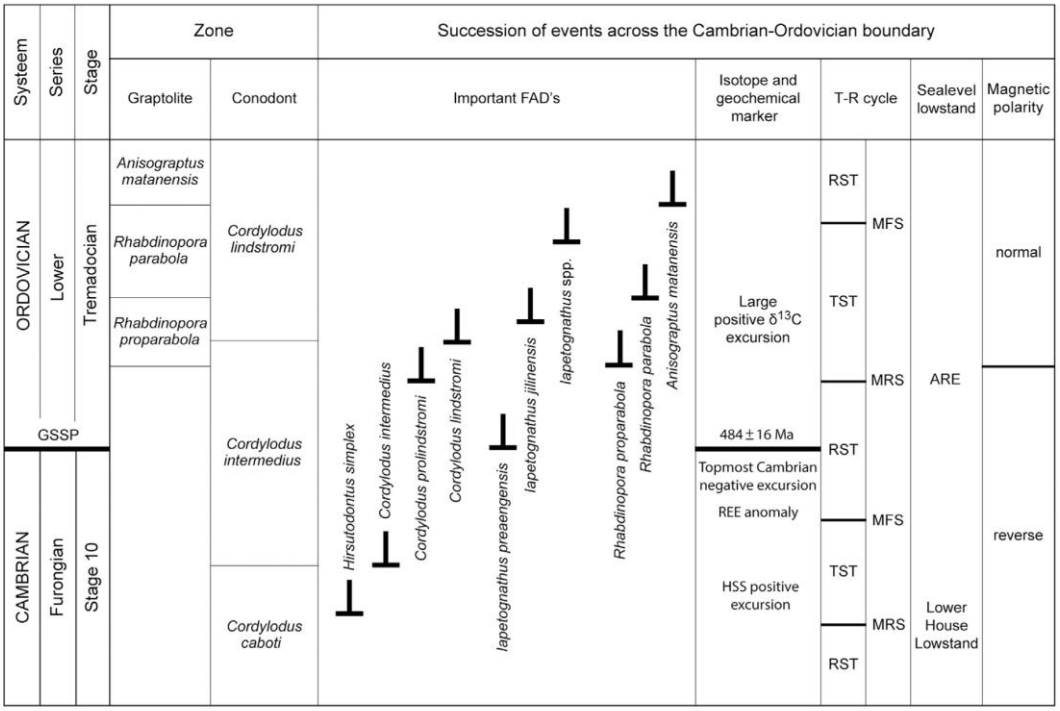

Fig. 18. Succession of events in the late Cambrian and earliest Ordovician. All events are useful as proxies for the recognition of the base of the global Ordovician System.

3. The Xiaoyangqiao section lies within the Cambrian–Ordovician boundary protection zone, 2 km to NEE of the town of Dayangcha, 25 km northeast of Baishan City (Hunjiang), and 7–8 km east of Jiangyuan County.
4. The upper Cambrian to Lower Ordovician succession, 32 m of which are exposed at the Xiaoyangqiao section, preserves the complete Cambrian–Ordovician transition (e.g., Chen, 1986; this study).
5. The succession is richly fossiliferous including benthos, nekton, phyto- and zooplankton.
6. All conodont and graptolite species that are important and used for long-distance or intercontinental correlation across different facies, are well displayed in the section.
7. Numerous trilobites and prolific acritarch assemblages are recorded from the Xiaoyangqiao section (Yin, 1985, 1986, 1995; Qian, 1986; Chen et al., 1988; Zhang et al., 1996; Wang et al., 2016; this study).
8. The investigated Cambrian–Ordovician interval in the Xiaoyangqiao section preserves a complete evolutionary succession from *Eoconodontus notchpeakensis* to the conodont genus *Cordylodus* Pander, via *Cordylodus primitivus*. This evolutionary lineage allows for the establishment of a series of conodont lineage zones in ascending order: the *Eoconodontus notchpeakensis*, *Cordylodus proavus*, *Cordylodus caboti*, *C. intermedius* and *C. lindstromi* biozones. The overlying *Cordylodus angulatus* Zone is recorded from the closely located exposures just to the east of the Xiaoyangqiao section (Chen, 1986).
9. The planktic Ordovician graptolites preserved in the section are referred to the *Rhabdinopora proparapola*, *Rhabdinopora parabola* and *Anisograptus matanensis* biozones.
10. The species *Rhabdinopora proparabola* (Lin, 1986) in the Xiaoyangqiao section represents the first representative of the *Rhabdinopora* lineage and is not known with certainty from other regions, except from perhaps Argentina (Zeballo et al., 2005).
11. The data mentioned above are directly comparable with the faunal succession at Green Point GSSP section and solve the correlation problems of the Cambrian–Ordovician boundary as it is fixed in the Green Point GSSP section.
12. The Xiaoyangqiao section is suitable for chemostratigraphic and magnetostratigraphic dating and provides the precise match with the Green Point GSSP section.
13. The geochemical REE anomaly first recorded in the Xiaoyangqiao section (Chen et al., 1986) from the *Cordylodus intermedius* Zone has been identified also in the Green Point section (Azmy et al., 2014). Like in the Xiaoyangqiao section, the REE anomaly is recorded above the HSS and below the GSSP horizon within the *Cordylodus intermedius* Zone in the Green Point GSSP section.

Please cite this article in press as: Wang, X.F., et al., Correlating the global Cambrian–Ordovician boundary: Precise comparison of the Xiaoyangqiao section, Dayangcha, North China with the Green Point GSSP section, Newfoundland, Canada. Palaeoworld (2019), https://doi.org/10.1016/j.palwor.2019.01.003

10. Conclusions

This contribution presents and summarizes new data on the Cambrian–Ordovician boundary interval obtained from the important Xiaoyangqiao section in North China and combined with the information from the Green Point section, i.e., the global GSSP section for the Cambrian–Ordovician boundary. This interdisciplinary study clearly demonstrates the strengths of the Xiaoyangqiao section for intercontinental correlation. We therefore recommend the section as a global ASSP section for the Cambrian–Ordovician boundary in order to provide a robust basis for the identification of the global Cambrian–Ordovician boundary level (Fig. 17).

The new results from this study — using integrated bio-, sequence-, chemo- and magnetostratigraphy from the Xiaoyangqiao section, Dayangcha, China, allowing for detailed comparison with the Green Point GSSP section — demonstrate that (1) the first planktic graptolite, *Rhabdinopora proparabola*, is recorded from the Xiaoyangqiao section; (2) the FAD of *Cordylodus lindstromi* is just above the appearance of the earliest planktic graptolite *Rhabdinopora proparabola;* (3) the Cambrian–Ordovician boundary is situated between the eustatic global Basal House Lowstand and the eustatic global 'Acerocare Regressive Event'; (4) the earliest Ordovician maximum positive $\delta^{12}C_{carb}$ isotope peak is recorded at the base of the *Rhabdinopora parabola* graptolite Zone; (5) the GSSP horizon representing the global Cambrian–Ordovician boundary lies immediately above a distinct negative excursion in the two investigated sections; (6) the prominent positive $d^{13}C_{carb}$ excursion named *Hirsutodontus simplex* spike (=HSS; i.e., Chen et al., 1995) and the REE anomaly, within the *Cordylodus intermedius* Zone, lie immediately below the Cambrian–Ordovician boundary in both sections.

All the points mentioned above can be applied as proxies — globally — for the identification of the Cambrian–Ordovician boundary (Fig. 18).

Problems concerning the Cambrian–Ordovician boundary remain to be solved. The first problem is when Cooper et al. (2001) fixed the position and placed the 'Golden Spike' for the Cambrian–Ordovician boundary in unit 23 in the Green Point section, they also assigned *Iapetognathus fluctivagus* Nicoll et al., 1999 as the biomarker for the Cambrian–Ordovician boundary. However, this chosen biomarker for the GSSP horizon is not present at the GSSP horizon, but instead the horizon is represented by *Iapetognathus preaengensis* Landing in Fortey et al., 1982 as correctly identified by Barnes (1988) in the proposal for the GSSP of the Cambrian–Ordovician boundary. The genus as defined by Nicoll et al. (1999) is probably polyphyletic and the chosen biomarker is not as widely distributed as previously thought.

The second problem is that the first planktic graptolite, *Rhabdinopora proparabola*, is recorded only from the Xiaoyangqiao section, and not observed from the Green Point GSSP section. The equivalent position for this first graptolite horizon, using high-resolution carbon isotope stratigraphy, is here estimated to be represented by the top bed of unit 24 into lowermost beds of unit 25 (Figs. 12, 15) — a level that is below the first appearance of *R. parabola* and above the global 'Acerocare Regressive Event' (=unit 24 in the Green Point section). In the Green Point section this interval only yields graptolite fragments and long-ranging conodonts. The estimated *R. proparabola* level is ca. 4 m above the GSSP horizon in the Green Point section and ca. 1 m above the estimated level representing the Cambrian–Ordovician boundary in the Xiaoyangqiao section.

Acknowledgements

The authors are deeply indebted to China Ministry of Sciences and Technology and China Geological Survey for their financial support to the research project (No. 2015FY310100-7, No. DD20160120-04). We also gratefully appreciate the support to the research project by Chinese Commission of Stratigraphy and Wuhan Center of China Geological Survey (WCGS). The isotopic geochemistry Laboratory of WCGS analyzed rock collected samples and prepared the samples for microfossils. A grant from the Carlsberg Foundation, Copenhagen, Denmark covering the travel to China for Svend Stouge is gratefully appreciated. Fieldwork by Jörg Maletz was supported by Grant MA 1269/7-1 of Deutsche Forschungsgemeinschaft (DFG).

Special thanks go the journal referees P. Ahlberg, C.R. Barnes, and an anonymous referee, who read the submitted manuscript and provided numerous suggestions and recommendations that all improved the final manuscript.

References

Albanesi, G.L.M., Giuliano, E., Pacheco, F.E., Ortega, G., Monaldi, R., 2015. Conodonts from the Cambrian Ordovician Boundary in the Cordillera Oriental, NW Argentina. Stratigraphy 12 (3–4), 237–256.

An, T.X., Zhang, F., Xiang, W.D., Zhang, Y.Q., Xu, W.H., Zhang, H.J., Jiang, D.B., Yang, C.S., Lin, L.D., Cui, Z.T., Yang, X.C., 1983. The Conodonts of North China and the Adjacent Regions. Science Press, Beijing, 223 pp. (in Chinese, with English abstract).

Azmy, K., Stouge, S., Brand, U., Bagnoli, G., Ripperdan, R., 2014. High-resolution chemostratigraphy of the Cambrian–Ordovician GSSP: enchanced global correlation tool. Palaeogeography, Palaeoclimatology, Palaeoecology 409, 135–144.

Bagnoli, G., Stouge, S., 2014. Upper Furongian (Cambrian) conodonts from the Degerhamn quarry road section, southern Öland, Sweden. GFF 136 (3), 436–458.

Bagnoli, G., Barnes, C.R., Stevens, R.K., 1987. Lower Ordovician (Tremadocian) conodonts from Broom Point and Green Point, Western Newfoundland. Bollettino della Società Paleontologica Italiana 25 (2), 145–158.

Barnes, C.R., 1988. The proposed Cambrian–Ordovician Global Boundary Stratotype and Point (GSSP) in Western Newfoundland, Canada. Geological Magazine 125 (4), 381–414.

Barnes, C.R., Williams, S.H. (Eds.), 1991. Advances in Ordovician Geology. Geological Survey of Canada, Paper 90-9, 336 pp.

Bassett, M.G., Dean, W.T. (Eds.), 1982. The Cambrian–Ordovician Boundary: Sections, Fossil Distributions, and Correlations. National Museum of Wales, Geological Series 3, Cardiff, 227 pp.

Bulman, O.M.B., 1954. The graptolite fauna of the *Dictyonema* shales of the Oslo region. Norsk Geologisk Tidsskrift 33 (1–2), 1–40.

Bulman, O.M.B., 1970. A new *Dictyonema* fauna from the Salmien of the Stavelot Massif (with a preface by F. Geukens). Bulletin de la Societé belge Geologie, Paleontologie, Hydrologie 79, 213–224.

Burrett, C., Zaw, K., Meffre, S., Lai, C.K., Khositanount, S., Chaodumrong, P., Udchachon, M., Ekins, S., Halpin, J., 2014. The configuration of Greater

Please cite this article in press as: Wang, X.F., et al., Correlating the global Cambrian–Ordovician boundary: Precise comparison of the Xiaoyangqiao section, Dayangcha, North China with the Green Point GSSP section, Newfoundland, Canada. Palaeoworld (2019), https://doi.org/10.1016/j.palwor.2019.01.003

Gondwana — evidence from LA ICPMS, U-PB geochronology of detrital zirkons from the Palaeozoic and Mesozoic of Southeast Asia and China. Gondwana Research 26, 31–51.

Catuneanu, O., Abreu, V., Bhattacharya, J.P., Blum, M.D., Dalrymple, R.W., Eriksson, P.G., Fielding, C.R., Fisher, W.L., Galloway, W.E., Gibling, M.R., Giles, K.A., Holbrook, J.M., Jordan, R., Kendall, C.G.St.C., Macurda, B., Martinsen, O.J., Miall, A.D., Neal, J.E., Nummedal, D., Pomar, L., Posamentier, H.W., Pratt, B.R., Sarg, J.F., Shanley, K.W., Steel, R.J., Strasser, A., Tucker, M.E., Winker, C., 2009. Towards the standardization of sequence stratigraphy. Earth-Science Reviews 92 (1–2), 1–33.

Catuneanu, O., Galloway, W.E., Kendall, C.G.C., Miall, A.D., Posamentier, W., Strasser, A., Tucker, M.E., 2011. Sequence stratigraphy: methodology and nomenclature. Newsletters on Stratigraphy 44 (3), 173–245.

Chen, J.T., 2014. Surface and subsurface reworking by storms on a Cambrian carbonate platform: evidence from limestone breccias and conglomerates. Geologos 20 (1), 13–23.

Chen, J.T., Lee, L.S., 2013. Soft-sediment deformation structures in Cambrian siliciclastic and carbonate storm deposits (Shandong Province, China): differential liquefaction and fluidization triggered by storm-wave loading. Sedimentary Geology 288, 81–94.

Chen, J.Y. (Ed.), 1986. Aspects of the Cambrian–Ordovician Boundary in Dayangcha, China. China Prospect Publishing House, Beijing, 410 pp.

Chen, J.Y., Gong, W.L., 1986. Conodonts. In: Chen, J.Y. (Ed.), Aspects of the Cambrian–Ordovician Boundary in Dayangcha, China. China Prospect Publishing House, Beijing, pp. 93–223.

Chen, J.Y., Zhang, J., 1986. Remark on sedimentary environment. In: Chen, J.Y. (Ed.), Aspects of the Cambrian–Ordovician Boundary in Dayangcha, China. China Prospect Publishing House, Beijing, pp. 35–49.

Chen, J.Y., Teichert, C., Zhou, Z., Lin, Y., Wang, Z., Xu, J., 1983. Faunal sequence across the Cambrian–Ordovician Boundary in northern China and its international correlation. Geological et Palaeontologica 17 (5), 1–15.

Chen, J.Y., Qian, Y.Y., Lin, Y.K., Zhang, J.M., Wang, Z.H., Yin, L.M., Erdtmann, B.-D. (Eds.), 1985. Study on Cambrian–Ordovician Boundary Strata and Its Biota in Dayangcha, Hunjiang, Jilin, China. China Prospect Publishing House, Beijing, 139 pp.

Chen, J.Y., Wang, Y.X., Yang, J.D., 1986. Rare earth and other trace elements in biogenic apatite across the Cambrian–Ordovician boundary. In: Chen, J.Y. (Ed.), Aspects of the Cambrian–Ordovician Boundary in Dayangcha, China. China Prospect Publishing House, Beijing, pp. 61–71.

Chen, J.Y., Qian, Y.Y., Zhang, J.M., Lin, Y.K., Yin, L.M., Wang, Z.H., Wang, Z.Z., Yang, J.D., Wang, Y.X., 1988. The recommended Cambrian–Ordovician boundary stratotype of the Xiaoyangqiao section (Dayangcha, Jilin Province), China. Geological Magazine 125 (4), 415–444.

Chen, J.Y., Zhang, J.M., Nicoll, R.S., Nowlan, G.S., 1995. Carbon and oxygen isotopes in carbonate rocks within Cambrian–Ordovician boundary interval at Dayangcha, China. Acta Palaeontologica Sinica 34 (4), 393–409.

Cooper, R.A., Stewart, I.R., 1979. The Tremadoc graptolite sequence of Lancefield, Victoria. Palaeontology 22 (4), 767–797.

Cooper, R.A., Maletz, J., Wang, H., Erdtmann, B.-D., 1998. Taxonomy and evolution of earliest Ordovician graptoloids. Norsk Geologisk Tidsskrift 78 (1), 3–32.

Cooper, R.A., Nowlan, G.S., Williams, S.H., 2001. Global Stratotype Section and Point for base of the Ordovician System. Episodes 24 (1), 19–28.

Dean, W.T., Martin, F., 1982. The sequence of trilobite faunas and acritarch microfloras at the Cambrian–Ordovician boundary, Wilcox Pass, Alberta, Canada. In: Bassett, M.G., Dean, W.T. (Eds.), The Cambrian–Ordovician Boundary: Sections, Fossil Distributions, and Correlations. National Museum of Wales, Geological Series 3, Cardiff, pp. 131–140.

Deunff, J., 1961. Un microplancton à Hystrichosphères dans le Tremadoc du Sahara. Revue de Micropaléontologie 4 (1), 37–52.

Deunff, J., 1964. Systématique de microplancton fossile à Acritarches; révision de deux genres de l'Ordovicien inférieur. Revue de Micropaléontologie 7 (2), 119–124.

Deunff, J., Gorka, H., Rauscher, R., 1974. Observations nouvelles et précisions sur les Acritarches a large ouverture polaire du Paleozoique inférieur. Geobios 7 (1), 5–18.

Druce, E.C., Jones, P.J., 1971. Cambro-Ordovician conodonts from the Burke River structural belt Queensland. Bureau of Mineral Resources, Geology and Geophysics, Bulletin 110, 1–159.

Dunham, R., 1962. Classification of carbonate rocks according to depositional textures. In: Ham, W.E. (Ed.), Classification of Carbonate Rocks — A Symposium. American Association of Petroleum Geologists, Memoir 1, 108–121.

Embry, A., Johannessen, E., 1992. T-R sequence stratigraphy, facies analysis and reservoir distribution in the uppermost Triassic and Lower Jurassic succession, western Sverdrup Basin, Arctic Canada. In: Vorren, T.O., Bergsager, E., Dahl-Stamnes, Ø.A., Holter, E., Johansen, B., Lie, E., Lund, T.B. (Eds.), Artic Geology and Petroleum Potential. Norvegian Petroleum Society, Special Publication 2, pp. 121–146.

Emmons, E., 1855. American Geology, containing a statement of the principles of the science, with full illustrations of the characteristic American fossils also an atlas and a geological map of the United States. Part II. J. Munsell, Albany, 251 pp.

Epstein, A.G., Epstein, J.P., Harris, L., 1977. Conodont alteration — an index to organic metamorphism. United States Geological Survey Professional Paper 995, 1–27.

Erdtmann, B.-D., 1982. A reorganization and proposed phylogenetic classification of planktic Tremadoc (early Ordovician) dendroid graptolites. Norsk Geologisk Tidsskrift 62 (2), 121–145.

Erdtmann, B.-D., 1986. Review of lithofacies and graptolite-based biofacies of three critical Cambrian–Ordovician boundary stratotype sections. In: Chen, J.Y. (Ed.), Aspects of the Cambrian–Ordovician Boundary in Dayangcha, China. China Prospect Publishing House, Beijing, pp. 374–391.

Erdtmann, B.-D., 1988. The earliest Ordovician nematophorid graptolites: taxonomy and correlation. Geological Magazine 125, 327–348.

Feng, Z.Z., Jin, Z.K., 1994. Types and origin of dolostones in the Lower Palaeozoic of the North China Platform. Sedimentary Geology 93 (3–4), 279–290.

Fortey, R.A., Landing, E., Skevington, D., 1982. Cambrian–Ordovician boundary sections in the Cow Head Group, western Newfoundland. In: Bassett, M.G., Dean, W.T. (Eds.), The Cambrian–Ordovician Boundary: Sections, Fossil Distributions, and Correlations. National Museum of Wales, Geological Series 3, Cardiff, pp. 95–129.

Frakes, L.A., Francis, J.E., Syktus, J.I., 2005. Climate Modes of the Phanerozoic. Cambridge University Press, Cambridge, 274 pp.

Fu, K., 1996. Palaeogeography map of the Early Ordovician of China. In: Wang, H. (Ed.), Atlas of the Palaeogeography of China. Cartographic Publishing House, Beijing, pt. I, pp. 1–143 (in Chinese).

Fu, K., Lai, C., 1996. Explanation of the 'Palaeogeographic map of the Early Ordovician of China'. In: Wang, H. (Ed.), Atlas of the Palaeogeography of China. Cartographic Publishing House, Beijing, pt. II, pp. 1–85, and pt. III, 1–25 (in Chinese (pt. II), with English abstract (pt. III)).

Furnish, W.M., 1938. Conodonts from the Prairie du Chien (Lower Ordovician) of the upper Mississippi Valley. Journal of Paleontology 12 (4), 318–340.

Gorka, H., 1967. Quelque nouveaux acritarches des silexites du Trémadocien supérieur de la région de Kielce (Montagne de Ste. Croix, Pologne). Cahiers de Micropaléontologie 1 (6), 1–8.

Grabau, A.W., 1922. Ordovician fossils from North China. Palaeontology Sinica, Series B, No. 1, 1–127.

Haq, B.U., Schutter, S.R., 2008. A chronology of Paleozoic sea-level changes. Science 322 (5898), 64–68.

Harris, W.J., Keble, R.A., 1928. The *Staurograptus* bed of Victoria. Proceedings of the Royal Society of Victoria (New Series) 40 (2), 91–95.

Hearing, T.W., Harvey, T.H.P., Williams, M., Leng, M.J., Lamb, A.L., Wilby, P.R., Gabbott, S.E., Pohl, A., Donnadieu, Y., 2018. An early Cambrian greenhouse climate. Science Advances 4, 1–11.

James, N.P., Stevens, P.K., 1986. Stratigraphy and correlation of the Cambro-Ordovician Cow Head Group western Newfoundland. Geological Survey of Canada, Bulletin 366, 1–143.

Kaljo, D., Borovko, N., Heinsalu, H., Hazanovits, K., Mens, K., Popov, L., Sergejeva, S., Sobolevskaja, R., Viira, V., 1986. The Cambro-Ordovician boundary in the Baltic Ladoga Clint Area (North Estonia and Leningrad Region, USSR). Proceedings of the Academy of Sciences of Estonian SSSR, Geology 35, 97–108 (in Russian, with English abstract).

Please cite this article in press as: Wang, X.F., et al., Correlating the global Cambrian–Ordovician boundary: Precise comparison of the Xiaoyangqiao section, Dayangcha, North China with the Green Point GSSP section, Newfoundland, Canada. Palaeoworld (2019), https://doi.org/10.1016/j.palwor.2019.01.003

Kozłowski, R., 1971. Early development stages and the mode of life of graptolites. Acta Palaeontologica Polonica 16 (4), 313–343.
Kozur, H.W., Mostler, H., Repetski, J.E., 1996. Well-preserved Tremadocian primitive Radiolaria from the Windfall Formation of the Antelope Range Eureka County, Nevada, U.S.A. Geologisch-Paläontologische Mitteilungen Innsbruck 21, 245–271.
Kuo, H.C., Duan, J.E., An, S.L., 1982. Cambrian–Ordovician boundary in the North China Platform with description of trilobites. Journal of Jiling University, Earth Science Edition 3, 9–28 (in Chinese, with English abstract).
Kusky, T.M., Windley, B.F., Zhai, M.G., 2007. Tectonic evolution of the North China Block: from orogen to craton to orogen. Geological Society of London, Special Publication 280, 1–34.
Kwon, Y.K., Chough, S.K., Choi, D.K., Lee, D.J., 2006. Sequence stratigraphy of the Taeback Group (Cambrian–Ordovician), mideast Korea. Sedimentary Geology 192, 19–53.
Landing, E., Westrop, S.R., 2006. Lower Ordovician faunas, stratigraphy, and sea-level history of the middle Beekmantown Group, northeastern New York. Journal of Paleontology 80 (5), 958–980.
Landing, E., Westrop, S.R., Knox, L., 1996. Conodonts, stratigraphy, and relative sea-level changes of the Tribes Hill Formation (Lower Ordovician, East-central New York). Journal of Paleontology 70 (4), 656–680.
Lee, H.S., Chough, S.K., 2011. Depositional processes of the Zhushadong and Mantou formations (Early to Middle Cambrian), Shandong Province, China: roles of archipelago and mixed carbonate-siliciclastic sedimentation on cycle genesis during initial flooding of the North China Platform. Sedimentology 58, 1530–1572.
Lee, J.H., Chen, J.T., Chough, S.K., 2012. Demise of an extensive biostromal microbialite in the Furongian (late Cambrian) Chaomidian Formation, Shandong Province, China. Geosciences Journal 16 (3), 275–287.
Li, Z.X., Powell, C.M., 2001. An outline of the palaeo-geographic evolution of the Australasian region since the beginning of the Neoproterozoic. Earth-Science Reviews 53, 237–277.
Lin, Y.K., 1986. A new planktonic graptolite fauna. In: Chen, J.Y. (Ed.), Aspects of the Cambrian–Ordovician Boundary in Dayangcha, China. China Prospect Publishing House, Beijing, pp. 224–254.
Lindström, M., 1955. Conodonts from the lowermost Ordovician of south-central Sweden. Geologiska Föreningens i Stockholms Förhandlingar 76, 517–604.
Liu, J.B., Zheng, Z.C., 1998. Stacking patterns and correlation of meter-scale shallowing upward cycles in the Lower Ordovician carbonates in Pingquan and Qinglongshan, North China. Journal of the Geological Society of Japan 104 (5), 327–345.
Liu, J.B., Wang, Y., Qian, X.L., 1997. Two Ordovician unconformities in North China: their origins and relationships to regional carbonate-reservoir characteristics. Carbonates Evaporites 12 (2), 177–184.
Magaritz, M., 1991. Carbon isotopes, time boundaries and evolution. Terra Nova 3, 251–256.
Maletz, J., 2011. Radiolarian skeletal structures and biostratigraphy in the Early Palaeozoic (Cambrian–Ordovician). Palaeoworld 20, 116–133.
Maletz, J., 2017. The identification of putative Lower Cambrian Radiolaria. Revue de Micropaléontologie 60, 233–240.
Maletz, J., Wang, X.F., Wang, C., Stouge, S., Yan, C., 2017. The earliest planktic graptolites: taxonony and correlation. In: Wang, X.F., Stouge, S., Maletz, J., Wang, C., Yan, C. (Eds.), Field Guide and Abstracts for the Dayangcah International Workshop on the Cambrian–Ordovician Boundary. Wuhan Center of China Geological Survey, Wuhan, pp. 64–65.
Martin, F., 1973. Les Acritarches de l'Ordovicien inférieur de la Montagne Noire (Hérault, Fance). Bulletin Institute Royal des Sciences Naturelles de Belgique 48 (10) (dated 1972), 61 pp.
Martin, F., 1983. Chitinozoires et Acritarches Ordoviciens de la plate-forme du Saint-Laurent (Québec et sud-est de l'Ontario). Geological Survey of Canada, Bulletin 310, 1–59.
Martin, F., Dean, W.T., 1982. The sequence of trilobite faunas and acritarch microfloras at the Cambrian–Ordovician boundary, Wilcox Pass, Alberta, Canada. In: Bassett, M.G., Dean, W.T. (Eds.), The Cambrian–Ordovician Boundary: Sections, Fossil Distributions, and Correlations. National Museum of Wales, Geological Series 3, Cardiff, pp. 131–140.
Martin, F., Dean, W.T., 1983. Late Early Cambrian and Early Middle Cambrian acritarchs from Manuels River, eastern Newfoundland. Geological Survey of Canada, Paper 83-1B, 353–363.
Martin, F., Dean, W.T., 1988. Middle and Upper Cambrian acritarchs and trilobite zonation at Manuels River and Random Island Eastern Newfoundland. Geological Survey of Canada, Bulletin 381, 1–91.
Meng, X., Ge, M., Taylor, M.E., 1997. Sequence stratigraphy, sea-level changes and depositional systems in the Cambro-Ordovician of the North China carbonate platform. Sedimentary Geology 114, 189–222.
Meyerhoff, A.A., Kamen-Kaye, M., Chen, C., Taner, I., 1991. Stratigraphy, Palaeogeography and Tectonics. Kluwer Academic Publishers, Dordrecht, 188 pp.
Miller, J.F., 1969. Conodont fauna of the Notch Peak Limestone (Cambro-Ordovician), House Range, Utah. Journal of Paleontology 43, 413–439.
Miller, J.F., 1980. Taxonomic revisions of some Upper Cambrian and Lower Ordovician conodonts with comments on their evolution. University of Kansas, Paleontological Contributions 99, 1–39.
Miller, J.F., 1984. Cambrian and earliest Ordovician conodont evolution, biofacies, and provincialism. In: Clark, D.L. (Ed.), Conodont Biofacies and Provincialism. Geological Society of America, Special Paper 196, 34–68.
Miller, J.F., 1992. The Lange Ranch Eustatic Event: a regressive-transgressive couplet near the base of the Ordovician System. In: Webby, B.D., Laurie, J.R. (Eds.), Global Perspectives on Ordovician Geology. A.A. Balkema, Rotterdam, pp. 396–407.
Miller, J.F., Flokstra, B.R., 1999. Graphic correlation of important Cambrian–Ordovician boundary sections. Quo Vadis Ordovician — Short Papers of the Eigth International Symposium on the Ordovician System. Acta Universitatis Carolinae, Geologica 43 (12), 81–84.
Miller, J.F., Evans, K.R., Loch, J.D., Ethington, R.L., Stitt, J.H., Holmer, L., Popov, L.E., 2003. Stratigraphy of the Sauk III Interval (Cambrian–Ordovivian) in the Ibex area, Wesern Millard County, Utah and Central Texa. Brigham Young University Geology Studies 47, 21–118.
Miller, J.F., Repetski, J.E., Nicoll, R.S., Nowlan, G., Ethington, R.L., 2014. The conodont *Iapetognathus* and its value for defining the base of the Ordovician System. GFF 136 (1), 185–188.
Moczydłowska, M., 1991. Acritarch biostratigraphy of the Lower Cambrian and the Precambrian–Cambrian boundary in southeastern Poland. Fossils and Strata 29, 1–127.
Mount, J., 1985. Mixed siliciclastic and carbonate sediments: a proposed first-order textural and compositional classification. Sedimentology 32 (3), 435–442.
Müller, K.J., 1959. Kambrische Conodonten. Zeitschift der Deutschen Geologischen Gesellschaft 111, 434–485.
Nicoll, R.S., 1990. The genus *Cordylodus* and latest Cambrian–earliest Ordovician biostratigraphy. BMR Journal of Australian Geology and Geophysics 11, 529–558.
Nicoll, R.S., 1991. Differentiation of Late Cambrian–Early Ordovician species of *Cordylodus* (Conodonta) with biapical basal cavities. BMR Journal of Australian Geology and Geophysics 12 (3), 223–244.
Nicoll, R.S., 1992. Evolution of the conodont genus *Cordylodus* and the Cambrian–Ordovician boundary. In: Webby, B.D., Laurie, J.R. (Eds.), Global Perspectives on Ordovician Geology. A.A. Balkema, Rotterdam, pp. 105–113.
Nicoll, R.S., Nielsen, A.T., Laurie, J.R., 1992. Preliminary correlation of latest Cambrian to Early Ordovician sea level events in Australia. In: Webby, B.D., Laurie, J.R. (Eds.), Global Perspectives on Ordovician Geology. A.A. Balkema, Rotterdam, pp. 381–394.
Nicoll, R.S., Miller, J.F., Nowlan, G.S., Repetski, J.E., Ethington, R.L., 1999. *Iapetonudus* (n. gen.) and *Iapetognathus* Landing: unusual earliest Ordovician multielement conodont taxa and their utility for biostratigraphy. Brigham Young University Geology Studies 44, 27–101.
Nogami, Y., 1967. Kambrische Conodonten von China, Teil 2: Conodonten aus den hoch oberkambrischen Yencho-Schichten. Memoirs of the College of Science, University of Kyoto, Geology and Mineralogy, Series B 33 (4), 211–218.
Norford, B.S., 1991. The international working group on the Cambrian–Ordovician boundary: report of progress. In: Barnes,

Please cite this article in press as: Wang, X.F., et al., Correlating the global Cambrian–Ordovician boundary: Precise comparison of the Xiaoyangqiao section, Dayangcha, North China with the Green Point GSSP section, Newfoundland, Canada. Palaeoworld (2019), https://doi.org/10.1016/j.palwor.2019.01.003

C.R., Williams, S.H. (Eds.), Advances in Ordovician Geology. Geological Survey of Canada, Paper 90-9, pp. 27–32.
Norford, B.S., Webby, B.D. (Eds.), 1988. Cambrian–Ordovician boundary. Geological Magazine 125 (4), 323–463.
Nowlan, G.S., 1995. Variations in marine carbon isotope ratios ($\delta^{13}C$) through the Cambrian–Ordovician boundary interval. International Cambrian–Ordovician boundary working group. St. John's, Newfoundland (Canada), December, 1995 (unpublished).
Nowlan, G.S., Nicoll, R.S., 1995. Re-examination of the conodont biostratigraphy at the Cambrian–Ordovician Xiaoyangqiao section, Dayangcha, Jilin Province, China. In: Cooper, J.D. (Ed.), Ordovician Odyssey: Short Papers for the Seventh International Symposium on the Ordovician System. Pacific Section of Society for Sedimentary Geology (SEPM), Book 77, 113–116.
Odin, G.S. (Ed.), 1988. Green Marine Clays. Development in Sedimentology, 45. Elsevier Amsterdam, 444 pp.
Pander, C.H., 1856. Monographie der fossilen Fische des silurischen Systems der Russich-Baltischen Gouvernements. Akademie der Wissenschaften, St. Petersburg, 91 pp.
Porrenga, D.H., 1967. Glauconite and chamosite as depth indicators in the marine environment. Marine Geology 5 (5–6), 495–501.
Pouille, L., Danelian, T., Maletz, J., 2014. Radiolarian diversity changes during the Late Cambrian–Early Ordovician transition as recorded in the Cow Head Group of Newfoundland (Canada). Marine Micropaleontology 110, 25–41.
Qian, Y.Y., 1986. Trilobites. In: Chen, J.Y. (Ed.), Aspects of the Cambrian–Ordovician Boundary in Dayangcha, China. China Prospect Publishing House, Beijing, pp. 255–306.
Raevskaya, E.G., 2000. Akritarkhi i biostratigraphija verkhov kembrija-srednego ordovika severo-zapada Vostochno-Evropejskoj Platformy [Acritarchs and biostratigraphy of the uppermost Cambrian–Middle Ordovician of the northwestern part of the East-European Platform]. PhD Thesis. Saint Petersburg State University, 174 pp. (in Russian).
Raevskaya, E.G., Servais, T., 2009. *Ninadiacrodium*: a new late Cambrian acritarch genus and index fossil. Palynology 33 (1), 219–239.
Rasul, S.M., 1974. The lower Palaeozoic acritarchs *Priscogalea* and *Cymatiogalea*. Palaeontology 17 (1), 41–63.
Rasul, S.M., 1976. New species of the genus *Vulcanisphaera* (Acritarcha) from the Tremadocian of England. Micropaleontology 22 (4), 479–484.
Remane, J., Bassett, M.G., Cowie, J.W., Gohrbandt, K.H., Lane, H.R., Michelsen, O., Naiwen, W., 1996. Revised guidelines for the establishment of Global chronostratigraphic standards by the International Commission on Stratigraphy (ICS). Episodes 19 (3), 77–81.
Ripperdan, R.L., Kirschvink, J.L., 1992. Paleomagnetic results from the Cambrian–Ordovician boundary sections at Black Mountain, Georgina Basin, western Queensland, Australia. In: Webby, B.D., Laurie, J.R. (Eds.), Global Perspectives on Ordovician Geology. A.A. Balkema, Rotterdam, pp. 93–103.
Ripperdan, R.L., Magaritz, M., Nicoll, R.S., Shergold, J.H., 1992. Simultaneous changes in carbon isotopes, sea level, and conodont biozones within the Cambrian–Ordovician boundary interval at Black Mountain, Australia. Geology 20, 1039–1042.
Ripperdan, R.L., Magaritz, M., Kirschvink, J.L., 1993. Carbon isotope and magnetic polarity evidence for non-depositional events within the Cambrian–Ordovician boundary section near Dayangcha, Jilin Province, China. Geological Magazine 130 (4), 443–452.
Ruedemann, R., 1937. A new North American graptolite faunule. American Journal of Science 33 (193), 57–62.
Runkel, A.C., Mackey, T.J., Cowan, C.A., Fox, D.L., 2010. Tropical shoreline ice in the late Cambrian: implications for Earth's climate between the Cambrian Explosion and the Great Ordovician Biodiversification Event. GSA Today 20 (11), 4–10.
Salvador, A. (Ed.), 1994. International Stratigraphic Guide: A Guide to Stratigraphic Classification, Terminology, and Procedure. , 2nd Edition. International Union of Geological Sciences and the Geological Society of America Boulder, Colorado, 214 pp.
Stouge, S., Bagnoli, G., McIlroy, D., 2017. Cambrian–Middle Ordovician Platform-slope Stratigraphy, Palaeontology and Geochemistry of Western Newfoundland. Geological Survey of Newfoundland and Labrador, Open File 012B/0692, 106 pp.
Taylor, J.F., Repetski, J.E., Orndorff, R.C., 1992. The Stonehenge Transgression: a rapid submergence of the central Appalachian platform in the Early Ordovician. In: Webby, B.D., Laurie, J.R. (Eds.), Global Perspectives on Ordovician Geology. A.A. Balkema Rotterdam, pp. 409–418.
Terfelt, F., Bagnoli, G., Stouge, S., 2012. Re-evaluation of the conodont *Iapetognathus* and implications for the base of the Ordovician System GSSP. Lethaia 45, 227–237.
Torsvik, T.H., Cocks, L.R., 2016. Earth History and Palaeogeography. Cambridge University Press, Cambridge, 317 pp.
Tripathy, G.R., Hannah, J.L., Stein, H.S., Yang, G., 2014. Re-Os age and depositional environment for black shales from the Cambrian–Ordovician boundary, Green Point, western Newfoundland. Geochemistry, Geophysics, Geosystems 15, 1021–1037.
Trotter, J.A., Williams, I.S., Barnes, C.R., Lecuyer, C., Nicoll, R.S., 2008. Did cooling oceans trigger Ordovician biodiversification? Evidence from conodont thermometry. Science 321, 550–554.
Tucker, M.E., 2003. Sedimentary Rocks in the Field. Wiley and Sons, Chichester, 237 pp.
Vanguestaine, M., 1973. New acritarchs from the Upper Cambrian of Belgium. In: Vozzhennikova, T.F., Timofeev, B.V. (Eds.), Microfossils of the Oldest Deposits. Proceedings of the Third International Palynological Conference, Novosibirsk, 1971. Akademiya Nauk SSSR, Siberskoe Otdelenie, Institut Geoogii I Geofizikii, Izdatelstvo, Nauka, Moskva, pp. 28–31.
Vanguestaine, M., 1978. Critères palynostratigraphiques conduisant a la reconnaissance d'un pli couche revinien dans le sondage de Grand-Halleux. Annales de la Société Géologique de Belgique 100, 249–276.
Viira, V., Sergeeva, S., Popov, L., 1987. Samye rannie predstaviteili roda *Cordylodus* (Conodonta) iz severnoj Ehstonii i Leningradskoj Oblasti [Earliest representatives of the genus *Cordylodus* (Conodonta) from Cambro–Ordovician boundary beds of North Estonia and Leningrad Region]. Proceedings of the Academy of Sciences of the Estonian SSR, Geology 36, 145–153 (in Russian).
Volkova, N.A., 1968. Akritarkhi dokembrijskikh i kembrijskikh otlozhenij Estonii. Problematika pogranichnykh sloev rifeja i kembrija Russkoj platformy, Urala i Kazakhstana. [Acritarchs from Precambrian and Cambrian strata of Estonia. Problems on boundary beds of the Riphean and Cambrian of the Russian Platform, Ural and Kazakhstan]. Trudy GIN AN SSSR 188, 34–37 (in Russian).
Volkova, N.A., 1990. Akritarkhi srednego i verkhnego Kembrija Vostochno-Evropeiskoj platformy [Middle and Upper Cambrian acritarchs of the East-European Platform]. Trudy 454, Nauka, Moscow, 115 pp. (in Russian).
Volkova, N.A., Kir'janov, V.V., 1995. Regional'naya stratigraphicheskaya skhema sredneverkhnekembrijskikh otlozhenij Vostochno Evropejskoj platformy [Regional stratigraphic scheme of the Middle–Upper Cambrian of the East European Platform]. Stratigraphy and Geological Correlation 3 (5), 66–74 (in Russian).
Wang, X.F., Erdtmann, B.-D., 1987. Zonation and correlation of the earliest Ordovician graptolites from Hunjiang, Jilin Province, China. Bulletin of the Geological Society of Denmark 35, 245–257.
Wang, X.F., Chen, X., Chen, X.H., Zhu, Z.Y., 1996. Stratigraphical Lexicon of China — The Ordovician System. Geological Publishing House, Beijing, 192 pp.
Wang, Z.C., Yang, J.D., 1986. Clay mineral composition aspects and relevant implication of diagenetic process. In: Chen, J.Y. (Ed.), Aspects of the Cambrian–Ordovician Boundary in Dayangcha, China. China Prospect Publishing House, Beijing, pp. 50–60.
Wang, Z.H., Zhen, Y.Y., Zhang, Y.D., Wu, R.C., 2016. Review of the Ordovician conodont biostratigraphy in the different facies of North China. Journal of Stratigraphy 46 (1), 1–16 (in Chinese, with English abstract).
Webby, B.D., Laurie, J.R. (Eds.), 1992. Global Perspectives on Ordovician Geology. A.A. Balkema Rotterdam, 513 pp.
Wentworth, C.K., 1922. A scale of grade and class terms for clastic sediments. The Journal of Geology 30 (5), 377–392.
Won, M.Z., Iams, W.J., Reed, K., 2005. Earliest Ordovician (early to Middle Tremadoc) radiolarian faunas of the Cow Head Group, western Newfoundland. Journal of Paleontology 79, 433–459.
Xiao, W.J., Windley, B.F., Yuan, C., Sun, M., Han, C.M., Lin, S.F., Chen, H.L., Yan, Q.R., Liu, D.Y., Qin, K.Z., Li, J.L., Sun, S., 2009. Paleozoic multiple

Please cite this article in press as: Wang, X.F., et al., Correlating the global Cambrian–Ordovician boundary: Precise comparison of the Xiaoyangqiao section, Dayangcha, North China with the Green Point GSSP section, Newfoundland, Canada. Palaeoworld (2019), https://doi.org/10.1016/j.palwor.2019.01.003

subduction–accretion processes of the southern Altaids. American Journal of Science 309, 221–270.

Yang, Y.D., Wang, Y.X., Tao, X.C., Li, H.M., Wang, Z.Z., 1986. Rb-Sr dating on the Cambrian–Ordovician boundary interval. In: Chen, J.Y. (Ed.), Aspects of the Cambrian–Ordovician Boundary in Dayangcha, China. China Prospect Publishing House, Beijing, pp. 72–82.

Yin, L.M., 1985. Acritarchs. In: Chen, J.Y., Qian, Y.Y., Lin, Y.K., Zhang, J.M., Wang, Z.H., Yin, L.M., Erdtmann, B.-D. (Eds.), Study on Cambrian–Ordovician Boundary Strata and Its Biota in Dayangcha, Hunjiang, Jilin, China. China Prospect Publishing House, Beijing, pp. 101–112.

Yin, L.M., 1986. Acritarchs. In: Chen, J.Y. (Ed.), Aspects of the Cambrian–Ordovician Boundary in Dayangcha, China. China Prospect Publishing House, Beijing, pp. 313–373.

Yin, L.M., 1995. Early Ordovician acritarchs from Hunjiang, Jilin and Yichang region, Hubei, China. Palaeontologica Sinica 185, New Series A 12, 1–170 (in Chinese and English).

Zeballo, F.J., Albanesi, G.L., Ortega, G., 2005. Conodontes y graptolitos de las formaciones Alfarcito y Rupasca (Tremadociano) en el área de Alfarcito, Tilcara, Cordillera Oriental de Jujuy, Argentina Parte 2: Paleontología sistema. Ameghiniana 42 (1), 47–66.

Zhai, M.G., Santosh, M., 2013. Metallogeny of the North China Craton: link with secular changes in the evolving Earth. Gondwana Research 16 (2), 321–341.

Zhang, J.M., 1986. Description of sections. In: Chen, J.Y. (Ed.), Aspects of the Cambrian–Ordovician Boundary in Dayangcha, China. China Prospect Publishing House, Beijing, pp. 7–14.

Zhang, J.M., Chen, J.Y., 1986. Lithofacies sequence. In: Chen, J.Y. (Ed.), Aspects of the Cambrian–Ordovician Boundary in Dayangcha, China. China Prospect Publishing House, Beijing, pp. 15–34.

Zhang, J.M., Wang, H.F., Li, G.X., Chen, J.Y., 1996. Redescription of the Dayangcha section as a candidate for the Global Cambrian–Ordovician Boundary Stratotype, Jilin Province, China. Journal of Stratigraphy 20 (2), 81–103 (in Chinese with English abstract).

Zhang, W.T., 1962. Ordovician of China. Symposium on Stratigraphy of China. Science Press Beijing, 62 pp. (in Chinese).

Zhang, Y.D., Erdtmann, B.-D., 2004. Tremadocian (Ordovician) biostratigraphy and graptolites at Dayangcha (Baishan, Jilin, NE China). Paläontologische Zeitschrift 78 (2), 323–354.

Zhao, G.C., Zhai, M.G., 2013. Lithotectonic elements of Precambrian basement in the North China Craton: review and tectonic implications. Gondwana Research 23, 1207–1240.

Zhen, Y.Y., Zhang, Y.D., Wang, Z.H., Percival, I.G., 2016. Huaiyuan Epeirogeny — Shaping Ordovician stratigraphy and sedimentation on the North China Platform. Palaeogeography, Palaeoclimatology, Palaeoecology 448, 363–370.

Zhen, Y.Y., Percival, I.G., Webby, B.D., 2017. Discovery of *Iapetognathus* fauna from far western New South Wales: towards a more precisely defined Cambrian–Ordovician boundary in Australia. Australia Journal of Earth Sciences 64 (4), 487–496.

Zheng, Y.F., Xiao, W.J., Zhao, G.C., 2013. Introduction to tectonics of China. Gondwana Research 23, 1189–1206.

Zhou, Z.Y., Wang, Z.H., Zhang, J.M., 1984. Cambrian–Ordovician boundary and the proposed candidates for stratotype in North and Northeastern China. In: Nanjing Institute of Geology and Palaeontology, Academia Sinica (Ed.), Cambrian–Ordovician Boundary (2). Anhui Science and Technology Publishing House, Hefei, pp. 1–62 (in Chinese).

Zhu, R.X., Yang, J.H., Wu, F.Y., 2012. Timing of destruction of the North China Craton. Lithos 149, 51–60.

Please cite this article in press as: Wang, X.F., et al., Correlating the global Cambrian–Ordovician boundary: Precise comparison of the Xiaoyangqiao section, Dayangcha, North China with the Green Point GSSP section, Newfoundland, Canada. Palaeoworld (2019), https://doi.org/10.1016/j.palwor.2019.01.003